PETROGRAPHIC AND ISOTOPIC STUDIES OF THE PRECAMBRIAN LESSER HIMALAYAN CLASTIC SEDIMENTS: IMPLICATION FOR THEIR PROVENANCES

By

MANJU NEGI

SAP ID 500033386

SCHOOL OF ENGINEERING

(DEPARTMENT OF PETROLEUM AND EARTH SCIENCES)

SUBMITTED

IN PARTIAL FULFILLMENT OF THE REQUIREMENT OF THE

DEGREE OF

DOCTOR OF PHILOSOPHY

TO

U UPES

UNIVERSITY WITH A PURPOSE

UNIVERSITY OF PETROLEUM AND ENERGY STUDIES

DEHRADUN

OCTOBER, 2018

UNDER THE GUIDANCE OF

EXTERNAL SUPERVISOR	INTERNAL SUPERVISOR
Dr. Santosh K. Rai **Scientist-D** **Wadia Institute of Himalayan Geology,** **Dehradun**	**Dr. Uday Bhan** **Associate Professor** **University of Petroleum and Energy Studies,** **Dehradun**

DEDICATED TO MAA

<u>Declaration</u>

I hereby declare that this submission entitled "PETROGRAPHIC AND ISOTOPIC STUDIES OF THE PRECAMBRIAN LESSER HIMALAYAN CLASTIC SEDIMENTS: IMPLICATION FOR THEIR PROVENANCES" is my own work and that, to the best of my knowledge and belief, it contains no material previously published or written by another person, nor material which has been accepted for the award of any other degree or diploma of the university or other institute of higher learning, except where due acknowledgment has been made in the text.

Manju Negi

Date   17.10.2018

WADIA INSTITUTE OF HIMALAYAN GEOLOGY

(An Autonomous Institution of Dept. of Science & Technology, Govt. of India)

33, General Mahadev Singh Road,
Dehradun (Uttarakhand) – 248001 (INDIA)

Dr. Santosh. K. Rai
Scientist-D & Coordinator
Petrology & Geochemistry Group

Phone : +91-0135-2525184
Fax : +91-0135-2625212
E-mail: rksant@wihg.res.in

THESIS COMPLETION CERTIFICATE

This is to certify that the thesis on **"PETROGRAPHIC AND ISOTOPIC STUDIES OF THE PRECAMBRIAN LESSER HIMALAYAN CLASTIC SEDIMENTS: IMPLICATION FOR THEIR PROVENANCES"** submitted by **MANJU NEGI** (SAP ID 500033386) in Partial completion of the requirements for the award of the degree of Doctor of Philosophy (Geo Sciences), is an original work carried out by her under my supervision and guidance.

It is certified that the work has not been submitted anywhere else for the award of any other diploma or degree of this or any other University.

External Guide

Dr. Santosh K. Rai
Scientist 'D'
Wadia Institute of Himalayan Geology,
33 GMS Road
Dehradun

Place: DEHRADUN   **Date:** 16·10·2018

THESIS COMPLETION CERTIFICATE

This is to certify that the thesis on **"PETROGRAPHIC AND ISOTOPIC STUDIES OF THE PRECAMBRIAN LESSER HIMALAYAN CLASTIC SEDIMENTS: IMPLICATION FOR THEIR PROVENANCES"** submitted by **MANJU NEGI** (SAP ID 500033386) in Partial completion of the requirements for the award of the degree of Doctor of Philosophy (Geo Sciences), is an original work carried out by her under my supervision and guidance.

It is certified that the work has not been submitted anywhere else for the award of any other diploma or degree of this or any other University.

Internal Guide

Dr. Uday Bhan

Associate Professor

University of Petroleum and Energy Studies

Dehradun

Place: Dehradun   **Date:** 17.10.2018

ACKNOWLEDGEMENTS

Table of Contents

EXECUTIVE SUMMARY

Clastics forming a major part of the sedimentary rocks in the Himalaya, exhibit varying chemical composition, protolith ages (pre-Himalayan) and depositional settings. The Himalayan Orogen is bounded by the Nanga Parbat Syntaxis in the northwest and the Namcha Barwa Syntaxis in the northeast with a length of ~2500 km and a width of 250 km. It is a young mountain chain which has resulted out of the continental collision between the Indian and the Eurasian plates. It consists of three principal lithotectonic zones, based on internal stratigraphy and bounding faults which were activated during the Cenozoic collision of India with Asia (Gansser, 1964; Lefort, 1975). To the south, the Lesser Himalayan domain, tectonically bound between the Main Central Thrust (MCT) and the Main Boundary Thrust (MBT) is constituted of deformed Proterozoic rock sequences. It comprises of Precambrian sedimentary packages and overlain by Permian and younger rocks. The Higher Himalaya is bounded between the Main Central Thrust (MCT) in the south and South Tibetan Detachment (STD) in the north and is comprises mainly of the high grade Precambrian metamorphics. The Tethys Himalaya comprises of the fossiliferous sedimentary rocks ranging in age from Late Proterozoic to Cretaceous or even Eocene.

Present study is focused on addressing the problems regarding the:-

- ➢ Controversy towards the information about the variability in the sources of sediments, chemical composition and nature of sedimentation (Ahmad et al., 2000; Jain, 1972; Spencer et al., 2011).
- ➢ The relative age of the Outer Lesser Himalaya (OLH) and Inner Lesser Himalaya (ILH) that, whether they are of the similar age? If not then which one is the younger?

The Lesser Himalaya (LH) sediments are unfossiliferous and thus most of the stratigraphic division are placed on the basis of the lithological and petrographic studies. Further, the sediments of the Lesser Himalaya are

characterized by higher degree of digenesis and low grade metamorphism and therefore petrographic studies alone may not be sufficient for their provenance identification. Towards this the theoretical and experimental approach has been a source of wide knowledge in the understanding of the geological processes like evolution, abrasion, transportation and finally changes in the chemical composition due to weathering of the sediments. With these new observations on the stratigraphy and geochronology of the LH has been proofed with the help of petrography, analytical and experimental methods in the laboratory.

The clastic samples were collected from the Proterozoic Lesser Himalayan sequence and have been analysed for their petrographic study, chemical composition, isotopic characteristics (Sr-Nd) and their U-Pb zircon geochronology.

Towards this, the chips of the collected samples were observed under the microscope for their petrographic features. From the petrographic study, it is observed that there occurs two sedimentary packages in the outer and inner part of the Lesser Himalaya and are classified as (i) Siliciclastic (SLC) and (ii) Recrystallized siliciclastic (RSLC). The SLC package has undergone diagenesis and is showing the preservation of original texture. The RSLC has undergone metamorphism due to which the original sedimentary textures are lost. Both the siliciclastics are mature as evidenced by a plenty of sub-rounded and rounded detrital and moderate degree of sorting. The detrital proportions of the clastics from the OLH and ILH are: $Q_{77}\pm_{12}F_{11}\pm_4R_{12}\pm_9$; $Mx_9\pm_5$ (n=17) and $Q_{86}\pm_{14}F_5\pm_4R_9\pm_{13}$; $Mx_{10}\pm_7$ (n=21), respectively. The petrographic studies suggest that clastic sediments were supplied from the felsic source rocks as a recycled material. The Scanning Electron Microscope (SEM) studies of these samples show the presence of surface features such as conchoidal fractures and clay alteration, which might have been developed due to diagenetic processes. The chemical composition of the clastics have also been measured during SEM-EDX method (quantitative-analysis), it indicates that clastics are dominated by the light minerals, quartz and clay and heavy minerals such as

ilmenite and rutile having the presence of Si, Mg, Fe, K and Ti. Presences of rutile have also been identified by their higher Zr and Nb content.

In addition, to get the detail of morphological and internal structures of zircon grains, cathodoluminescence (CL) imaging was done using a Chroma CL-2 detector (Gatan make), attached to Secondary Electron Microscope (SEM). This shows that zircons from both the units (OLH and ILH) are generally euhedral shape. However, the OLH zircons are bigger (117μm ± 21 with L/B ratio 1.87 ± 0.11) than the ILH (101 μm ±30 with L/B ratio1.75 ± 0.10). The zircons are irregular and euhedral to anhedral in the ILH domain and prismatic euhedral to anhedral whereas these are more elongated in case of the OLH. The zoning in ILH zircons is only faintly visible as compared to OLH.

For the chemical composition of the clastics the major, trace and rare earth elements (REEs) were measured. Towards this, X-Ray Fluorescence technique (XRF) used for the analysis of major and trace elements using pressed powder pellets and REEs by using Inductively Coupled Plasma Mass Spectrometry (ICP-MS) in solution mode. Geochemical analysis of the clastics indicates that they are sourced from both the felsic and mafic source rocks which has gone under varying degrees of denudation. Towards this, the Chemical Index of Alteration (CIA) is used for evaluating the degree of chemical weathering through which these clastics were faced with during their transport from their protoliths to depositional sites. The present study shows that the CIA values of the Lesser Himalayan clastic sediments ranges between 47 and 81, with an average of 70±8. The CIA values thus show moderate weathering in the source region. A-CN-K (Al_2O_3-(CaO^*+Na_2O)-K_2O) plot was also used for knowing the weathering trend of a source rock which further indicates that these clastic sediments are derived from a protolith with felsic nature.

The isotopic (Sr-Nd) concentrations of the siliciclastics were analysed on Multi-collector Inductively coupled plasma Mass Spectrometer (MC-ICP-MS) to understand the plausible provenance of these sediments. Present study shows that isotopic signatures of the Lesser Himalaya showing the εNd values range from -19.6 to -6.7 for OLH and -14.6 to -37.6 for ILH.Similarly, the

$^{87}Sr/^{86}Sr$ ratio of ILH ranges from 0.7434 to 1.4789 and 0.7392 to 0.8638 for OLH. A comparison of these values in clastic sediments with those from the potential source regions, it appears that these (OLH and ILH) are sourced from the mixing end members like Aravalli craton, Bundelkhand craton and other Archean cratons. These observations are also reflected in the two isotope plot constructed between εNd and $^{87}Sr/^{86}Sr$ where majority of the sample composition lie within three end members.

The unfossiliferous nature of the Damtha Group (Chakrata and Rautgara formations) and Jaunsar Group (Chandpur and Nagthat formations) of the Lesser Himalayan sediments has made it inappropriate for measuring the age of these Formations with biostraigraphic tools. Therefore, the U-Pb dating of the detrital zircon of the siliciclastics were attempted to constrain their maximum age. Towards this, U-Pb analysis of the zircon grains was performed by using LASER Ablation Multi Collector Inductively Coupled Mass Spectrometer (LA-ICP-MS). Age distribution for these zircon grains, recovered from the clastic rocks of inner and outer zones of the Lesser Himalaya, shows that the most of these zircons have affinities for a bimodal age with peaking at Paleoproterozoic (between 1.6 and 1.8 Ma.) and Neoproterozoic (800 Ma). This study shows the presence of mono-crystalline quartz, polycrystalline quartz, potash-feldspar, plagioclase and rock fragments like phyllite, slate, schist and felsic volcanic fragments. These attributes are also present in the source rocks which consist of Archean banded gneissic complex (BGC; >2.5Ga), Palaeoproterozoic Aravalli -Delhi Supergroup overlain by sedimentary succession of Meso-Neoproterozoic Vindhyan Supergroup (Verma and Greiling, 1995). This seems to indicate that they are derived from the cratons as a recycled material. It is also inferred from the isotopic composition of the LH clastics by the isotopic differences between the Outer and inner zones and relates its differences with their source rocks (Aravalli craton, Bundelkhand craton and other Archean craton) and proposes that these clastics of the Lesser Himalaya were in sediment source continuity with the Indian craton. The bimodal age distributions of the zircons from clastic samples (1.8 Ga and 800Ma) from the Lesser Himalaya are correlated

with the Vindhyan Supergroup, Banded Gneissic complex (BGC)/Marwar Supergroup (Aravalli craton) and Tonalite-trondhjemite-granodiorite (TTG, Bundelkhand craton). Thus form the petrographic, isotopic and geochronology it is suggested that Aravalli craton and Bundelkhand craton are the possible end members of the Lesser Himalayan clastics which has a varied pattern of sediment supply to these clastic with time.

List of Abbreviations

ALG	Argillite
BDL	Below detection limit
BGC	Banded Gneissic complex
CGS	Coarse-grained siliciclastic facies
CH	Chert
CIA	Chemical Index of Alteration
CIW	Chemical Index of Weathering
CIW'	Modified CIW
CL	Cathodoluminescence
EDX	Energy Dispersive X-Ray Analysis
F	Feldspar
FGS	Fine- grained siliciclastic facies
HF	Hydrofluoric acid
ICP-MS	Inductively Coupled Plasma Mass Spectrometry
ILH	Inner Lesser Himalaya
IMFS	Interbedded medium to fine grained siliciclastic facies
ITZS	Indus -Tsangpo Suture Zone
LA-MC-ICPMS	Laser Ablation Multi-collector Inductively coupled plasma Mass Spectrometer
LGM	Low grade metamorphics
LH	Lesser Himalayan
LOI	Loss on Ignition
LST	Limestone
m	Molar
MBT	Main Boundary Thrust
Mc	Microcline
MC-ICP-MS	Multi-collector Inductively coupled plasma Mass Spectrometer
MCT	Main Central Thrust
MFT	Main Frontal Thrust
MQ	Metaquartzite
Mx	Matrix

OLH	Outer Lesser Himalaya
PAAS	Post-Archean Australian average shale
PIA	Plagioclase Index of Alteration
PPM	Part per million
PRL	Physical Research Laboratory
PVA	Polyvinyl alcohol
QC	Quality control
Q_m	Mono-crystalline quartz
QMA	Quartz mica aggregate
Q_{mnu}	Monocrystalline non undulatory quartz
Q_{mu}	Monocrystalline undulatory quartz
Q_p	Polycrystalline quartz
R	Rock fragment
REEs	Rare earth elements
Ri	Igneous rock
Rm	Metamorphic rock
Rs	Sedimentary rock
RSLC	Recrystallized Siliciclastic
SEM	Scanning Electron Microscope
SLC	Siliciclastic
SRBD	Sundernagar – Rampur - Berinag - Damtha
SSD	Soft sediment deformation
STD	South Tibetan Detachment
TTG	Tonalite-trondhjemite-granodiorite
UCC	Upper continental crust
UND	Undifferentiated rock fragments
VLC	Volcanics
WIHG	Wadia Institute of Himalayan Geology
wt. %)	Weight percentage
XRF	X-Ray Fluorescence technique

List of Figures

List of Tables

CHAPTER 1: INTRODUCTION

CHAPTER 1: INTRODUCTION

1.1 Outline

Clastics form the major part of the sedimentary rocks in the Himalaya and exhibit varying chemical composition, protolith ages (pre-Himalayan) and depositional settings. However, the information about the variability in the sources of sediments, chemical composition and nature of sedimentation is debated (Ahmad et al., 2000; Jain, 1972; Spencer et al., 2011). Petrography is a fundamental tool for understanding the textural and compositional properties of rocks. It is regarded as the most useful parameters for the reconstruction of the source lithology, diagenetic and depositional characteristics, collectively used for provenance studies. However, in many cases the petrographic parameters do not work because of deformation, metamorphism and intense weathering of rocks due to the alteration of their inherited structures, texture and composition. In such cases, the geochemical and isotopic studies are helpful for the determination of the provenance. In addition, the zircon geochronology can also be used for tracking the changes during transportation and depositional processes and eventually determining the age of the rocks.

The Himalayan range is bounded by the Nanga Parbat syntaxis in the northwest and the Namche-Barwa syntaxis in the northeast. This range is divided into four major subdivisions from south to north as Sub-Himalaya, Lesser Himalaya, Higher Himalaya, and Tethys Himalaya (Figure 1.1). Detailed description about the lithology, stratigraphy and tectonic features of the Himalayan orogen is described in Chapter 2.

1.2 Lesser Himalaya and the vital issues

The Lesser Himalaya is about 13-16 km wide with moderate to high relief topography. The Lesser Himalayan sequence essentially comprises Proterozoic to Early Cambrian sediments derived from the passive Indian margin intercalated with some granites and acid volcanism of Early Proterozoic age (Frank et al.,1973).
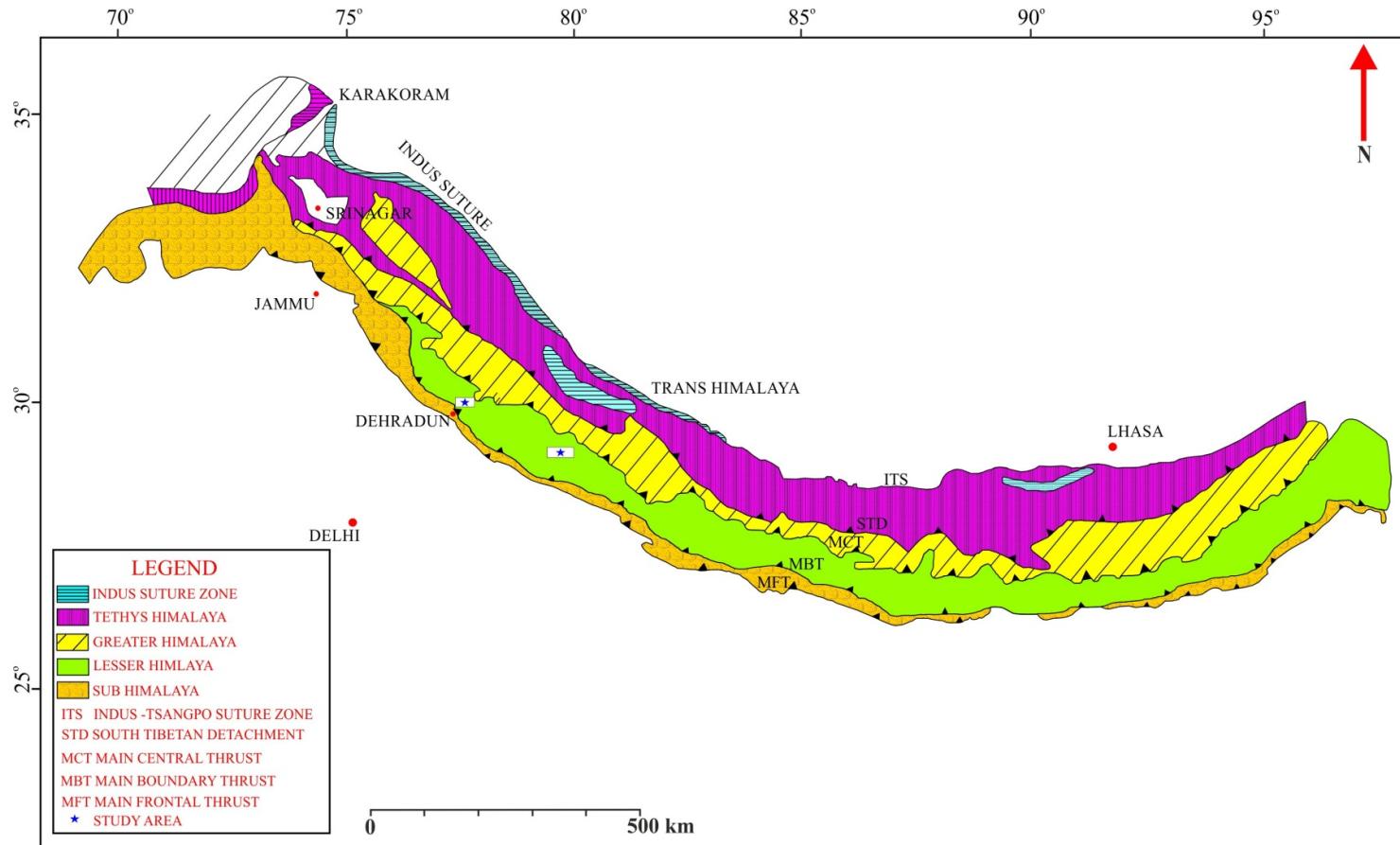
Figure 1.1 Simplified geological map of the Himalaya (after Gansser, 1964) showing the study area.

The sedimentation and other events in the Lesser and Higher Himalaya have much in common with those noted from the sediment lying to the north of the Central Indian Tectonic Zone of the peninsular region. Holland (1908) was first to propose the Precambrian age for the Lesser Himalayan rocks in Shimla, Kumaun and Bhutan and equated them with the Aravalli, Vindhyan and Cuddapah successions of the Peninsular India. Subsequently, the Lesser Himalayan sediments were termed as the Peninsular Himalaya by Auden (1935). Further, he added that, even though the Lesser Himalaya and the northern end of the Peninsular India are separated by the Indo-Gangetic plain, to a large extent, the Himalaya should be considered as made up of a foreland to the Tethys Ocean and its continental shelf. A lot of work has been done to bring out significant details on the structural and stratigraphic set up of the Lesser Himalaya zone (Medlicott, 1864; Oldham, 1883, 1888; Auden 1934, 1937; Rupke 1974; Valdiya 1980). Also the significant study of the depositional history of the Lesser Himalaya, provenance and weathering details have been done by several researchers (Ghosh, 1991; Pant and Shukla, 1999) on the basis of detrital modes and geochemical studies (Islam et al., 2002).

The Proterozoic Lesser Himalayan basin is unique owing to its extremely long stratigraphy at least from Palaeoproterozoic to early Phanerozoic, encompassing a sedimentary record of virtually 1000 My. Collectively, the Late Neoproterozoic (between 650-542 Ma) part of the Lesser Himalaya is relatively fairly constrained and understood in terms of litho- and bio-stratigraphy, sedimentology, structure, tectonics and isotopic constrain. However, the Late Paleoproterozoic-Neoproterozoic (~1800-650 Ma) part is least attended due to some inherited geological problems. On the basis of the published records, it has been noticed that the sedimentological studies of these successions are available only from the siliciclastic-carbonate succession of Uttarakhand and in part from the carbonate dominated succession of Himachal Pradesh (Figure 1.2). Recently Ghosh et al (2016b) has reviewed the published work (Figure 1.2) and indicated the issues that needs the attention on the following counts-

- Stratigraphy, particularly the litho-stratigraphy and bio-stratigraphy of these Precambrian sedimentary successions has been documented, even though disagreement persist,

- Methodical sedimentologic study (except in the Garhwal- Kumaun Lesser Himalaya), which is lacking in the western and eastern Himalayan sectors and constrains us to evolve an overall evolutionary sedimentologic model,

- It is still unclear whether the Proterozoic succession in the Himalaya is a part of the Aravalli or Bundelkhand craton or a combination of both. Consequently, it will be appropriate to consider the Himalayan Proterozoic succession as a part of the Aravalli- Bundelkhand craton, and near absence of consistent radiometric age data for these sedimentary successions has resulted in highly speculative paleogeography models because the intercontinental geological correlations of formations deposited during this time-span is based primarily on a comparison of stratigraphic records.
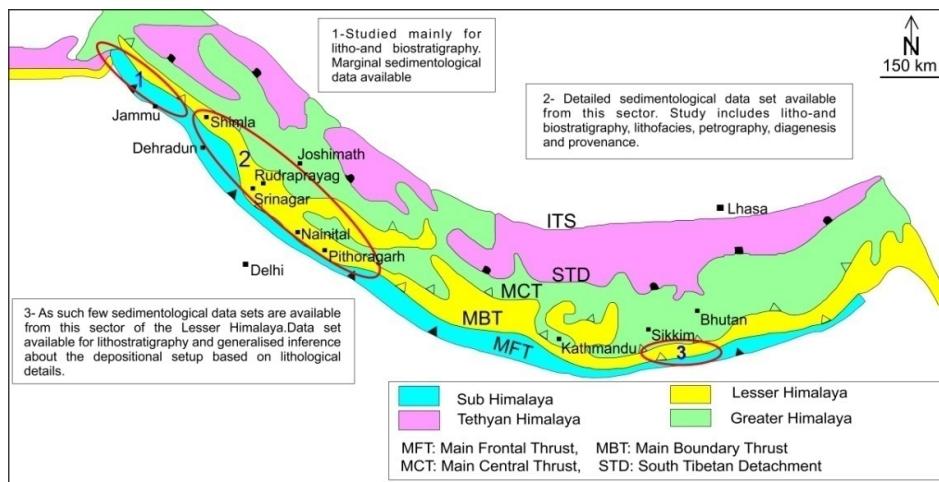
Figure 1.2 Status of sedimentological work in the Lesser Himalayan domain.

The primary goals of my thesis are to determine (i) the provenance of the clastics from the Lesser Himalayan region, and (ii) the geochronological age of the Lesser Himalayan siliciclastics. Accomplishing of these goals requires sampling of the clastics sediments, knowledge of the stratigraphy and lithology of the area. Keeping these in view, efforts have been made in this

chapter to summarize available information about the lithology, stratigraphy, geochronology and provenance, of the Lesser Himalaya.

1.3 Objectives

- To address the stratigraphic setting and source rock compositional aspects of the Lesser Himalayan sedimentary packages (in particular Garhwal and Kumaun regions) by petrographic and geochemical (major, trace and rare earth element) studies.
- To track the provenance of Lesser Himalayan clastic sediments using Sr-Nd isotopic proxy.
- To obtain the relative ages for these unfossiliferous siliciclastics using U-Pb zircon geochronology.

1.4 Global and National significance of the research problem

Proterozoic span (2500-542Ma) constitutes nearly 43 percent of the earth history. Which, it has witnessed various major global events including extensive glaciations, progressive rifting, break-up and dispersals of the Archean supercontinents, formation of sediment dominated passive margin sequences, amalgamation of Earth's first supercontinent Nuna. Subsequently, during a Neoproterozoic time (1000-542Ma), the amalgamation of supercontinent Rodinia and global glaciations-Snowball earth and near the terminal Neoproterozoic, emergence of Ediacaran metazoans took place. The Proterozoic Lesser Himalayan sedimentary and associated volcanic packages offer an excellent area for the investigation of the northern margin of the Proto-Tethys prior to split of the Gondwanaland. This study in the Lesser Himalayan domain lies in its exceptionally long stratigraphic records, at least Paleoproterozoic to early Phanerozoic time span. The present understanding about crustal evolution comes chiefly from detrital modes, geochemical and isotopic data gathered on sedimentary rocks. The data set generated from these study will help in evolving a better chrono-constrained Proterozoic sedimentary basin evolution aspect of the Himalayan Orogen and their relationship with the adjoining contemporary sedimentary basin of the peninsular regions.

1.5 Importance of the study

Based on these studies Lesser Himalaya is divided into two zones which are the Inner Lesser Himalaya (ILH) and Outer Lesser Himalaya (OLH). Here question arises that out of these two zone which one is younger or whether they are of same age and if, then when they were deposited and from where they were sourced using petrography studies. The Proterozoic clastics of the Lesser Himalaya sedimentary packages are of two types (Ghosh et al., 2016b): i) Siliciclastic and Recrystallized Siliciclastic. The weathering history of the source area is determined by using parameter such as Chemical Index of Alteration (CIA- Nesbitt and Young, 1982), Plagioclase Index of Alteration (PIA- Nesbitt and Young, 1982, 1984; Fedo et al., 1995) and Chemical Index of Weathering (CIW- Harnois, 1988). The simplest and useful tool for determining the chemical weathering is A-CN-K (Al_2O_3-($CaO*+Na_2O$)-K_2O) plot. This diagram interprets the mobility of elements during chemical weathering of the source rock and also explains the chemical modifications in sediments after deposition (Nesbitt and Young, 1982, 1984). These studies are helpful to evaluate the provenance of the Lesser Himalaya. Studies of the $^{87}Sr/^{86}Sr$ in the Lesser Himalaya clastics shows that the ILH is more radiogenic than OLH, as the former contain high radiogenic $^{87}Sr/^{86}Sr$ ratio. Also ILH has more negative εNd values. This suggests that Bundelkhand craton and Aravalli craton could be the potential source of sediments to these clastics. Along with the geochemical and isotopic studies the U-Pb dating of the detrital zircon has been carried out. In this study an attempt were made to determine the geochronological age of the global and national relevance of the research problem.

1.6 Framework of the Thesis

It consists of seven chapters as -.

Chapter 1 provides a brief introduction of the problem in the study area, review of work done, objectives and importance of the thesis in a larger prospective.

Chapter 2 contains the overall description of the stratigraphy and lithology of the Lesser Himalayan successions. Detailed descriptions of the Lesser Himalayan Formations were discussed.

Chapter 3describes the various methods and experimental procedure adopted in order to achieve the objectives of the thesis.

Chapter 4 petrographic and SEM studies of the clastic sediments are given in this chapter. To determine the composition and textures of the samples thin section rock slides were studied under polarising microscope. Scanning Electron Microscope (SEM) was used for studying the surface features present in rocks coupled with the elemental composition of the surface/subsurface of the sample when combined with EDX (Energy Dispersive X-Ray Analysis).

Chapter 5 geochemical and Sr-Nd isotopic studies for provenance of the Proterozoic Lesser Himalayan clastics and chemical relations of the major oxides and trace elements are provided. Also, the attempts were made to quantify the weathering and mineral alteration of the source area.

Chapter 6 provides the geochronological ages of the Proterozoic Lesser Himalayan clastic sediments. In this chapter emphasis has been given on the extraction of the zircon grains and their analysis in the LA-MC-ICP-MS followed by CL images in SEM.

Chapter 7 consists of conclusions of the present studies with suggestions for future direction of research work.
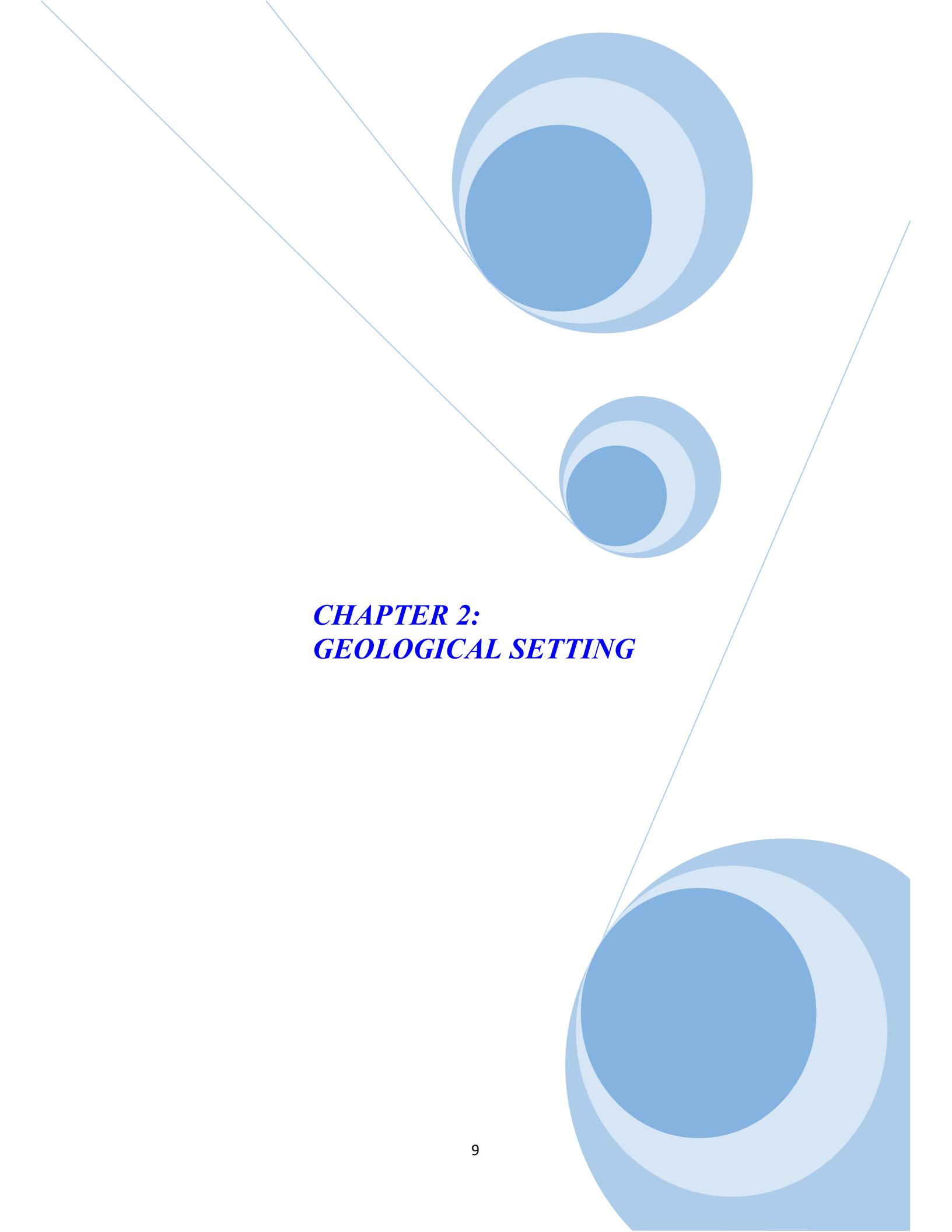
CHAPTER 2:
GEOLOGICAL SETTING

CHAPTER 2: GEOLOGICAL SETTING

2.1 Himalayan Orogen

The Himalaya is a young mountain chain situated between 75° and 95° east longitude, and 27° and 35° north latitude, originated as a result of collision between the Indian plate and the Eurasian plate. The Himalayan mountain range shows a perfect southwards-convex arcuate bulge (Heim and Gansser, 1939). It is bounded by the Nanga Parbat (8066.6m) syntaxis in the northwest and the Namcha Barwa (7710.6m) syntaxis in the northeast with an average length of ~2500 km. and width of ~250 km. The Himalayan orogen has suffered intense deformation and high-grade metamorphism (Yin, 2006). The Himalaya is divided into four major subdivisions from south to north are as the Sub/Outer Himalaya, Lesser Himalaya, Higher Himalaya and the Tethys Himalaya (Figure 1.1).

2.1.1 Sub-Himalaya/Outer Himalaya

The Sub-Himalaya is also known as the Siwaliks or Himalayan Foreland basin and lies north of the Indo-Gangetic alluvium plain. The boundary between the Outer Himalaya and the Indo-Gangetic alluvium plain is marked by Main Frontal Thrust (MFT). The Outer Himalayan hills are relatively low in height from 1000-1200m above mean sea level and lies in the generally 10-12 km wide region. This region is mainly consisting of sedimentary packages of Late Cretaceous and Tertiary period. Generally, this sequence represents detrital rocks of the nature of freshwater molasses, consisting of coarsely bedded sandstone, clays and conglomerates. In terms of sedimentary content, the Sub-Himalaya has the highest sedimentary content followed by the Tethys Himalaya and the Lesser Himalaya.

2.1.2 Lesser Himalaya

The Lesser Himalayan is about 13–16 km wide with an average altitude of 3000 m and has a moderate to high relief topography. This zone is

structurally separated by the Main Boundary Thrust (MBT) in the south and Main Central Thrust (MCT) in the north from Siwaliks and the Higher Himalaya, respectively. The significant lithological, stratigraphy and tectonic setting variations between the northern and southern parts of the Lesser Himalaya, traditionally divide it into two zones- Inner Lesser Himalaya (ILH) and Outer Lesser Himalaya (OLH) (Valdiya, 1980). The OLH and ILH are separated by Tons Thrust (Figure 2.1). OLH consist of Jaunsar Group (Chandpur and Nagthat formations) and Mussoorie Group (Blaini, Krol and Tal formations). Litho-stratigraphically, it comprises Mandhali at the base, succeeded by the Chandpur and Nagthat formations of the Jaunsar Group, forming the bulk of the tectonic unit and are capped by the Late Neoproterozoic Krol (mostly limestones) and Tal (mostly siliciclastics) formations. ILH consists of Damtha Group (Chakrata and Rautgara Formations) and Tejam Group (Deoban and Mandhali formation). The siliciclastics of the outer and inner zones of the Lesser Himalaya typically consist of the wackes and arenites. Schistose gneisses are most commonly occur at the base of thrust sheets such as, the Berinag, Ramgarh, and Almora Thrusts and are widely exposed across the Garhwal and Kumaun Himalaya in the Main Central Thrust footwall (Celerier et al., 2009).

2.1.3 Higher Himalaya

The Higher Himalaya, also refer as Central Crystallines, represents the area of highest topographic elevation above 61,00m and an average width of ~25km. These regions comprise of higher-grade Precambrian metamorphics, which constitute the basement on which the Proterozoic-Phanerozoic sediments of the Tethyan sub province deposited. Cambro-Ordovician and Miocene granites invade the Precambrian metamorphic rocks extensively. The STD marks the northern limit and MCT marks the southern limits of the Higher Himalaya.

2.1.4 Tethys Himalaya

The Tethys Himalaya extending north of the Higher Himalaya and comprises predominantly fossiliferous sedimentary rocks ranging from Late

Proterozoic to Cretaceous or even Eocene. These are bounded between the Indus-Tsangpo Suture Zone (ITZS) in the north and Tethyan Fault in the south. These argillite dominated packages are mainly observed in Tethys Himalayan basin (1,20,000 sq.km), consistsing of nearly 5-16 km thick, reasonably continuous and undeformed sedimentary successions (Valdiya, 1995).

2.2 Domain of the present study --Lesser Himalaya

The Lesser Himalayan (LH) basin is unique from other contemporary basins of the Indian sub-continent as former being suffered by the Tertiary Himalayan orogeny.These clastic sediments are unfossiliferous and thus most of the stratigraphic divisions are placed on the basis of the lithological and petrographic studies. Further, the sediments of the LH are characterized by the higher degree of diagenesis and low-grade metamorphism. The Proterozoic Lesser Himalayan basin is exclusive due to its long stratigraphy at least from Palaeoproterozoic to early Phanerozoic, also it has a sedimentary record more than a period of nearly 1000 Ma Late Neoproterozoic (between 650–542 Ma) part of the LH is mainly constrained and understood in terms of litho- and bio-stratigraphy, sedimentology, structure, tectonics and isotopic constrains. However, Late Palaeoproterozoic-Neoproterozoic (~1800-650 Ma) parts of the LH is least attended because of the geological problems such as metamorphism and unfossiliferous. Ghosh et al (2016b) identified four sedimentary successions in the central part of the LH orogen are described as -

1. *Palaeoproterozoic Argillite = Siliciclastic packages*
2. *Mesoproterozoic Calcareous(limestone) > Argillite packages*
3. *Neoproterozoic Siliciclastic = Argillite*
4. *Late Neoproterozoic- Early Palaeozoic Mixed Siliciclastic - Argillite – Calcareous (limestone).*
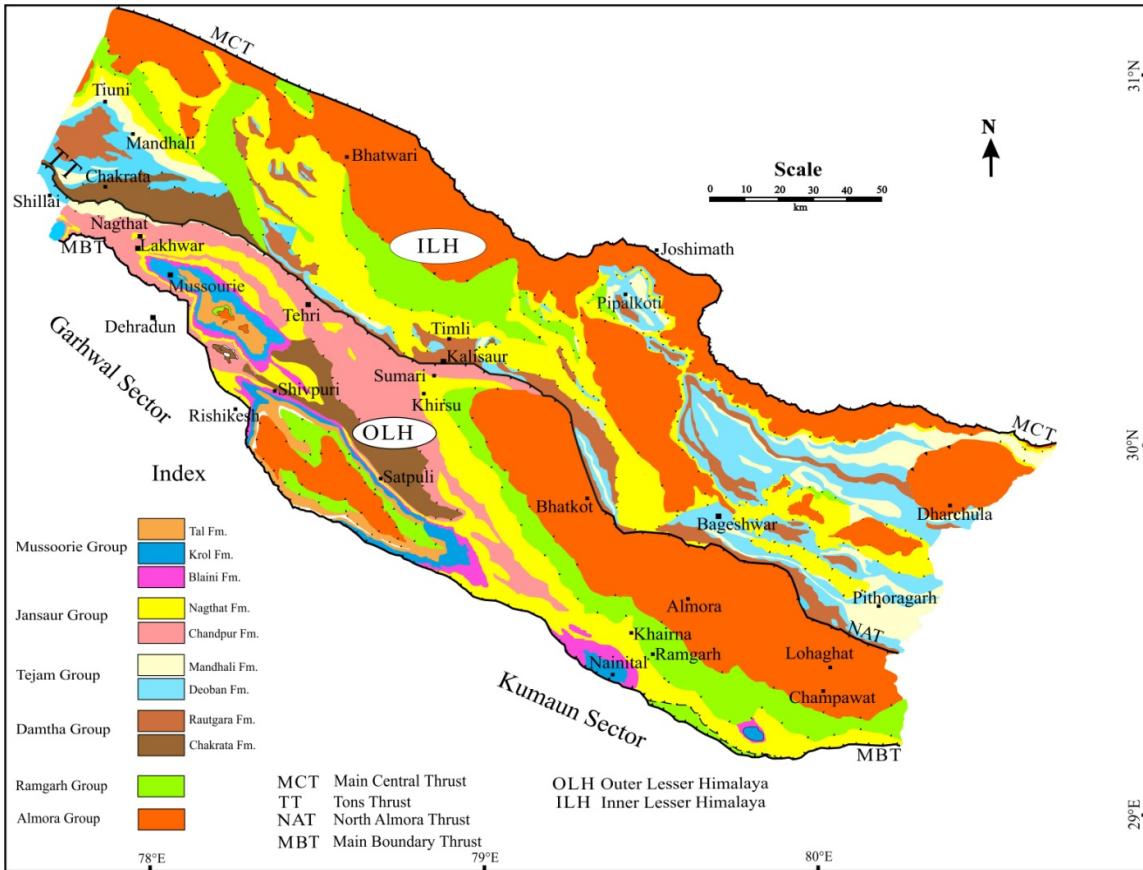
Figure 2.1 Geological map of the Lesser Himalaya (after Valdiya, 1980) showing the division of the Lesser Himalayan zones of the Kumaun and Garhwal region.

2.2.1 Palaeoproterozoic Lesser Himalayan packages

The characteristic features of the Palaeoproterozoic package of the LH are the occurrences of the thick sequence of argillite, siliciclastic and metavolcanics followed by carbonate dominated shallow marine shelf succession in the top part (Figure 2.2). This package represents one of the oldest known sedimentary sequences and is exposed from Himachal in the west to Arunachal Pradesh in the east through Uttarakhand Himalayan orogen, commonly referred as - Sundarnagar /Kistawar /Rampur, Damtha, Nawakot/Kuncha, Phuntsholing and Bichom Group in Himachal, Garhwal-Kumaun, Nepal, Bhutan and Arunachal Pradesh, respectively (Valdiya, 1995).
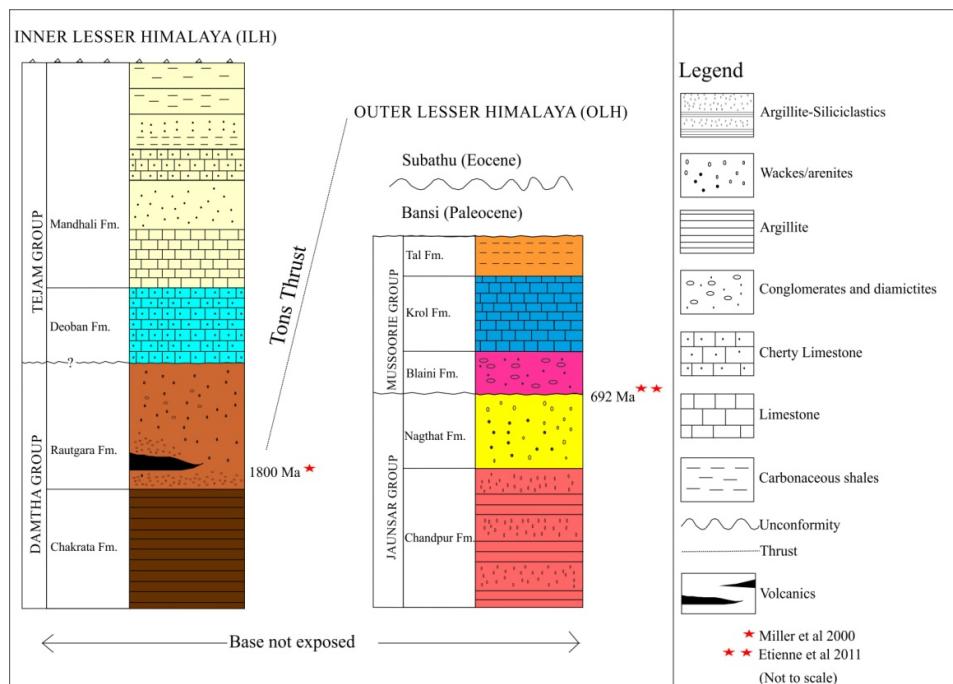
Figure 2.2 Lithostratigraphic division of the Lesser Himalaya (modified after Azmi and Paul, 2004; Kohn et al., 2010).

The sedimentological attributes are best described only from the well-exposed sections of Garhwal and Kumaun sectors of Uttarakhand. In the Garhwal-Kumaun Lesser Himalaya, the Paleoproterozoic package of the LH is represented by the Damtha Group. Stratigraphically, Damtha Group occurs at the base of the LH Formation. It is further subdivided into the Lower Chakrata

Formation and the Upper Rautgara Formation. The Damtha Group represents shallow marine argillo-arenaceous deposits with characteristic differences in the lateral and vertical facies (Rupke, 1974; Valdiya, 1970, 1980, 1995, Ghosh et al., 2011, 2012, 2016b). The Damtha Group shows the occurrences of soft sediment deformation (SSD) structures which are formed as a result of liquefication due to which the unconsolidated sediments are deformed prior or soon after the burial of sediments. The primary depositional structures such as parallel and wavy laminations small to medium-scale cross stratification, flaser bedding, ripple marks, flute casts, tool and scour marks (Ghosh et al., 2011, 2012). The SSD structures are well recorded from the sandstone-shale rhythmite facies in the Chakrata Formation. The Chakrata Formation consisting of argillite> siliciclastic assemblage and followed by the Rautgara Formation. The SSD structures observed in the Chakrata Formation resemble seismites, and are older than 1.8 Ga are recorded as the oldest seismites on the earth (Ghosh et al., 2011, 2012). Rautgara Formation is characterized by the presence of quartz-arenites/sub-litharenite with penecontemporaneous mafic volcanic (1.8Ga) and tuffs. The mafic volcanics and intrusive in the Rautgara formations have suffered surprisingly slight metamorphism. The oldest mafic rocks (sub-alkaline basalt through andesite to andesitic basalt) of the Himalaya are associated with Damtha Group. The age of these mafic rocks are constrained as Palaeoproterozoic (1.8 Ga; Miller et al., 2000) in terms of regional correlation. These rocks are correlated with the rocks of Aravalli and Bundelkhand regions of the Indian shield as they show similarities (Islam et al., 2002). The Damtha-Tejam succession of the LH is comparable with the Tethyan Himalaya, Martoli flysch-Ralam quartz-arenites-Garbyang carbonates sequence (Valdiya, 1995). The Rampur/Sundernagar packages are similar to that of with the Damtha Group package except it lacks the argillite facies in basal part. On the basis of the lithostratigraphic characteristics, Saha (2013) suggested that the Daling-Buxa group is comparable to the Bomdila group (Arunachal Pradesh).

2.2.2 Mesoproterozoic Lesser Himalayan packages

The Mesoproterozoic Lesser Himalaya is characterized by non- clastic Calcareous> Argillite packages. The sedimentary package of Mesoproterozoic succession are marked by stromatolites (Valdiya, 1969) and consisting of the Calc Zone in Kumaun, the Jaunsar-Deoban in Garhwal, the Sirban in Jammu, and the Shali-Simla in Himachal. In this package, the sedimentation is marked by desiccation and formation of salt with abundant growth of stromatolites and algal assemblage under very shallow marine stable tidal-flat conditions (Virdi, 1995). The comparative packages of dolomitic limestone is associated with syn-sedimentary pebbly conglomerate are known as- Great limestone (Jammu region), Aut and Shali limestone (Himachal Pradesh), Deoban (Uttarakhand), Dhading (Nepal), Buxa (Bhutan), and Dedza (Arunachal Pradesh). The Deoban sequence rests disconformably over the Dharagad Groupand is characterized by red siliciclastic and limestone in the basal part, followed by an argillite sequence and grey carbonates in middle and upper parts, respectively (Bhargava, 1976). Different types of stromatolites also occur in this package of the LH. The lentiform deposits of magnesite are noticed in the carbonate succession, and are found associated with the disseminated clusters of lead sulfide mineralization dated as 1000Ma (Raha et al., 1978). The ca. 1800-Ma quartzite is overlain above a regional unconformity by argillite-Siliciclastics of the Damtha Group that are succeeded by Deoban dolomites and Mandhali carbonaceous slates and carbonates. Tejam Group includes the Deoban-Mandhali succession and assigned to the period of Late Neoproterozoic. The Mandhali sediments were deposited in a poorly ventilated anoxic environment, although there are differences in opinion about the age of this group. The Gangolihat Dolomite (Proterozoic) of Kumaun Lesser Himalaya signifies the presence of small ancestral sponges during Neoproterozoic. Fossils of entire sponges are still not known from the Neoproterozoic era. Likewise, in the northeastern Lesser Himalaya, there is reported positive C-isotope ratios (δ^{13}C=+3.7 to +5.4‰ PDB) and remarkable consistency in the δ^{18}O fluctuation within a narrow range (between –8.9 and –7.2‰ PDB; Tewari and Sial, 2007) from the Buxa Dolomite (Neoproterozoic).

2.2.3 Neoproterozoic Lesser Himalayan packages

The Mesoproterozoic package of the LH is followed by the Neoproterozoic package. The Neoproterozoic Jaunsar Group consists of a siliciclastics and is unconformably covered by 692 Ma Blaini Formation (Etienne et al, 2011). From this package of the LH, both the sedimentological and stratigraphic data are available. The Jaunsar Group consisting of Chandpur (argillite dominated) and Nagthat Formations (siliciclastics) from base to top. The Jaunsar Group consisting of Chandpur and Nagthat formations from base to top and constitutes an integral part of the Krol belt succession. The Chandpur Formation deposited in muddy shelf conditions and comprises of argillite dominated succession. However its equivalent Pauri Phyllite is characterized by grey thinly bedded and foliated argillite. Pauri Phyllite is well developed in Alaknanda valley of the Garhwal Himalaya. This type of near homogenous argillite sediments (transitional shale–phyllite) are not observed in the LH, however, Simla slate around Solan region of Himachal is closely related to this. Above Chandpur there occurs a purple, green, and grey colored fine-to coarse-grained sandstones, Nagthat Formation representing the uppermost lithostratigraphic unit of the Neoproterozoic Jaunsar Group and are associated with the penecontemporaneous mafic lava flows (?). The thickness of Nagthat Formation varies from 400 to 1000 m from south to north, respectively. The Nagthat Formation is characterized by an open asymmetrical and symmetrical folds are forms part of syncline (Nagtibba-Pauri syncline) together with Chandpur Formation (Valdiya, 1980). Ghosh et al (1991) identified three major lithofacies in the Nagthat Formation. These lithofacies are coarse grained siliciclastic facies (CGS), interbedded medium to fine grained siliciclastic facies (IMFS), and (c) fine grained siliciclastic facies (FGS). Overall coarsening upward stratigraphic sequence of the Jaunsar suggests the gradual shallowing of the basin and thus indicates prograding behaviour of the Jaunsar litho-succession.

2.2.4 Late Neoproterozoic- Early Palaeozoic Lesser Himalayan Packages

Late Neoproterozic- Early Palaeozoic is characterized by a sequence of coarse clastic and carbonates lies over the Jaunsar Group and is referred as Krol belt. This package comprises of Blaini, Infra -Krol and Krol and Tal formations from base to top. The Blaini Formation consisting of 8-10 km thick succession of Neoproterozoic to Lower Palaeozoic sediments lies over Jaunsar Group. It is characterized by diamictite-shale- diamictite succession followed by a pink microcrystalline dolomite, which forms the base of the Infra-Krol Formation. A glaciogenic origin for Blaini diamictite has long been recognized and further supported by relatively abundant striated clasts and local preservation of polished and striated pavement on the underlying Simla Group clastics. New ^{207}Pb/^{206}Pb detrital zircon ages of the diamictite of the Blaini Formation provide a depositional age limit of 692±18 Ma (Etienne et al, 2011). The palaeocurrent indicators of the underlying Jaunsar Groups indicates there is a possibility that the basin margin oriented roughly east-west, consistent with detrital sources in the Blaini Formation from the Aravalli belt to the south. The Blaini diamictites followed by Infra Krol argillite. The Infra Krol comprises of shale-dominated unit and are confined mostly to the area near Solan. The Infra Krol argillite is followed by the carbonate and siliciclastic of Krol and Tal units. The regional stratigraphic terminology proposed by Auden (1934) in ascending order as- the Infra Krol, Krol sandstone, Lower Krol (Krol A), Middle Krol (Krol B), and Upper Krol (Krol C, D, and E). The Krol sandstone is mainly consisting of coarse- to fine-grained quartz sandstone. The Krol A and B having argillaceous limestone interbedded with greenish-grey calcareous shale, greyish-red shale and siltstone with thin, lenticular beds of dolomite. The Krol C consisting of bluish-grey crystalline limestone and dolomitic limestone. The Krol D showing an assemblage of dolomitic limestone, microbial cherty dolomite, calcareous shale, siltstone, and minor sandstone. The Krol E consists of limestone interbedded with calcareous shale, siltstone, argillaceous limestone, and dolomite. The Krol belt has numerous stratigraphic profiles which are studied in details. Between Solan (NW) and Nainital (SE) in the Lesser

Himalaya nearly 12 km thick Neoproterozoic and Lower Cambrian Infra Krol-Krol succession are exposed. The Infra- Krol and lower and upper parts of the Krol shows upward transitions from shale and mixed shale-limestone to more massive carbonate rocks together with microbial dolomite collectively indicates shoaling-upward trends. Azmi et al., 1981 proposed a Cambro-Ordovician age to the Lower Tal Formation on the basis of the presence of small shelly fauna (SSF) in the phosphorites deposits. Afterward, Bhatt et al (1983) and Brasier and Singh (1987) revised and assigned Tommotian (Early Cambrian) age for the Tal Formation. And thus with all this, the Krol-Tal succession has been assigned a Neoproterozoic-Early Cambrian age.

2.2.5 Relationship of the Outer and Inner Lesser Himalayan succession

Despite contesting views, the LH, by and large, is believed to be consisting of two zones- Inner Lesser Himalaya (ILH) and Outer Lesser Himalaya (OLH) on the basis of different lithology and ages (Singh et al., 1999; Valdiya, 1980; Ghosh et al., 2016 a and b).Virdi (1995) proposed a number of criteria for differentiating between these two successions on the basis of geological features. ILH sediments are characterized by a higher degree of diagenesis and low-grade metamorphism and are associated with crystalline metamorphic bodies. These successions are isolated due to erosion and show greenschist to upper amphibolite grade of metamorphism. The siliciclastic succession of ILH (Berinag – Rampur – Rudraprayag) is associated with syn-sedimentary basic magmatism, seismites (Ghosh et al., 2012) acid tuff, intrusive granites and uranium mineralization, which in the OLH is relatively rare. The two sedimentary- cycles, namely the Paleoproterozoic Sundernagar - Rampur - Berinag - Damtha (SRBD; siliciclastic>argillite) and Mesoproterozoic Shali –Tejam (calcareous >argillite) are recorded in the ILH. The distal end of SRBD, towards further north consisting of more argillaceous facies and represent as Chail-Ramgarh metamorphics associated with 1.8Ga and 1.2Ga granitoids (Virdi, 1988). Rupke (1974) and Valdiya (1980) equated this SRBD package of the ILH with that of the Simla –Jaunsar (SJ) package of the OLH, which is still debatable. Further, Azmi and Paul (2004) reported bio-stratigraphically the

protoconodont assemblages from the Gangolihat Dolomite of the ILH, and proposed revised stratigraphic setting, correlated the Jaunsar Group of the OLH with that of the Damtha Group of the ILH of the Kumaun and Garhwal Lesser Himalaya, and thus shown single siliciclastic, carbonate horizons, and placed in Palaeoproterozoic Eon. However, Gangolihat Dolomite has been assigned Neoproterozoic age on the basis of well-preserved microbial assemblage (Tiwari and Pant, 2009). The Palaeoproterozoic Damtha Group and Neoproterozoic Jaunsar Group preserve a thick pile of coarsening upward argillite/ (muddy) and siliciclastic (sandy) succession. In both zones of the LH, the lower part of the succession is characterized by transgressive argillite dominated packages (Chakrata and Chandpur formations). These successions further pass upward into the regressive facies of the Rautgara and Nagthat formations, which comprise sand bodies (Ghosh 1991; Ghosh et al., 2010, 2011). In the Tons valley, the Tejam Group consists of Deoban Formation and is coeval to Gangolihat Dolomite of Kumaun (Ghosh et al, 2016b). On the basis of "Riphean" stromatolite bio-stratigraphy, the Deoban Formation of ILH has been assigned as Mesoproterozoic (Bhattacharya, 1983; Rupke, 1974; Valdiya, 1969, 1980). Miller et al., (2000) further constrained the age of underlying Damtha (Garhwal-Kumaun) and Rampur Group (Sutlej valley, Himachal Pradesh) by interbedded ca. 1.8 Ga metabasalt flows. Age constraints of the OLH (Jaunsar Group) successions are established on the basis of the presence of the Marinoan-aged (ca. 635 Ma) diamictite and cap-carbonate of the Baliana Group (Jiang et al., 2002, 2003a,b) and are considered to be early Neoproterozoic in age.New $^{207}Pb/^{206}Pb$ detrital zircon ages of the diamictite of the Blaini Formation provide a depositional age limit of 692±18 Ma (Etienne et al, 2011)

Ghosh et al (2016a), proposed a demarcating plane (Figure 2.3) between the younger (Neoproterozoic-Cambrian age; 800-500 Ma) OLH and older (Palaeoproterozoic-Mesoproterozoic;1900-1600 Ma) ILH. In the present study, the samples are collected from the LH formations on the basis of the map as shown in Figure 2.3.
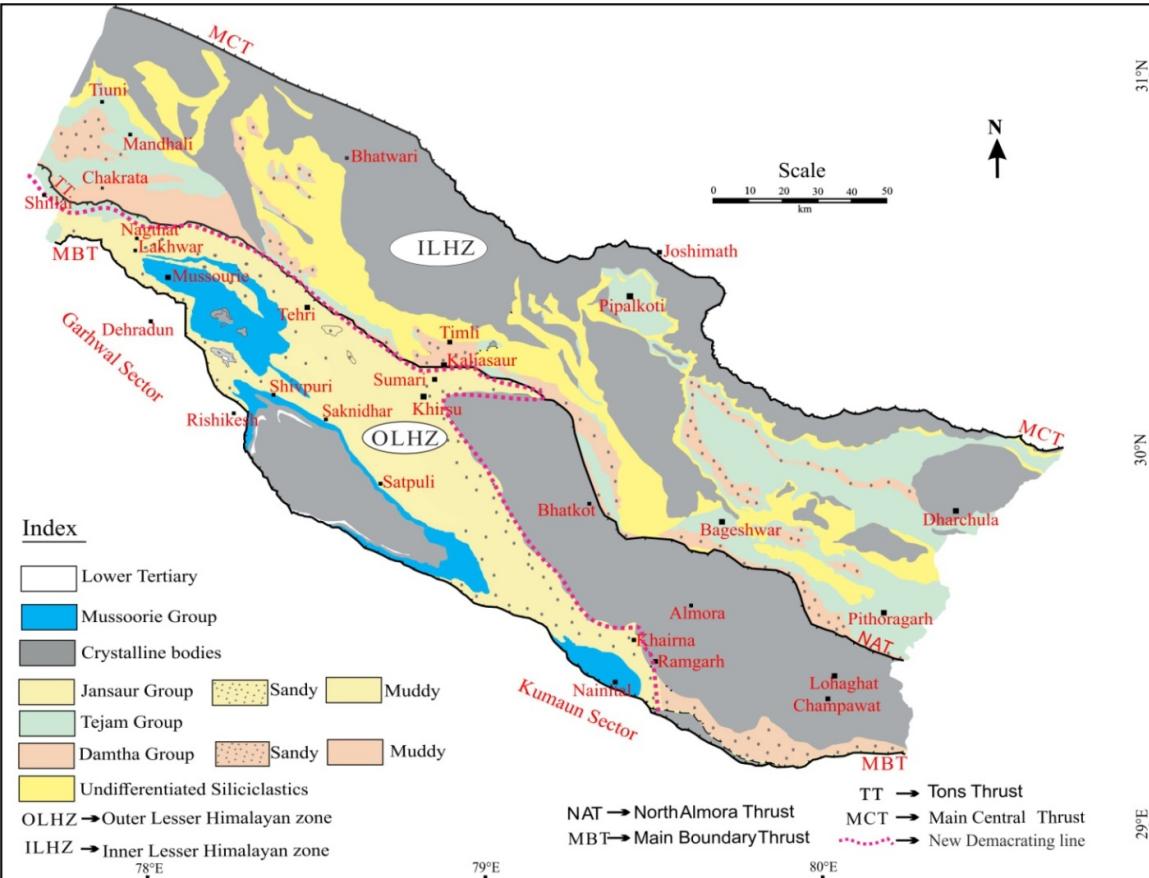
Figure 2.3 Geological map of the Lesser Himalaya (after Valdiya 1980) with Tons Thrust between the Outer Lesser Himalaya (OLH) and Inner Lesser Himalaya (ILH) (Ghosh et al., 2016a).
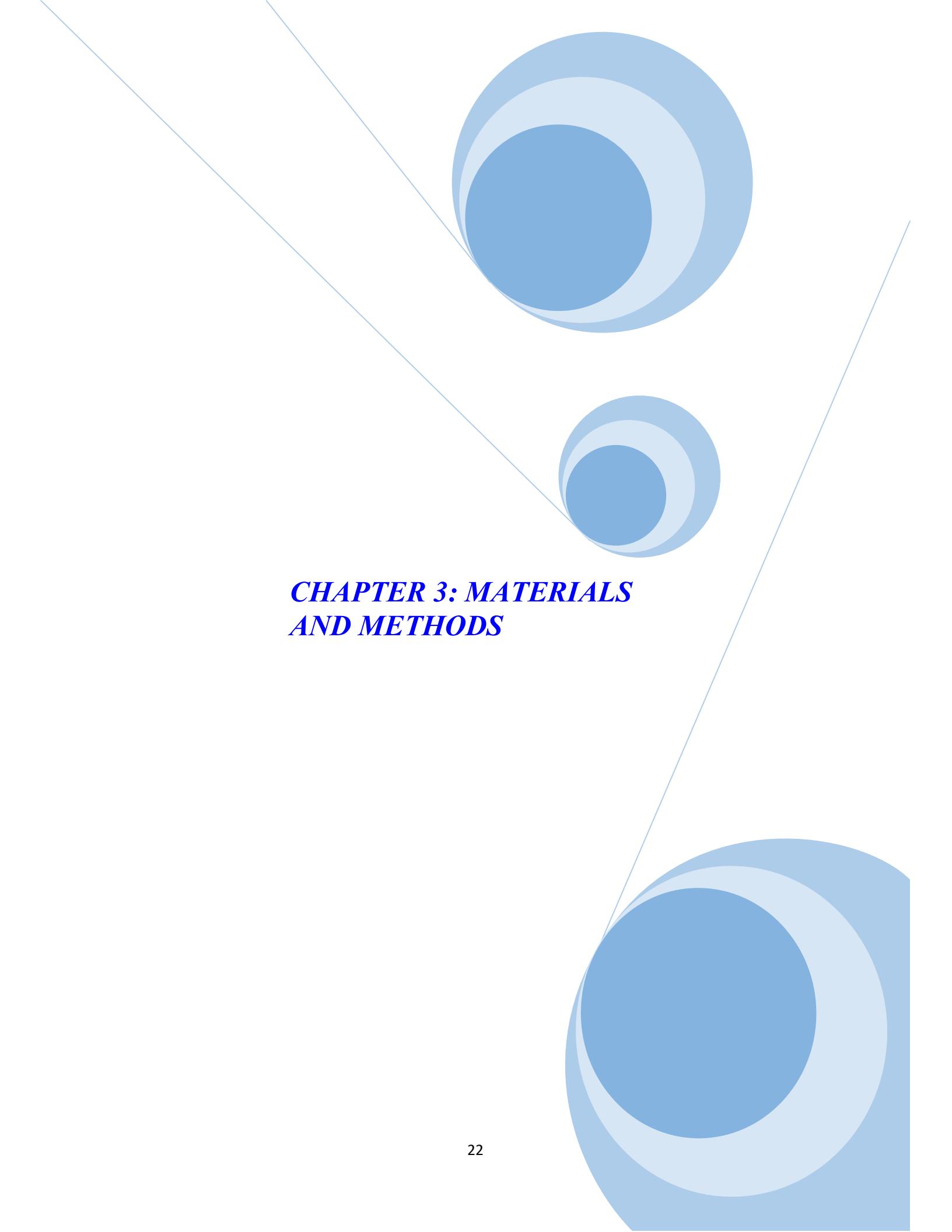
CHAPTER 3: MATERIALS AND METHODS

CHAPTER 3: MATERIALS AND METHODS

Suitable sampling and field observations with proper scientific protocols for analyses are the primary requirements for any study. Towards this, the present study has also followed these steps which are incorporated in terms of the determination of provenance and radiometric age constraints for the Proterozoic LH clastics (argillite and siliciclastic) using petrographic, geochemical and geochronological approaches. Among these, petrography is used as a fundamental tool for understanding the textural and compositional properties of the rocks through their thin sections. Such information is found to be useful in the reconstruction of source lithology, diagenetic and depositional attributes which also indicates the provenance identifications. However, in many cases like metamorphism, diagenetic alterations and weathering where the rocks lost their original texture, structures and the composition, the petrographic parameters do not work effectively. Therefore, in these cases, geochemical, isotopic and geochronological studies are helpful for the determination of the provenance, lithology, and intensity of weathering experiences by the source areas and dating of the sediments. As the LH region has undergone several changes since their depositions, a suit of analytical tools are used to extract meaningful information from the analyses of the representative samples which are discussed as follows.

3.1 Field work

Representative samples (nos 113) were collected from the northern (Chakrata and Rautgara formations) and southern (Chandpur and Nagthat formations) parts of the Garhwal LH (Figure 3.1). Some samples were also collected from the Rautgara and Nagthat Formations of the Kumaun LH. The geographical coordinates of the location of the sample are given in Table 3.1. The Proterozoic clastic sediments recognized from the LH are mainly siliciclastic and argillite type. The siliciclastic of the LH are composed of arenites (sub-lithic, lithic and quartz arenites) and wackes (quartz wacke and lithic greywacke), and argillites are mainly greenish- grey silty detritus.

Figure 3.1 Representative field photographs (with sample site) of Lesser Himalayan clastics; a and b are ILH clastics; c, d, e and f shows OLH clastics.

3.2 Methodology

Measurement of different parameters requires their associated ways of analyses to derive useful information from the samples towards their meaningful interpretation. These can be classified into three basic parts. 1) Field observation in the field, 2) petrographical observation of sample under the thin section and 3) chemical composition of the sample. Out of these, petrography is of vital importance towards the selection of samples for further geochemical analysis. In order to get a comprehensive data set, a variety of analyses was conducted and is presented in scheme format as given as-

SCHEMES OF ANALYSIS

```
                              ┌──────────┐
                              │ CLASTICS │
                              └────┬─────┘
              ┌────────────────────┴────────────────────┐
              ▼                                          ▼
   ┌──────────────────────┐               ┌──────────────────────┐
   │ Physical characteristic│             │ Chemical characteristic│
   └──────────┬───────────┘               └───────────┬──────────┘
```

Physical characteristic

- Petrography → Texture
- Scanning Electron Microscope (SEM) → Surface features

Chemical characteristic

- X-Ray Fluorescence (XRF) → Major and trace element → Weathering intensity and protolith characterization
- Inductively Coupled Plasma Mass Spectrometry (ICP-MS) → Rare earth element (REEs) → Source rock identification
- Multi-collector Inductively Coupled Plasma Mass Spectrometry (MC-ICPMS) → Isotopic ($^{87}Sr/^{86}Sr$, εNd) → Provenance identification
- LA-Multi-collector Inductively Coupled Plasma Mass Spectrometry (LA-MC-ICP-MS) → U-Pb detrital zircon geochronology → Age constraint

25

Table 3.1: Location of clastic samples from the outer and inner Lesser Himalaya (Garhwal-Kumaun) with coordinates.

S.No	Sample	Formation	Locality	Rock type	OLH/ILH	Latitude (N)	Longitude (E)
1	MN3R	Nagthat	Khairwa Village	SLC	OLH	30° 33' 38.28"	78° 48' 48.75"
2	MN3S	Nagthat	Khairwa Village	SLC	OLH	30° 33' 38.28"	78° 48' 48.75"
3	MN3T	Nagthat	Khairwa Village	SLC	OLH	30° 33' 38.28"	78° 48' 48.75"
4	MN3U	Nagthat	Khairwa Village	SLC	OLH	30° 33' 38.28"	78° 48' 48.75"
5	MN3Z	Nagthat	Around Sahastradhara Area	SLC	OLH	30° 23' 5.66"	78° 7' 28.35"
6	MN4A	Nagthat	Around Sahastradhara Area	SLC	OLH	30° 23' 5.66"	78° 7' 28.35"
7	MN4B	Nagthat	Around Sahastradhara Area	SLC	OLH	30° 23' 5.66"	78° 7' 28.35"
8	MN4C	Nagthat	Around Sahastradhara Area	SLC	OLH	30° 23' 5.66"	78° 7' 28.35"
9	MN4D	Nagthat	Around Sahastradhara Area	SLC	OLH	30° 23' 5.66"	78° 7' 28.35"
10	MN4F	Nagthat	Around Sahastradhara Area	SLC	OLH	30° 23' 5.66"	78° 7' 28.35"
11	MN4G	Nagthat	Around Sahastradhara Area	SLC	OLH	30° 23' 5.66"	78° 7' 28.35"
12	MN4H	Nagthat	Around Sahastradhara Area	SLC	OLH	30° 23' 5.66"	78° 7' 28.35"
13	MN4I	Nagthat	Around Sahastradhara Area	SLC	OLH	30° 23' 5.66"	78° 7' 28.35"
14	MN4J	Nagthat	Around Sahastradhara Area	SLC	OLH	30° 23' 5.66"	78° 7' 28.35"
15	MN4K	Nagthat	Around Sahastradhara Area	SLC	OLH	30° 23' 5.66"	78° 7' 28.35"
16	MN4L	Nagthat	Around Sahastradhara Area	SLC	OLH	30° 23' 5.66"	78° 7' 28.35"
17	MN5E	Nagthat	Aglar river	SLC	OLH	30° 31' 28.92"	77° 54' 21.81"
18	MN5F	Nagthat	Aglar river	ARG	OLH	30° 31' 28.92"	77° 54' 21.81"
19	MN5G	Nagthat	Aglar river	SLC	OLH	30° 30' 51.55"	77° 59' 57.26'
20	MN5H	Nagthat	Aglar river	SLC	OLH	30° 30' 51.55"	77° 59' 57.26"
21	MN5I	Nagthat	Aglar river	SLC	OLH	30° 30' 51.62"	77° 59' 57.3"
22	MN5J	Nagthat	Aglar river	SLC	OLH	30° 30' 51.62"	77° 59' 57.3"
23	MN5K	Nagthat	Maldeota section	SLC	OLH	30° 20' 40.56"	78° 7' 39.25"
24	MN5L	Nagthat	Maldeota section	SLC	OLH	30° 20' 40.56"	78° 7' 39.25"
25	MN5M	Nagthat	Maldeota section	SLC	OLH	30° 20' 38.47"	78° 7' 38.35"
26	MN5N	Nagthat	Maldeota section	SLC	OLH	30° 20' 41.39"	78° 7' 43.07"
27	MN5NB	Nagthat	Maldeota section	SLC	OLH	30° 20' 41.39"	78° 7' 43.07"
28	MN5P	Nagthat	Tons valley	SLC	OLH	30° 32' 44.59"	77° 49' 14.05"
29	MN5Q	Nagthat	Tons valley	SLC	OLH	30° 33' 23.00"	77° 49' 17.68"
30	MN5R	Nagthat	Tons valley	SLC	OLH	30° 34' 33.99"	77° 45' 48.45"

Continued-

S.No	Sample	Formation	Locality	Rock type	OLH/ILH	Latitude (N)	Longitude (E)
31	MN5S	Nagthat	Tons valley	SLC	OLH	30° 34' 33.99"	77° 45' 48.45"
32	MN5T	Nagthat	Tons valley	SLC	OLH	30° 35' 43.65"	77° 44' 44.44"
33	MN5V	Nagthat	Saknidhar	SLC	OLH	30° 3' 38.7"	78° 30' 39.81"
34	MN5W	Nagthat	Saknidhar	SLC	OLH	30° 3' 38.7"	78° 30' 39.81"
35	MN5X	Nagthat	Saknidhar	SLC	OLH	30° 4' 52.10"	78° 33' 17.13"
36	MN5Y	Nagthat	Sahastradhara	SLC	OLH	30° 23' 0.78"	78° 7' 14.80"
37	MN5Z	Nagthat	Saknidhar	SLC	OLH	30°04' 56.75"	78°32' 48.91"
38	MN6A	Nagthat	Saknidhar	SLC	OLH	30°04' 56.75"	78°32' 48.91"
39	MN1S	Chandpur	Shivpuri -Timli Road	ARG	OLH	30° 08' 31.11"	78° 23' 47.34"
40	MN1T	Chandpur	Shivpuri -Timli Road	ARG	OLH	30° 08' 31.11"	78° 23' 47.34"
41	MN1U	Chandpur	Shivpuri -Timli Road	SLC	OLH	30° 08' 31.11"	78° 23' 47.34"
42	MN1V	Chandpur	Shivpuri -Timli Road	SLC	OLH	30° 08' 31.11"	78° 23' 47.34"
43	MN1W	Chandpur	Shivpuri -Timli Road	SLC	OLH	30° 08' 31.11"	78° 23' 47.34"
44	MN1X	Chandpur	Shivpuri -Timli Road	SLC	OLH	30° 08' 31.11"	78° 23' 47.34"
45	MN1Y	Chandpur	Shivpuri -Timli Road	ARG	OLH	30° 08' 31.11"	78° 23' 47.34"
46	MN1Z	Chandpur	Shivpuri -Timli Road	SLC	OLH	30° 08' 31.11"	78° 23' 47.34"
47	MN2A	Chandpur	Shivpuri -Timli Road	SLC	OLH	30° 08' 31.11"	78° 23' 47.34"
48	MN2B	Chandpur	Shivpuri -Timli Road	ARG	OLH	30° 08' 31.11"	78° 23' 47.34"
49	MN2C	Chandpur	Shivpuri -Timli Road	SLC	OLH	30° 08' 31.11"	78° 23' 47.34"
50	MN2D	Chandpur	Shivpuri -Timli Road	ARG	OLH	30° 08' 31.11"	78° 23' 47.34"
51	MN2E	Chandpur	Shivpuri -Timli Road	ARG	OLH	30° 08' 31.11"	77° 23' 47.34"
52	MN3L	Chandpur	Dhamogh-Khairwa Road	ARG	OLH	30° 33' 38.28"	77° 48' 48.75"
53	MN3M	Chandpur	Dhamogh-Khairwa Road	ARG	OLH	30° 33' 38.28"	77° 48' 48.75"
54	MN3N	Chandpur	Dhamogh-Khairwa Road	ARG	OLH	30° 33' 38.28"	77° 48' 48.75"
55	MN3O	Chandpur	Dhamogh-Khairwa Road	ARG	OLH	30° 33' 38.28"	77° 48' 48.75"
56	MN3P	Chandpur	Dhamogh-Khairwa Road	ARG	OLH	30° 33' 38.28"	77° 48' 48.75"
57	MN3Q	Chandpur	Dhamogh-Khairwa Road	ARG	OLH	30° 33' 38.28"	77° 48' 48.75"
58	MN2G	Rautgara	8 km. NNW from Lamgaon	SLC	ILH	30° 31' 49.25"	78° 30' 21.97"
59	MN2H	Rautgara	9 km. NNW from Lamgaon	ARG	ILH	30° 31' 14.27"	78° 30' 2.14"
60	MN2I	Rautgara	9 km. North of Lamgaon	SLC	ILH	30° 31' 14.27"	78° 30' 2.14"

Continued-

S.No	Sample	Formation	Locality	Rock type	OLH/ILH	Latitude (N)	Longitude (E)
61	MN2J	Rautgara	3 km down from Pratapnagar	SLC	ILH	30° 30' 50.57"	78° 29' 41.3"
62	MN2K	Rautgara	Along Mandakini , 2km from Tilwara	SLC	ILH	30° 21' 35.38"	78° 58' 43.74"
63	MN2L	Rautgara	Along Mandakini , 2km from Tilwara	SLC	ILH	30° 21' 35.38"	78° 58' 43.74"
64	MN2M	Rautgara	Along Mandakini , 2km from Tilwara	SLC	ILH	30° 21' 35.38"	78° 58' 43.74"
65	MN2N	Rautgara	Along Mandakini , 2km from Tilwara	SLC	ILH	30° 21' 35.38"	78° 58' 43.74"
66	MN2R	Rautgara	Chopta, Garhwal	SLC	ILH	30° 21' 3.3"	79° 2' 41.58"
67	MN2Z	Rautgara	Srinagar Rudraprayag (Kaliasaur Road)	SLC	ILH	30° 15' 19.28"	78° 53' 10.43"
68	MN3A	Rautgara	Srinagar Rudraprayag (Kaliasaur Road)	SLC	ILH	30° 15' 19.28"	78° 53' 10.43"
69	MN3B	Rautgara	Srinagar Rudraprayag (Kaliasaur Road)	SLC	ILH	30° 15' 19.28"	78° 53' 10.43"
70	MN3C	Rautgara	Srinagar Rudraprayag (Kaliasaur Road)	SLC	ILH	30° 15' 19.28"	78° 53' 10.43"
71	MN3D	Rautgara	Srinagar Rudraprayag (Kaliasaur Road)	SLC	ILH	30° 15' 19.28"	78° 53' 10.43"
72	MN3E	Rautgara	Srinagar Rudraprayag (Kaliasaur Road)	SLC	ILH	30° 15' 19.28"	78° 53' 10.43"
73	MN3F	Rautgara	Srinagar Rudraprayag (Kaliasaur Road)	SLC	ILH	30° 15' 19.28"	78° 53' 10.43"
74	MN3G	Rautgara	Srinagar Rudraprayag (Kaliasaur Road)	SLC	ILH	30° 15' 19.28"	78° 53' 10.43"
75	MN3H	Rautgara	Srinagar Rudraprayag (Kaliasaur Road)	SLC	ILH	30° 15' 19.28"	78° 53' 10.43"
76	MN3I	Rautgara	Srinagar Rudraprayag (Kaliasaur Road)	SLC	ILH	30° 15' 19.28"	78° 53' 10.43"
77	MN3J	Rautgara	Srinagar Rudraprayag (Kaliasaur Road)	SLC	ILH	30° 15' 19.28"	78° 53' 10.43"
78	MN3K	Rautgara	Srinagar Rudraprayag (Kaliasaur Road)	SLC	ILH	30° 15' 19.28"	78° 53' 10.43"
79	MN6B	Rautgara	Srinagar Rudraprayag (Kaliasaur Road)	SLC	ILH	30° 15' 19.28"	78° 53' 10.43"
80	MN4O	Rautgara	Kaliasaur Road	SLC	ILH	30° 15' 19.28"	78° 53' 10.43"
81	MN4P	Rautgara	Kaliasaur Road	SLC	ILH	30° 15' 19.28"	78° 53' 10.43"
82	MN4Q	Rautgara	Kaliasaur Road	SLC	ILH	30° 15' 19.28"	78° 53' 10.43"
83	MN4R	Rautgara	Kaliasaur Road	SLC	ILH	30° 15' 19.28"	78° 53' 10.43"
84	MN4S	Rautgara	Kaliasaur Road	SLC	ILH	30° 15' 19.28"	78° 53' 10.43"
85	MN4T	Rautgara	Kaliasaur Road	SLC	ILH	30° 15' 19.28"	78° 53' 10.43"
86	MN4U	Rautgara	Kaliasaur Road	SLC	ILH	30° 15' 19.28"	78° 53' 10.43"
87	MN4V	Rautgara	Kaliasaur Road	SLC	ILH	30° 15' 19.28"	78° 53' 10.43"
88	MN4W	Rautgara	Kaliasaur Road	SLC	ILH	30° 15' 19.28"	78° 53' 10.43"
89	MN4X	Rautgara	Kaliasaur Road	SLC	ILH	30° 15' 19.28"	78° 53' 10.43"
90	MN4Y	Rautgara	2 km from Ghat, Gurna 14 km (Kumaun)	SLC	ILH	29° 29' 31.06"	80° 7' 32.62"

Continued-

S.No	Sample	Formation	Locality	Rock type	OLH/ILH	Latitude (N)	Longitude (E)
91	MN4Z	Rautgara	2 km from Ghat, Gurna 14 km (Kumaun)	SLC	ILH	29° 29' 31.06"	80° 7' 32.62"
92	MN5A	Rautgara	4 km from Ghat, Gurna 14 km (Kumaun)	SLC	ILH	29° 29' 45.74"	80° 7' 36.84"
93	MN5B	Rautgara	(Bhimtal -Kathgodam)Kumaun	SLC	ILH	29° 19' 04.1"	79° 33' 12.3"
94	MN5C	Rautgara	(Bhimtal -Kathgodam)Kumaun	SLC	ILH	29° 19' 04.1"	79° 33' 12.3"
95	MN5D	Rautgara	(Bhimtal-Kathgodam)Kumaun	SLC	ILH	29° 19' 04.1"	79° 33' 12.3"
96	MN1A	Chakrata	Rikhae Khand section road, 6.5 km from Damtha	LST	ILH	30° 38' 87.34"	78° 01' 14.62"
97	MN1B	Chakrata	Rikhae Khand section road, 6.5 km from Damtha	ARG	ILH	30° 38' 87.34"	78° 01' 14.62"
98	MN1C	Chakrata	Barkat-Damtha Road section Damtha	SLC	ILH	30° 38' 87.34"	78° 01' 14.62"
99	MN1D	Chakrata	Barkat-Damtha Road section Damtha	SLC	ILH	30° 38' 87.34"	78° 01' 14.62"
100	MN1E	Chakrata	Barkat-Damtha Road section Damtha	ARG	ILH	30° 38' 87.34"	78° 01' 14.62"
101	MN1F	Chakrata	1 km North of Damtha, Naingaon road	ARG	ILH	30° 36' 25.95"	78° 00' 59.34"
102	MN1G	Chakrata	2 km North of Damtha, Naingaon road	ARG	ILH	30° 36' 25.95"	78° 00' 59.34"
103	MN1H	Chakrata	3 km North of Damtha, Naingaon road	ARG	ILH	30° 36' 25.95"	78° 00' 59.34"
104	MN1I	Chakrata	8 km south of Noagaon	ARG	ILH	30° 47' 20.09"	78° 08' 26.66"
105	MN1J	Chakrata	9 km south of Noagaon	SLC	ILH	30° 47' 20.09"	78° 08' 26.66"
106	MN1K	Chakrata	Near Dakra village Chakrata-Lakhmandal road section	ARG	ILH	30° 43' 37.16"	78° 04' 45.35"
107	MN1L	Chakrata	Near Dakra village Chakrata-Lakhmandal road section	ARG	ILH	30° 43' 37.16"	78° 04' 45.35"
108	MN1M	Chakrata	Near Dakra village Chakrata-Lakhmandal road section	SLC	ILH	30° 43' 37.16"	78° 04' 45.35"
109	MN1N	Chakrata	Near Dakra village Chakrata-Lakhmandal road section	SLC	ILH	30° 43' 37.16"	78° 04' 45.35"
110	MN1O	Chakrata	Near Dakra village Chakrata-Lakhmandal road section	SLC	ILH	30° 43' 37.16"	78° 04' 45.35"
111	MN1P	Chakrata	Near Dakra village Chakrata-Lakhmandal road section	ARG	ILH	30° 43' 37.16"	78° 04' 45.35"
112	MN1Q	Chakrata	Near Dakra village Chakrata-Lakhmandal road section	ARG	ILH	30° 43' 37.16"	78° 04' 45.35"
113	MN1R	Chakrata	Kalsi-Sahiya road	ARG	ILH	30° 42' 01.23"	77° 52' 5.82"

3.2.1 Petrography

A total of ninty samples including both siliciclastics and argillites were studied for detailed petrographic properties using the polarising microscope. The slides (30µ thin sections of the rock samples) for the petrographic studies were prepared in a standard procedure at Wadia Institute of Himalayan Geology (WIHG). Each rock samples were sliced into a rectangular piece and polished successively with carborundum powder of 200 to 600 meshes. The polished pieces are then mounted on glass slides using resin Araldite. Rock slides were studied under a microscope to determine the textural and mineralogical composition of the samples.

3.2.2 Scanning Electron Microscope (SEM)

The samples were studied for their finer details and qualitative information using Scanning Electron Microscope (SEM) to see the surface features present in rocks (Figure 3.2). The qualitative elemental composition of the surface of the samples was obtained when SEM attributes were combined with the Energy Dispersive X-Ray Analysis (EDX).
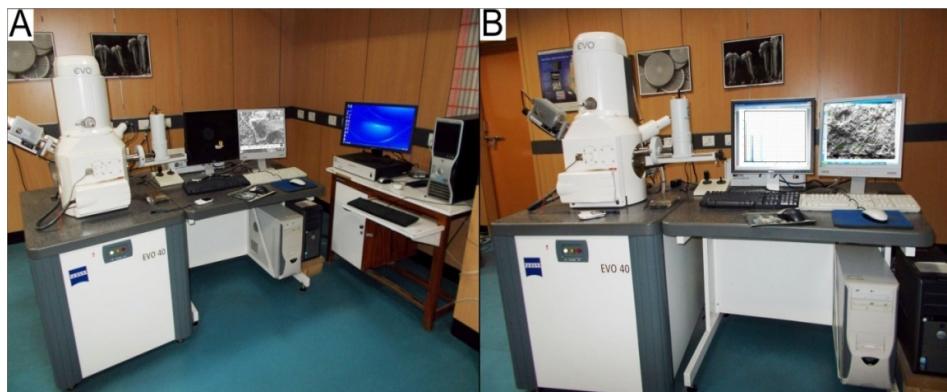
Figure- 3.2 Scanning Electron Microscope (SEM) instrument used for the analyses of the siliciclastics at WIHG.

Scanning Electron Microscope (SEM) is a scientific instrument that uses a beam of energetic electron to examine the objects (of the micro structural characteristic of solid object)on a very fine scale by scanning it with a high-energy beam of electrons. The most important features of a SEM are:

1. It is capable of providing the topographic features (surface features of an object or "how it looks", its texture) and thus helps in developing the direct relation between these features and material.
2. It provides the composition (the elements and compounds that the object is composed of and the relative amounts of them) and their relationship with the materials properties.

An Energy Dispersive X-ray detector System (EDX or EDS) is the widely used detector that can display all the elements present in the specimen (all object). The composition of the objects determined to an overall accuracy of about 1% and detection sensitivity down to 0.1% by weight. A semiconductor material is used to detect the x-rays together with processing electronics to analyze the spectrum.

Technical Specification of SEM and EDX

SEM	:	**ZEISS EVO 40 EP**
Resolution	:	3.0nm SE and HV
Magnification	:	7 to 10,00,000 X
Accelerating Voltage	:	0.2 to 30 KV
Sample Environment	:	High Vacuum
Detectors Available	:	No vacuum-up to 3000Pa
		SE in HV
		SE in VPSE mode
		BSD in all modes
Goniometer	:	5-axis motorized
		Tilt:- 1 to 90
		Z: 35mm
		Y: 80 mm
		X: 80 mm
		Rotation: nX360˚
Specimen Exchange Time	:	3 Minutes
Max. Specimen Size	:	200 X 200 X 100mm

Energy Dispersive	:	**Bruker LN2 free X-Flash**
X-ray Microanalyser		**4010 SDD Detector**
Resolution	:	129 eV at Mn kα (5.98KeV)
Analytical Software	:	QUANTAX 200 Full qualitative & quantitative Analysis Software with a point, Line and area Scanning and Elemental mapping

Prior to SEM studies, two small rock chips for each sample were rinsed with Hydrogen Peroxide (H_2O_2) for removing the organic material, if any. The rock chips were then washed with acetone and kept for air drying for a whole day. Thereafter, these two chips were coated with thin film of Gold foil (5nm thick) for SEM and carbon foil (5nm thick) for SEM-EDX analysis using Quorum (Q150RES). The coating on the surface of samples are used because of the following reasons

1. It makes them electrically conductive, necessary for the analysis.
2. It increased the mechanical stability of the sample due to increased heat conduction.
3. Increase in primary and secondary electron emission.
4. Decrease in beam penetration, resulting in better spatial resolution.

The SEM-EDX analyses were carried out with the help of a computer controlled field emission SEM (ZEISS EVO 40 EPA).

3.2.3 Major and Trace elements

Major and trace elements are useful in describing the nature of rock and its origin under given geological condition and therefore their precise measurement is crucial for interpretation. For this study, the X-Ray

Fluorescence technique (XRF) were used for the analysis of rock samples for their major and trace elements using pressed powder pellets following the established procedures of Saini et al., 2000. Prior to the major and trace elements analysis, the samples were cleaned with distilled water, air-dried and powdered. About 50 grams of each sample was powdered up to 200 mesh size using a Tema mill (N.V.TEMA) at the WIHG. The powdered samples were then used for further geochemical and isotopic analyses as follows.

3.2.3.1 Loss on ignition (LOI)

Loss on ignition (LOI) determines the amount of organic matter and carbonate content in the samples. This is also required for the accurate measurement of major and trace elements composition of any material in X-Ray Fluorescence (XRF) technique.

The procedure for the LOI calculation includes is

1. 5 gm of each sample was taken in a precleaned alumina crucible.
2. The crucibles were kept in a furnace in a closed environment at 550°C for four hours and 950 °C for 8 hours.
3. Crucibles were allowed to be cool in the furnace at each step so that convection current do not absorb atmosphere water.
4. The crucibles were then reweighed along with the samples. The difference in the weights gives the amount of organic matter and carbonate mineral content in sediments. The formula for the LOI can be written as:

LOI_{550} or $LOI_{950}= (W_1\text{-}W_2/W_1)*100$

Where W_1= Initial weight of sample plus crucible

W_2=Weight of sample plus crucible after heating at 550°C or950 °C

Figure 3.3 Wavelength dispersive X-ray Fluorescence (WDXRF) Spectrometer for analyses of the major and trace elements (at WIHG).

3.2.3.2 Elemental abundance

A total of 112 samples were analysed for major and trace elements concentration using X-ray Fluorescence (WDXRF) Spectrometer; Bruker S8 Tiger at WIHG (Figure 3.3). Prior to analysis, the pressed pellets were prepared. Around 6gm of every sample was taken and 4-5 drops of polyvinyl alcohol (PVA) solution added to it in an agate mortar and then mixed thoroughly with the pestle. PVA does not react with the sample and therefore used as a binder. The mixture was then pressed under hydraulic pressure machine at a pressure of 17 tons for around 60 seconds. These pellets are then measured for major and trace elements. Major oxides are measured in weight percentage (wt. %) and the trace elements in part per million (ppm). The abundance of major oxides was converted to major elements with their respective conversion factors. Analytical precision for major elements is well within $\pm$ 2 to 3% and $\pm$ 5 to 6% for trace elements.

3.2.4 Rare earth elements (REEs)

The samples studied for rare earth elements (REEs) were analyzed using Inductively Coupled Plasma Mass Spectrometer (ICP-MS), Perkin Elmer SCIEX Quadrupole, ELAN DRC-e, at WIHG. It works on the principle of mass spectrometry using a Quadrupole which acts as an analyzer that differentiates the different isotopes of the element on the basis of their mass/charge ratio. The samples were prepared by the open acid digestion method as described in Khanna, (2009). Towards this, ~0.1gm of each sample was taken in teflon crucible and a mixture of Hydrofluoric acid (HF) and Nitric acid (HNO_3) in a ratio of 2:1 was added to it. 5 ml of perchloric acid ($HClO_4$) was also added to it, for decreasing the boiling point of the solution. The ceramic crucibles containing mixture of the samples and acids were then covered with a lid and heated at the hot plate at a temperature around 180°C for 8-10 hrs, for the complete dissolution. This treatment was given thrice until the complete digestion is obtained. After dissolution, the samples were allowed to evaporate till incipient dryness. Thereafter, 10 ml of 10% HNO_3 was added to it and warmed gently for 10 minutes. The final solution was volume made up to 100 ml by adding distilled water to it. The solution was then stored in polypropylene bottles for the before the final analysis. The international standards of JGR-1 and BMG-1 were used to calibrate the instrument and results. Repeated measurements were carried out for maintaining the accuracy of the results. Accuracy of rare earth elements ranges from 2 to 12% and precision varies from 1 to 8%. The values of the REEs is reported in part per million (ppm).

3.2.5 Strontium and Neodymium ($^{87}Sr/^{86}Sr$ & $^{143}Nd/^{144}Nd$) studies

Radiogenic isotopes (Sr-Nd) are found to be useful as tracers of the provenance of sediments in geological processes. Towards this the $^{87}Sr/^{86}Sr$ and $^{143}Nd/^{144}Nd$ were measured in their silicate fraction recovered after the decarbonation of the bulk powdered sediments.

3.2.5.1 Decarbonation and ashing

For sample preparation for Sr-Nd isotopic studies, 1gm of each sample was taken in 50 ml centrifuge tube and treated with 0.6 N Hydrochloric acids (HCl) with intermittent ultra-sonication at 60°C for 30 minutes, for removing the carbonates (Figure 3.4). Subsequently, the acid was decanted and sample washed thrice with high purity MQ water to remove the total acid content. To avoid interference of organic matter with the Sr-Nd chemistry, the samples were also ashed at 600° C for ~8 hrs. The ashed samples than brought to solution form by acid digestion. At each step, the samples were weighed for knowing the amount of carbonates and organic matter in the samples.

3.2.5.2 Acid dissolution

About 0.1 gm of each ashed sample (free from carbonates and organic matter) was taken in a 7ml Savillex vial along with a known amount of ^{84}Sr and ^{150}Nd spikes. In order to bring a sample to a complete solution the samples were treated with ultra-pure $HF+HNO_3$ (3:1.5) twice and HNO_3+HCl (3:1) acid digestion process. After the complete dissolution, samples were dissolved in 1.5ml 2N HCL. After this, Sr and REEs were separated from the solution by passing the solution through the ion exchange columns as described in Singh et al., 2008. From the REE fraction, Nd was further separated using Ln specific resin. Sr and Nd concentration and ^{87}Sr/^{86}Sr and ^{143}Nd/^{144}Nd were analyzed on a Multi-collector Inductively coupled plasma Mass Spectrometer (MC-ICP-MS) at Physical Research Laboratory, Ahmedabad (Figure 3.4). The corresponding Standards to Sr and Nd are SRM987 and JNdi-1 are also analyzed repeatedly and yielded value of 0.710316±0.00001.2 (1σ, N=14) for ^{87}Sr/^{86}Sr and 0.511719±0.000007 (1σ, n=10) for ^{143}Nd/^{144}Nd, respectively (Figure 3.5).

Figure 3.4 Sample preparation method for the Sr-Nd isotopic studies (at PRL, Ahmedabad).
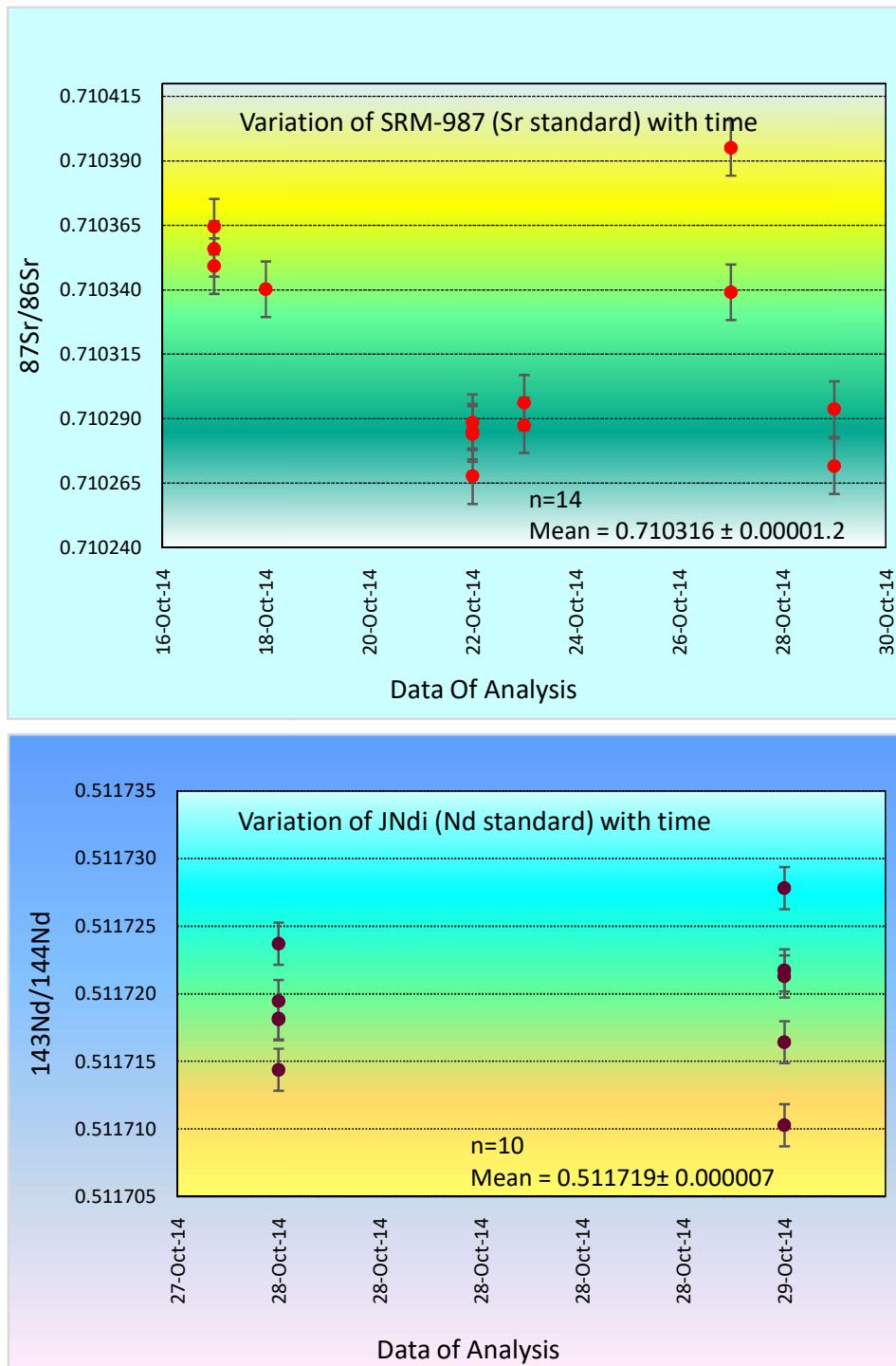
Figure 3.5 Variations in ^{87}Sr/^{86}Sr and ^{143}Nd/^{144}Nd measured in standards.

38

3.2.6 U-Pb Zircon geochronology

3.2.6.1 Zircon separation and dating

The samples (nos 12) for the detrital zircon study were collected from the Damtha and Jaunsar Group. Prior to the analysis, the bulk samples (4-5 kg) were cleaned properly (Figure 3.6). Then using hammer these samples were crushed to ~1 cm dimension. After that these samples were powdered using jaw crusher and disc mill up to a size of about 0.5 mm. The area where the sample were crushed using jaw crusher and disc mill were properly cleaned before and after the powdering of each sample using compressed air and vacuum cleaner. To segregate heavy fraction from this powder a sieve of 60-200 mesh was used. Sieve is also properly cleaned after sieving the samples in order to avoid any contamination. The sieved powder is used for gravity separation using Wilfley hydrodynamic shake table using water. Using the vibration and slope of Wilfley table, the heavier and lighter minerals are segregated by a divider and wash into different collection buckets. Heavier fraction after gravity separation contains heavy mineral present in the sample like pyroxenes, zircon, micas, amphiboles, magnetite, pyrite, apatite, etc. Thisheavier fraction was used for heavy liquid separation using Bromoform (Specific gravity: sp.gr. 2.89 gml^{-1}) in order to separate the lighter minerals like quartz, feldspar, muscovite etc (those mineral which are having lower sp. gr. than Bromoform). Remaining powder contains heavier minerals like Zircon apatite etc. Magnetic minerals were firstly separated by hand magnetic bar and then using an isodynamic magnetic separator. After that, the non-magnetic part is again separated by heavy liquid separator using Di-iodomethane (sp.gr. 3.32 gml^{-1}). After that, the zircons were handpicked and arranged in a matrix pattern on a quartz slide under a binocular microscope. The mounts were grinded using 8, 3, 1, 0.5 and 0.25 micron diamond suspensions and make sure that the grains are sufficiently cut through their centres in order to get the excess of complete morphology.

3.2.6.2 Instrumentation

In order to get the detail of internal structure (core and rim) of zircon grains, cathodoluminescence (CL) imaging was done using a Chroma CL-2 detector (Gatan make), attached to Secondary Electron Microscope (SEM) Make Carl Zeiss Model No: EVO40 after gold coating of the mounts. The mounts were cleaned or polished with the diamond suspension of 0.25 micron in order to remove the gold coating before using for LA-MC-ICPMS analysis. In-situ U-Pb geochronology work was done at Wadia Institute of Himalayan Geology, Dehra Dun, using a 193 nm UV EXCIMER LASER Ablation sampling device (Analyte-G2 (Cetac-Teledyne), attached to the Neptune Plus (make Thermo Fisher Scientific) Multi-collector ICPMS. Analyses were done using mixed collector configuration, following the procedure of Mukherjee et al., 2017 for zircon U-Pb dating and used Z91500 as a primary standard and Plešovice zircon standard for QC. Detail of parameters of LA-MC-ICP-MS is mentioned in the Table 3.2.

Table 3.2: Optimized Instrumental parameters.

MC-ICPMS	Description/optimized value	LASER Ablation system	Description/optimized value
Make	Thermo Fisher Scientific	Make	Photon Machine
Model	Neptune Plus	Model	Analyte-G2
Cool Gas	~16 L/min	Type	193nm Excimer
Auxiliary Gas	0.7-0.9 L/min	Wavelength	193 nm
Sample Gas	~0.9 to 1.1 L/min	Repetition rate	5 Hz
RF Power	1350 Watts	Energy density	$4Jcm^{-2}$
Guard Electrode	Off	Spot size	20 μm
i.		MFC1	~0.6 L/min
Detector Mode	Faraday+ICs		
Integration Time	~0.5 s	MFC2	~0.4 L/min
Scan Mode	Static	Shot count	150
Software used for data reduction		Iolite Software	

Masses measured	Detector:	IC5	IC4 ^{204}Hg+	IC2	IC1B	IC6	H3	H4
	Mass:	^{202}Hg	^{204}Pb	^{206}Pb	^{207}Pb	^{208}Pb	^{232}Th	^{238}U

Figure 3.6 Zircon separation and Analytical instrumentation (at WIHG) for U-Pb dating.
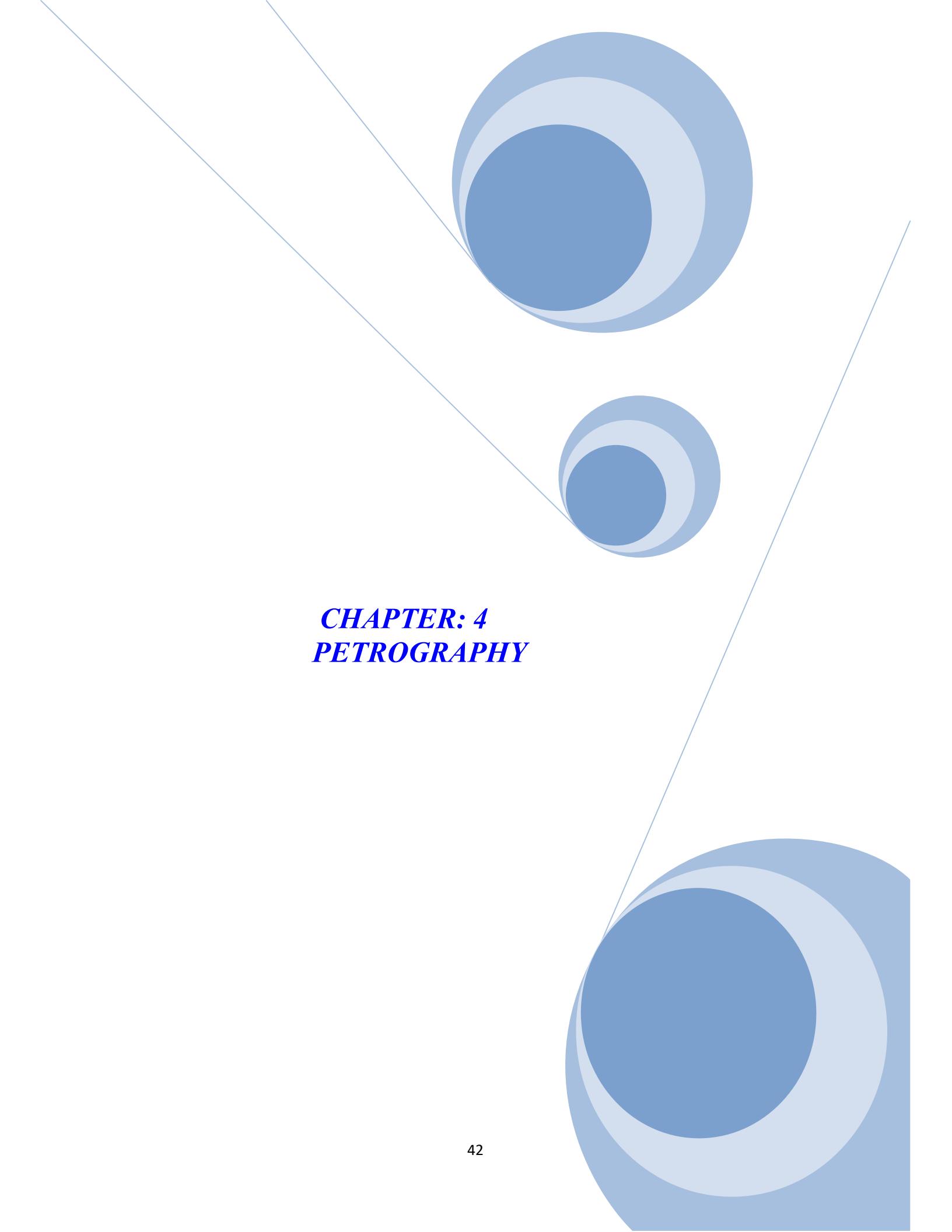
CHAPTER: 4
PETROGRAPHY

CHAPTER: 4 PETROGRAPHY

4.1 Introduction

Petrography is a useful tool for deriving first-order information of rock samples. Overall the Proterozoic siliciclastics of the Lesser Himalayan sedimentary packages may be categorized into two broad types - i) Siliciclastic (SLC) associated with the autochthon and para- autochthon bodies, which has undergone diagenesis and preserved the sedimentary textures. It generally has an association with syn-sedimentary basic volcanic rocks, particularly the Rautgara Siliciclastics of Inner Lesser Himalaya (ILH), and ii) Recrystallized Siliciclastic (RSLC) associated mainly with the crystalline sheets (gneissic bodies) and has lost the sedimentary textures and structures due to metamorphism. There are significant lithologic variations between the northern and southern parts of the Lesser Himalaya and traditionally divided into two zones (Figure 2.1) – Inner Lesser Himalaya (ILH) and Outer Lesser Himalaya (OLH). The siliciclastics of outer and inner Lesser Himalaya are usually grey, purple, and green and dirty white, medium- to fine-grained having sub-angular to well-rounded detritals (Ghosh et al., 2016a and b). Interestingly, purple, green types are common with syn-sedimentary basic volcanics and noticed mainly in ILH and subordinately in OLH (eastern part- Kumaun sector) of the Lesser Himalaya. Compositionally, the siliciclastics are of arenite and wacke types. Arenites include sublithic arenite, lithic arenite, quartz- arenite, and subarkose. Wackes include quartz wacke and lithic greywacke. These are abundant in the argillite facies of Chakrata and Chandpur formations. The occurrence of clayey materials and a reasonable amount of siliceous rock fragments and feldspars brands in both the clastics makes them compositionally sub-mature. Non-appearance of non-siliceous rock fragments may be because of diagenesis. Texturally, both the siliciclastics are mature as evidenced by a plenty of sub-rounded and rounded detrital and moderate degree of sorting. In general, coarser detritals show a

higher degree of roundness. The interstices between the coarse detritals (~2mm) are filled with finer size detritals.

4.2 Petrographic features

4.2.1 Detrital modes

The clastics of OLH and ILH are mostly grey, purple, green and dirty white and having medium- to fine-grained, sub-angular to well-rounded detritals. Remarkably, the purple, green clastics are noticed mainly in ILH associated with syn-sedimentary basic volcanics and subordinately in OLH (eastern part- Kumaun sector) of the Lesser Himalaya. Compositionally, the siliciclastics of the Lesser Himalaya are of arenite and wacke types. Arenites comprise of sublithic arenite, lithic arenite, quartz arenite, and subarkose and wackes comprise quartz wacke and lithic greywacke. On the basis of the petrographical studies, minor changes are observed in the clastics of OLH and ILH. The detrital from both the belts of the Lesser Himalaya are sub-rounded and rounded and exhibit a moderate degree of sorting which makes them mature. The quartz grains are mostly in the form of sub-rounded to rounded grains and thus indicating reworked sedimentary origin. The quartz grains generally exhibit straight extinction, yet many are feebly undulose. Generally, the coarse detrital grains are showing the higher degree of roundness (Figure 4.1 to 4.3), and the spaces between the coarse detrital grains are occupied by the finer size detritals. Clayey components and presence of siliceous rock fragments and feldspars make the clastics from both the OLH and ILH compositionally submature. The non-siliceous rock fragments are found in the negligible amount due to diagenesis.

Quartz (Q) detritus are sub-rounded to rounded and constitute of 95 percent of the overall detrital components. Quartz (Q) detritus are of three types- monocrystalline non-undulatory, monocrystalline undulatory, and polycrystalline. The detrital are consisting of maximum nearly 92 percent of mono-crystalline quartz (Qm) exhibiting both undulose and non-undulose extinction (Figure 4.1 to 4.3). The rareness of Qp and strained (undulose) quartz detritus might be related to the mechanical stability and are less stable than the unstrained (non-undulose) quartz detritus. Qp grains are bigger than

Qm grains. The presence of Qp and Qm in the Lesser Himalaya indicates different sources (granitic and granitic gneiss source). The siliceous materials are the common cementing material of the quartz grains in the form of silica overgrowth (Figure 4.1 to 4.3). The presence of siliceous rock fragment and silica overgrowth indicates several phases of recycling from older rocks. The grain boundaries are typically sutured and uncommon concavo-convex and long contacts.

Feldspar (F) detritus occur as the second most abundant detrital constitute of sub-rounded, fine sand-sized grains (Figure 4.1 to 4.3) including plagioclase and K-feldspar. During locomorphic diagenetic stage, feldspars have been transformed into clayey and sericite matrix, (Ghosh, 1991) due to which feldspar are present in scarcity. The most common types are Microcline- orthoclase, and albite and labradorite - andesine types are rare.

Rock fragments(R) are the assemblage of multiple mineral grains. Rock fragments of sedimentary (Rs), metamorphic (Rm), and igneous (Ri) types, includes varied proportion of siliciclastics (SLC), argillite (ALG), chert (CH), meta- chert and metaquartzite (MQ), low grade metamorphics (LGM), quartz mica aggregate (QMA), volcanics (VLC)and some undifferentiated rock fragments (UND). Amongst the rock fragment types in both the siliciclastics (OLH and ILH), sedimentary fragments dominates over the metamorphic. However, igneous fragments are insignificant due to post-depositional alterations.

4.2.2 Accessory components

The accessories are like matrix, cement and heavy mineral includes minor amount of chlorite, sericite and iron oxides found generally in the intergranular spaces. The most common cementing materials are clay, silica (quartz overgrowth) and iron oxide. Clayey fraction includes sericite and chlorite flakes. Ferruginous cement occurs as a thin film bordering the detritals. Chlorite fills the interstices and frequently replaces the ferruginous material. Quartz cement commonly found as quartz overgrowth. These overgrowths are seen as the rim of the quartz grain around the detrital grains.

The heavy minerals are zircon, tourmaline, apatite, rutile with few opaque grains. A few coarser detritals contain inclusions of needle-shaped rutile and tourmaline. The heavy minerals which are commonly found in both the clastics of the OLH and ILH include zircon, tourmaline, garnet, apatite, staurolite, and rutile. Glauconite found in form of pale green to dark green (Figure 4.1, A).
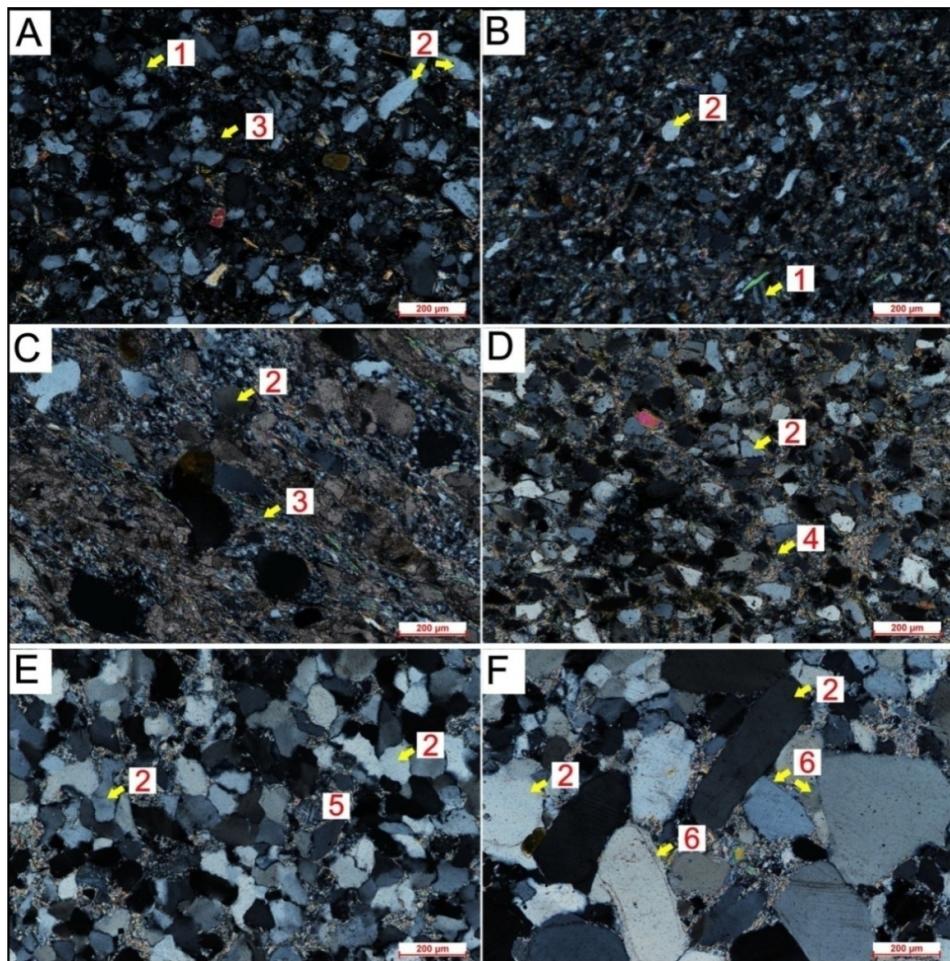
Figure 4.1 Photomicrographs of the clastics (Chakrata and Rautgara formations), (A) Well sorted, fine-grained, subrounded quartz grain (Chakrata ARG), (B) Moderately-sorted fine quartz grain (Chakrata ARG), (C) Fine-grained, moderately-sorted and sub-rounded quartz grain showing feldspar alteration (Chakrata ARG), (D) Grains are subrounded with sericitic matrix (showing late diagenetic process resulting into the dissolution of quartz by sericitic matrix (Rautgara SLC), (E) Well sorted quartz grain showing initial

stage of recrystallization (may be near volcanic or tectonic zone, showing presence of microcline(Rautgara SLC), (F) Moderately sorted, elongated coarse grain quartz showing quartz intergrowth due to highest degree of diagenesis (Rautgara SLC).

1-Plagioclase, 2-Monocrystalline quartz, 3-Altered Feldspar, 4-sericitic matrix, 5-Microcline, 6-Quartz overgrowth. All photomicrographs are in polarised light mode.
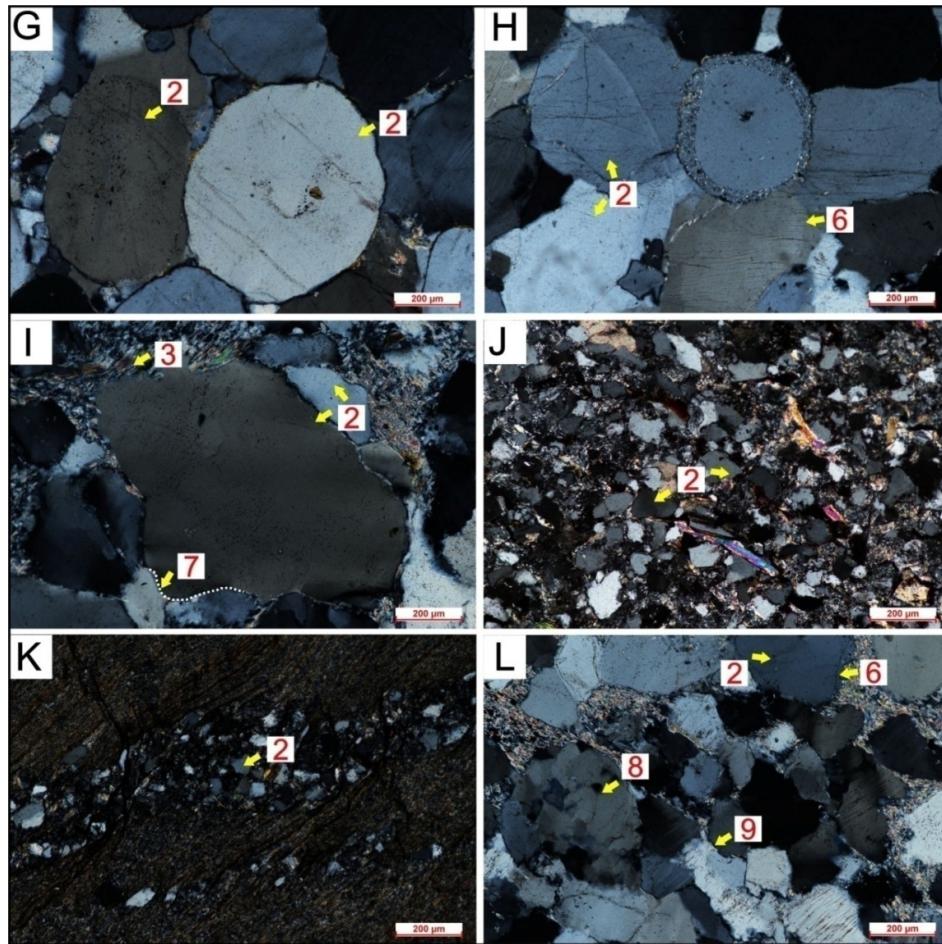
Figure 4.2 Photomicrographs of the clastics (Rautgara and Chandpur formations), (G) Coarse grain siliciclastic showing well rounded quartz grain (Rautgara SLC), (H) Siliciclastic showing silica coating around quartz grain (Rautgara SLC), (I) Siliciclastic having concavo-convex contact (Rautgara SLC), (J) Poorly sorted angular to sub-rounded quartz grain showing presence of micaceous mineral and iron oxide cement (Chandpur ARG), (K)

Recrystallized quartz ribbon showing moderately sorted rounded to sub-rounded fine grain siliciclastic (Chandpur ARG), (L) Well sorted coarse grain siliciclastics with sharp boundaries (Nagthat SLC).

1- Plagioclase, 2-Monocrystalline quartz, 3-Altered Feldspar, 4-sericitic matrix, 5-Microcline, 6-Quartz overgrowth 7-Concavo-convex boundary, 8-Polycrystalline quartz and 9-Suture boundary. All photomicrographs are in polarised light mode.
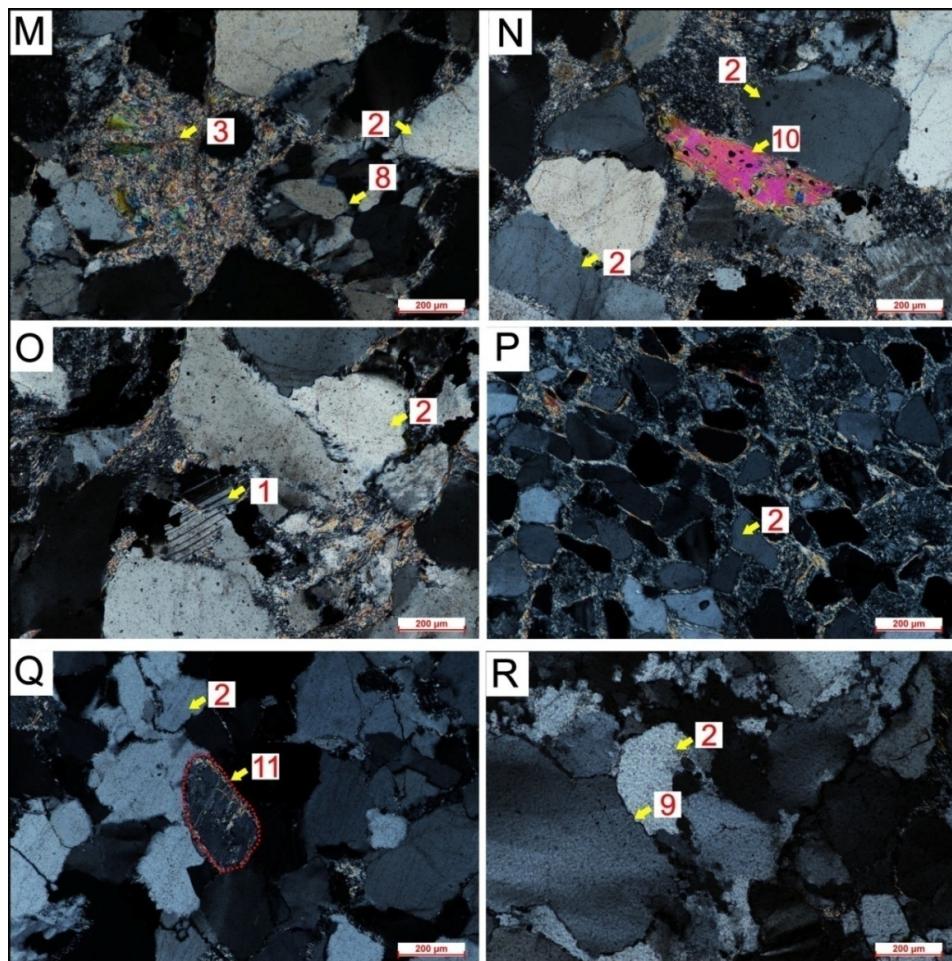
Figure 4.3 Photomicrographs of the clastics (Nagthat Formation), (M) Well sorted rounded to sub-rounded coarse-grained siliciclastic showing altered feldspar (Nagthat SLC), (N) Siliciclastic with muscovite flakes (Nagthat SLC), (O, P) Well sorted siliciclastic showing presence of plagioclase feldspar (Nagthat SLC), (Q) Siliciclastic showing feldspar coating in quartz grain (Nagthat SLC), (R) Sub rounded coarse grain quartz (Nagthat SLC).

1-Plagioclase, 2-Monocrystalline quartz, 3-Altered Feldspar, 4-sericitic matrix, 5-Microcline, 6-Quartz overgrowth 7-Concavo- convex boundary, 8-Polycrystalline quartz and 9-Suture boundary, 10-Mica and 11-Feldspar layering. All photomicrographs are in polarised light mode.

Modal composition of 38 samples from the Lesser Himalayan clastics is shown in Table 4.1. The QFR diagram of the clastics of the OLH and ILH are plotted in the Figure 4.4. The clastics with lesser amount of matrix (<15%) are plotted in Figure 4.4a and the clastics with matrix >15% are plotted in the Figure 4.4 b. Major detrital framework components of the clastics, especially quartz, feldspar and rock fragments have been recalculated as 100% for QFR diagrams. QFR diagrams for the clastics are plotted as proposed by Pettijohn (1987). The detrital proportion of the clastics from the OLH and ILH is: $Q_{77\pm12}F_{11\pm4}R_{12\pm9}$; $Mx_{9\pm5}$(n=17)   and $Q_{86\pm14}F_{5\pm4}R_{9\pm13}$; $Mx_{10\pm7}$(n=21) respectively.

Table 4.1: Recalculated modal composition (in percentage) of the Outer and the Inner Lesser Himalayan clastics.

Samples	Q	F	R	Mx	Classified as
MN-3Z	84.14	13.29	2.57	4.06	Subarkose
MN-4A	85.35	9.34	5.32	18.17	Arkosic wacke
MN-4B	88.67	7.13	4.21	8.61	Subarkose
MN-4D	84.74	13.36	1.91	10.51	Subarkose
MN-4E	76.62	12.39	10.99	5.13	Subarkose
MN-4F	75.50	7.00	17.50	18.14	Lithic greywacke
MN-4G	74.35	13.76	11.88	3.27	Subarkose
MN-4H	43.45	20.56	35.98	8.90	Lithic arenite
MN-4I	72.22	9.72	18.06	18.25	Lithic greywacke
MN-4J	72.52	14.29	13.19	11.06	Subarkose
MN-4K	86.29	9.14	4.57	10.88	Subarkose
MN-4L	80.46	13.79	5.75	4.95	Subarkose

Continued-

Samples	Q	F	R	Mx	Classified as
MN-5K	94.27	1.83	3.90	9.55	Quartz arenite
MN-5L	88.88	3.88	7.24	4.30	Sublitharenite
MN-5M	69.94	8.91	21.15	5.69	Sublitharenite
MN-5N	66.29	12.78	20.92	3.61	Sublitharenite
MN-5NB	73.78	9.89	16.33	2.80	Sublitharenite
MN-1J	76.92	7.69	15.38	20.00	Lithic greywacke
MN-1M	85.37	12.20	2.44	16.00	Arkosic wacke
MN-1N	83.33	11.11	5.56	0.00	Subarkose
MN-1Q	43.09	0.70	56.21	19.96	Lithic greywacke
MN-2J	75.87	3.90	20.23	8.42	Sublitharenite
MN-2Z	94.09	4.33	1.58	7.79	Quartz arenite
MN-3A	94.06	2.31	3.63	15.40	Quartz wacke
MN-3B	88.24	1.91	9.86	20.04	Lithic greywacke
MN-3C	98.69	0.33	0.98	1.10	Quartz arenite
MN-3D	100.00	0.00	0.00	0.62	Quartz arenite
MN-3E	97.19	2.41	0.41	8.43	Quartz arenite
MN-3F	94.45	4.14	1.41	3.75	Quartz arenite
MN-3G	99.23	0.77	0.00	2.92	Quartz arenite
MN-3H	98.60	1.40	0.00	7.73	Quartz arenite
MN-3I	98.24	1.76	0.00	16.67	Quartz wacke
MN-3Q	86.08	7.59	6.33	12.00	Subarkose
MN-4V	66.33	13.72	19.96	12.89	Sublitharenite
MN-4Y	69.37	7.84	22.79	6.14	Sublitharenite
MN-4Z	80.28	9.86	9.86	11.00	subarkose -sublitharenite
MN-5A	85.53	6.58	7.89	13.00	Sublitharenite
MN-6B	98.12	1.88	0.00	1.37	Quartz arenite

Abbreviations used: Q-Quartz, F-Feldspar, R-Rock Fragments, Mx- Matrix
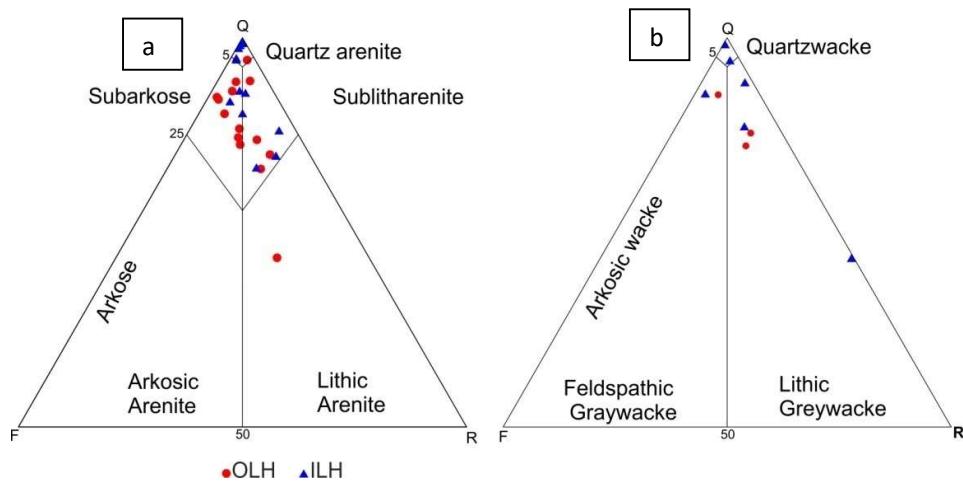
Figure 4.4 Q-F-R ternary plot: Petrographic classification of sandstones (following Pettijohn et.al 1987).

4.3 Scanning electron microscope (SEM) analysis

A total of 22 samples (gold coated samples) were analysed for the morphological features using ZEISS EVO 40 EPA Secondary Electron Microscope (SEM). Present studies shows that the quartz occur as one of the most common diagenetic mineral in the Lesser Himalayan succession. Of particular interest is the presence of quartz overgrowth showing well-formed crystal faces which are formed as a result of diagenesis (Figure 4.5-A, B).The samples analysed, exhibiting various diagenetic features as arc-shaped steps, conchoidal fractures and clay alteration (Figure 4.6).

The quartz overgrowth includes the small isolated growth of the quartz around the detrital grains. The chemical composition of the clastic sediments (carbon coated) are measured using SEM-EDX mode (quantitative- analysis). This analysis shows that the clastic sediment are rich in light minerals such as quartz and clay minerals and heavy minerals such as ilmenite and rutile due to the presence of Si, Mg, Fe, K and Ti (Figure 4.7 and 4.8).
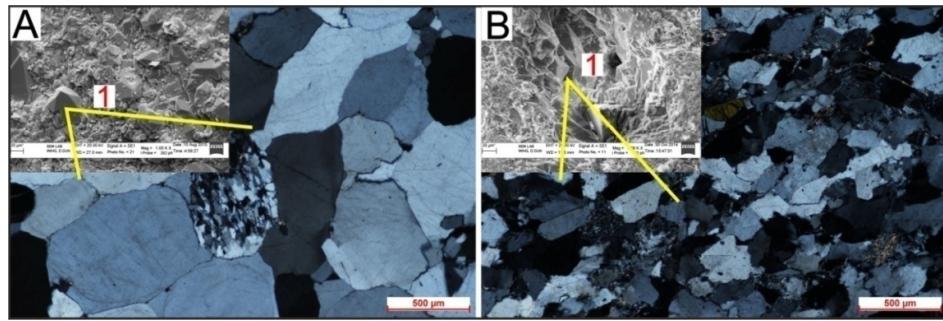
Figure 4.5 SEM images, (A) Quartz overgrowth in siliciclastic of ILH in SEM image, (B) Quartz overgrowth in siliciclastic of OLH in SEM image.
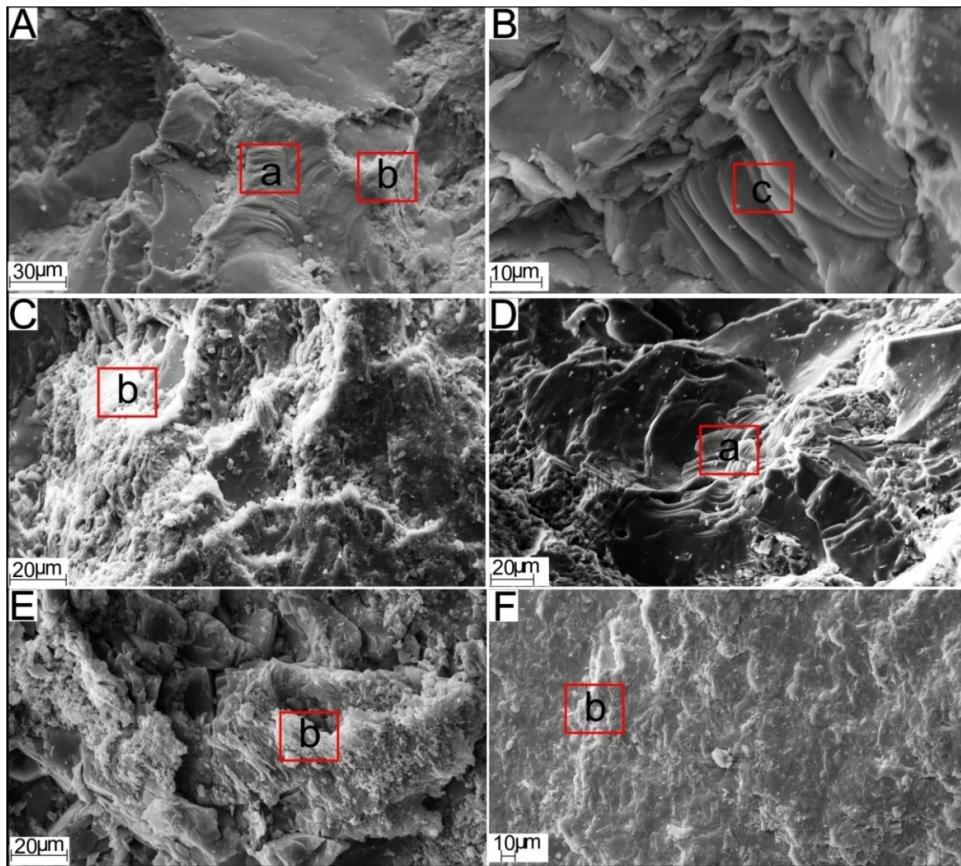
Figure 4.6 SEM images, (A) Smooth surface with conchoidal fractures and clay alteration, (B) Step like fractures, (C) Clay mineral alteration (D) Clay alteration crushing features (E) Clay alteration and crushing features (F) Clay alteration.
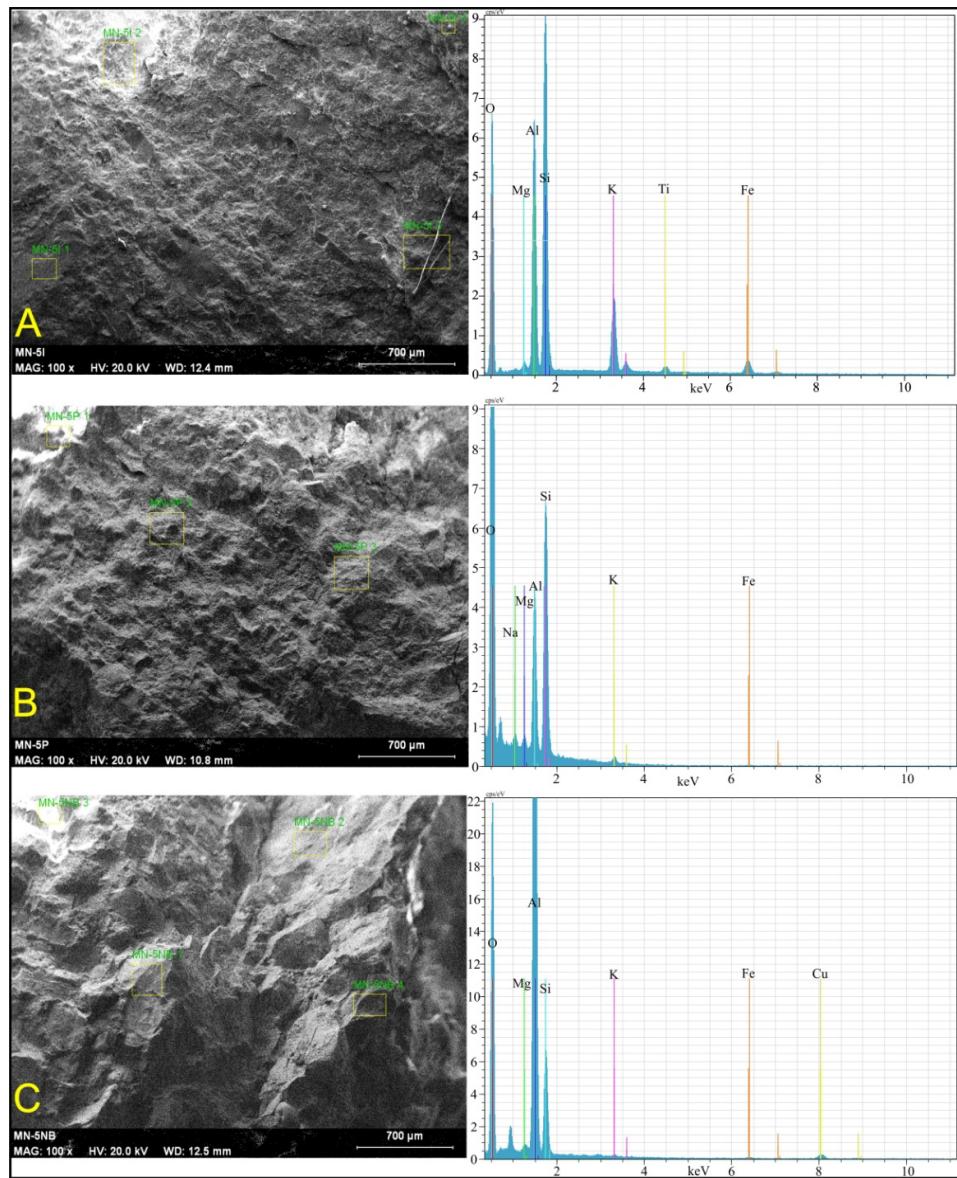
Figure 4.7 SEM and EDX spectrum for Lesser Himalayan clastics showing the presence of light minerals such as quartz and clay minerals and heavy minerals such as ilmenite and rutile due to the presence of Si, Mg, Fe, K and Ti.
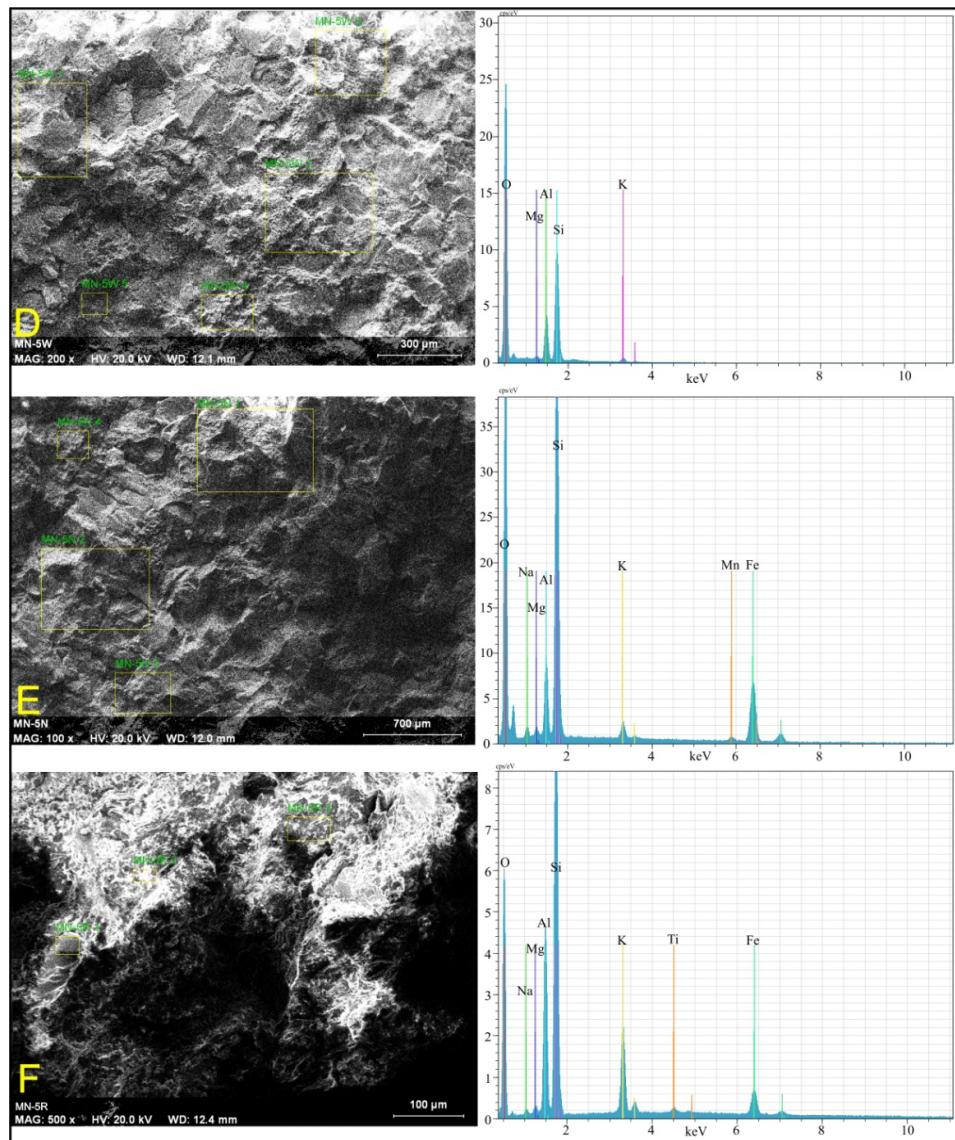
Figure 4.8 SEM and EDX spectrum for Lesser Himalayan clastics showing the presence of light minerals such as quartz and clay minerals and heavy minerals such as ilmenite and rutile due to the presence of Si, Mg, Fe, K and Ti.

4.4 Zircon morphology

The present study concerns mainly with the following three major issues as -a) regarding the characterisation of the detrital zircon obtained from the Proterozoic Lesser Himalayan clastics for creating a first-hand data base, b) using the data set for relooking the stratigraphic correlation of the OLH and ILH clastics, and c) the provenance appraisal of the Lesser Himalayan clastics.

The separated zircon grains (for dating purpose–Chapter-6) from the Outer and Inner belts of the Lesser Himalaya are analyzed for their morphological and internal features.

Zircon ($ZrSiO_4$) is a key mineral having widespread use in geoscience application covering the streams of U-Pb geochronology and tracer studies. It records the ages representing major events in Earth history, including crustal modifications, the oldest sediments, episodes of non-depositions, orogenic events, and relative movements of supercontinent (Rubatto and Hermann 2007; Harley et al., 2007). The ability to survive magmatic, erosion and metamorphic processes makes zircon an important tool to infer detail information regarding the geological history of the magmatic, metamorphic and sedimentary rocks. Detrital zircon from clastics provides important information into provenance protolith characteristics. The most common shape of the zircon is tetragonal, elongated and euhedral prismatic crystals having length-to-width ratio within a range of 1–5 (Corfu et al., 2003). Reconstructing the stratigraphic relationship and unroofing the history of the unfossiliferous, deformed Lesser Himalayan clastics is problematical, particularly in the absence of notable marker horizons. The major problem in polydeformed terranes is that the earlier structures are often over-printed, and their significance gets obscured by later deformation events (Ghosh et al., 2016a). Consequently, perhaps for the first time, the detrital zircons are used as a proxy for comparing the variability of their physical attributes for understanding the detrital derivation (provenance) of the Proterozoic Lesser Himalayan sediments.

Characterisation of the detrital zircon largely takes care of three imperative features like shape, elongation, and. zoning pattern for its implication towards the provenance interpretations. The optical imaging of shape and elongation of the zircon grains has been done using the camera with transmitted light mode attached to LASER Ablation system and for internal features (like zoning and their types), the backscattered electron (BSE) and cathodoluminescence (CL) imaging method are used. The elongation of the zircon is defined by its length-to-width ratio. This ratio defines the crystallization rate of zircon i.e. the higher the ratio the faster will be the crystallization rate (Corfu et al., 2003). Magmatic zircons grains are euhedral to subhedral with smooth prismatic crystals with distinct core and rim usually having the longest axis between 20 and 250µm (Hoskin and Schaltegger, 2003). The most common features of the magmatic zircon are the development of the oscillatory and sector zoning (Vavra et al., 1996; Hoskin and Schaltegger, 2003). Post-magmatic processes (such as erosion, transportation, metamorphism, and fluid inclusion) can also affect the morphology of the zircon grain. It may result in the partial or complete deformation of the morphology and inner texture. Metamorphic zircons produced by recrystallization (intra-grain"reworking" of earlier formed zircon) under the certain pressure-temperature condition, T≥ 400˚C (Pidgeon, 1992; Pidgeon et al., 1998; Corfu et al., 2003; Hoskin and Schaltegger, 2003; Wu and Zheng, 2004) and are euhedral to anhedral in shape. Zircons of Granulitic facies rock are subhedral, anhedral or isometric and poorly zoned with strong CL intensity, Amphibolite facies zircon are mostly euhedral prismatic crystals with low CL intensity. Similar, the Eclogite facies zircons are characterised by overgrowths with or without zoning, cloudy zoning and sector zoning and are generally subhedral to anhedral (Wu and Zheng, 2004). During migmatization and crystallization, the zircon may react with the existing melt due to disequilibrium and results in the formation of resorption structure. The zircons, which are altered by the metamorphic fluid, show homogeneous texture with high CL brightness (Schaltegger et al., 1999; Vavra et al., 1996). Hydrothermal alteration also results in the loss of radiogenic Pb due to which

zircon shows white CL image. Zonation may also be lost in specific environment responsible for forming compositionally homogeneous texture.

The external and internal features of the separated zircon grains from the outer and inner Lesser Himalaya are documented in Table 4.2. Zircons from the Lesser Himalayan lithounits comprise of texturally variable in terms of external morphology and internal texture (Figures.4.9 to 4.20). Zircons with different physical features (Shape, roundness and crystallinity etc) reveal that they were formed under variable conditions Negi et al., 2018 (communicated). However, these features are dependent upon zircon saturation in the crystallization history of a rock (Hoskin and Schaltegger, 2003). The shapes of the zircons are anhedral to euhedral which display well developed prismatic to stumpy crystals. The occurrences of irregular or sub-rounded zircon grains are formed because of fluid induced processes (e.g. metasomatism and metamorphism; Corfu and Ayres, 1984; Corfu et al., 2003). The zircons grains show a size range of 75-250μm. Broken detrital zircon fragments were considered carefully (as there is a likely chance of fragmentation during processing). Zircon grains exhibit moderate roundness of their edges also in some cases sub- roundness to rounded grains is present. The variable physical feature of zircon depends on the degree of transportation, durability and density. The more rounded grains suggestive of more transportation from the source region. In the ILH domain, the grains are irregular and euhedral to anhedral in shape whereas in the OLH, these are prismatic euhedral to anhedral and more elongated. Core-rim texture indicates magmatic growth, Alternate bright and dark rim indicate recrystallization/overgrowths from fluids, and fracture in zircon shows metamictization and external pressure. The zoning in ILH zircons is faintly visible as compared to OLH. The zircon grains from both the OLH and ILH show nearly similar morphological and internal features. However, the differences are observed within the grains of same sample which suggest that each formation (Nagthat, Chandpur and Rautgara) of the Lesser Himalaya are sourced from protoliths, which had undergone different process of zircon formation as well as different degrees of transportation. The resorption structure in the grains may be due to the

disequilibrium of the zircon grains with the melt during magmatic processes and can occur due to metamorphic fluid/hydrothermal process due to the activity of the Main Central Thrust during Himalayan tectonism.

Detrital zircons from the Proterozoic Lesser Himalayan sediments comprise of texturally variable in terms of external and internal features. The calculated average size of the detrital zircon obtained from the Lesser Himalayan clastics is 112 μm ±SD 24 with length: breadth (L/B) ratio 1.83 ± 0.12. The zircon grains are dominantly euhedral to subhedral in shape and with angular to sub angular perimeter (Table 4.2 (overall) and Table 4.3 OLH/ILH). All these parameters can be used as a new type of proxy for inter- and intra-basinal stratigraphic correlations. Zircons with different physical features reveal that they were formed under variable conditions and obviously dependent upon zircon saturation in the crystallization history of a rock (Hoskin and Schaltegger, 2003).The shapes of the zircons are anhedral to euhedral which display well developed prismatic to stumpy crystals. The occurrences of irregular or sub-rounded zircon grains are formed because of fluid induced processes (e.g. metasomatism and metamorphism; Corfu and Ayres, 1984; Corfu et al., 2003). Zircon grains exhibit moderate roundness of their edges also in some cases sub- roundness to rounded grains is present. The variable physical features of zircon depend on the degree of transportation, durability and density. The more rounded grains suggestive of more transportation from the source region. Majority of the detrital zircons of the Lesser Himalayan clastics are euhedral to anhedral. Typical external morphologies are euhedral, rounded to sub-rounded grains. The rounded shapes are interpreted to be formed by resorption by a zircon-undersaturated intergranular fluid (Hoskin and Black 2000).

Table 4.2: The external and internal features of the zircons from the Inner and Outer Lesser Himalaya (after Negi et al., 2018, in communicated).

	Sample Id	Formation	Zircon domain						Inferences
			Shape	Size range	Average size (± SD)	Roundness	L/B ratio	Zoning pattern	
Outer Lesser Himalaya	MN-6A	Nagthat	Eu>>Su>An	72-186µm	124 µm(±22, n=201)	Ar>>Sr>>>R	3.8:1to1.1:1(avg. 1.89±0.42)	OsZ (Figure 4.9 to 4.16)	Zircon showing affinity towards Amphibolite facies metamorphism (low CL contrast)
	MN-5Z	Nagthat	Eu>Su>>An	53-218µm	102µm(±34, n=150)	Ar>Sr>>R	3.5:1 to 1:1 (avg. 1.92±0.46)	PoZ (Figure 4.9 to 4.16)	Zircon showing affinity towards metamorphism
	MN-5X	Nagthat	Eu>Su>>An	87-251µm	156µm(±26, n=185)	Ar>>>Sr>>R	3.3:1to1:1(avg. 1.92±0.35)	HmZ (low CL contrast) (Figure 4.9 to 4.16)	Zircon showing affinity towards Amphibolite facies metamorphism
	MN-5W	Nagthat	EuI>>>Su>An	89-291µm	135µm(±24, n=322)	Ar>>Sr>>>R	3.9:1 to 1:1 (avg. 1.76± 0.40)	Cl/PoZ (Figure 4.9 to 4.16)	Zircon affected by metamorphism.
	MN-5P	Nagthat	Eu>>Su>>An	70-192µm	120 µm (±24,n=212)	Ar>>Sr>>R	3.5:1 to 1:1(avg. 1.95±0.42)	OsZ (Figure 4.9 to 4.16)	
	MN-5K	Nagthat	Eu>>Su>>.An	54-180µm	96 µm(±22, n=122)	Ar>>Sr>>>R	2.7:1 to 1:1(avg. 1.71±0.37)		Magmatic zircon (strong CL contrast).
	MN-5I	Nagthat	Eu>>Su>>>An	67-185µm	105 µm (±19, n=229)	Ar>>Sr>>R	3:1 to 1:1 (avg. 1.76 ±0.38)	HmZ (bright CL contrast) (Figure 4.9 to 4.16)	Zircon showing affinity towards metamorphic fluid (showing reabsorbed structure).
	MN-1U	Chandpur	Eu>>>Su>>>An	57-156µm	97 µm(±15, n=176)	Ar>>Sr>>>R	3.4:1 to 1.1:1(avg. 2.02 ± 0.44)	HmZ (perfectly euhedral) (Figure 4.9 to 4.16) PaZ (Figure 4.13)	Uncertain (environmental condition?). Zircon showing affinity towards metamorphism

Continued-

Inner Lesser Himalaya	Sample Id	Formation	Zircon domain						Inferences
			Shape	Size range	Average size (σ)	Roundness	L/B ratio	Zoning pattern	
	MN-4T	Rautgara (Garhwal)	Eu~Su>An	60-167μm	107 μm (±20,n=280)	Ar~Sr>>R	3.2:1 to 1.1:1(avg. 1.89 ±0.43)	Irregular HmZ (Figure 4.17 to 4.18)	Magmatic zircon modified during late and post-magmatic cooling.
	MN-6B	Rautgara) (Garhwal)	Eu>Su>>An	80-215μm	136 μm (±25,n=198)	Ar>Sr>>R	2.8:1 to 1:1(avg. 1.66±0.41)	SZ (Figure 4.17 to 4.18)	Zircon showing affinity towards metamorphism. Formed by unsteady growth of small and numerous crystal faces
	MN-4Y	Rautgara (Kumaun)	Eu>Su>>An	44-115μm	64 μm(±12, n=130)	Ar>Sr>>R	3:1 to 1.1:1 (avg. 1.74±0.36)	PoZ (Figure 4.19 to 4.20)	Magmatic zircon (low CL intensity) showing involvement in Amphibolite facies metamorphism
	MN-4Z	Rautgara (Kumaun)	Su~Eu>>An	61-176μm	97 μm (±18,n=308)	Sr~Ar>>R	3.2:1 to 1:1(avg. 1.72±0.33)	OsZ (Figure 4.19 to 4.20)	Magmatic zircon showing affinity towards metamorphism
								HmZ (low CL contrast) (Figure 4.19 to 4.20)	Zircon showing affinity towards Amphibolite facies metamorphism

L-Length , B- Breadth, Eu – Euhedral, Su- Subhedral, An- Anhedral, Ar- Angular, Sr- Subrounded, R- Rounded, PoZ-Poor zoning OsZ-Oscillatory zoning, HmZ-Homogenous zoning, Cl- Cloudy zoning, PaZ-Planar zoning, SZ- Sector zoning, n-number of grains, SD-standard deviation.Inferences are based on Vavra et al., (1996); Schaltegger et al., (1999) and Hoskin and Schaltegger, (2003).

Table 4.3: Length/Breath ratio of the zircon grains separated from the siliciclastics of the OLH and ILH, n-number of grains, SD-standard deviation.

	Average size (± SD)	Average L/B ratio (± SD)
OLH	117μm ± 21 (n=1606)	1.87 ± 0.11
ILH	101 μm ± 30 (n=916)	1.75 ± 0.10
Total (ILH and OLH)	112 μm ± 24 (n=2522)	1.83 ± 0.12

The siliciclastic samples for characterization of the internal structure were collected from the Neoproterozoic Chandpur and Nagthat formation (OLH) and Paleoproterozoic Rautgara Formation (ILH) of the Lesser Himalaya. Dimension wise the OLH zircons are bigger (117μm ± 21 with L/B ratio 1.87 ± 0.11) than the ILH (101 μm ±30 with L/B ratio1.75 ± 0.10) (Table 4.3). The internal structure of the zircon shows low-to-high-luminescence growth zone sequentially overgrown by sector or oscillatory zoned domains. The Lesser Himalayan zircon separates are usually inherited from the protolith and showing the sign of resorption or metamorphic overgrowth. The resorption features in the grains may be due to the disequilibrium of the zircon grains with the melt during magmatic processes, it can also occur due to metamorphic fluid/hydrothermal process due to activity during the Himalayan Orogeny. The Lesser Himalayan sediment has been recorded to have suffered up to amphibolite facies. Towards this, formation of new zircon is rare at P-T conditions lower than upper-amphibolite and granulite-grade, and therefore recrystallization of protolith zircon (igneous or metamorphic) is responsible for producing metamorphic zircon. Zircons formed under different conditions have typical internal structure.
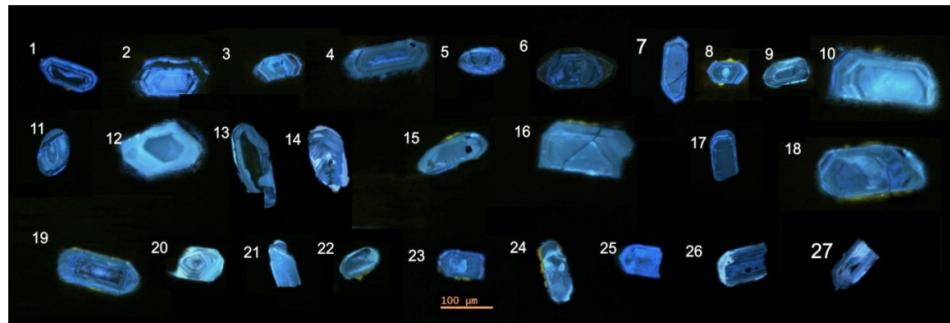
Figure 4.9 Cathodoluminescence (CL) images of different types of zircon of OLH (Nagthat Formation), **(1-9)** Euhedral, oscillatory zoned crystal grain, **(10)** Oscillatory zoned zircon grain, **(11-19)** Poorly zoned and homogeneous zircon grain, **(20)** Broken grain with oscillatory zoning, **(21-25)** Homogeneous grain, **(26-27)** Grain with broken surfaces.
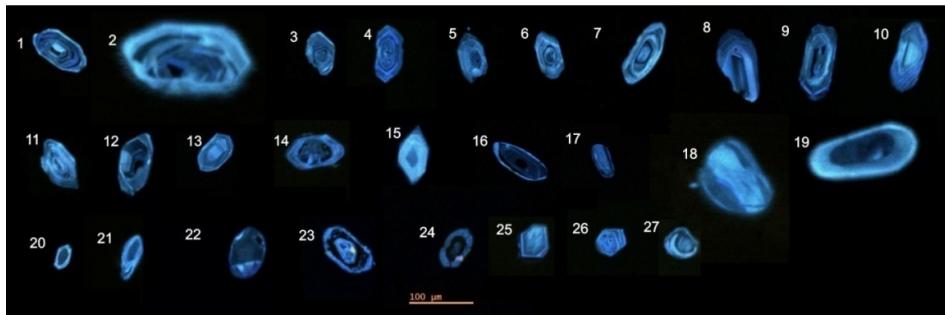
Figure 4.10 CL images of the zircons of OLH (Nagthat Formation), **(1-11)** Euhedral to anhedral zircon with oscillatory zoning, magmatic grains with high CL intensity, **(12-14)** Poorly zoned, **(15)** Zircon with bright luminescent displaying homogeneous texture, **(16-17)** Elongated zircon grains with planar zoning, **(18)** Poorly zoned sub-rounded zircon, **(19-21)** Euhedral to anhedral zircon showing bright rim, **(22)** Rounded unzoned zircon grain, **(23-24)** euhedral zircon grain, **(25-27)** Anhedral, sub-rounded unzoned to poorly zoned zircon grains.
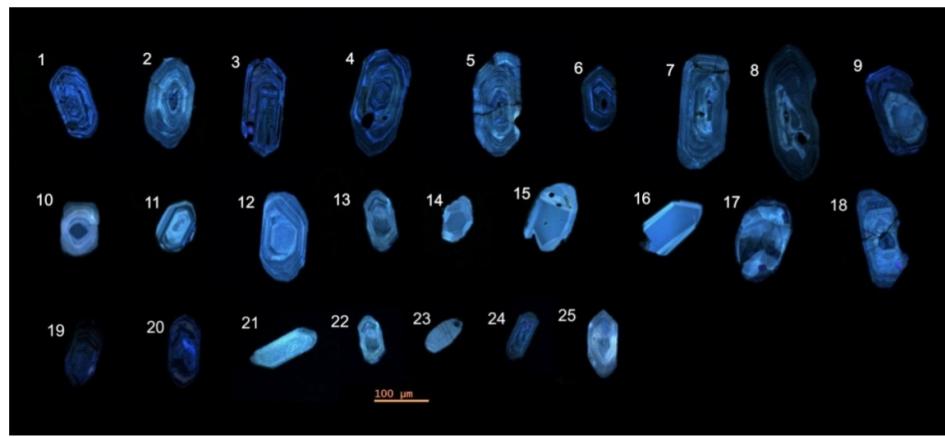
Figure 4.11 CL images of the zircon of OLH (Nagthat Formation), **(1-7)** euhedral to subhedral zircon grains with oscillatory zoning, **(8-9)** Euhedral to anhedral zircon grains with irregular zoning, **(10)** Anhedral zircon grain with thick and bright rim, **(11-13)** Euhedral zircon grains with magmatic core and recrystallized rim, **(14-16)** Poorly or cloudy zoned zircon, **(17)** Zircon with fir-tree zoning, **(18)** Multiple fractures, **(19-20, 24)** Poor or no zoning, **(21-23, 25)** Homogeneous zircon.
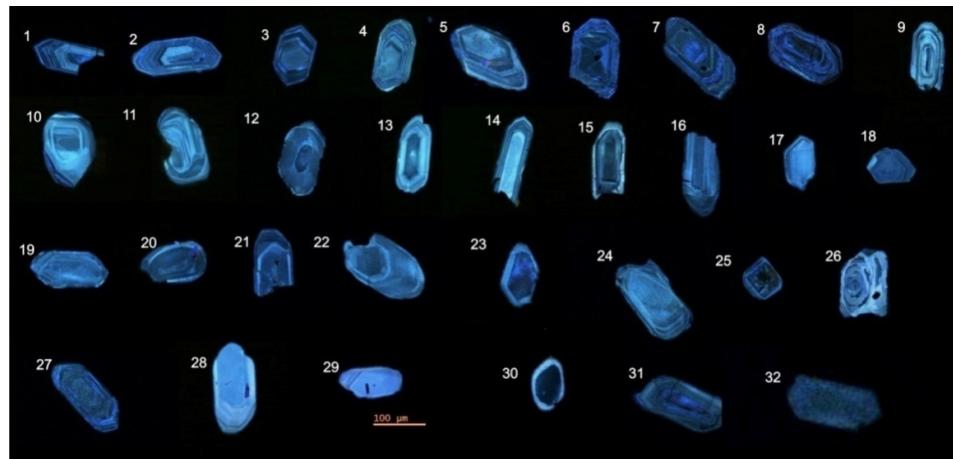
Figure 4.12 Internal structure of zircon of OLH (Nagthat Formation) in CL images, (**1-11**) Oscillatory zoned euhedral crystal grain, **(12)** Planar zoning, **(13-16)** Grains with euhedral and are prismatic and elongate in habit, **(17-27)** Poorly zoned grains with euhedral to sub-rounded in habit, 26- stubby grain,

(28-29) Unzoned crystal grains displaying homogeneous texture, **(30)** Sub-rounded zircon grain with bright metamorphic rim, **(31)** Zoning with multiple fractures, **(32)** Homogeneous grain with low CL intensity.
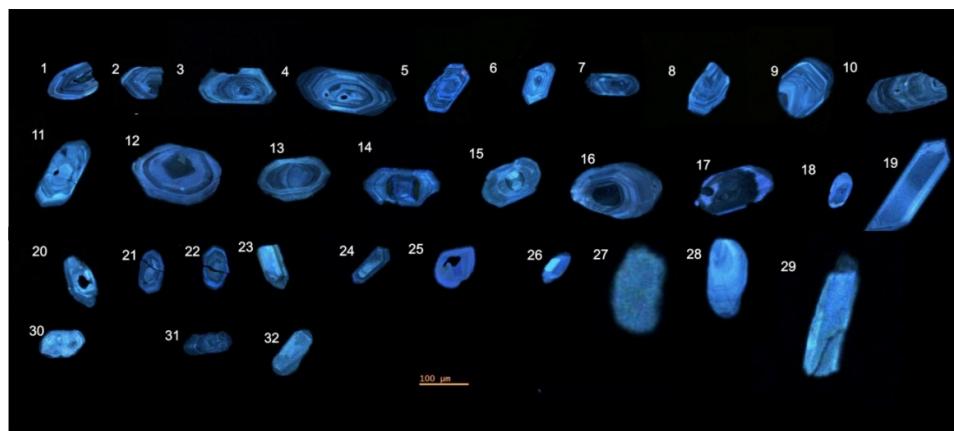
Figure 4.13 CL images of different types of zircon of OLH (Nagthat Formation), **(1-11)** Euhedral zircon grains with or without core displaying oscillatory zoning, **(12-16)** Planar zoning with bright rim, **(17-18)** Cloudy zoning, **(19)** needle shaped crystal grain with unzoned morphology, (**20-24)** Poorly zoned zircon, **(25-32)** Homogeneously textured zircon grain.
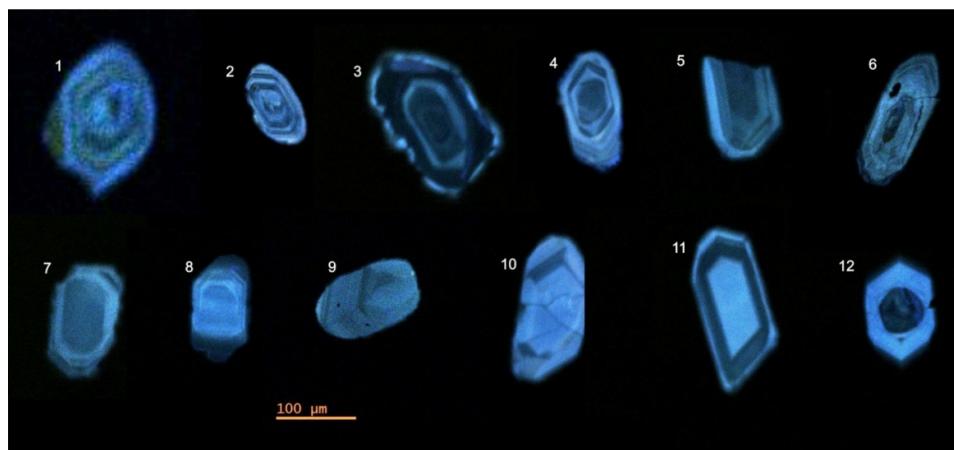
Figure 4.14 CL images of different types of zircon of OLH (Nagthat Formation)**, (1-6)** Detrital cores show oscillatory zoning and are surrounded by a bright metamorphic rim or thin luminescent boundary, **(7-9**) Poorly or unzoned zircon grains with homogeneous texture**, (10)** Zoning is apparently

replaced by strongly luminescent, the habit of zircon overgrowth is stubby (short prismatic), **(11)** Detrital cores shows bright core and are surrounded by a dark overgrowth rim, the dark rim is often also surrounded by a bright metamorphic rim, **(12)** Euhedral crystal grain surrounded by bright metamorphic rim.
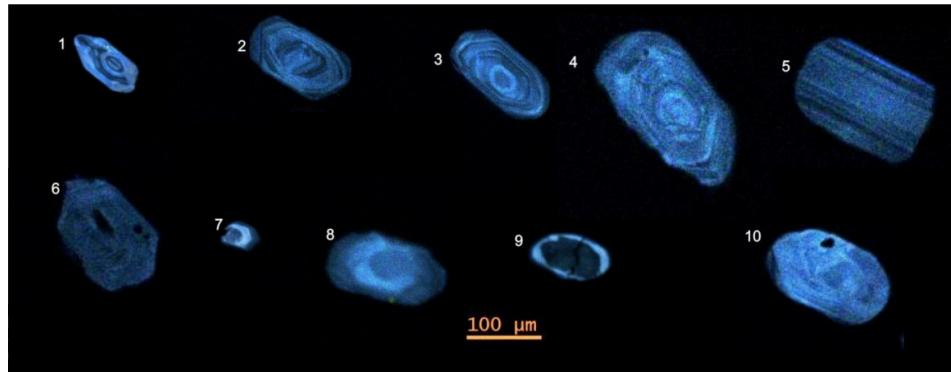
Figure 4.15 CL images of different types of zircon of OLH (Nagthat Formation), **(1- 4)** Oscillatory zoning in the grains of magmatic zircon, **(5)** zircon grain with elongated morphology displaying moderate core-rim texture, **(6)** Homogeneous unzoned zircon grain, **(7-8)** Poorly or cloudy zoned crystal grain, (**9**) Large segment of homogeneously texture zircon grain, (**10**) Poorly zone highly luminescent crystal grain, core is not revealed.
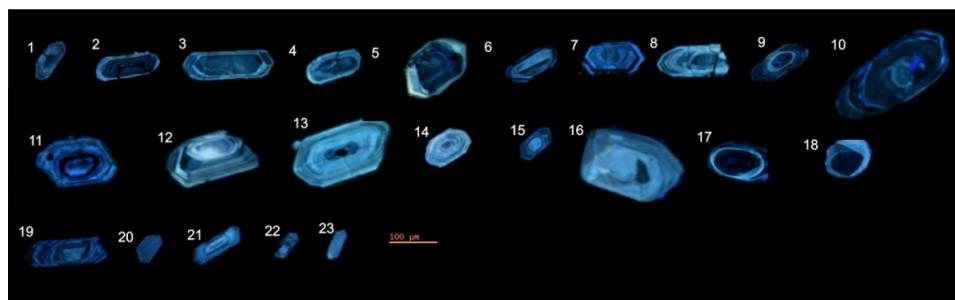
Figure 4.16 CL images of the zircons of the OLH (Chandpur Formation), **(1- 7)** Zircon images with bright metamorphic rim**, (8- 16)** Euhedral to subhedral zircon grains with oscillatory zoning, **(17- 18)** Subrounded grains of the zircon

with dark core, **(19)** Magmatic zircon modified during late and post-magmatic cooling, **(20, 23)** Homogeneous grain with low CL intensity, **(21-22**) Bright core.
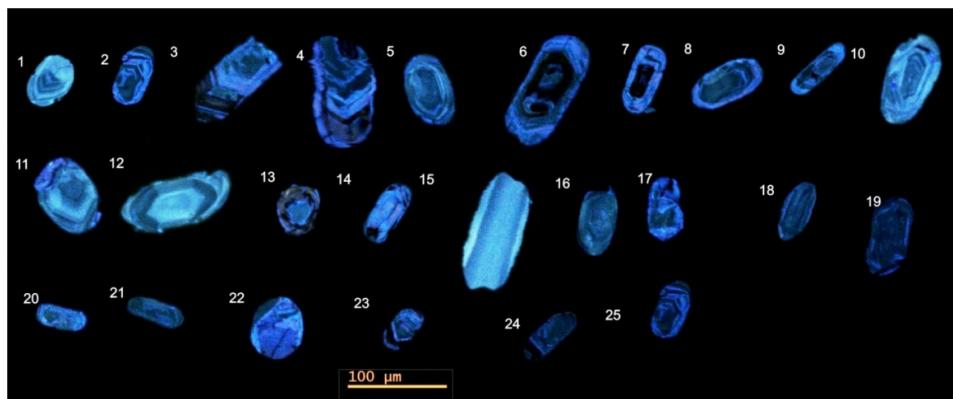
Figure 4.17 CL images for different zircon grains of the siliciclastic of the Rautgara Formation of ILH from the Garhwal section, **(1-5)** Magmatic zircons with or without inherited core showing irregular oscillatory zoning, **(6–12)** Grains with bright metamorphic rim formed by alteration of protolith zircon due to recrystallization,(12) Euhedral core, **(13–15)** Poorly zoned or unzoned zircon grain, **(16–21)** Homogeneous grain formed in amphibolite facies with low CL intensity, (**22**) Anhedral grain without core, **(23–25)** Magmatic zircon modified during late and post-magmatic cooling.
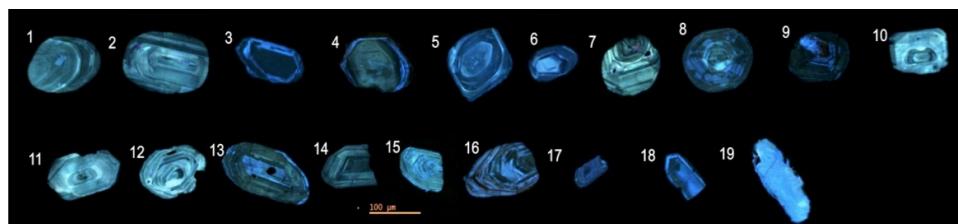
Figure 4.18 CL imaging of zircon grains of different morphological characteristic of the Rautgara Formation of inner Lesser Himalaya, **(1-2)** Planar zoning, **(3-4)** Zircons with bright metamorphic rim, **(5- 6)** Bright core

surrounded by dark rim which are further surrounded by bright rim, **(7- 8)** Grains with sector zoning, **(9)** Grain exhibiting irregular, patchy luminescence, **(10- 11)** Bright luminescence grains with euhedral cores, **(12- 16)** All grains exhibit straight-edged zonation, **(17- 19)** Homogeneous unzoned or poorly zoned grains.
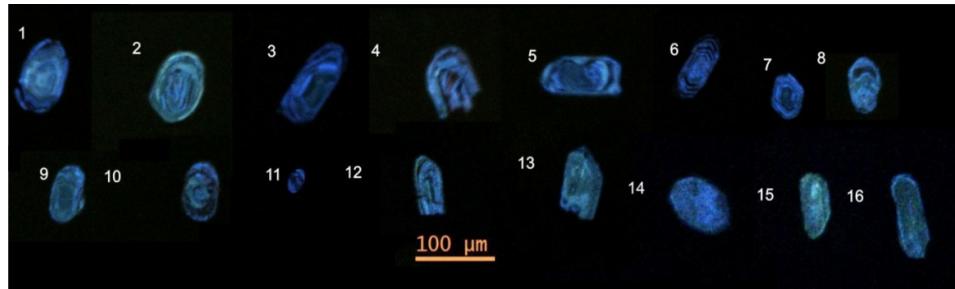
Figure 4.19 CL images of zircon grains of the siliciclastic of the Inner Lesser Himalaya (Rautgara Formation) from the Kumaun section, **(1-7)** Euhedral to anhedral crystals with irregular oscillatory zoning **(3 and 7)** Dark core surrounded by bright metamorphic rim, **(8-12)** Very fine anhedral to subrounded zircon grains with poor or cloudy zoning, **(13-16)** Homogeneous unzoned zoned grains.
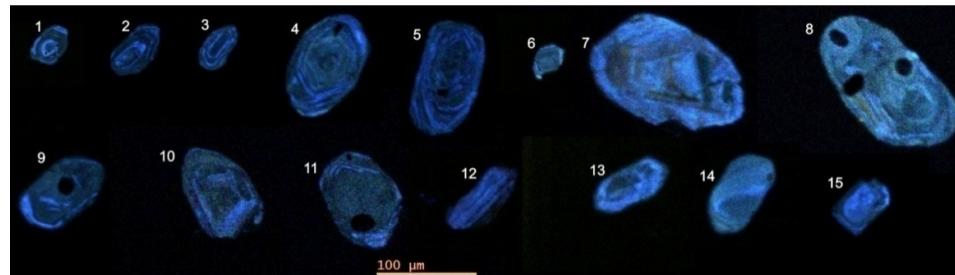
Figure 4.20 Recrystallized zircon in the Rautgara Formation of the inner Lesser Himalaya (Kumaun section) **(1-5)** Oscillatory zoning, **(1, 2 and 3)** Showing dark core is surrounded by light rim which is further surrounded by dark rim succeeded by light rim suggesting recrystallization, **(6-13)** Poorly zoned or cloudy zoned zircon grains, **(13-15)** Unzoned zircon grains lacking magmatic overgrowths having sub-rounded anhedral outlines.
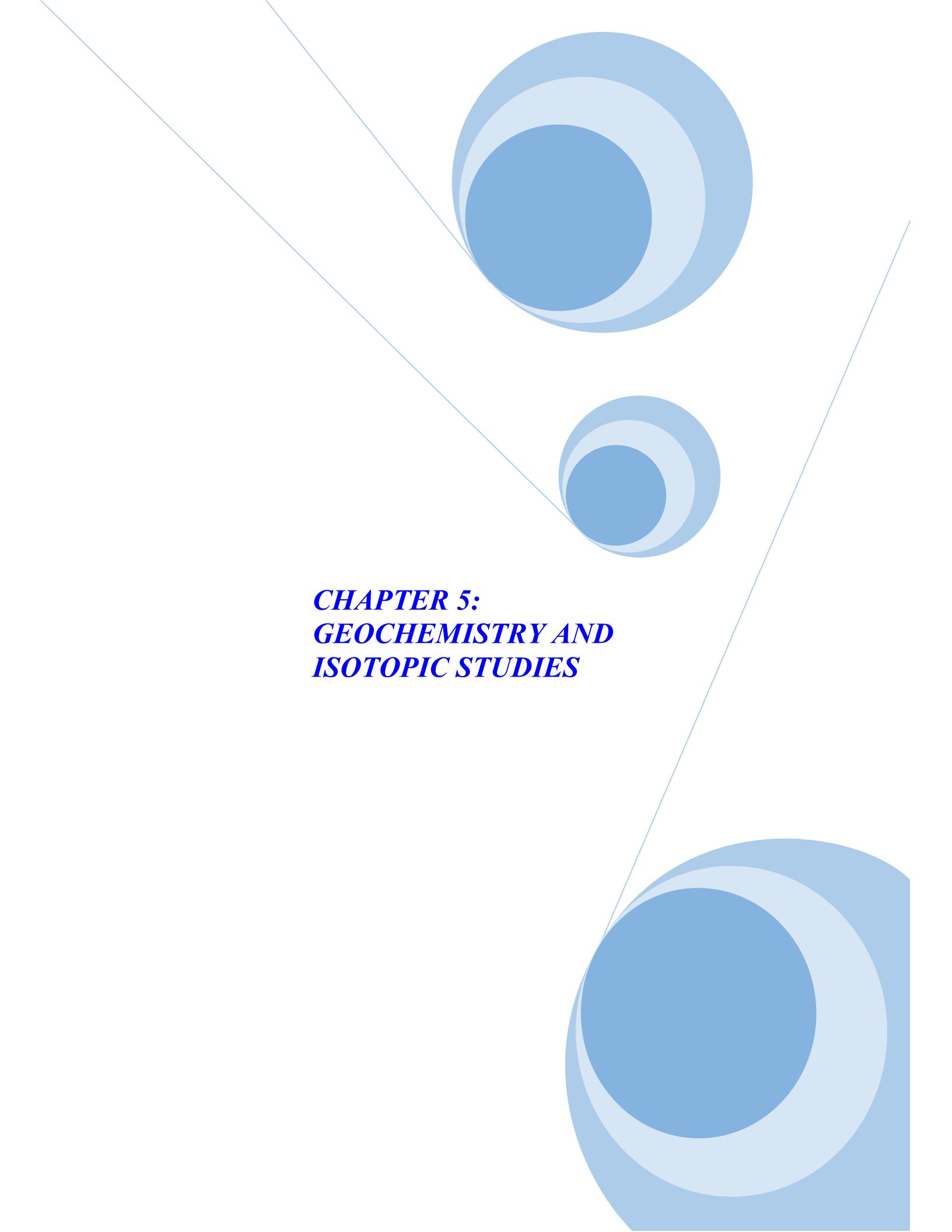
CHAPTER 5:
GEOCHEMISTRY AND
ISOTOPIC STUDIES

CHAPTER 5: GEOCHEMISTRY AND ISOTOPIC STUDIES

5.1 Introduction

Chemical and mineralogical composition of the sediments is defined in many ways and the most common method is based on the relative abundance of the element or their major oxides in the bulk samples (Johnsson et al., 1993). These are controlled mainly by the composition of their protolith, intensities of weathering (e.g. chemical and mechanical weathering), duration of weathering, fluid rock interaction time, transportation of clastic sediments from the source areas to depositional sites, depositional environments (marine or fresh water), and post depositional processes (such as diagenesis and hydrothermal alteration). The geochemistry of clastic sediments therefore, reflects a combination of its source rock, chemical weathering, hydraulic sorting, and abrasion etc. (Taylor and McLennan,1985; Wronkiewicz and Condie, 1987; McLennan et al.,1993; Condie, 1993, Nesbitt et al., 1997). The Lesser Himalayan succession are represented by medium- to coarse- grained clastics (siliciclastic) and fine -to very fine- clastic (argillite). Both the siliciclastic and argillite are present in the Neoproterozoic Jaunsar Group (representing the OLH) and similarly the Paleoproterozoic-Mesoproterozoic Damtha Group (representing the ILH). The present study includes the major and trace element geochemistry, and isotopic signatures of the Garhwal and Kumaun Lesser Himalayan (includes OLH and ILH) siliciclastics and argillites and attempts to constrain their source rocks characterisation and provenance.

5.2 Major elements

Major element abundances in the clastic sediments from the Lesser Himalaya are presented in Table 5.1. The Chakrata argillite show a large variation of 59.5to 80.2 wt.% SiO_2; 9.6 to 20.0 wt.% Al_2O_3; 0.3 to 0.8 wt.% TiO_2; 2.9 to 9.9 wt.% Fe_2O_3; 0.02 to 0.2 wt.% MnO; 0.4 to 5.5 wt.% CaO; 1.3 to 2. 1 wt.% MgO; 0.2 to 2.0 wt.% Na_2O; 1.5 to 5.4 wt.% K_2O and 0.05 to 0.4

wt.% P_2O_5. Al_2O_3 content of the argillites ranges from 9.55 to 20.04 wt. % which indicates the presence of clay minerals (secondary weathering products). Among the major elements, the abundance of Al_2O_3 and K_2O is negatively correlated with SiO_2 (Table 5.2). Al and Ti being immobile elements, the Al_2O_3/ TiO_2 ratio may be used to denote the relative compositional loss in clastics as compared to that of protoliths rocks. The Al_2O_3/TiO_2 ratio of the Chakrata argillite ranges from 15-31. The ratio ranges from 3 to 11 for mafic rocks, 11-21 for intermediate rocks, and 21-70 for felsic rocks (Sugitani et al., 1996; Hayashi et al., 1997). Consequently, the Al_2O_3/TiO_2 ratio of the Chakrata argillite suggests these clastics have either derived from felsic source rock or may be as a result of cation loss during intense weathering during their transport and depositions. The K_2O/Al_2O_3 is often used in defining the original composition of source rock (Ramachandran et al., 2016). Shales with K_2O/Al_2O_3 ratio > 0.5 indicate a significant amount of alkali feldspar present in the original shale relative to other minerals (Cox et al., 1995). The K_2O/Al_2O_3 ratio of the Chakrata argillite has an average value of 0.19 indicative of minimum amount of alkali feldspar relative to other minerals.

However, the values of K_2O/Na_2O ratio vary from 1.19 to 19.9, the high values seem to indicate the presence of K-bearing minerals such as K-feldspar, muscovite and biotite (Nath et al., 2000; Osae et al., 2006) in their protoliths. The negative correlation of SiO_2 and K_2O hints towards the richness of quartz grain with decreasing clay content.

Table 5.1: Major elements (wt%) in the clastics of the Lesser Himalaya (Garhwal- Kumaun region).

S.No	Sample no	Na_2O %	MgO %	Al_2O_3 %	SiO_2 %	P_2O_5 %	K_2O %	CaO %	TiO_2 %	MnO %	Fe_2O_3 %	SUM %	LOI %	CIA (m)	CIA* (m)	PIA (m)	CIW (m)	CIW' (m)
1	MN3R	0.54	0.4	3.71	91.7	0.02	1.07	0.29	0.1	0.044	2.73	100.6	1.64	59	64	65	100	81
2	MN3S	1.4	0.24	6.42	85.08	0.07	1.1	0.11	0.1	0.033	2.61	97.16	1.15	63	65	68	100	74
3	MN3T	1.3	0.42	10.24	80.52	0.03	2.05	0.13	0.15	0.05	3.65	98.54	2.14	69	70	77	100	83
4	MN3U	1.57	0.24	6.67	85.32	0.06	1.12	0.08	0.11	0.065	3.43	98.67	1.54	63	64	67	100	72
5	MN3Z	2.95	1.04	8.07	81.17	0.04	2.0	0.76	0.3	0.078	1.21	97.62	2.25	49	53	49	99	62
6	MN4A	2.0	1.28	16.26	66.62	0.06	5.1	0.17	0.64	0.01	3.7	95.84	2.19	64	65	75	100	83
7	MN4B	2.68	0.89	12.5	73.95	0.07	3.6	0.18	0.64	0.007	3.36	97.88	1.67	59	60	65	100	74
8	MN4C	3.36	0.55	9.13	80.45	0.05	1.91	0.12	0.66	0.006	1.8	98.04	1.21	54	55	55	100	62
9	MN4D	3.39	1.27	11.33	75.84	0.03	2.41	0.09	0.26	0.014	2.11	96.74	1.41	58	58	60	100	67
10	MN4F	1.26	1.17	12.8	75.04	0.03	4.37	0.09	0.34	0.006	1.57	96.68	1.7	65	65	78	100	86
11	MN4G	2.03	0.57	8.75	82.25	0.04	2.69	0.07	0.15	0.004	1.08	97.63	1.26	58	58	63	100	72
12	MN4H	1.18	1.39	17.99	66.95	0.06	5.64	0.16	0.17	0.007	1.99	95.54	2.48	68	69	84	100	90
13	MN4I	1.25	1.15	14.7	71.42	0.04	4.93	0.14	0.31	0.007	3.42	97.37	2.47	66	66	80	100	88
14	MN4J	2.33	0.51	7.29	84.86	0.02	1.62	0.05	0.22	0.005	1.02	97.93	0.76	56	57	59	100	66
15	MN4K	0.66	2.06	20.16	56.5	0.07	7.08	0.18	0.92	0.013	6.74	94.38	3.76	69	70	90	100	95
16	MN4L	1.23	0.52	4.05	92.85	0.01	0.71	0.05	0.09	0.006	0.44	99.96	0.81	58	59	61	100	67
17	MN5E	1.7	1.06	11.71	74.47	0.02	2.1	0.58	0.49	0.07	4.21	96.41	1.97	66	70	71	100	81
18	MN5F	1.02	2.03	20.29	62.37	0.03	5.01	0.11	0.72	0.05	5.68	97.31	3.39	74	74	89	100	92
19	MN5G	0.12	0.15	9.72	86.02	0.02	2.21	0.03	0.13	0.0	0.95	99.35	1.23	79	79	97	100	98
20	MN5H	0.19	1.07	23.35	58.02	0.05	6.09	0.07	1.05	0.01	7.6	97.5	2.97	77	77	97	100	99
21	MN5I	1.19	0.65	7.12	82.72	0.06	0.93	0.29	0.27	0.16	3.51	96.9	1.59	67	71	71	100	78
22	MN5J	1.1	2.19	21.37	60.09	0.12	5.24	0.23	1.15	0.02	5.44	96.95	3.84	73	74	88	100	92
23	MN5K	1.23	1.29	13.79	73.44	0.11	3.15	0.74	0.5	0.12	2.78	97.15	3.06	67	72	76	100	87
24	MN5L	1.29	0.68	6.24	84.77	0.05	1.15	1.57	0.19	0.18	1.71	97.83	2.59	51	65	51	99	75
25	MN5M	1.85	0.18	8.64	86.06	0.02	3.03	0.05	0.1	0.0	0.52	100.45	0.79	57	58	63	100	74
26	MN5N	0.65	0.09	3.9	94.1	0.02	1.39	0.02	0.12	0.03	0.6	100.92	0.79	60	60	68	100	78
27	MN5NB	0.38	0.08	3.46	95.49	0.01	1.58	0.03	0.03	0.0	0.25	101.31	0.59	59	60	72	100	85
28	MN5P	1.49	0.54	19.55	67.65	0.05	4.44	0.09	0.53	0.01	3.24	97.59	2.08	72	73	85	100	89

Continued-

S.No	Sample no	Na$_2$O %	MgO %	Al$_2$O$_3$ %	SiO$_2$ %	P$_2$O$_5$ %	K$_2$O %	CaO %	TiO$_2$ %	MnO %	Fe$_2$O$_3$ %	SUM %	LOI %	CIA (m)	CIA* (m)	PIA (m)	CIW (m)	CIW' (m)
29	MN5Q	1.31	2.34	14.51	60.51	0.01	3.27	5.21	0.52	0.026	5.51	93.22	7.3	49	72	49	99	87
30	MN5R	1.46	1.12	17.08	65.68	0.03	3.82	0.04	0.39	0.0	6.17	95.79	1.97	72	72	84	100	88
31	MN5S	0.08	0.1	4.25	94.65	0.01	1.1	0.02	0.15	0.0	0.53	100.89	0.71	76	76	95	100	97
32	MN5T	0.45	0.29	3.55	90.75	0.01	0.62	1.02	0.08	0.22	1.95	98.94	1.92	53	72	54	100	83
33	MN5W	0.08	0.27	8.22	84.19	0.07	2.06	0.1	0.61	0.01	2.62	98.23	1.04	76	78	95	100	98
34	MN5X	0.08	0.97	11.22	77.71	0.07	2.67	0.22	0.58	0.06	3.42	97	1.88	77	79	94	100	99
35	MN5Y	1.6	0.3	6.58	88.62	0.02	1.45	0.07	0.25	0.01	1.14	100.04	0.73	60	61	65	100	71
36	MN6A	0.3	0.32	8.29	83.54	0.05	2.18	0.07	0.14	0.1	2.56	97.55	1.82	74	74	91	100	94
37	MN1S	0.63	1.13	18.38	63.39	0.18	3.99	0.7	0.62	0.07	6.17	95.26	4.46	74	77	86	100	95
38	MN1T	1.37	0.82	19	64.59	0.14	3.89	0.59	0.68	0.046	3.97	95.1	3.59	72	75	82	100	89
39	MN1U	1.11	0.74	15.02	75.48	0.12	2.92	0.45	0.6	0.03	2.62	99.09	2.52	72	75	82	100	89
40	MN1V	1.36	0.92	14.24	71.31	0.11	2.89	0.74	0.43	0.04	5.45	97.49	3.08	68	73	76	100	86
41	MN1W	1.05	1.25	17.76	64.11	0.14	4.04	0.5	0.79	0.049	5.73	95.42	3.29	72	74	84	100	91
42	MN1X	1.55	0.98	13.08	73.22	0.15	2.7	1.02	0.52	0.06	4.89	98.17	3.15	64	70	70	100	84
43	MN1Y	0.46	1.1	19.88	60.86	0.17	5.33	0.64	0.7	0.08	5.37	94.59	4.2	72	75	88	100	96
44	MN1Z	1.23	1.26	14.5	68.45	0.09	2.97	1.16	0.49	0.062	5.12	95.33	3.66	67	73	75	100	88
45	MN2A	1.36	0.91	14.09	71.99	0.09	2.82	0.66	0.41	0.033	4.26	96.62	2.69	69	73	77	100	86
46	MN2B	0.51	1.1	20.95	62.59	0.27	5.32	0.6	0.69	0.014	3.01	95.05	3.38	73	76	89	100	96
47	MN2C	1.25	1.08	15.56	69.4	0.1	3.39	0.91	0.51	0.038	4.18	96.42	3.48	68	73	77	100	88
48	MN2D	0.38	1.06	20.59	61.47	0.09	5.67	0.96	0.7	0.082	5.4	96.4	5.27	71	75	86	100	97
49	MN2E	1.2	1.12	13.98	70.85	0.11	2.92	1.2	0.57	0.107	4.98	97.04	4.21	66	73	73	100	88
50	MN3L	0.79	1.77	16.55	58.47	0.09	4.13	0.09	0.62	0.251	11.59	94.35	4.5	74	74	89	100	93
51	MN3M	0.96	1.85	18.5	55.88	0.17	4.78	0.2	0.7	0.25	10.44	93.73	4.8	72	73	87	100	92
52	MN3N	0.92	2.13	17.26	59.46	0.24	4.27	0.52	0.69	0.254	8.91	94.65	5.54	71	74	84	100	92
53	MN3O	0.87	2.13	18.57	58.3	0.12	4.69	0.23	0.7	0.149	8.36	94.12	4.35	73	74	88	100	93
54	MN3P	0.88	1.7	16.95	65.11	0.08	4.04	0.17	0.57	0.033	5.44	94.97	3.47	73	74	88	100	92
55	MN3Q	1.28	1.51	8.12	76.66	0.05	1.08	0.12	0.25	0.047	6.84	95.96	3.4	70	71	75	100	79

Continued-

S.No	Sample no	Na$_2$O %	MgO %	Al$_2$O$_3$ %	SiO$_2$ %	P$_2$O$_5$ %	K$_2$O %	CaO %	TiO$_2$ %	MnO %	Fe$_2$O$_3$ %	SUM %	LOI %	CIA (m)	CIA* (m)	PIA (m)	CIW (m)	CIW' (m)
56	MN2G	0.01	0.14	0.53	99.56	0.06	0.03	0.07	0.03	0.006	0.45	100.89	0.37	76	92	78	100	97
57	MN2I	0.03	0.46	1.37	97.41	0.1	0.14	0.06	0.09	0.006	0.35	100.02	0.42	82	87	89	100	97
58	MN2J	0.02	0.12	1.38	97.4	0.11	0.23	0.07	0.04	0.002	0.42	99.79	0.38	78	83	88	100	98
59	MN2K	0.08	0.19	4.23	93.51	0.09	0.87	0.05	0.05	0.003	0.15	99.22	0.76	78	80	94	100	97
60	MN2L	0.02	0.13	0.89	99.32	0.05	0.13	0.02	0.03	0.001	0.12	100.71	0.26	81	84	92	100	96
61	MN2M	0.05	0.2	3.06	96.05	0.05	0.61	0.03	0.1	0.001	0.15	100.3	0.61	79	80	95	100	97
62	MN2N	0.05	0.1	2.9	94.94	0.06	0.61	0.04	0.03	0.001	0.09	98.82	0.67	78	80	94	100	97
63	MN2R	0.05	0.01	2.05	94.58	0.04	0.43	0.03	0.16	0.002	0.66	98.01	0.32	77	79	92	100	96
64	MN2Z	0.19	0.15	3.58	94.85	0.02	0.63	0.02	0.03	0.001	0.19	99.66	0.62	78	78	89	100	92
65	MN3A	0.4	0.18	5.94	91.1	0.02	0.99	0.02	0.1	0.001	0.19	98.94	1.3	77	77	88	100	90
66	MN3B	0.08	0.07	4.88	92.49	0.04	1.54	0.05	0.05	0.001	0.42	99.62	0.67	72	73	94	100	97
67	MN3C	0.2	0.14	4.96	92.85	0.02	0.89	0.04	0.07	0.001	0.2	99.37	0.97	78	79	91	100	94
68	MN3D	0.03	0.02	0.65	>95.90	0.02	0.09	0.01	0.02	0.001	0.13	0.97	0.23	80	82	89	100	93
69	MN3E	0.31	0.21	5.88	92.06	0.02	1.1	0.01	0.06	0.001	0.15	99.8	1.08	77	78	90	100	92
70	MN3F	0.12	0.02	2.37	97.73	0.01	0.4	0.01	0.05	0.002	0.1	100.81	0.5	79	79	90	100	92
71	MN3G	0.24	0.14	5.61	93.17	0.02	1.03	0.01	0.05	0.001	0.19	100.46	0.78	79	79	92	100	93
72	MN3H	0.11	0.03	2.16	97.05	0.02	0.37	0.01	0.03	0.001	0.15	99.93	0.37	78	79	90	100	92
73	MN3I	0.39	0.11	5.65	92.04	0.02	0.93	0.02	0.06	0.001	0.2	99.42	0.79	77	77	87	100	90
74	MN3J	0.08	0.07	2.21	96.47	0.02	0.41	0.02	0.03	0.001	0.15	99.46	0.36	78	79	91	100	94
75	MN3K	0.03	0.03	1.24	98.25	0.02	0.23	0.02	0.02	0.002	0.11	99.95	0.24	79	81	92	100	96
76	MN4O	0.11	1.35	11.86	76.06	0.17	3.12	0.24	0.35	0.006	3.36	96.63	2.67	75	77	93	100	98
77	MN4P	0.12	1.8	10.22	78.19	0.14	2.71	0.19	0.2	0.01	3.11	96.69	2.31	75	77	93	100	98
78	MN4Q	0	0.8	3.41	92.64	0.11	0.7	0.14	0.11	0.006	1.66	99.58	1.39	77	82	92	100	100
79	MN4R	0.07	0.74	6.95	87.43	0.17	1.97	0.22	0.12	0.004	1.24	98.91	1.93	73	76	91	100	98
80	MN4S	1.42	0.36	8.77	82.63	0.08	2.34	0.17	0.38	0.085	2.71	98.95	1.85	63	64	70	100	79
81	MN4T	0.06	0.64	1.84	95.53	0.03	0.54	0.05	0.21	0.007	1.2	100.11	0.93	70	73	87	100	95
82	MN4U	0.15	1.25	21.41	58.93	0.19	6.4	0.32	0.69	0.006	5.44	94.79	3.25	73	75	95	100	99

Continued-

S.No	Sample no	Na₂O %	MgO %	Al₂O₃ %	SiO₂ %	P₂O₅ %	K₂O %	CaO %	TiO₂ %	MnO %	Fe₂O₃ %	SUM %	LOI %	CIA (m)	CIA* (m)	PIA (m)	CIW (m)	CIW' (m)
83	MN4V	0.1	0.76	4.69	89.99	0.06	1.87	0.1	0.13	0.003	0.74	98.44	1.34	66	68	89	100	97
84	MN4W	0.08	0.28	3.76	93.46	0.02	1.67	0.04	0.05	0.001	0.27	99.63	0.96	65	66	91	100	97
85	MN4X	0	1.29	3.82	89.84	0.02	1.09	0.04	0.07	0.005	1.18	97.36	1.41	75	76	97	100	100
86	MN4Y	0.15	1.24	12.83	72.91	0.04	3.68	0.06	0.42	0.018	3.38	94.73	3.31	75	75	96	100	98
87	MN4Z	0.05	0.09	1.55	>95.90	0.01	0.82	0.09	0.08	0.01	0.76	3.46	0.8	58	61	74	100	95
88	MN5A	0.04	0.07	0.94	96.55	0.02	0.24	0.05	0.04	0.004	0.89	98.84	0.77	70	74	82	100	93
89	MN5B	0.04	0.02	2.52	95.19	0.04	0.84	0.04	0.06	0.001	0.48	99.23	0.73	71	72	92	100	97
90	MN5C	0.07	0.1	5.11	90.03	0.05	1.58	0.04	0.08	0.001	0.44	97.5	1.4	73	74	95	100	98
91	MN5D	0.02	0	2.15	96.66	0.03	0.7	0.02	0.04	0.001	0.3	99.92	0.88	72	73	95	100	98
92	MN6B	0.32	0.05	2.88	95.64	0.01	0.5	0.02	0.05	BDL	0.03	99.5	0.67	72	73	81	100	85
93	MN1B	0.96	2.04	18.01	61.87	0.11	3.3	0.52	0.68	0.092	6.98	94.56	3.86	75	78	85	100	92
94	MN1C	0.09	0.13	2.08	94.96	0.01	0.41	0.36	0.07	0.002	2.43	100.54	0.33	63	78	68	100	93
95	MN1D	1.56	0.97	12.23	76.27	0.15	1.88	0.52	0.36	0.028	4.46	98.43	2.38	69	73	75	100	83
96	MN1E	1.2	1.79	14.44	67.59	0.13	2.65	1.04	0.58	0.111	5.7	95.23	3.74	69	75	76	100	88
97	MN1F	1.1	1.98	14.22	65.66	0.11	2.39	1.23	0.56	0.079	6.74	94.07	4.04	68	76	74	100	89
98	MN1G	2.0	1.34	12.39	74.43	0.18	2.37	1.21	0.83	0.063	4.65	99.46	2.09	61	68	65	99	79
99	MN1H	1.5	2.8	13.97	63.95	0.38	1.8	1.44	0.57	0.045	9.49	95.95	2.12	68	76	72	100	85
100	MN1I	0.27	2.46	18.63	61.68	0.05	5.38	0.39	0.6	0.019	6.98	96.46	3.9	73	75	92	100	98
101	MN1J	2.44	0.86	8.15	84.21	0.05	2.18	0.41	0.3	0.076	1.52	100.2	1.3	54	56	55	100	67
102	MN1K	0.68	1.71	17.85	63.61	0.11	3.27	0.46	0.74	0.048	6.57	95.05	4.05	77	79	88	100	94
103	MN1L	0.55	1.85	19.14	62.2	0.1	4.05	0.46	0.74	0.041	6.35	95.48	4.32	76	78	90	100	95
104	MN1M	1.3	1.19	12.27	75.67	0.11	1.79	0.45	0.48	0.061	4.41	97.73	2.73	72	75	78	100	85
105	MN1N	1.49	1.06	11.25	78.02	0.1	1.87	0.39	0.55	0.102	3.97	98.8	2.56	69	72	75	100	82
106	MN1O	0.18	0.67	7.11	87.25	0.08	1.31	0.4	0.22	0.009	2.61	99.84	1.68	75	81	85	100	96
107	MN1P	0.28	1.16	10.15	80.92	0.09	2.21	0.7	0.36	0.035	2.91	98.82	2.25	71	78	82	100	96
108	MN1Q	0.17	1.25	9.55	66.32	2.78	1.53	5.5	0.32	0.173	6.24	93.83	5.01	47	83	46	100	97
109	MN1R	0.61	1.67	20.04	59.45	0.09	4.38	0.49	0.75	0.046	5.63	93.16	5.29	75	78	89	100	95

Details about the sample location, stratigraphy etc. are given in Table 3.1

The major element composition of the Chakrata siliciclastic, Rautgara siliciclastics, Chandpur argillite, Chandpur siliciclastics and Nagthat siliciclastics are shown in the Table5.1. The samples from Chakrata region show a strong negative correlation of SiO_2 with all other major oxides. This indicates that the bulk of quartz grains are present in the samples leaving other cations lost during the recycling and transport from protoliths to the depositional sites. All the other major oxides (Al_2O_3, MgO, TiO_2, MnO, CaO, Na_2O, K_2O and Fe_2O_3) showing positive correlations between themselves (Table 5.3). Such a trend is expected as the quartz enrichment is the result of weathering of source rocks loosing cations like (Na, Ca Mg, K etc.). There is a strong positive correlation of Al_2O_3 with K_2O (r = 0.83) suggestive of K-bearing minerals have significant influence on Al distribution. It also suggests that the majority of Al and K is predominantly contributed by clay minerals (e.g., illite) (McLennan et al., 1983; Jin et al., 2006). The Al_2O_3/TiO_2ratio ranges from 20.45 to33.97 indicative of felsic nature of source rock. The average value of ~0.19±0.04 (n=6) of K_2O/Al_2O_3 of the Chakrata siliciclastics indicative of alkali depletion in source rock. The values of K_2O/Na_2O ratio vary from 0.9 to 7.3 with higher values manifests the presence of K-bearing minerals such as K-feldspar, muscovite and biotite (McLennan et al., 1983; Nath et al., 2000; Osae et al., 2006), however such a composition could also arise with intense mobilisation of cations from the source composition during denudation processes. The Rautgara siliciclastic showing a negative correlation of SiO_2 with other oxides. The Al_2O_3/TiO_2 ratios range from 8.8 to 119. The values of K_2O/Na_2O ratio vary from 1.56 to 42.67. TiO_2, Fe_2O_3, MgO, and K_2O exhibit positive correlation with Al_2O_3 (Table 5.4 and 5.5). Increase in the abundance of these elements in the sample indicates enrichment of clay minerals (Nagarajan et al., 2007a, b) and residual phases. In these samples, the K_2O/Al_2O_3 ranges from 0.05 to 0.52. The samples from the Chandpur argillites also show a negative correlation of SiO_2 with all major oxides except Na_2O and CaO (Table 5.6). The K_2O/Al_2O_3 ratio ranges from 0.13 to 0.28 and the Al_2O_3/TiO_2ratio varies from 24.53 to 32.48 suggesting affinity with felsic nature source rocks. There is a positive correlation of K_2O with Al_2O_3, Th and Rb. TiO_2 concentration indicates the presence of Ti-

bearing minerals (Table 5.1). SiO_2 of Chandpur siliciclastic shows negative correlation with all other major oxides, except Na_2O (Table 5.7). K_2O shows a positive correlation with Al_2O_3, Th and Rb which is a manifestation of clay mineral formation during deposition that can attract Thorium (being particle reactive). The Nagthat siliciclastics also shows negative correlation of SiO_2 with other oxides (Table 5.8) suggesting very high quartz residual content resulted after weathering. The moderate amount of K_2O is due to K-feldspars and mica contribution. High content of the Al_2O_3 in the sediment indicate the presence of clay minerals and mica.

Table 5.2: Correlation coefficient of major elements of Chakrata argillite.

Elements	Na$_2$O	MgO	Al$_2$O$_3$	SiO$_2$	P$_2$O$_5$	K$_2$O	CaO	TiO$_2$	MnO	Fe$_2$O$_3$
Na$_2$O	1.00									
MgO	0.20	1.00								
Al$_2$O$_3$	-0.11	0.47	1.00							
SiO$_2$	0.15	-0.60	-0.77	1.00						
P$_2$O$_5$	-0.33	-0.33	-0.55	0.01	1.00					
K$_2$O	-0.35	0.30	0.85	-0.55	-0.48	1.00				
CaO	-0.19	-0.33	-0.65	0.09	0.98	-0.59	1.00			
TiO$_2$	0.51	0.20	0.70	-0.38	-0.60	0.49	-0.68	1.00		
MnO	-0.03	-0.36	-0.50	0.01	0.79	-0.57	0.82	-0.44	1.00	
Fe$_2$O$_3$	0.20	0.86	0.34	-0.72	0.07	0.05	0.07	0.14	0.02	1.00

Table 5.3: Correlation coefficient of major elements of Chakrata siliciclastic.

Elements	Na$_2$O	MgO	Al$_2$O$_3$	SiO$_2$	P$_2$O$_5$	K$_2$O	CaO	TiO$_2$	MnO	Fe$_2$O$_3$
Na$_2$O	1.00									
MgO	0.66	1.00								
Al$_2$O$_3$	0.60	0.97	1.00							
SiO$_2$	-0.61	-0.96	-1.00	1.00						
P$_2$O$_5$	0.34	0.80	0.91	-0.90	1.00					
K$_2$O	0.89	0.89	0.83	-0.81	0.63	1.00				
CaO	0.42	0.59	0.73	-0.73	0.86	0.54	1.00			
TiO$_2$	0.58	0.93	0.90	-0.91	0.71	0.76	0.39	1.00		
MnO	0.77	0.70	0.58	-0.60	0.24	0.75	0.00	0.81	1.00	
Fe$_2$O$_3$	0.03	0.60	0.73	-0.76	0.82	0.24	0.62	0.66	0.15	1.00

Table 5.4: Correlation coefficient of major elements of Rautgara siliciclastic (Garhwal).

Element	Na$_2$O	MgO	Al$_2$O$_3$	SiO$_2$	P$_2$O$_5$	K$_2$O	CaO	TiO$_2$	MnO	Fe$_2$O$_3$
Na$_2$O	1.00									
MgO	-0.06	1.00								
Al$_2$O$_3$	0.31	0.64	1.00							
SiO$_2$	-0.27	-0.73	-0.98	1.00						
P$_2$O$_5$	-0.03	0.67	0.64	-0.70	1.00					
K$_2$O	0.24	0.67	0.97	-0.98	0.66	1.00				
CaO	0.17	0.76	0.81	-0.87	0.92	0.85	1.00			
TiO$_2$	0.35	0.60	0.87	-0.91	0.66	0.89	0.83	1.00		
MnO	0.88	0.12	0.24	-0.28	0.18	0.24	0.34	0.43	1.00	
Fe$_2$O$_3$	0.24	0.79	0.87	-0.94	0.76	0.89	0.92	0.93	0.39	1.00

Table 5.5: Correlation coefficient of major elements of Rautgara siliciclastics (Kumaun).

Element	Na$_2$O	MgO	Al$_2$O$_3$	SiO$_2$	P$_2$O$_5$	K$_2$O	CaO	TiO$_2$	MnO	Fe$_2$O$_3$
Na$_2$O	1.00									
MgO	0.96	1.00								
Al$_2$O$_3$	0.96	0.95	1.00							
SiO$_2$	-0.98	-0.97	-0.99	1.00						
P$_2$O$_5$	0.38	0.27	0.53	-0.46	1.00					
K$_2$O	0.97	0.95	0.99	-0.99	0.49	1.00				
CaO	0.33	0.26	0.09	-0.17	-0.57	0.17	1.00			
TiO$_2$	0.96	1.00	0.96	-0.98	0.29	0.96	0.27	1.00		
MnO	0.83	0.88	0.74	-0.79	-0.17	0.76	0.65	0.88	1.00	
Fe$_2$O$_3$	0.93	0.99	0.90	-0.93	0.15	0.89	0.33	0.98	0.91	1.00

Table 5.6: Correlation coefficient of major elements of Chandpur argillite.

Element	Na$_2$O	MgO	Al$_2$O$_3$	SiO$_2$	P$_2$O$_5$	K$_2$O	CaO	TiO$_2$	MnO	Fe$_2$O$_3$
Na$_2$O	1.00									
MgO	0.12	1.00								
Al$_2$O$_3$	-0.66	-0.19	1.00							
SiO$_2$	0.50	-0.37	-0.78	1.00						
P$_2$O$_5$	-0.34	-0.03	0.56	-0.44	1.00					
K$_2$O	-0.76	-0.05	0.96	-0.83	0.49	1.00				
CaO	-0.20	-0.65	0.26	0.18	0.21	0.20	1.00			
TiO$_2$	-0.50	-0.01	0.94	-0.86	0.57	0.91	0.28	1.00		
MnO	0.06	0.70	0.01	-0.59	0.11	0.13	-0.29	0.29	1.00	
Fe$_2$O$_3$	0.09	0.78	-0.19	-0.46	-0.16	-0.05	-0.58	0.01	0.90	1.00

Table 5.7: Correlation coefficient of major elements of Chandpur siliciclastics.

Elements	Na_2O	MgO	Al_2O_3	SiO_2	P_2O_5	K_2O	CaO	TiO_2	MnO	Fe_2O_3
Na_2O	1.00									
MgO	-0.24	1.00								
Al_2O_3	-0.86	0.47	1.00							
SiO_2	0.45	-0.90	-0.74	1.00						
P_2O_5	0.09	-0.03	0.15	-0.03	1.00					
K_2O	-0.71	0.61	0.97	-0.84	0.24	1.00				
CaO	0.56	0.45	-0.52	-0.06	-0.23	-0.36	1.00			
TiO_2	-0.66	0.36	0.82	-0.53	0.62	0.81	-0.48	1.00		
MnO	0.28	0.69	-0.14	-0.39	0.31	0.02	0.72	0.13	1.00	
Fe_2O_3	0.17	0.72	0.18	-0.72	0.18	0.35	0.33	0.12	0.63	1.00

Table 5.8: Correlation coefficient of major elements of Nagthat siliciclastics.

Elements	Na_2O	MgO	Al_2O_3	SiO_2	P_2O_5	K_2O	CaO	TiO_2	MnO	Fe_2O_3
Na_2O	1.00									
MgO	0.15	1.00								
Al_2O_3	0.03	0.77	1.00							
SiO_2	-0.11	-0.87	-0.96	1.00						
P_2O_5	0.03	0.36	0.46	-0.45	1.00					
K_2O	-0.02	0.72	0.93	-0.89	0.40	1.00				
CaO	0.02	0.42	0.05	-0.24	-0.15	-0.03	1.00			
TiO_2	0.02	0.69	0.79	-0.79	0.57	0.71	0.07	1.00		
MnO	-0.14	-0.07	-0.28	0.19	0.12	-0.38	0.25	-0.18	1.00	
Fe_2O_3	-0.14	0.69	0.77	-0.84	0.38	0.64	0.21	0.75	0.00	1.00

5.3 Trace elements

In addition to the major elements and their ratios, trace elements are also used to determine the provenance and for the understanding of source rock characteristics. However, the trace elements behaviour during sedimentary processes is complex because of the factors such as source rock composition, weathering, physical sorting and diagenetic alterations (e.g. Mackenzie et al., 1971; Taylor and McLennan, 1985; Wronkiewicz and Condie, 1987; Nesbitt et al., 1980). Changes during sediment transport and diagenesis may affect the sedimentary and geochemical record, and therefore prone to uncertainties in the interpretation may occur from this geochemical data (McLennan, 1989). Trace elements, especially the immobile ones like La,

Y, Sc, Cr, Th, Zr, Hf and Nb are useful in tracing the source rock and therefore are the best suited for provenance identification as they are transported quantitatively into clastic sediments during sedimentary process (McLennan et al., 1983). The samples having $Al_2O_3 > 15\%$ are characterized by the higher contents of trace elements. Present study also contains information of trace element concentrations of clastic sediments which are provided in (Table 5.9).

Table 5.9: Trace elements (in ppm) of the clastics of the Lesser Himalayan Formation (Garhwal-Kumaun region).

S.No	Sample Nos	Ba	Cr	V	Sc	Co	Ni	Cu	Zn	Ga	Pb	Th	Rb	U	Sr	Y	Zr	Nb
1	MN3R	224	4	21	BDL	-	15	26	20	8	14	3	39	-	14	8	69	4
2	MN3S	182	26	20	BDL	-	8	5	9	9	22	4	41	-	16	11	75	4
3	MN3T	276	20	29	BDL	-	16	6	11	10	23	3	72	-	19	15	89	5
4	MN3U	187	12	16	BDL	-	11	8	11	9	18	5	42	-	16	13	86	4
5	MN3Z	363	28	28	1.2	-	6	6	BDL	10	25	6	56	-	27	13	279	7
6	MN4A	315	118	73	5.3	-	15	5	8	19	22	13	186	-	30	29	475	14
7	MN4B	249	126	58	4.3	-	12	5	4	14	27	12	129	-	33	22	541	13
8	MN4C	1338	57	47	2.2	-	7	5	1	10	19	11	67	-	100	16	469	10
9	MN4D	338	70	25	1.4	-	14	4	14	12	17	7	90	-	29	21	204	7
10	MN4F	261	95	33	BDL	-	12	5	8	14	23	11	143	-	23	20	506	11
11	MN4G	273	194	16	BDL	-	7	4	BDL	10	14	4	84	-	21	11	138	4
12	MN4H	439	94	20	1.5	-	14	3	2	18	13	5	161	-	21	18	103	5
13	MN4I	362	114	30	1.7	-	15	3	1	17	20	11	180	-	25	27	329	10
14	MN4J	843	66	13	BDL	-	7	3	BDL	9	16	5	51	-	42	9	258	6
15	MN4K	484	103	91	10.7	-	33	4	16	22	25	20	282	-	21	45	325	17
16	MN4L	574	48	BDL	BDL	-	3	3	3	7	11	2	22	-	25	3	58	2
17	MN5E	377	26	48	6.5	-	18	5	57	14	8	16	117	2.5	53	31	241	15
18	MN5F	579	43	90	10.2	-	26	4	60	24	4	25	272	4.3	36	55	277	29
19	MN5G	205	20	10	3	-	2	2	12	7	2	4	73	2.8	6	16	89	2
20	MN5H	560	37	90	14.3	-	24	4	33	20	16	12	266	<1.0	40	36	305	18
21	MN5I	154	27	34	6.1	-	13	34	31	5	10	5	42	<1.0	42	10	169	5
22	MN5J	624	68	119	14.4	-	39	12	46	23	23	18	265	2.8	43	38	245	22
23	MN5K	562	37	47	6.4	-	13	7	32	13	59	12	121	2.7	26	25	213	10
24	MN5L	211	27	18	1.6	-	5	9	182	6	38	4	38	<1.0	21	10	90	4
25	MN5M	410	11	7	2.3	-	<1.0	17	10	8	7	7	90	<1.0	24	15	90	3
26	MN5N	355	13	9		-	-	-	-	-	-	-	-	-	-	-	-	
27	MN5NB	349	9	3	1.5	-	<1.0	5	2	3	3	2	41	<1.0	5	6	53	<2.0
28	MN5P	712	23	41	6.9	-	15	18	101	15	65	12	156	2.4	46	27	167	12
29	MN5Q	422	59	96	7.2	-	18	2	34	17	3	8	216	<1.0	25	32	291	9

Continued-

S.No	Sample Nos	Ba	Cr	V	Sc	Co	Ni	Cu	Zn	Ga	Pb	Th	Rb	U	Sr	Y	Zr	Nb
30	MN5R	401	22	46	12.7	-	30	7	105	19	21	19	192	2.4	81	27	131	18
31	MN5S	193	13	14		-	-	-	-	-	-	-	-	-	-	-	-	-
32	MN5T	83	32	7	2.6	-	2	4	44	3	10	3	24	<1.0	29	7	56	<2.0
33	MN5W	294	27	37	4.5	-	9	4	12	6	8	15	70	4.1	17	16	279	12
34	MN5X	814	34	51	5.9	-	13	5	26	9	5	18	98	4.3	23	20	361	11
35	MN5Y	376	30	15	3.7	-	4	2	17	5	4	8	46	<1.0	18	11	320	5
36	MN-6A	-	19	26	3.7	170.5	3	3	10	4	6	5	73	BDL	104	12	53	2
37	MN1S	700	53	81	8.1	30	31	46	87	20	29	36	197	11.49	283	40	248	16
38	MN1T	443	115	100	11.5	36	31	16	56	19	49	14	175	24.54	82	29	214	14
39	MN1U	372	69	70	6.7	78	18	7	30	13	33	22	120	1.2	60	25	460	14
40	MN1V	282	44	63	5.4	56	25	9	47	14	22	10	134	BDL	68	26	168	9
41	MN1W	422	79	95	9.7	45	32	31	65	20	31	21	204	2.06	95	32	411	18
42	MN1X	354	47	65	7	57	25	61	51	14	28	15	123	0.78	115	27	244	11
43	MN1Y	565	74	109	12.5	26	35	51	71	22	48	17	258	6.36	103	28	193	13
44	MN1Z	410	46	71	11.2	61	24	55	65	14	23	11	133	BDL	82	26	182	9
45	MN2A	304	38	57	5.4	64	21	53	40	13	23	10	112	2.32	72	22	166	8
46	MN2B	565	105	99	8.6	55	27	173	73	22	38	21	202	15.9	93	29	247	14
47	MN2C	365	51	66	6	77	20	24	29	14	25	14	131	2.11	85	25	242	10
48	MN2D	553	92	118	11.6	26	34	9	55	22	37	19	244	BDL	119	27	193	14
49	MN2E	477	83	77	10.5	51	23	20	46	13	23	17	115	1.48	82	27	337	12
50	MN3L	402	56	118	13.2	-	36	27	160	21	14	17	227	-	36	41	185	12
51	MN3M	567	66	130	14.5	-	38	35	86	22	22	20	259	-	51	46	204	13
52	MN3N	456	57	115	14.6	-	31	16	76	21	20	18	230	-	66	44	204	13
53	MN3O	476	59	128	15.3	-	35	19	121	23	17	18	257	-	48	43	205	13
54	MN3P	443	52	104	12.4	-	28	27	115	18	38	16	205	-	36	31	191	12
55	MN3Q	136	27	40	4.6	-	26	29	510	10	35	7	49	-	32	14	105	6
56	MN1B	519	85	115	12.1	37	45	57	93	20	30	20	161	2.5	39	32	241	16
57	MN1K	562	72	109	10.9	44	42	41	103	17	27	18	145	3.02	48	29	242	17
58	MN1L	543	71	115	11.4	33	35	46	79	21	21	18	214	3.28	52	30	209	16

81

Continued-

S.No	Sample Nos	Ba	Cr	V	Sc	Co	Ni	Cu	Zn	Ga	Pb	Th	Rb	U	Sr	Y	Zr	Nb
59	MN1P	417	59	50	5.4	144	13	6	35	11	25	11	93	BDL	12	23	181	9
60	MN1E	467	144	93	9.1	39	39	50	79	17	35	17	129	BDL	44	30	221	13
61	MN1F	376	60	86	9.6	45	47	60	93	16	30	14	114	3.29	35	26	191	13
62	MN1G	698	77	84	8.8	60	22	27	54	14	42	33	99	4.15	101	37	663	19
63	MN1H	259	88	142	10.6	95	33	28	89	14	19	10	99	1.91	86	26	109	8
64	MN1I	520	74	107	12.5	29	26	290	99	22	24	24	321	BDL	10	27	142	14
65	MN1Q	497	41	53	9	43	15	6	39	11	21	8	56	2.74	136	80	127	5
66	MN1R	636	81	117	14.7	36	33	63	83	21	43	25	213	5.74	69	32	253	17
67	MN1D	478	41	56	4.6	58	22	23	50	12	20	9	89	1.96	36	23	141	8
68	MN1J	574	28	25	BDL	186	6	7	2	10	27	8	61	BDL	24	16	348	8
69	MN1M	387	50	68	5.9	64	19	21	39	13	22	15	82	1.92	33	23	189	11
70	MN1N	441	52	66	4.8	94	21	29	39	12	24	19	90	2.35	42	24	189	12
71	MN1O	251	63	33	1.1	124	14	5	42	9	21	5	52	1.26	9	14	119	5
72	MN1C	540	87	41	BDL	264	4	4	0	5	17	1	14	BDL	3	3	120	3
73	MN2G	73	51	2	BDL	-	BDL	6	BDL	5	11	2	2	-	BDL	BDL	71	2
74	MN2I	85	22	4	BDL	-	1	8	BDL	5	12	19	2	-	1	2	201	3
75	MN2J	106	15	10	BDL	-	BDL	9	BDL	6	13	3	8	-	2	3	52	3
76	MN2K	115	55	BDL	BDL	-	1	5	BDL	6	11	10	20	-	4	6	68	3
77	MN2L	93	30	BDL	BDL	-	3	4	BDL	5	12	6	2	-	2	2	48	2
78	MN2M	114	19	6	BDL	-	1	6	BDL	6	12	19	13	-	3	5	124	5
79	MN2N	100	30	BDL	BDL	-	BDL	5	BDL	5	12	9	12	-	2	4	68	2
80	MN2R	72	28	5	BDL	-	1	3	BDL	5	12	24	8	-	3	3	249	6
81	MN2Z	39	71	BDL	BDL	-	6	6	BDL	5	12	3	11	-	9	4	68	2
82	MN3A	116	19	7	0.9	-	2	5	BDL	7	14	5	16	-	20	7	208	4
83	MN3B	272	75	BDL	BDL	-	7	6	BDL	7	16	2	42	-	20	6	60	3
84	MN3C	149	31	8	0.3	-	3	5	BDL	7	13	4	19	-	9	5	113	2
85	MN3D	90	28	BDL	BDL	-	BDL	4	BDL	5	12	3	3	-	3	2	47	2
86	MN3E	164	23	5	BDL	-	2	5	BDL	8	12	3	21	-	11	5	127	3
87	MN3F	113	26	BDL	BDL	-	BDL	5	BDL	6	11	3	8	-	4	4	61	3

Continued-

S.No	Sample Nos	Ba	Cr	V	Sc	Co	Ni	Cu	Zn	Ga	Pb	Th	Rb	U	Sr	Y	Zr	Nb
88	MN3G	101	39	3	BDL	-	6	6	BDL	7	13	4	19	-	9	5	95	2
89	MN3H	49	50	BDL	BDL	-	6	5	BDL	5	12	4	9	-	2	2	44	3
90	MN3I	83	28	6	BDL	-	4	5	BDL	7	13	4	17	-	15	5	129	3
91	MN3J	30	31	BDL	BDL	-	5	5	BDL	6	12	3	7	-	3	3	106	3
92	MN3K	13	64	BDL	BDL	-	5	4	BDL	6	12	3	5	-	1	2	44	2
93	MN-6B	65	14	4	2.8	263.5	BDL	2	3	2	4	3	12	4.1	6	4	36	BDL
94	MN4O	309	9	34	2.3	-	8	3	BDL	12	16	10	87	-	6	17	266	9
95	MN4P	273	92	17	3.2	-	6	3	BDL	10	17	8	82	-	3	13	308	5
96	MN4Q	157	11	6	BDL	-	3	3	BDL	6	15	4	23	-	3	8	141	4
97	MN4R	280	5	8	BDL	-	5	3	BDL	10	15	4	58	-	3	13	198	2
98	MN4S	818	24	41	2.1	-	9	6	BDL	10	17	13	78	-	24	18	250	8
99	MN4T	128	13	15	0.3	-	0	4	BDL	5	28	6	14	-	1	11	753	7
100	MN4U	529	87	78	11.1	-	7	4	BDL	19	21	14	168	-	9	26	332	13
101	MN4V	232	6	10	BDL	-	2	4	BDL	7	15	4	50	-	6	11	214	4
102	MN4W	198	BDL	BDL	BDL	-	1	4	BDL	7	12	1	42	-	6	6	58	3
103	MN4X	130	14	5	BDL	-	5	7	BDL	7	12	4	32	-	1	9	105	3
104	MN4Y	410	112	46	5.2	-	8	12	5	12	49	15	142	-	25	27	764	13
105	MN4Z	172	BDL	BDL	0.5	-	BDL	6	2	5	19	2	27	-	7	6	399	5
106	MN5A	106	20	BDL	1	-	BDL	8	2	6	14	1	8	-	2	10	152	2
107	MN5B	88	42	BDL	BDL	-	1	4	BDL	7	12	4	14	-	11	2	70	3
108	MN5C	70	97	BDL	BDL	-	4	6	BDL	8	13	4	21	-	13	4	107	3
109	MN5D	91	33	BDL	BDL	-	1	4	BDL	6	12	4	9	-	10	2	86	3

Details about the sample location, stratigraphy etc. are given in Table 3.1

BDL- Below Detection Limit

There is a positive correlation of K_2O with Al_2O_3 and Th (Figure 5.1). This indicates that the concentrations of these elements are controlled by the clay minerals (McLennan et al., 1983).
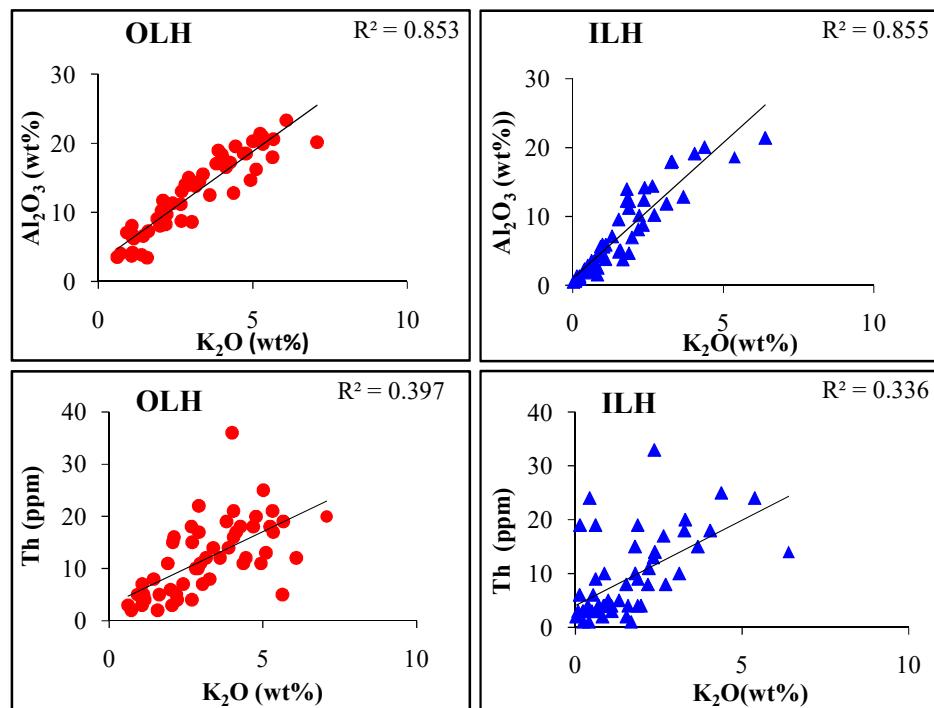
Figure 5.1 Positive correlations of K_2O with Al_2O_3 and Th from Outer and Inner Lesser Himalayan samples; OLH (Chandpur and Nagthat fms), ILH (Chakrata and Rautgara fms).

In the Inner Lesser Himalaya, Ni, Zn and Rb exhibit positive correlations when plotted against Al_2O_3 and K_2O (Figure 5.2), whereas in the outer Lesser Himalaya Ni, and Rb exhibit positive correlations while Zn is poorly correlated with Al_2O_3 and K_2O (Figure 5.3). Positive correlations of Ni, Zn and Rb with Al_2O_3 and K_2O also indicate that these elements are mainly controlled by clay minerals (Nagarajan et al., 2007a, b; Ramachandran et al., 2016) constituting the fine grained clastics. Correlation of Al_2O_3 with Rb suggests that it may be derived from source rock rich in potassium feldspar. As potassium can be replaced by the rubidium (Rb) having ionic radii and charge ratio similar to that of Rb.
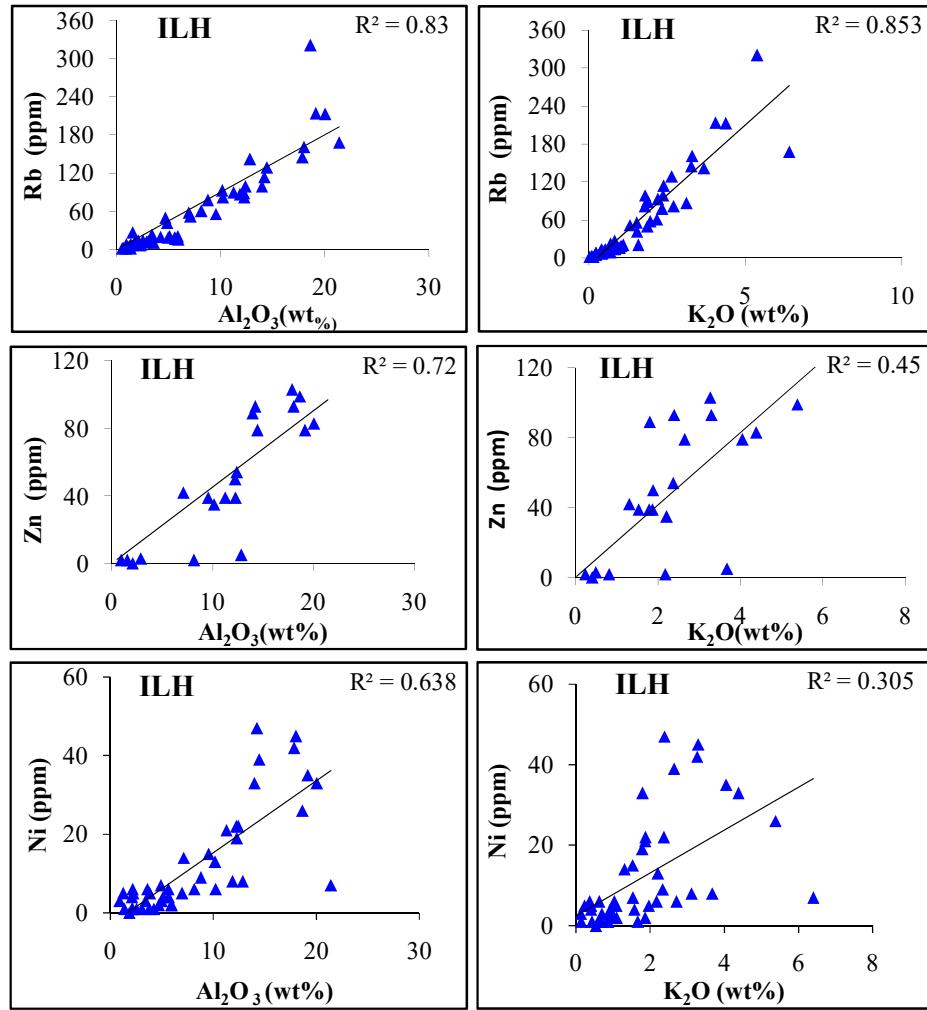
Figure 5.2 Positive correlations of Rb, Zn and Ni with Al_2O_3 and K_2O from Inner Lesser Himalayan samples, ILH (Chakrata and Rautgara fms).

This is also evident from the petrographic observations that show the presence of K-feldspar. The relation between the Al_2O_3 and Ni shows Ni gets saturated with the higher the concentration of Al_2O_3 and the degree of enrichment of Ni shows the degree of absorption of Fe in clay.
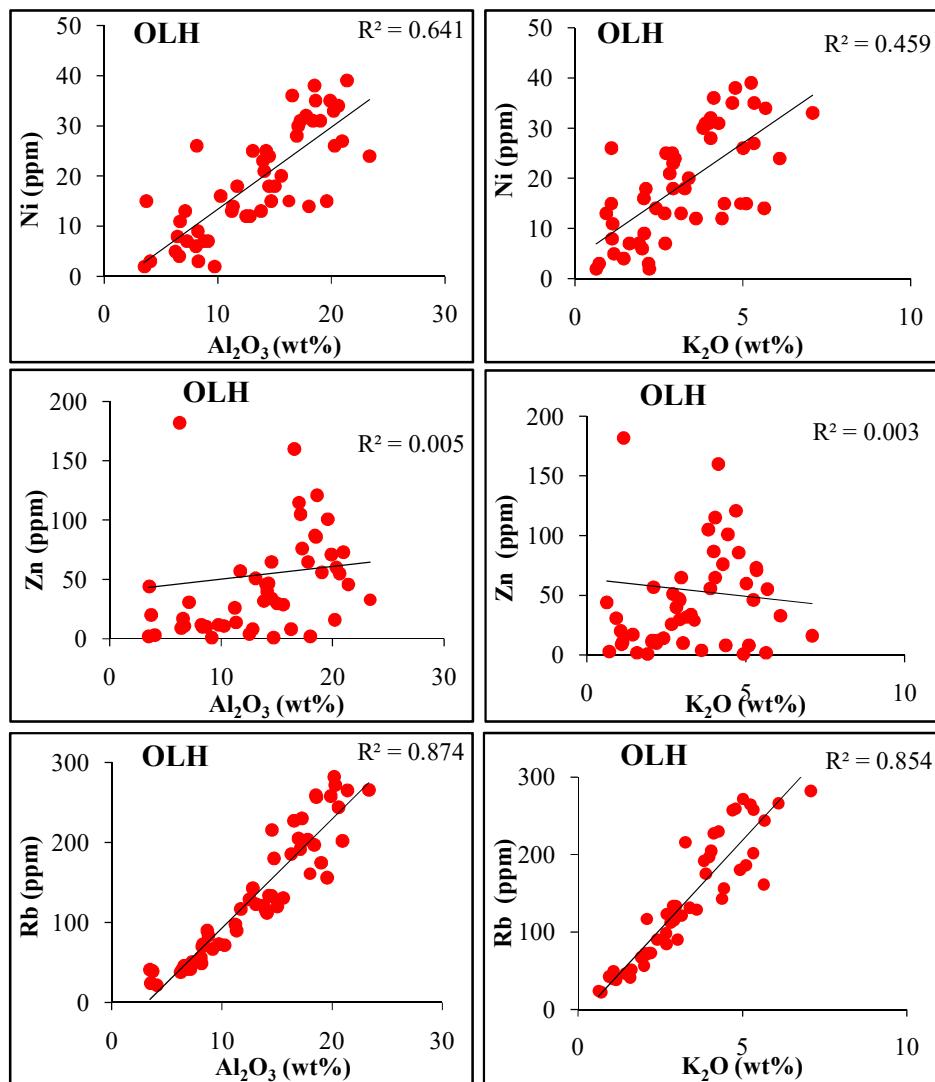
Figure 5.3 Correlations of Ni, Zn and Rb with Al_2O_3 and K_2O from Outer Lesser Himalayan samples OLH (Chandpur and Nagthat fms).

In both the Inner and Outer Lesser Himalaya Nb and Ga shows positive correlation with Al_2O_3 (Figure 5.4). MgO also shows positive correlation with Ni and Zn (Figure 5.5) which suggest that the Ni and Zn are the constituent components of clay minerals (McCann 1991). Sc is mainly below detection limit (BDL) in the Nagthat and Rautgara siliciclastics, and Zn in the former.
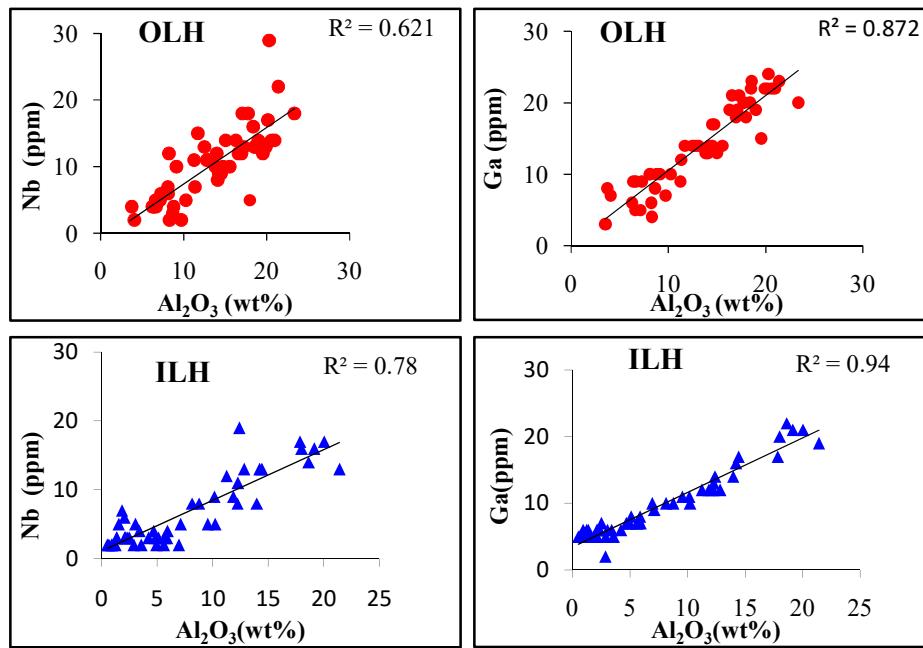
Figure 5.4 Positive correlations of Nb and Ga with Al_2O_3 from outer and inner Lesser Himalayan samples; OLH (Chandpur and Nagthat fms.), ILH (Chakrata and Rautgara fms.).
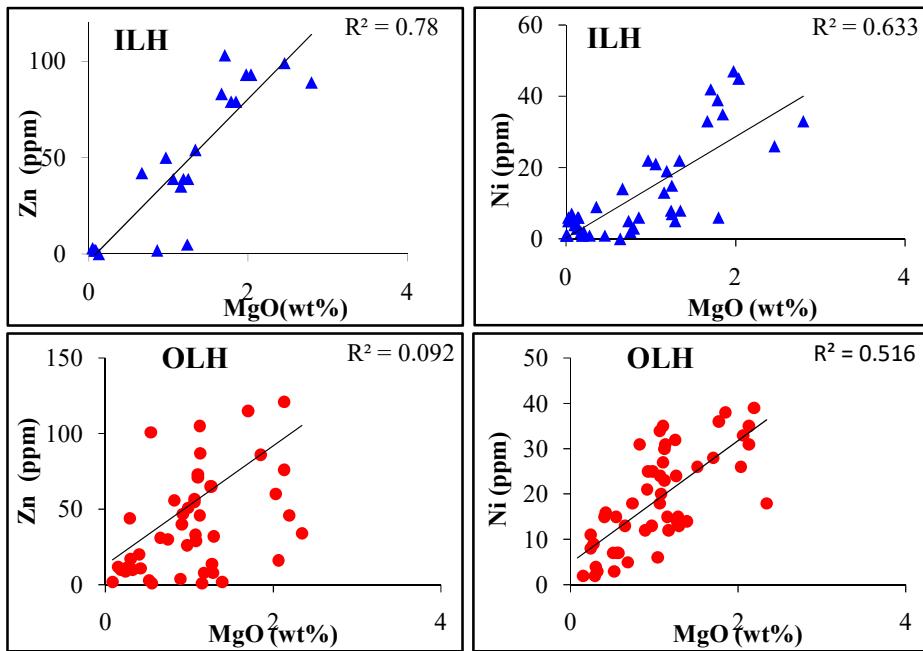
Figure 5.5 Positive correlations of Zn and Ni with MgO from outer and inner Lesser Himalayan samples; OLH (Chandpur and Nagthat fms), ILH (Chakrata and Rautgara fms).

Co is present mainly in Chakrata and Chandpur clastic sediments and exhibit negative correlation when plotted against Al_2O_3, K_2O and MgO (Figure 5.6).
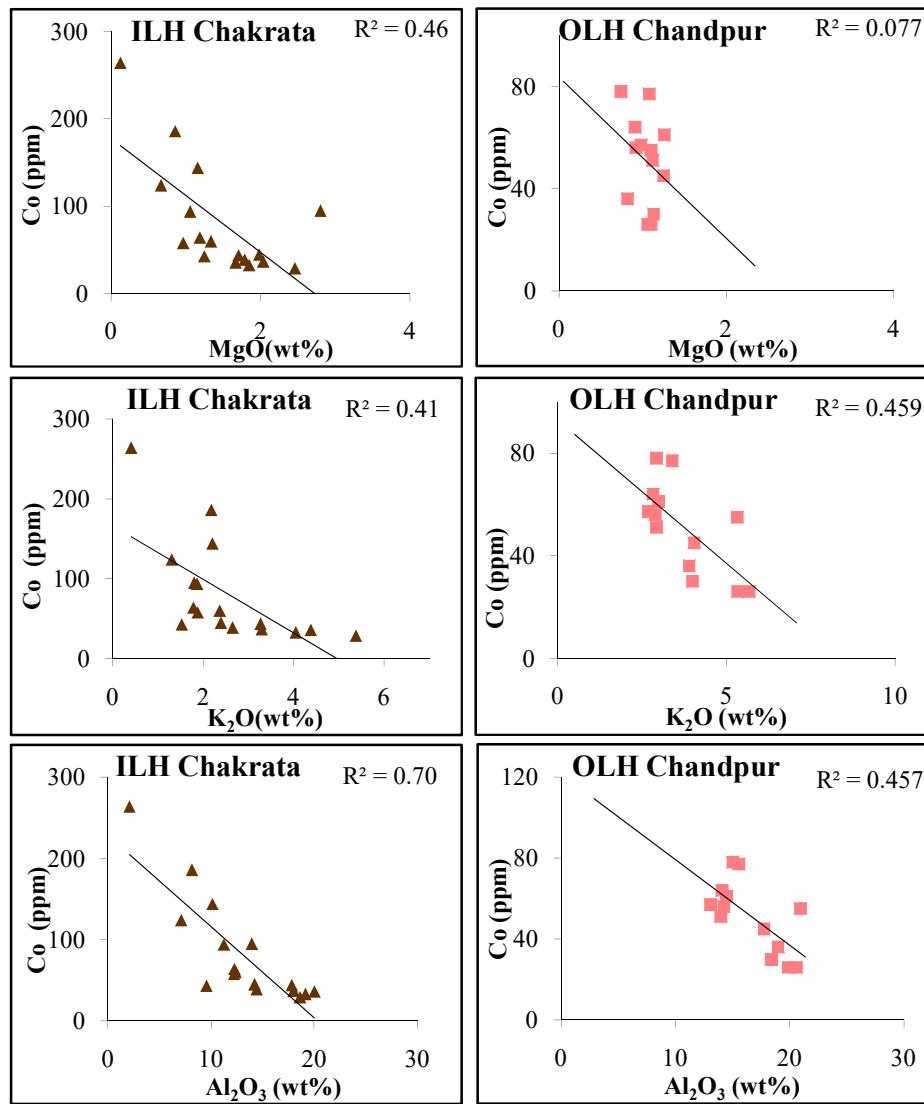
Figure 5.6 Negative correlations of Co with MgO, K_2O and Al_2O_3 from outer and inner Lesser Himalayan samples; OLH (Chandpur and Nagthat fms.), ILH (Chakrata and Rautgara fms.).

SiO_2 showing negative correlation with Cr, Ni and Nb (Figure 5.7) reflects the quartz dilution effect. Higher SiO_2 content in the clastic sediments implies that the important constituents of their provenance be granites and granitic gneisses.
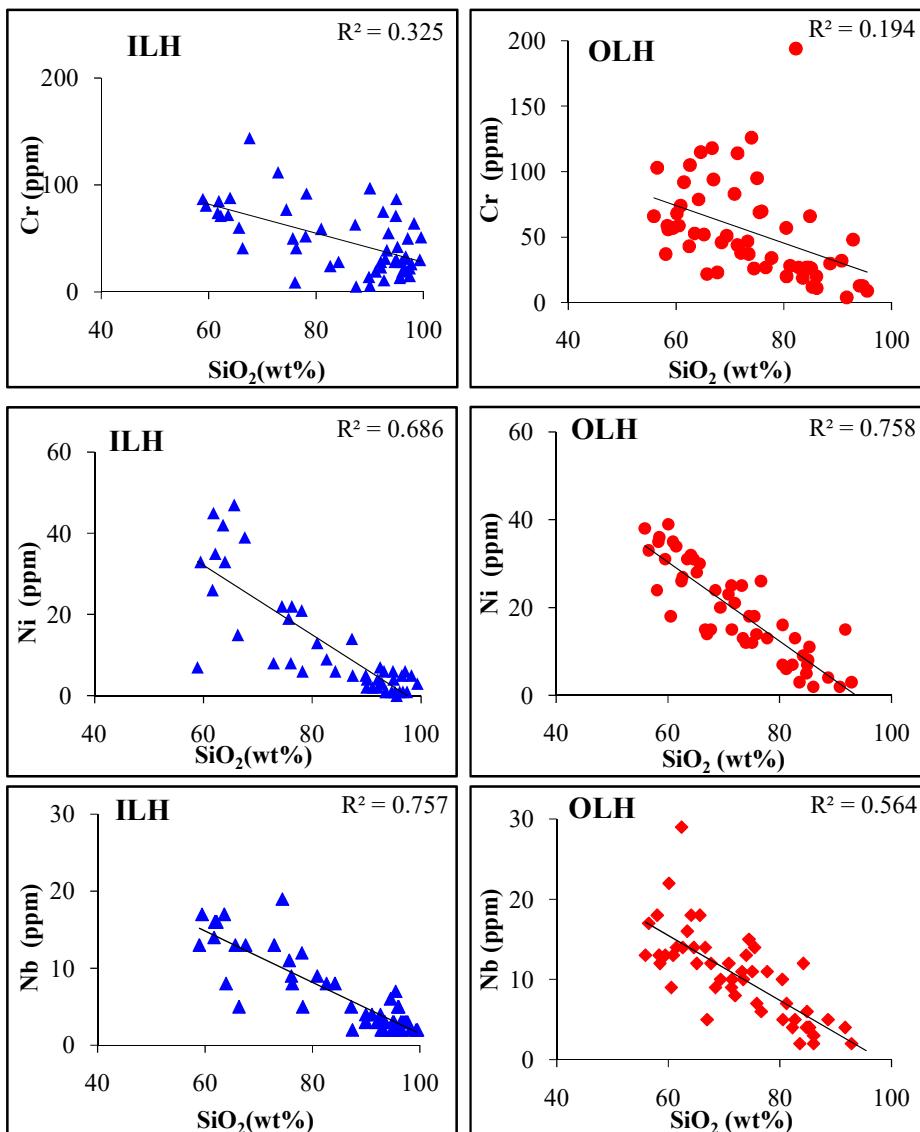
Figure 5.7 Negative correlations of Cr Ni and Nb with SiO_2 from Outer and Inner Lesser Himalayan samples.

The high values of Th/Sc and Zr/Sc ratio in the clastics suggest their concentration in the zircons present. The presence of U content in the Chakrata, Chandpur and Nagthat formation is evident from the Th/U ratio ranging from 2.9- 8.1,0.57-19.2 and 1.4- 7.9, respectively. However, it is found <1.0 ppm in many of the Nagthat siliciclastics. Except in one sample (MN-6B), such a higher U content is not noticed in the Rautgara clastics, may be loss due to weathering and sedimentary recycling under oxidising conditions.

The U^{4+} is less soluble and converts to U^{6+} and prone gets lost during sedimentation (Singh and Khan, 2017). The Th/U ratio of the clastics of the Chakrata and Nagthat formation is higher this may be interpreted as the results of the higher chemical weathering of the source rock and accumulation of Th bearing mineral through sorting. The upper continental Crust (UCC) normalized (McLennan, 2001) plot of the trace elements are plotted in (Figure 5.8). The Sr content of Chakrata, Chandpur and Nagthat are higher than the Rautgara. The low content of Sr in the Rautgara siliciclastics is mainly due to the intensive weathering in the source area. As Sr substitutes for Ca and Mg, mainly supposed to be mobilized during long transportation of these clastics. This also explains that depletion of Se being a member of second group appears to be consistent. The Rb concentration is higher in the Chakrata argillite, Chandpur argillite and Chandpur siliciclastics. Kessler and Ramasamy (2012) suggest that the high Rb concentration indicates that the sediments consist of very fine grain clays and silts. The Zr content is higher in both the parts of the Lesser Himalaya. The higher content of zirconium is mainly due to the concentration of zircon, which indicates the felsic nature of source area (Nagarajan et al., 2017). Ba concentration is quite variables in clastics of the Lesser Himalaya. This could be a result of clay mineral proportion in different types of rock (Nagarajan et al., 2017).
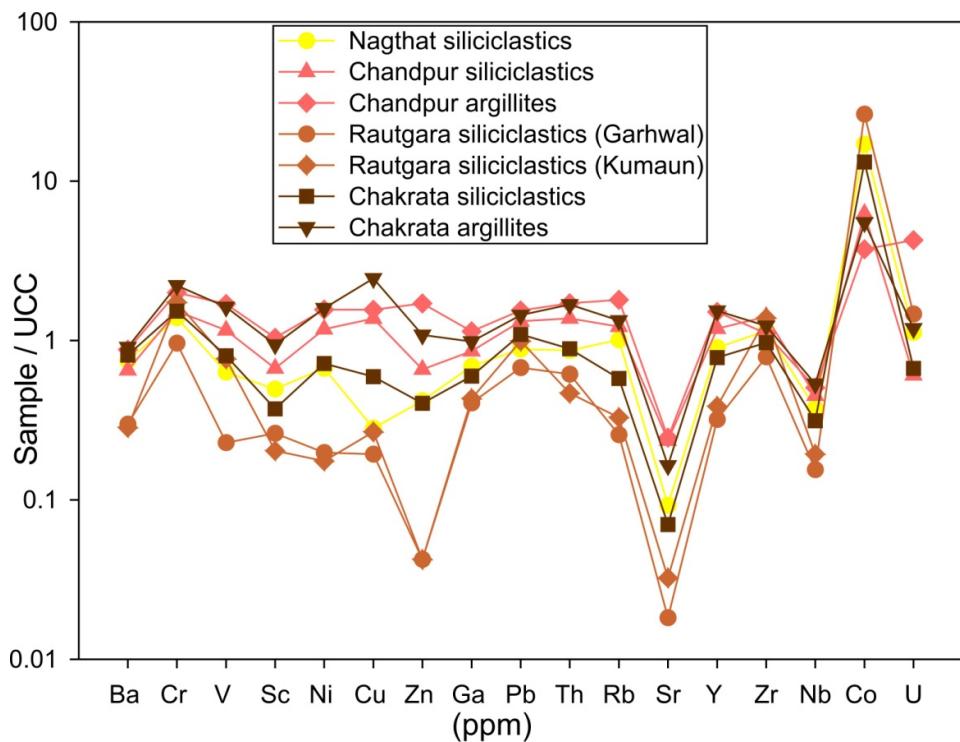
Figure 5.8 UCC normalized trace elements (ppm) plot of the Lesser Himalaya (UCC; McLennan, 2001); Chandpur and Nagthat fms (OLH), Chakrata and Rautgara fms (ILH).

5.4 Weathering intensity-implication for Provenance

As mentioned earlier, the composition of the clastic sediments is mainly affected by the processes of weathering and mixing of sediments. Weathering is not only responsible for changing the composition of the sediments but also removes the mineral grains from the parent rock for sedimentary processes. As most of the mobilization of the cations take place in this process, the original composition of the source rock changes during the course of time from its detachment from the source rock to its deposition after its recycling and transport. The extent of fractionation depends upon the conditions of weathering related to climate. For example, warm and humid climate may result in strong chemical weathering. On the contrary, arid climate is mainly related with weak chemical weathering. During chemical weathering large cations (Rb, Sr) are stable in the weathered residue in preference to

smaller cations such as Na, Ca, K, which are particularly leached out (Nesbitt et al., 1980). However in certain instances like, recoil of the daughter element ([87]Rb) due to radioactive decay it is likely that [87]Sr may loosen and released easily to the solution. The mobile element Ca, Na and K are largely removed from the feldspar during weathering. Such a loss of cations is also reflected in the residual sediment composition of the source rocks and may be assessed by different indices of alterations. Chemical Index of Alteration (CIA) is the widely useful tool for evaluating the degree of chemical weathering in the source area proposed by Nesbitt and Young (1982). The Chemical Index of Alteration is calculated as- $\mathbf{CIA = [Al_2O_3*100/Al_2O_3+CaO*+Na_2O+K_2O].}$ Oxides are expressed in molecular proportions and CaO* is the amount of CaO measured in the silica fraction of the rock. Towards this, the total CaO is corrected by considering that the loss of decarbonation.CIA is suitable for determining the paleo-weathering condition as it monitors the gradual weathering of feldspar to clay minerals (Fedo et al. 1995; Armstrong-Altrin et al. 2004). Concentration of CIA evaluates the progressive alteration of plagioclase and potassium feldspars to clay minerals and is used as an indicator to measure the intensity of weathering in the source area. Removal of labile elements like Ca, Na, K during chemical weathering results in the high value of CIA (Nesbitt and Young, 1982), and low CIA values indicate less or absence of chemical weathering, which reflects cool or arid condition. High SiO_2/Al_2O_3, K_2O/Na_2O and CIA content shows the clastic are derived from upper crustal granitic source and extreme weathering. Nesbitt and Young (1982) and Fedo et *al,*(1995) proposed that the higher CIA values, ranges between 76 and 100, suggest the intensive chemical weathering in the source areas whereas CIA having <50 values indicates less or absence of chemical alteration. The values of CIA for the Lesser Himalaya are given in (Table 5.1). In the present study, the derived CIA values of the Lesser Himalaya clastic sediments ranges between 47 and 81 with an average of 70±8 (n=109). The average CIA value of ILH (Chakrata and Rautgara formations) is 72.7±6.9 and OLH (Chandpur and Nagthat formations) is 66.6±7.5. The CIA values accordingly show a moderate weathering in the source region. The average CIA values are higher than the UCC suggestive of intense weathering of the

source area and indicating warm and humid climate. In certain cases where CaO from the carbonate source is not known, once can use the CIA*. It is called the modified Chemical Index of Alteration (CIA*; Colin et al., 1999) it does not include CaO. The modified Chemical Index of Alteration given by **CIA* = (100*Al$_2$O$_3$/ (Al$_2$O$_3$ + Na$_2$O + K$_2$O).** The average CIA* of the ILH and OLH clastics are 76.3±5.9 and 69.41±6.8, respectively which indicate moderate to extreme weathering of the source region. Weathering of source rock and redistribution of elements during diagenesis can also be determined by using Plagioclase Index of Alteration (PIA; Nesbitt and Young 1982, 1984, Fedo et al., 1995) and Chemical Index of Weathering (CIW; Harnois, 1988). Modified version of CIW (CIW'; Cullers, 2000) used for determining source weathering of carbonate-bearing siliciclastic rocks where CaO is excluded from the CIW. The equation for the PIA, CIW and CIW' are given below.

PIA = {(Al$_2$O$_3$ – K$_2$O) / ((Al$_2$O$_3$ - K$_2$O) + CaO* + Na$_2$O)} x 100   ……..

CIW = {Al$_2$O$_3$ / (Al$_2$O$_3$ + CaO* + Na$_2$O)} x 100   ………………..

CIW'= {Al$_2$O$_3$ / (Al$_2$O$_3$ + Na$_2$O)} x 100   …………………..

The PIA values indicate the intensities of weathering of the clastic samples. The PIA of the ILH and OLH are 85.44±10.53 and 76.5±12.89. CIW values suggest the degree of source weathering in the range from 99 to 100 % (average = 100%). The CIW of the ILH and OLH are 99.9±0.11 and 99.9±0.23. CIW′ values of ILH and OLH are 93.18±6.3 and 85.13±9.93. Average PIA and CIW values (81±13; 100, n=109) indicate higher degree of source weathering than the degree of weathering inferred from CIA values (70±8). PIA calculates the moderate weathering of feldspar to clay minerals (Fedo et al., 1995). PIA values of the clastics from present study suggest intense loss of feldspar during sedimentary process. The CIA, CIA*, PIA and CIW′ values of the inner Lesser Himalaya are higher than that of outer Lesser Himalaya and thus indicating higher degree of weathering in ILH.

The simplified tool to evaluate chemical weathering is the A-CN-K [**Al$_2$O$_3$- (CaO*+Na$_2$O)-K$_2$O**] plot. This diagram depicts the mobility of elements during chemical weathering of the source rock and hence quantifies the degree of chemical modification in sediments after deposition (Nesbitt and

Young, 1982, 1984). Mobile element such as Ca, Na and Sr (corresponding to the intensity of weathering) are lost during weathering (Nyakairu and Koeberl, 2001; Nesbitt et al., 1997). In this plot, Al_2O_3 (A) is plotted at the top apex, at the bottom left CaO* +Na_2O (CN) and at the bottom right K_2O (K) is plotted. This plot helps in understanding weathering trends and mineralogical compositions (Nesbitt and Young, 1984, 1989). It shows that the weathering of the protolith yield Al-rich sediments e.g. kaolinite, gibbsite and chlorite (Bhat and Ghosh, 2001). On the A-CN-K diagram, Lesser Himalayan clastics are plotted in scattered way which indicates that they are derived from different source (Figure 5.9). These data lie above the feldspar join in A-CN-K plot.However, few samples are also plotted below the feldspar join which suggests that they are relatively unweathered (<50). On an average, the Chakrata and Rautgara clastics are clustered near the illite field. It implies that they have more illite than Nagthat and Chandpur clastics and hints to potassium metamorphism, where kaolinite is converted into illite post metamorphism (Nagarajan et al., 2015). However, some of the Nagthat and Rautgara clastics are clustered towards A-K line, indicative of ample separation of Na_2O and CaO from the bulk composition (Khan and Khan, 2015) during chemical weathering. The samples are plotted on a weathering trend derived from TTG, average Granite and UCC. Data sets of tonalite-trondhjemite-granodiorite (TTG) and granite (Condie, 1993); and the average composition of UCC and PAAS (Taylor and McLennan, 1985) has been used. The plot of the present study indicates that these sediments are derived from a felsic source rock.
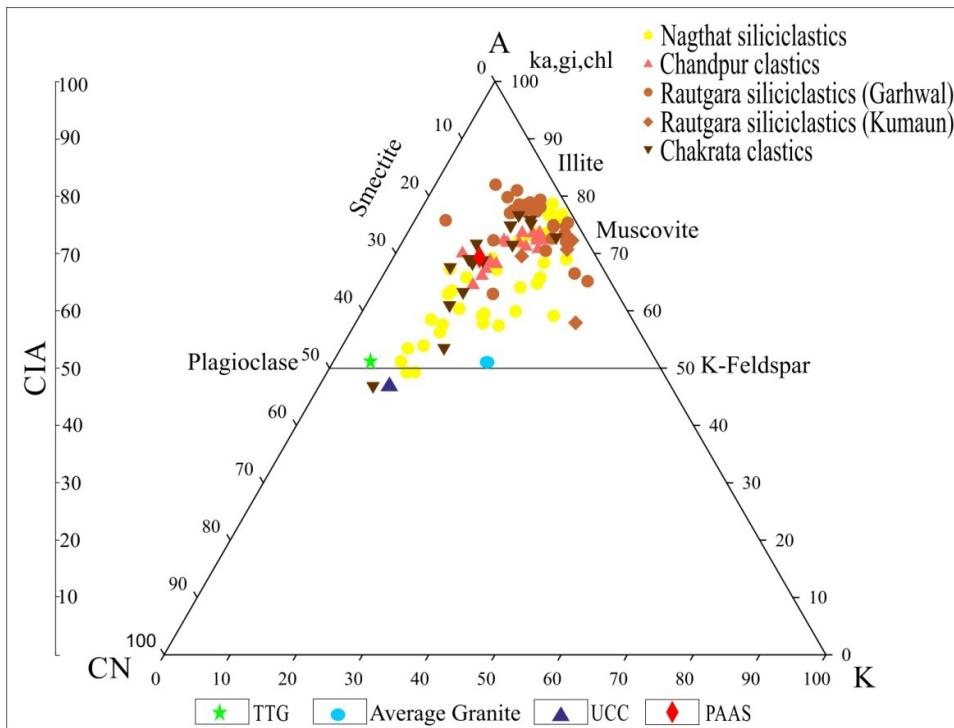
Figure 5.9 A-CN-K ternary plot of the clastics of Lesser Himalayan formation; Chandpur and Nagthat fms (OLH), Chakrata and Rautgara fms (ILH).

5.5 Rare earth elements (REEs)

REEs pattern of the Lesser Himalayan clastic sediments are given in (Table 5.10) which is used as tracers for provenance and diagenesis of clastic sediments. As the elements are less soluble and preserved in the sediments even after going through different alteration processes like low grade metamorphism, weathering and hydrothermal alterations. Therefore, REE ratios (e.g. $(La/Yb)_N$, $(Gd/Yb)_N$, $(La/Sm)_N$, Eu/Eu^*]) of clastic sediments are used as a tool for determining the provenance and bulk source composition (Singh and Rajamani, 2001; Garzanti et al., 2010; Dabard and Loi, 2012). The $(La/Yb)_N$ ratios for Chakrata ranges from 9.23 to 27.37 (average =15.7±4.6,n=17), Rautgara from 4.92 to 56.04 (average=19.21±11.99,n=37). For Chandpur $(La/Yb)_N$ ratio ranges from 13.04 to 20.90, (average=17.01±2.3,n=13) and for Nagthat from 7.38 to 25.35 (average =15.54±4.3,n=37). Also the $(Gd/Yb)_N$ for Chakrata clastics ranges from1.75 to

4.64, (average=2.41±.71) for Rautgara clastics 1.23 to 6.65 (average=2.92±1.3). For Chandpur clastics the $(Gd/Yb)_N$ ratio ranges from 6.65 to 3.42 (average=2.44±.35) and for Nagthat clastics 1.27 to 4.38 (average=2.62±.59). The clastics exhibit high total REE fractionation with $(La/Yb)_N$ ranging from 9.23 to 56.04 (ILH), 7.38 to 25.35 (OLH) and are characterized by relatively higher HREE fractionation with $(Gd/Yb)_N$ ranging from 1.23 to 6.65 (ILH) and 1.27 to 6.65 (OLH). All the clastics in the OLH and ILH formation shows negative europium (Eu) anomaly (Figure 5.10). The HREE depleted, high $(La/Yb)_N$ ratio and negative europium anomaly suggestive of granitic source characteristics of the Lesser Himalayan clastics. Some siliciclastic of the Nagthat and Rautgara Formation are showing the positive Eu anomaly. Eu enrichment in some of the siliciclastic is likely due to the plagioclase enrichment formed during sediment sorting. For felsic rock have higher Th/Cr ratio which ranges from 0.13 to 2.7 whereas it is 0.018 to 0.046 for basic rocks (Cullers, 2000). The present study shows that the Th/Cr ratio for the Outer and Inner Lesser Himalayan clastics ranges from 0.02 to 0. 86 (average 0.28±0.22, n=) and 0.01 to 1.11 (average 0.27±0.26), respectively, which shows that these clastics are derived from felsic sources with minor contribution from basic components. Trace elements, LREE enriched, high Th/Sc, La/Sc indicating felsic source rock and High Rb/Sr reflecting recycled sediments. The range of Th/Sc ratio for the OLH (Chandpur and Nagthat fms.) ranges from 0.832 to 6.47 and for ILH (Chakrata and Rautgara fms.) ranges from 0.89 to 20 suggestive of detrital derivation from felsic source rock. It thus indicates various source areas (Bundelkhand craton and Aravalli craton) for Proterozoic clastics of the Garhwal-Kumaun Lesser Himalayan. According to Sharma, (1998) the Lesser Himalayan gneiss basement represents the northern extension of the Bundelkhand craton and northern Indian shield elements of the Aravalli-Delhi mobile belt thereby implying that the Lesser Himalayan part represents the northern component of the Bundelkhand craton and Aravalli-Delhi mobile belt (Kumar et al., 2013).

Table 5.10: REES (ppm) of the Lesser Himalayan clastics (Garhwal-Kumaun region).

Sample	La	Ce	Pr	Nd	Sm	Eu	Gd	Tb	Dy	Ho	Er	Tm	Yb	Lu	(La/Yb)cn	(Gd/Yb)cn	Ce/Ce*	Eu/Eu*
MN3R	11.50	23.80	2.50	10.20	1.80	0.41	1.22	0.20	1.01	0.20	0.58	0.08	0.44	0.07	18.75	2.29	1.09	0.85
MN3S	15.40	35.20	3.90	16.40	3.26	0.71	3.17	0.40	1.88	0.36	0.93	0.13	0.83	0.13	13.31	3.15	1.11	0.68
MN3T	20.00	43.80	5.00	20.80	3.50	0.78	2.97	0.40	1.98	0.40	1.06	0.15	0.98	0.16	14.64	2.50	1.07	0.74
MN3U	16.80	35.80	4.20	17.30	3.47	0.75	3.34	0.44	2.03	0.40	1.02	0.14	0.93	0.15	12.96	2.96	1.04	0.67
MN3Z	20.00	43.50	4.90	19.60	3.77	0.83	3.39	0.44	2.11	0.43	1.11	0.16	0.98	0.15	14.64	2.85	1.08	0.71
MN4A	44.00	90.00	9.60	36.50	6.58	1.45	6.41	0.89	4.58	0.95	2.53	0.36	2.34	0.38	13.49	2.26	1.07	0.68
MN4B	33.80	67.00	8.20	33.70	7.12	1.31	5.51	0.65	2.95	0.57	1.50	0.21	1.42	0.23	17.07	3.20	0.99	0.64
MN4C	25.00	55.50	6.10	24.40	4.84	1.31	3.84	0.44	2.08	0.42	1.10	0.16	1.04	0.16	17.24	3.05	1.10	0.93
MN4D	34.60	66.70	7.20	27.50	4.78	1.30	5.52	0.77	3.77	0.70	1.65	0.22	1.28	0.20	19.39	3.56	1.04	0.77
MN4E	14.50	32.30	3.50	13.70	2.22	0.69	1.95	0.24	1.14	0.23	0.59	0.08	0.51	0.08	20.39	3.16	1.11	1.02
MN4F	28.00	58.40	6.40	26.10	4.75	1.04	3.55	0.47	2.37	0.47	1.25	0.18	1.17	0.19	17.17	2.50	1.07	0.78
MN4G	18.30	36.00	3.80	14.50	2.48	0.63	2.20	0.29	1.44	0.30	0.76	0.11	0.70	0.11	18.75	2.59	1.06	0.83
MN4H	38.00	86.00	9.60	38.00	2.28	1.41	6.63	0.70	2.82	0.53	1.46	0.20	1.25	0.20	21.81	4.38	1.10	1.11
MN4I	42.00	77.00	9.50	37.50	7.63	1.39	6.47	0.82	3.94	0.81	2.10	0.31	1.98	0.33	15.22	2.70	0.95	0.61
MN4J	12.70	26.20	2.70	10.30	1.68	0.59	1.54	0.20	0.94	0.20	0.56	0.08	0.52	0.09	17.52	2.44	1.10	1.12
MN4K	61.50	128.0	14.00	50.00	10.89	2.07	11.13	1.58	7.75	1.58	4.08	0.56	3.42	0.55	12.90	2.69	1.07	0.58
MN4L	5.10	9.50	1.00	3.50	0.52	0.29	0.58	0.08	0.41	0.09	0.27	0.04	0.30	0.05	12.19	1.60	1.03	1.62
MN5E	39.00	78.00	8.40	33.30	7.22	0.98	6.98	1.01	5.07	1.05	2.64	0.40	2.51	0.40	11.15	2.29	1.06	0.42
MN5F	56.00	115.0	12.10	47.10	9.53	1.38	8.35	1.99	12.33	2.45	6.80	1.01	5.44	0.75	7.38	1.27	1.08	0.47
MN5G	11.40	25.50	3.10	12.70	2.44	0.50	2.16	0.31	1.65	0.37	1.01	0.16	1.05	0.18	7.79	1.70	1.05	0.67
MN5H	52.00	107.0	12.10	49.00	9.73	1.99	7.68	0.93	4.57	0.94	2.49	0.38	2.45	0.40	15.22	2.59	1.05	0.70
MN5I	13.90	28.90	3.10	12.20	2.35	0.51	2.52	0.36	1.75	0.35	0.92	0.14	0.89	0.14	11.20	2.34	1.08	0.64
MN5J	58.00	121.0	13.30	49.00	9.51	1.85	8.03	1.05	5.28	1.10	2.94	0.46	3.00	0.50	13.87	2.21	1.07	0.65
MN5K	31.40	64.30	7.20	29.00	5.31	1.01	4.79	0.64	3.24	0.66	1.78	0.26	1.73	0.29	13.02	2.28	1.05	0.61
MN5L	13.60	27.40	2.90	11.20	2.01	0.42	2.12	0.30	1.48	0.30	0.75	0.12	0.74	0.13	13.18	2.36	1.07	0.62
MN5M	18.30	34.20	3.90	15.00	2.61	0.71	2.22	0.28	1.38	0.27	0.73	0.10	0.68	0.11	19.30	2.69	0.99	0.90
MN5N	8.10	15.10	1.80	6.80	1.09	0.27	1.05	0.15	0.81	0.18	0.48	0.07	0.46	0.07	12.63	1.88	0.97	0.77
MN5NB	6.30	10.70	1.30	4.70	0.69	0.24	0.65	0.09	0.45	0.10	0.26	0.04	0.26	0.04	17.38	2.06	0.92	1.10
MN5P	32.40	67.60	7.90	31.80	5.13	0.99	4.09	0.54	2.76	0.60	1.70	0.26	1.66	0.28	14.00	2.03	1.04	0.66
MN5Q	48.00	93.00	10.00	38.30	6.62	1.16	6.16	0.77	3.56	0.69	1.85	0.27	1.82	0.31	18.92	2.79	1.04	0.56

Continued-

Sample	La	Ce	Pr	Nd	Sm	Eu	Gd	Tb	Dy	Ho	Er	Tm	Yb	Lu	(La/Yb)cn	(Gd/Yb)cn	Ce/Ce*	Eu/Eu*
MN5R	60.00	130.0	13.70	53.50	10.63	1.46	9.41	1.18	5.47	1.08	2.82	0.41	2.55	0.40	16.88	3.05	1.11	0.45
MN5S	19.20	43.00	4.30	17.00	2.82	0.40	2.28	0.27	1.21	0.24	0.66	0.09	0.57	0.09	24.16	3.30	1.16	0.48
MN5T	7.00	14.80	1.80	7.50	1.58	0.32	1.69	0.26	1.21	0.23	0.56	0.08	0.51	0.09	9.85	2.73	1.02	0.60
MN5V	28.60	56.40	7.70	33.90	7.13	1.72	7.37	1.11	5.64	1.22	2.98	0.40	2.50	0.41	8.21	2.43	0.93	0.73
MN5W	35.70	75.20	7.50	29.10	4.72	0.81	4.06	0.43	1.96	0.40	1.09	0.15	1.01	0.17	25.35	3.32	1.13	0.57
MN5X	41.00	82.00	8.20	31.00	5.99	1.01	5.03	0.58	2.61	0.53	1.47	0.21	1.37	0.24	21.47	3.03	1.10	0.56
MN5Y	12.60	27.70	3.00	11.90	2.07	0.52	1.87	0.24	1.16	0.23	0.62	0.09	0.54	0.08	16.74	2.86	1.10	0.81
MN1U	44.40	90.90	9.20	34.70	6.11	0.96	5.06	0.61	3.04	0.62	1.65	0.27	1.74	0.28	18.30	2.40	1.10	0.53
MN1V	30.10	61.00	6.40	25.10	4.65	0.98	4.02	0.55	2.69	0.55	1.42	0.21	1.36	0.22	15.88	2.44	1.08	0.69
MN1W	56.50	115.0	12.20	46.90	8.44	1.55	7.18	0.90	4.30	0.89	2.37	0.34	2.29	0.38	17.70	2.59	1.07	0.61
MN1X	39.00	77.40	8.30	32.40	5.84	1.03	4.89	0.65	3.25	0.68	1.78	0.27	1.65	0.28	16.95	2.45	1.05	0.59
MN1Z	36.10	72.70	7.80	30.60	5.31	1.04	4.56	0.65	3.25	0.72	1.93	0.29	1.95	0.33	13.28	1.93	1.06	0.65
MN2A	26.90	57.70	5.60	22.10	4.11	0.78	3.78	0.54	2.73	0.59	1.53	0.23	1.48	0.25	13.04	2.11	1.15	0.61
MN2C	38.50	82.40	8.30	32.00	5.77	1.07	4.91	0.61	3.05	0.61	1.66	0.25	1.61	0.27	17.15	2.52	1.13	0.62
MN3L	41.50	82.00	8.50	35.90	6.12	1.16	4.49	0.76	3.65	0.67	1.93	0.28	1.55	0.22	19.21	2.39	1.07	0.68
MN3M	51.00	108.0	11.50	44.00	10.24	1.74	6.91	1.13	5.23	0.93	2.65	0.39	2.25	0.33	16.26	2.53	1.09	0.63
MN3N	51.00	108.0	11.40	45.00	10.29	1.72	7.25	1.17	5.32	0.91	2.40	0.32	1.75	0.25	20.90	3.42	1.10	0.61
MN3O	51.40	105.0	10.60	40.40	8.17	1.51	5.90	1.02	4.93	0.90	2.49	0.36	1.91	0.27	19.30	2.55	1.10	0.67
MN3P	40.80	80.50	8.10	33.20	5.84	1.09	4.11	0.72	3.52	0.66	1.94	0.29	1.61	0.24	18.18	2.11	1.09	0.68
MN3Q	15.10	30.00	3.10	13.10	2.52	0.52	2.01	0.36	1.80	0.33	0.93	0.14	0.72	0.10	15.04	2.30	1.08	0.71
MN2G	4.00	7.10	0.80	2.90	0.52	0.08	0.54	0.07	0.36	0.08	0.19	0.03	0.18	0.03	15.94	2.48	0.97	0.46
MN2H	29.40	58.90	7.50	32.70	10.80	3.43	12.72	1.64	7.31	1.27	2.85	0.38	2.39	0.34	8.82	4.39	0.97	0.90
MN2I	10.50	20.00	2.00	6.90	1.07	0.12	0.99	0.13	0.63	0.12	0.31	0.04	0.25	0.04	30.13	3.27	1.07	0.36
MN2J	5.30	11.40	1.20	4.70	0.99	0.18	0.99	0.16	0.86	0.17	0.43	0.06	0.38	0.07	10.00	2.15	1.11	0.56
MN2K	13.70	28.10	3.00	11.20	1.96	0.21	1.41	0.19	0.88	0.17	0.49	0.06	0.36	0.05	27.30	3.23	1.07	0.39
MN2L	7.90	17.50	1.90	7.10	1.31	0.07	1.01	0.14	0.65	0.12	0.30	0.04	0.25	0.04	22.67	3.33	1.11	0.19
MN2M	13.50	28.50	3.00	11.30	2.16	0.18	1.70	0.21	1.03	0.19	0.49	0.07	0.45	0.07	21.52	3.12	1.10	0.29
MN2N	11.90	24.60	2.60	9.70	1.72	0.14	1.59	0.23	1.04	0.20	0.48	0.06	0.38	0.06	22.46	3.45	1.08	0.26
MN2R	10.00	20.30	2.10	7.60	1.38	0.20	1.08	0.12	0.47	0.09	0.23	0.03	0.17	0.03	42.19	5.24	1.09	0.50
MN2Z	9.10	19.40	2.00	7.90	1.38	0.22	1.16	0.15	0.75	0.16	0.40	0.06	0.37	0.06	17.64	2.59	1.11	0.53

Continued-

Sample	La	Ce	Pr	Nd	Sm	Eu	Gd	Tb	Dy	Ho	Er	Tm	Yb	Lu	(La/Yb)cn	(Gd/Yb)cn	Ce/Ce*	Eu/Eu*
MN3A	12.50	25.50	2.70	10.50	1.93	0.44	1.77	0.23	1.16	0.26	0.61	0.09	0.59	0.09	15.20	2.48	1.08	0.73
MN3B	6.70	11.00	1.30	5.00	0.89	0.30	0.81	0.12	0.63	0.14	0.36	0.06	0.35	0.06	13.73	1.91	0.91	1.08
MN3C	14.30	26.00	2.60	9.30	1.37	0.23	1.15	0.16	0.88	0.20	0.52	0.07	0.51	0.08	20.11	1.86	1.05	0.56
MN3D	6.40	12.00	1.30	4.90	0.81	0.11	0.66	0.09	0.40	0.08	0.22	0.03	0.21	0.03	21.86	2.59	1.02	0.46
MN3E	21.10	37.80	3.90	13.90	1.99	0.29	1.71	0.18	0.82	0.17	0.50	0.07	0.48	0.08	31.53	2.94	1.02	0.48
MN3F	3.40	7.70	0.90	3.40	0.78	0.15	0.91	0.15	0.85	0.19	0.47	0.07	0.47	0.08	5.19	1.60	1.08	0.54
MN3G	18.50	37.00	3.90	14.40	2.18	0.28	1.65	0.18	0.87	0.17	0.48	0.07	0.45	0.08	29.49	3.03	1.07	0.45
MN3H	2.50	5.10	0.60	2.30	0.51	0.09	0.62	0.10	0.54	0.12	0.32	0.05	0.32	0.05	5.60	1.60	1.02	0.49
MN3I	14.30	28.00	3.00	11.30	1.86	0.29	1.55	0.18	0.93	0.20	0.57	0.08	0.55	0.09	18.65	2.33	1.05	0.52
MN3J	7.40	14.40	1.60	6.30	1.09	0.20	1.05	0.13	0.62	0.12	0.33	0.05	0.31	0.05	17.12	2.80	1.03	0.57
MN3K	4.70	9.10	1.00	3.90	0.74	0.12	0.71	0.09	0.45	0.09	0.23	0.03	0.23	0.04	14.66	2.55	1.03	0.51
MN4O	14.00	25.40	3.10	12.60	2.64	0.72	2.81	0.41	2.25	0.50	1.37	0.23	1.52	0.27	6.61	1.53	0.95	0.81
MN4P	25.10	47.80	5.50	22.70	4.16	0.87	3.68	0.44	1.88	0.37	1.02	0.15	1.03	0.18	17.48	2.95	1.00	0.68
MN4Q	24.30	49.00	5.90	24.00	4.76	1.08	4.50	0.58	2.83	0.54	1.39	0.20	1.22	0.20	14.29	3.04	1.00	0.71
MN4R	29.00	50.80	6.90	29.20	6.20	1.48	5.83	0.76	3.66	0.74	1.83	0.27	1.63	0.26	12.76	2.95	0.88	0.75
MN4S	32.10	66.30	6.70	25.60	4.63	1.06	4.55	0.61	2.94	0.61	1.61	0.23	1.50	0.25	15.35	2.50	1.11	0.71
MN4T	9.80	19.20	2.50	10.30	2.19	0.49	2.25	0.38	2.27	0.50	1.30	0.20	1.31	0.22	5.37	1.42	0.95	0.68
MN4U	15.60	25.80	3.30	14.50	3.66	1.13	3.92	0.62	3.56	0.83	2.34	0.39	2.63	0.46	4.25	1.23	0.88	0.91
MN4V	16.20	31.60	3.50	13.80	2.68	0.71	2.74	0.37	1.91	0.41	1.05	0.16	1.02	0.17	11.39	2.22	1.03	0.80
MN4W	8.70	15.90	1.80	6.70	1.11	0.27	0.96	0.11	0.47	0.10	0.28	0.05	0.33	0.06	18.91	2.40	0.99	0.80
MN4X	18.90	37.90	4.60	18.80	3.05	0.60	2.55	0.30	1.32	0.26	0.73	0.10	0.68	0.11	19.94	3.09	1.00	0.66
MN4Y	46.00	92.00	9.40	34.20	5.95	0.94	5.50	0.71	3.66	0.80	2.19	0.36	2.32	0.40	14.22	1.96	1.08	0.50
MN4Z	10.00	20.90	2.20	8.80	1.76	0.33	1.68	0.23	1.10	0.23	0.61	0.09	0.61	0.11	11.76	2.27	1.09	0.59
MN5A	5.10	9.40	1.40	6.50	1.69	0.42	2.84	0.50	2.62	0.53	1.13	0.14	0.81	0.13	4.52	2.89	0.86	0.59
MN5B	10.30	19.50	2.20	8.90	1.65	0.34	1.22	0.09	0.28	0.05	0.16	0.02	0.17	0.03	43.46	5.92	1.00	0.73
MN5C	14.30	27.10	3.20	11.90	2.14	0.47	1.72	0.15	0.55	0.10	0.26	0.03	0.24	0.04	42.74	5.91	0.98	0.75
MN5D	12.50	23.00	2.60	10.10	1.59	0.30	1.29	0.13	0.44	0.07	0.21	0.03	0.16	0.03	56.04	6.65	0.99	0.64
MN1B	44.50	90.00	9.40	36.50	6.41	1.24	5.20	0.64	2.95	0.57	1.45	0.22	1.41	0.24	22.64	3.04	1.08	0.66
MN1C	5.10	10.90	1.10	3.90	0.58	0.13	0.55	0.09	0.46	0.10	0.27	0.04	0.26	0.04	14.07	1.75	1.13	0.70
MN1D	25.80	54.20	5.60	22.40	4.24	0.89	4.01	0.56	2.92	0.61	1.55	0.24	1.54	0.25	12.02	2.15	1.11	0.66

Continued-

Sample	La	Ce	Pr	Nd	Sm	Eu	Gd	Tb	Dy	Ho	Er	Tm	Yb	Lu	(La/Yb)cn	(Gd/Yb)cn	Ce/Ce*	Eu/Eu*
MN1E	46.90	94.10	9.90	38.00	6.96	1.26	5.90	0.80	3.88	0.77	2.04	0.30	2.06	0.34	16.33	2.36	1.07	0.60
MN1F	37.30	74.90	7.90	29.80	5.25	1.07	4.45	0.60	3.05	0.62	1.63	0.25	1.61	0.26	16.62	2.28	1.07	0.68
MN1G	86.50	174.0	18.40	71.00	12.76	1.84	11.41	1.61	8.19	1.76	4.49	0.67	4.24	0.66	14.63	2.22	1.07	0.47
MN1H	23.30	48.60	5.30	21.60	4.56	0.86	4.56	0.74	4.00	0.84	1.99	0.28	1.81	0.29	9.23	2.08	1.07	0.58
MN1I	60.80	124.0	13.10	50.50	7.86	1.33	7.28	1.07	5.56	1.17	3.10	0.47	3.06	0.50	14.25	1.96	1.08	0.54
MN1J	17.90	32.20	4.00	15.60	2.93	0.71	2.44	0.34	1.65	0.35	0.90	0.14	0.89	0.15	14.43	2.26	0.93	0.81
MN1K	55.50	114.0	12.00	44.00	7.07	1.47	5.74	0.74	3.74	0.78	2.11	0.34	2.26	0.37	17.62	2.10	1.08	0.71
MN1L	46.70	94.00	10.00	38.40	6.64	1.16	5.82	0.90	4.79	1.09	2.99	0.48	3.24	0.55	10.34	1.48	1.07	0.57
MN1M	39.60	77.60	8.20	30.50	5.15	0.87	4.40	0.58	2.81	0.55	1.47	0.21	1.43	0.23	19.86	2.54	1.06	0.56
MN1N	58.00	112.0	11.90	44.80	7.29	1.25	5.76	0.67	3.00	0.60	1.62	0.24	1.52	0.25	27.37	3.13	1.05	0.59
MN1O	17.80	37.20	3.80	15.00	2.59	0.61	2.71	0.38	1.87	0.38	0.97	0.14	0.93	0.15	13.73	2.40	1.11	0.70
MN1P	34.20	65.40	7.50	28.80	5.26	0.89	4.37	0.59	2.76	0.54	1.41	0.21	1.33	0.21	18.44	2.71	1.00	0.57
MN1Q	63.00	143.0	17.30	85.00	22.00	6.08	25.30	3.70	18.70	3.50	7.40	0.84	4.50	0.66	10.04	4.64	1.06	0.79
MN1R	72.40	147.0	15.40	57.30	9.65	1.52	7.71	1.05	5.22	1.11	3.06	0.49	3.34	0.57	15.55	1.90	1.08	0.54

Details about the sample location, stratigraphy etc. are given in Table 3.1

cn-chondrite normalized
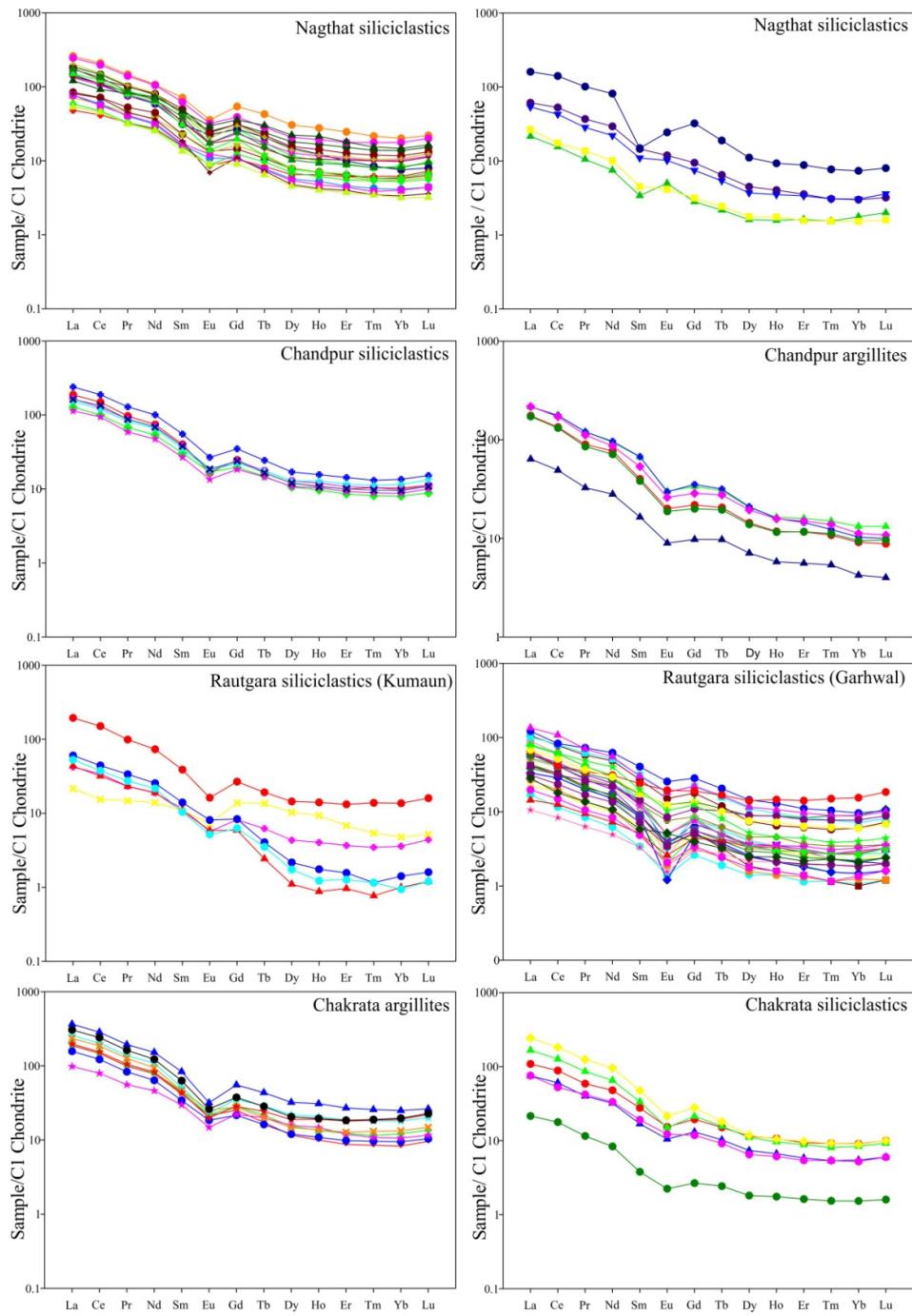
Figure 5.10 C1 chondrite normalized REEs (ppm) plots of Outer and Inner Lesser Himalayan clastics (C1 Chondrite; Sun and McDonough, 1989).

5.6 Isotopic characteristics (Sr-Nd)

Since the isotopes of Sr and Nd are not much affected by the crustal processes and climate, their signatures are widely used for understanding the provenance characteristics (Singh et al., 2008).Towards this, a two-isotope plot ($^{87}Sr/^{86}Sr$ vs. εNd) is used to understand the provenance characteristics of the Lesser Himalayan clastics. Strontium is an alkaline earth element which is reasonably soluble in water and hydrous fluids. It is a moderately mobile element with ionic radius (113 picometer) which substitutes for Ca (99 picometer) to varying degrees in the Ca bearing minerals like plagioclase, calcite, apatite, limestone and gypsum etc. ^{87}Sr is one of its four isotopes (^{88}Sr, ^{87}Sr,^{86}Sr&^{84}Sr) which is also produced from the radioactive decay of ^{87}Rb with half-life of 48.8 By. Therefore, the $^{87}Sr/^{86}Sr$ of any rock depends upon the initial Rb/Sr ratio of the parent rock and its age which may provide the radiogenic strontium (^{87}Sr) to grow during the course of time.

^{147}Sm decays to ^{143}Nd by alpha decay process with a long half-life of 106 Ga resulting small variations in Nd isotopic composition and therefore inquires their precise measurement. Sm and Nd are both intermediate rare earth elements and generally have a +3 valence. The ionic radius of REEs shrinks systematically from 115 pm for La (A=57) to 93 pm for Lu (A=71). They form predominately ionic bonds with oxygen in the solid Earth and therefore their ionic radius controls the observed variation in their abundances in rocks, minerals, and solutions. The ionic radii of Sm and Nd, which are very close and separated by only 4 pm (Nd=108, Sm=104). The ionic radii and relatively high charge of the REEs make them unsuitable in many mineral lattices and therefore they are identified as moderately incompatible elements. The Proterozoic clastic sediments (siliciclastics and argillites) of the Garhwal Lesser Himalaya has been analysed for their isotopic (Sr–Nd) composition. The present study shows that $^{87}Sr/^{86}Sr$ and $^{143}Nd/^{144}Nd$ values in these clastic rocks vary from 0.7392 to 1.4789 and 0.5116±0.0004, respectively. The εNd values of these sediments exhibit a range from -6.7 to -37.6 hints towards diverse provenance for these clastic sediments.

5.7 ^{87}Sr/^{86}Sr and ^{143}Nd/^{144}Nd of the Lesser Himalayan clastics

The Sr and Nd isotopic data for all the samples is given in Table 5.11. Sr concentration in these clastic rocks varies in the range of 0 .4 to 105 ppm and the values of ^{87}Sr/^{86}Sr ratio are in the range of 0.7392 to 1.4789. The samples are showing crustal signatures. This indicates that the Lesser Himalayan sediments getting their detritus from different regions of Indian craton. The εNd values ranges from -6.7 to -27.3 for OLH and -14.6 to -37.6 for ILH. εNd value of Chakrata clastics ranges from -14.59 to -37.98 whereas -16.19 to -31.37 for Rautgara, Garhwal region, -27.3 to -15.0 for Rautgara, Garhwal region, -15.42 to -19.56 for Chandpur and -6.66 to -15.06 for Nagthat. This shows that the ILH clastic sediments have more negative εNd values than that of the OLH. ^{87}Sr/^{86}Sr ratio of ILH for Garhwal region ranges from 0.7445 to 0.9386 for Chakrata Formation and 0.7434 to 1.4788 for Rautgara Formation, 0.7529 to 0.9864 for Rautgara, Kumaun region. Similarly, ^{87}Sr/^{86}Sr ratio for OLH ranges from 0.7392 to 0.8638 for Chandpur Formation and 0.7476 to 0.8105 for Nagthat Formation. The Sr and Nd isotopic composition for samples are plotted on a two-isotope diagram (Figure 5.11a). The possible peninsular sources, Bundelkhand craton and Aravalli craton for these sediments are also plotted in the diagram.

Among these end members the Bundelkhand craton showing range of radiogenic ^{87}Sr/^{86}Sr ratio from 0.71–1.24 and εNd from − 26.86 to -47.46 (Chakrabarti et al., 2007; Joshi et al., 2016) (Table 5.12). The Aravalli craton are more radiogenic in Sr but less in εNd with typical value of Sr is 0.71–1.79 and εNd is −30.30 to 0.82 (Dhar et al., 1996, Rathore et al., 1999, Pandit et al., 2003, George and Ray, 2017) as compared to Bundelkhand craton. The comparison of our data with the values from the peninsular sources suggests the possible sources for the ILH and OLH are the Aravalli craton and the Bundelkhand Craton (Figure 5.11a).

Table 5.11: Sr- Nd isotopic concentration in the silicate fraction of the Proterozoic Garhwal-Kumaun Lesser Himalayan clastics.

S.No	Sample Nos	$^{87}Sr/_{86}Sr$	$[Sr]_{ppm}$	$^{143}Nd/^{144}Nd$	$\varepsilon Nd_{(CHUR)0}$	$[Nd]_{ppm}$
1	MN-3S	0.7787	12.3	0.5123	-6.7	8.2
2	MN-3T	0.7876	15.8	0.5123	-7.0	11.0
3	MN-3Z	0.7857	21.4	0.5119	-13.5	9.5
4	MN-4A	0.8105	27.2	0.5120	-13.3	21.1
5	MN-4B	0.7727	31.5	0.5121	-11.0	17.3
6	MN-4C	0.7476	59.0	0.5120	-12.4	12.4
7	MN-4D	0.7777	22.2	0.5119	-15.1	15.0
8	MN-1U	0.7522	53.9	0.5116	-19.6	20.6
9	MN-1V	0.7524	61.9	0.5117	-19.1	13.9
10	MN-1W	0.7579	84.1	0.5117	-19.2	25.6
11	MN-1X	0.7392	105.1	0.5116	-19.5	18.5
12	MN-1Z	0.7504	71.0	0.5116	-19.5	15.6
13	MN-2A	0.7495	65.9	0.5117	-19.2	12.6
14	MN-2C	0.7488	75.6	0.5117	-19.2	17.2
15	MN-3L	0.8575	23.9	0.5118	-16.9	14.6
16	MN-3M	0.8511	30.1	0.5118	-15.5	26.0
17	MN-3N	0.8638	25.0	0.5118	-15.4	24.5
18	MN-2G	0.7434	0.4	0.5112	-27.5	0.7
19	MN-2I	0.8465	0.6	0.5110	-31.4	2.7
20	MN-2J	1.1591	1.3	0.5116	-20.9	1.7
21	MN-2L	0.8664	0.9	0.5112	-28.2	3.3
22	MN-2M	0.9554	1.6	-	-	-
23	MN-2R	0.8877	1.5	0.5112	-27.9	4.5
24	MN-2Z	0.8094	7.5	0.5114	-24.8	4.3
25	MN-3A	0.7995	15.6	0.5114	-25.0	5.7
26	MN-3B	0.7498	13.8	0.5118	-16.2	2.6
27	MN-3C	0.8210	7.1	0.5111	-29.2	4.9
28	MN-3D	0.7860	2.1	0.5113	-26.8	2.2
29	MN-3E	0.8248	8.0	0.5112	-28.9	7.1
30	MN-4Q	1.4789	1.3	0.5113	-25.2	9.2
31	MN-4R	1.2744	2.5	0.5114	-23.9	11.4
32	MN-4S	0.8204	14.7	0.5117	-19.1	12.8
33	MN-4Y	0.9864	21.9	0.5114	-23.7	22.1
34	MN-4Z	0.9207	5.1	0.5115	-21.2	3.2
35	MN-5A	0.8244	1.5	0.5119	-15.0	2.6
36	MN-5B	0.7529	9.2	0.5114	-24.7	5.9
37	MN-5C	0.7642	11.9	0.5112	-27.3	7.3
38	MN-1G	0.7445	98.0	0.5116	-19.9	32.4
39	MN-1H	0.7488	92.4	0.5117	-18.1	14.3
40	MN-1J	0.7797	22.0	0.5119	-14.6	8.9
41	MN-1N	0.7870	40.0	0.5115	-21.9	25.9
42	MN-1O	0.9386	6.0	0.5116	-19.8	8.7
43	MN-1P	0.8903	6.4	0.5101	-37.6	18.8

Details about the sample location, stratigraphy etc. are given in Table 3.1

The histogram of εNd values for the Lesser Himalaya (OLH and ILH) and the potential sources shows an overlapping trend (Figure 5.11 b and c). The variation in the εNd of the Lesser Himalayan sediments suggests multiple source area for these sediments. The ILH showing highly negative εNd values and high $^{87}Sr/^{86}Sr$ ratios show the Bundelkhand craton as a potential provenance whereas OLH had multiple sources.The $^{87}Sr/^{86}Sr$ ratio of the Chandpur and Berinag Formation are 0.79±0.03 (n= 6) and 0.88± 0.27(n=3) (Ahmad et al., 2000). Also the $^{87}Sr/^{86}Sr$ values from the Vindhyan Supergroup by Awasthi et al., 2018 is 0.83 ± 0.20 (n= 43). Aravalli has $^{87}Sr/^{86}Sr$ value 0.94 ±0.28 (n=52) and Bundelkhand has 0.89 ± 0.25($n = 4$) (Table 5.12).

Sample collected from Jaunsar Group yield εNd values-11.3 ± 3.3 ($n = 7$) for Nagthat Formation and -18.3 ± 1.7($n = 10$) for the Chandpur Formation. These values are similar to the reported value of -17 from the Neoproterozoic strata of the Jaunsar group (Kumaun Himalaya) (McKenzie et al, (2011). Ahmed et al, (2000) also reported the similar εNd isotopic values -17.9±0.5 (n=6) from Chandpur Formation, Garhwal region. The Aravalli craton having εNd value $−13.23 ± 9.8$ ($n = 15$) (Table 5.12). On the basis of isotopic between the OLH and Aravalli craton similarities it is suggested that the OLH received maximum sediments from the Aravalli craton. The values of the εNd for the Bundelkhand craton ranges from $− 34.95 ± 7.99$($n = 5$) (Table 5.12).

Table 5.12: Isotopic characteristics of sources to the Lesser Himalayan clastics (Garhwal-Kumaun region).

	Major lithology	$^{87}Sr/^{86}Sr$	Average $^{87}Sr/^{86}Sr \pm 2\sigma$	εNd	Average εNd ± 2σ
Present study					
Nagthat	siliciclastics	0.75–.81	0.78 ± 0.02($n = 7$)	− 15.1 to − 6.7	− 11.3 ± 3.3($n = 7$)
Chandpur	siliciclastics and argillites	0.74–.86	0.78 ± 0.05($n = 10$)	− 19.6 to − 15.4	− 18.3 ± 1.7($n = 10$)
Rautgara (Garhwal)	siliciclastics	0.74–1.48	0.92 ± 0.21($n = 15$)	− 31.4 to − 16.2	-25.3 ± 4.2($n = 14$)
Rautgara (Kumaun)	siliciclastics	0.75– .99	0.85 ± 0.10($n = 5$)	− 27.3 to − 15.0	− 22.4 ± 4.7($n = 5$)
Chakrata	siliciclastics and argillites	0.74– .94	0.81 ± 0.08($n = 6$)	− 37.6 to − 14.6	− 22.0 ± 8.0($n = 6$)
Peninsular cratonic source					
Aravalli Delhi Supergroup[a]	Biotite granite gneiss, Aplitic leucogranite, Hornblende-biotite. granodiorite and Granite, Quartzite, Schist, calc silicate and metapelite	0.72–1.79	.94 ±0.28 (n=52)	−30.30 to 0.82	−13.23 ± 9.8 ($n = 15$)
Chota Nagpur plateau (CNP)[b]	Gneisses, migmatites, granites, meta–basic rocks and schists along with their sedimentary derivatives	0.76–0.98	0.89 ± 0.13($n = 29$)	− 48.8 to − 4	− 31.9 ± 24.2($n = 32$)
Bundelkhand Granite[c]	Granite, K-granitoids, TTGs	0.71–1.24	0.89 ± 0.25($n = 4$)	− 26.86 to - 47.46	− 34.95 ± 7.99($n = 5$)

(a) M.K. Pandit et al, (2003); Dhar et al, (1996); Rathore et al, (1999); George and Ray, (2017)
(b) Awasthi et al, (2018)
(c) Chakrabarti et al, (2007); Joshi et al, (2016)
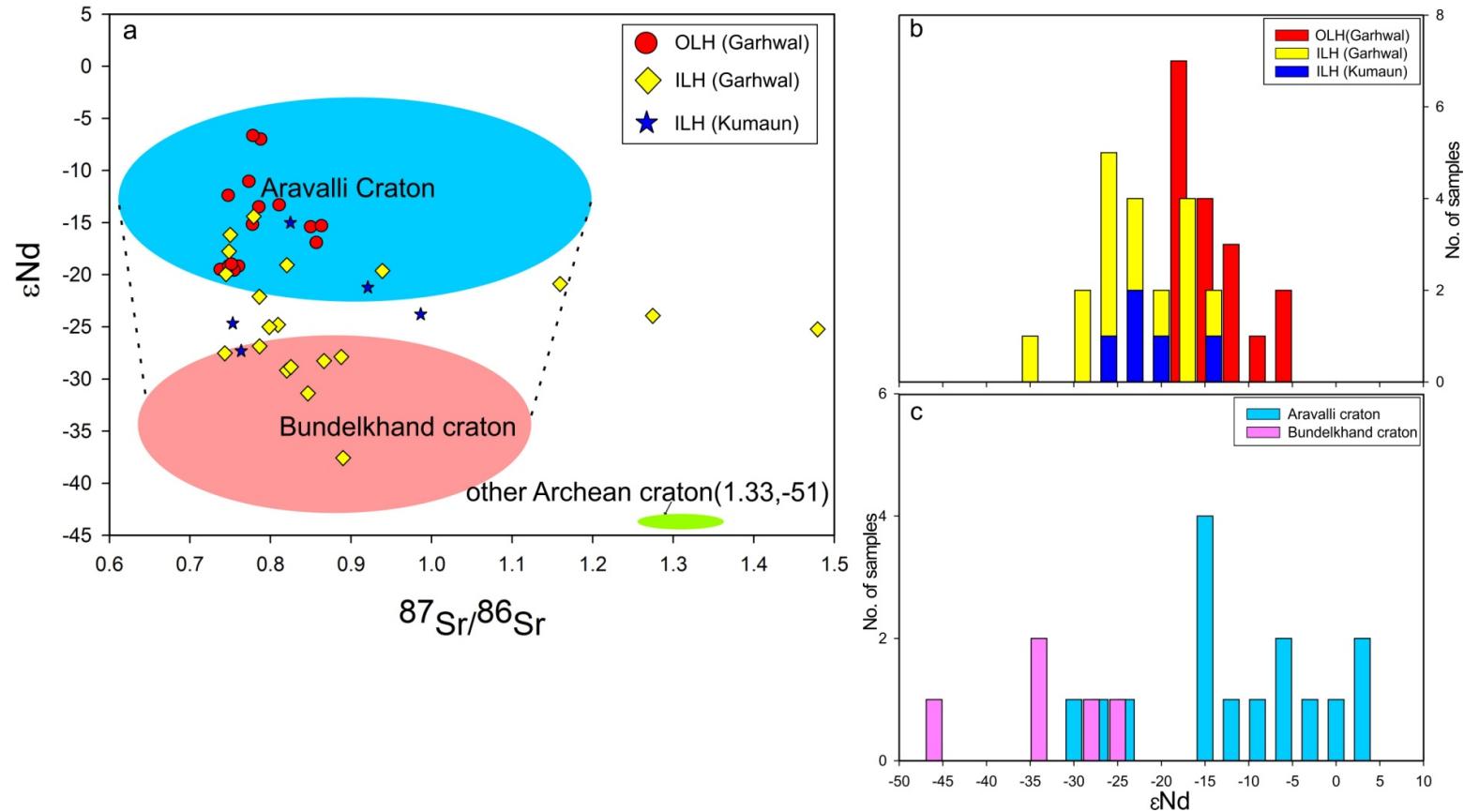
Figure 5.11 (a) Two isotope system plot, $^{87}Sr/^{86}Sr$ and εNd, in the clastics of Garhwal and Kumaun Lesser Himalaya, (b) Histogram of εNd distribution for the Lesser Himalayan clastics, (c) εNd distribution for the potential sources in a stacked histogram.

Our data suggest that the Aravalli craton is the major source lithology for the OLH whereas the ILH had received material from both Aravalli and Bundelkhand cratons (Figure 5.11a). The samples show highly radiogenic $^{87}Sr/^{86}Sr$ ratios with depleted εNd values. This is consistent with the evolved nature of crustal material with older age which causes to accumulate ^{87}Sr as a result of decay of ^{87}Rb. Such a scenario looks plausible that the clastic material were sourced from other Archean cratons (Figure 5.11a). The values of the Inner Lesser Himalaya and the Bundelkhand craton are showing the similar εNd isotopic distribution and thus suggest that most of the ILH sediments are supplied from the Bundelkhand cratons. Based on study it is interpreted that the OLH has less negative εNd and less radiogenic $^{87}Sr/^{86}Sr$ value than that of the ILH and thus suggest that these two belts of the LH are isotopically differentiated and ILH are older than the OLH.This indicates that the OLH and ILH are sourced from the mixing end members (Aravalli and Bundelkhand craton).
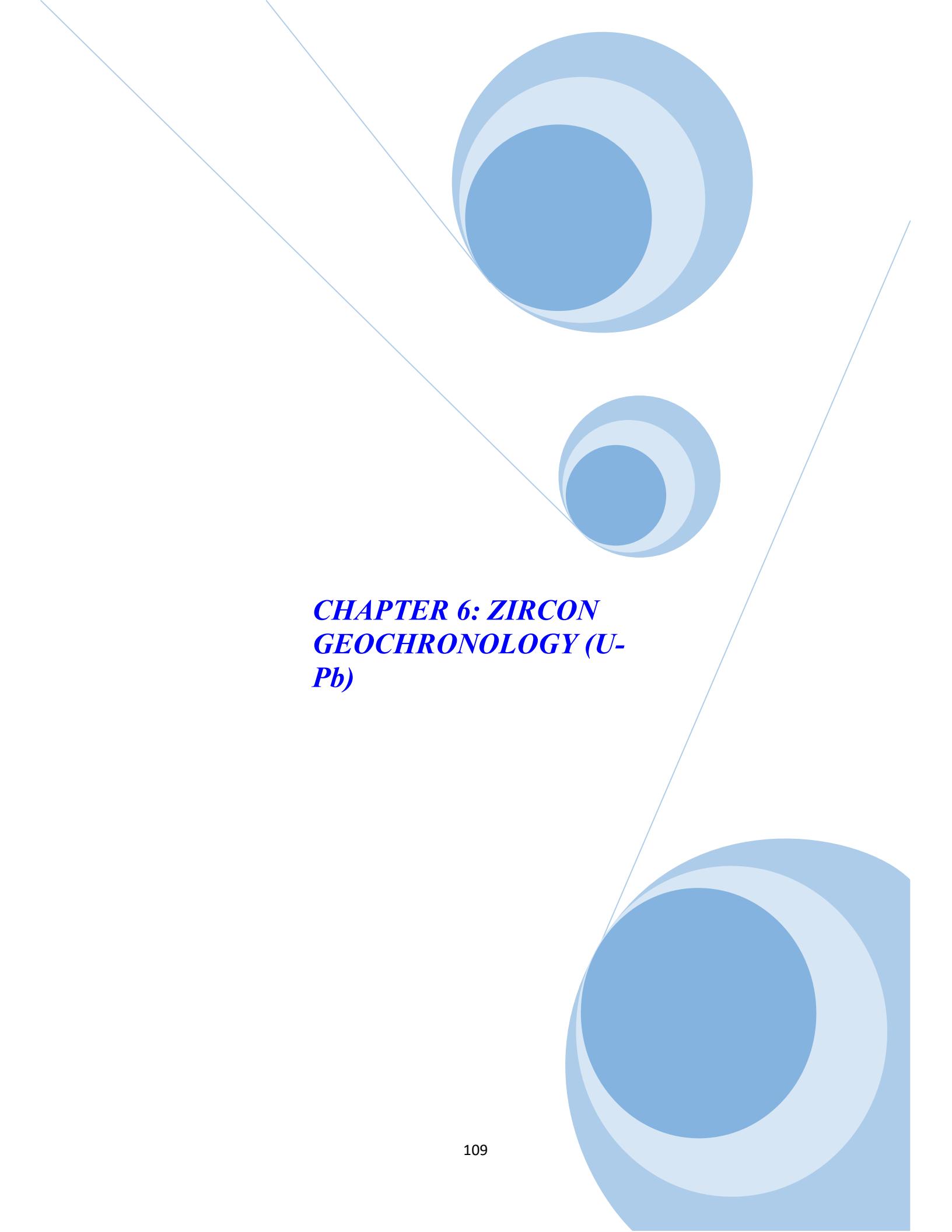
CHAPTER 6: ZIRCON GEOCHRONOLOGY (U-Pb)

CHAPTER 6: ZIRCON GEOCHRONOLOGY (U-Pb)

6.1 Introduction

Zircon grains are the most important mineral for U-Pb dating to characterize the radiometric age constraints of the sediments. Detrital zircon geochronology has become an important tool for lithostratigraphic study of the Himalayan sediments (e.g., DeCelles et al., 2000; Martin et al., 2005; McQuarrie et al., 2008; Myrow et al., 2003, 2010; Long et al.,2011; McKenzie et al., 2011; Webb et al., 2011; Spencer et al., 2012). Such studies have facilitated towards a better understanding the stratigraphic setup towards reconstructing the age of the Lesser Himalayan formation. The detailed informations regarding the litho-stratigraphic setup of the Garhwal-Kumaun (GK) Lesser Himalaya are discussed in Chapter 2.

As the sediments of the Damtha (Chakrata and Rautgara formations) and the Jaunsar Group (Chandpur and Nagthat formations) of the Lesser Himalayan sediments are unfossiliferous and therefore it is tricky to provide an age constrains. The U-Pb dating of detrital zircon of the siliciclastics has been attempted to constrain their maximum depositional ages. The detrital sediments also provide information about the plausible provenance (Gehrels et al., 2011). Among the earlier works on the geochronological studies using U-Pb zircon in the Lesser Himalayan lithounits, Richards et al, (2005) stated that, the zircons from the ILH (Rampur Formation) yielded age population between 2.26 to 1.87 Ga. Similarly, Kohn et al, (2010) and Miller et al, (2000) have reported as the maximum depositional age of ~1.8 Ga for the Berinag–Rampur groups. The age of the lower Damtha group yielded a peak of 1870 Ma and upper Damtha group yielded older peaks at 1750, 1880, and 2500 Ma having no grains younger than 1600 Ma (McKenzie et al., 2011). Further, the younger Mandhali Formation yielded an age distribution with the youngest peak at 950 Ma and older peaks at 1560, 1750, and 2500 Ma. Zircon grains extracted from the rocks from the Baliana Group from Nainital region yielded the youngest age with a peak of 770 Ma and an assemblage of grains yielded older age of

peak 850, 1100, 1600, 1880, and 2500 Ma (McKenzie et al., 2011). Hofmann (2011) suggested the age of the Nagthat Formation (Garhwal) as Neoproterozoic, with a minimum age of 733±10Ma using U-Pb method. Schistose gneisses lying at the base of Lesser Himalaya Sequence in both the units, the OLH and the ILH yield an age range of 1856 to 1868Ma (Celerier et al., 2009). However, age estimates for the siliciclastics are poorly constrained for the Lesser Himalaya sedimentary successions. Towards this, a total of sixteen clastic samples representing the OLH and ILH have been taken for the U-Pb dating of the zircon grains recovered from these rocks. Mineral separation analysis of the separated zircon grains was performed at the Wadia Institute of Himalayan Geology (WIHG) Dehradun, following the established methods and protocol (Mukherjee et al., 2017). The euhedral to anhedral shaped zircons with size range 74-250µm extracted from the Lesser Garhwal-Kumaun Lesser Himalayan sediment were taken for analyses. The extracted zircon under binocular microscope show are transparent, light pink, light brown to dark brown colour After their characterisation the detrital zircon grains were also examined under SEM for cathodoluminescence imaging (CL) prior to analyse in LA-MC-ICPMS.

6.2 U–Pb zircon geochronology

A total number of sixteen samples were taken for the zircon grain separation and their U-Pb dating using an in-house multi collector Inductively Coupled Mass Spectrometer (MC-ICP-MS; Thermo Neptune Plus) in laser ablation mode of analyses. Out of these sixteen samples, zircon grains are found only in twelve samples (Figure 6.1). The detailed description of their morphological features and internal structures are mentioned in Chapter-4. U-Pb analyses were performed with Laser spot of 20 µm diameter. Cathodoluminescence (CL) images were acquired from each grain for the features such as shape, size, internal zoning and core-rim (Figure 6.2).
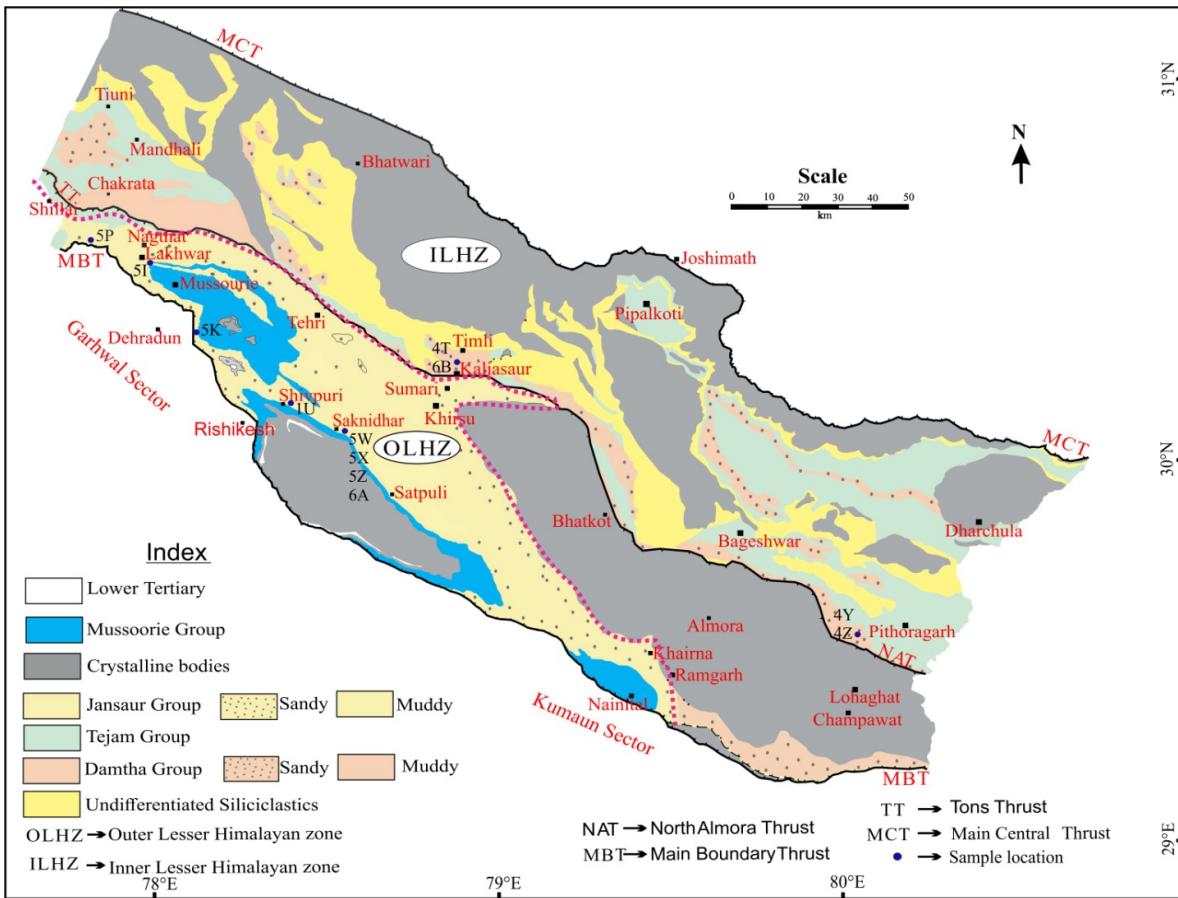
Figure 6.1 Geological map of the Kumaun and Garhwal Lesser Himalaya (after Ghosh et al., 2016a; modified from Valdiya, 1980), showing the location of samples for U-Pb geochronology.
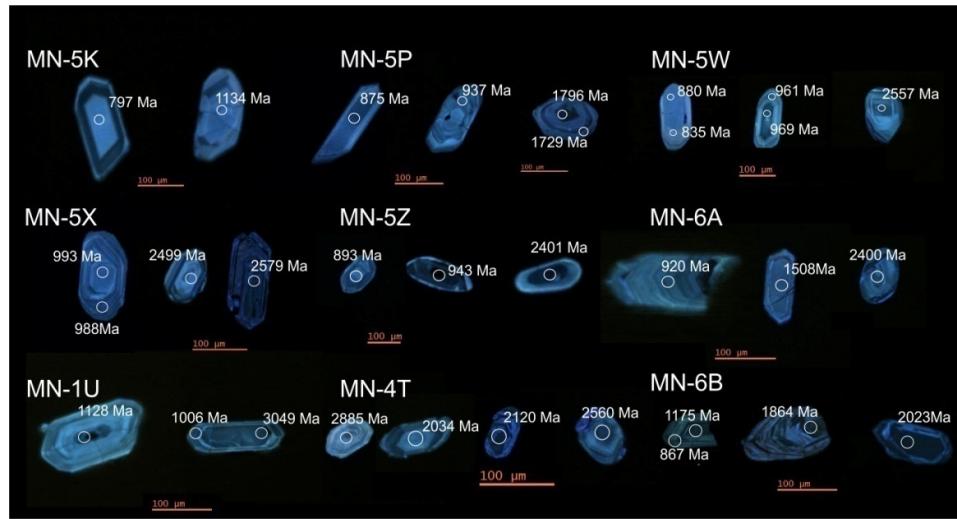
Figure 6.2 Cathodoluminescence images of representative zircon grains from the siliciclastics of Garhwal-Kumaun Lesser Himalaya. Circles indicate position of U–Pb laser spots with ^{207}Pb/^{206}Pb ages.

In the Inner Lesser Himalaya, samples from the Rautgara Formation of the Garhwal and Kumaun section were taken up for the U-Pb zircon dating. The detailed description of the U-Pb geochronology of outer and inner Lesser Himalayan (Garhwal-Kumaun) clastics are provided in Table 6.1 to 6.12 (in appendix). Towards this, two samples MN-4T and MN-6B were collected from the upper Damtha Group (Rautgara Fm.) of Garhwal Lesser Himalaya (for details please refer to Table 3.1). Also two samples MN-4Y and MN-4Z from Rautgara formation of the Kumaun Lesser Himalaya (Ghat Gurna) were analysed for the U-Pb ages. In the Outer Lesser Himalaya the samples from the Chandpur Formation (Shivpuri and Timli road) and Nagthat Formation (from Aglar river valley, Maldeota, Tons Valley and Saknidhar) of Garhwal Lesser Himalaya (for details please refer to Table 3.1) were analysed for the U- Pb detrital zircon ages. The details of the morphological and internal features of the zircon are given in Chapter 4.

Sample MN-4T

Zircon grains were extracted from the siliciclastic is generally euhedral in shape. The total number of 92 spots were analysed with Th/U ratio ranges 0.02 to 4.22 and yielded an age distribution with a large peak 2100 Ma. This

sample yielded no grains younger than 1823±40Ma, with older peaks at 2565, 2655 and 3000 Ma (Figure 6.3).

Sample MN-6B

The detrital zircons grains are euhedral to anhedral in shape. 122 analysis were made on the zircons. Most spots reveal Th/ U ratio between 0.05 and 3.5. Sample MN-6B yielded an age distribution with large peak 1920 Ma with youngest peak at 861± 31Ma (Figure 6.3) and older peaks at 1100, 1630, 1800 and 2565 Ma.

Sample MN- 4Y

The zircon gains are mostly euhedral to anhedral crystal. For this sample 69 spots were analysed. The Th/U ratio ranges from 0.17 to 1.52. The size of the zircon varies from 44-115µm with length and width ration of 3:1 to 1.1:1. The age spectra shows two pronounced age peak at 1880 Ma and 2022 Ma (Figure 6.3) with no grains younger than 1600 Ma. The oldest peaks are noticed at 2506 and 2860 Ma.

Sample MN- 4Z

The zircons are represented by a dominancy of both the euhedral and subhedral zircon grains. 84 spots were analysed with Th/U ratio between 0.02 and 1.76. This sample yielding dominant age peaks at 1900 and 2585 Ma (Figure 6.3) with no peaks younger than 1600 Ma. In addition the older age peaks of the same sample noticed at 1850, 2100, 2585 and 3000 Ma.

Sample MN-1U

This zircon grains extracted from the Chandpur Formation are mostly euhedral in shape. 102 analytical spot were analysed having Th/U ratio between 0.23 and 3.38. The detrital zircon clustering is at 888, 1000, 1100, 1600, 1800, 2488, 2686 and 3000 Ma (Figure 6.4).

Sample MN-5I

This sample is taken from Nagthat Formation. The zircons from this siliciclastic are generally euhedral. A total of 78 spots were analyzed for dating. The Th/ U ratio of the analyzed zircon spots widely ranges from 0.09 to 1. 71. The dominant age peaks at 864±20Ma (one spot yielding age at 792 Ma) (Figure 6.4) with the older peaks at 1670, 1830, 2550 and 3013 Ma.

Sample MN-5K

The zircon grains from the siliclastics of the Nagthat Formation are representing euhedral zircon. 87spots were analysed for this sample with Th/U ratio ranging from 1.12 to 2.77. The zircon grain yielded youngest grains with an 820 Ma age peak (Figure 6.4). Furthermore, the six spots showing the younger age at 783 ± 18 Ma and an array of older grains of nearly at 900, 1100, 1737, 1891, 2169 and 2571 Ma.

Sample MN-5P

This sample is collected from the Tons valley section of the Nagthat Formation. In general the grains are euhedral. 91 spot analysed from the sample with Th/U ratio between 0.11 and 2.75. The analysed grains yielded a detrital zircon age distributions with pronounced peak at 870 Ma (Figure 6.4). In addition the four spots showing younger age at 791 ± 3.9 Ma and older peaks at 1550, 1750, 2290 and 2510 Ma.

Samples MN-5W

This sample is collected from Saknidhar (Nagthat Formation) area of Garhwal Lesser Himalaya. The grains are mostly euhedral. 107 spots were analyzed in sample MN-5W with Th/U ratio from 0.072 to 8.92. The analysed grains yielded younger age peak 868±22 Ma (Figure 6.4) and the older peaks at 1500, 1700, 1995, 2521 and 3000 Ma.

Samples MN-5X

This sample is collected from the same location as from MN-5W. These zircon grains are representing euhedral to subhedral shape. The Th/U ratio of the 117 spots ranges from 0.18 to 2.24. The grains yield younger age at 873 ±18Ma (Figure 6.4) and older age at 1150, 1550, 2040, 2523 and 3030 Ma.

Sample MN-5Z

This sample is collected from the same location as from MN-5W. The grains are usually euhedral. A total of 82 spot were analyzed with Th/U ratio from 0.09 to 1.83. These grains shows younger age peak at 922 Ma with 6 spots showing younger age peak at 886.95 ±12.3 Ma (Figure 6.4) and older peaks at 1700, 1883, 1900, 2684 and 3200 Ma.

Sample MN-6A

This sample is also collected from the same location as from MN-5W. The grains are mostly euhedral. 117 spot are analyzed with Th/U ratio from 0.15

to 2.05 and yielded younger age peak at 847Ma (Figure 6.4) and 931 Ma (six spots with age 876±20 Ma) and the older peaks are at 1231, 1559, 1878, 2562 and 2880 Ma.
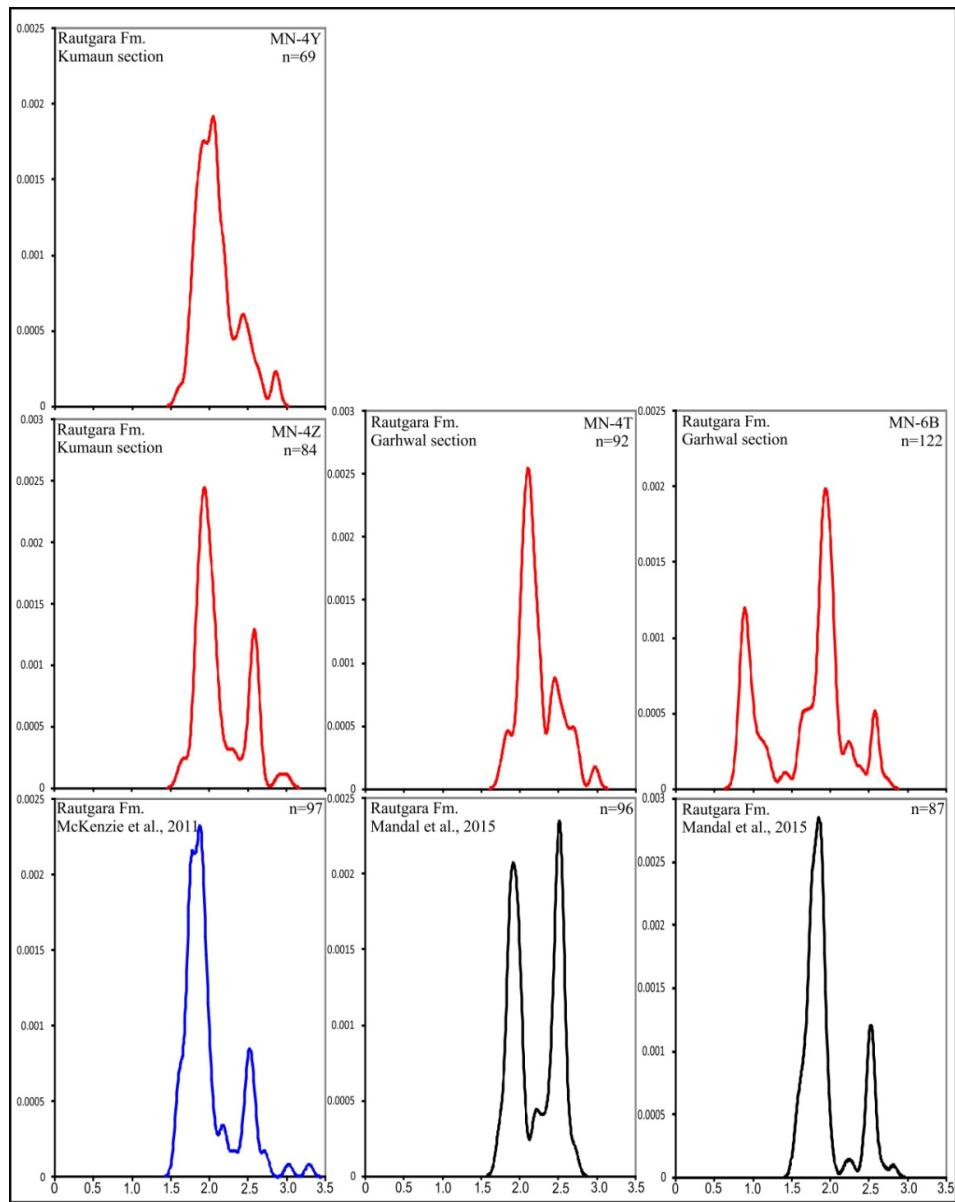
Age (Ga)

Figure 6.3 Detrital zircon age distributions curves of siliciclastic of inner Lesser Himalaya (Garhwal-Kumaun section) and their comparison with the published data of McKenzie et al., (2011) and Mandal et al., (2015).

n= number of analysis.
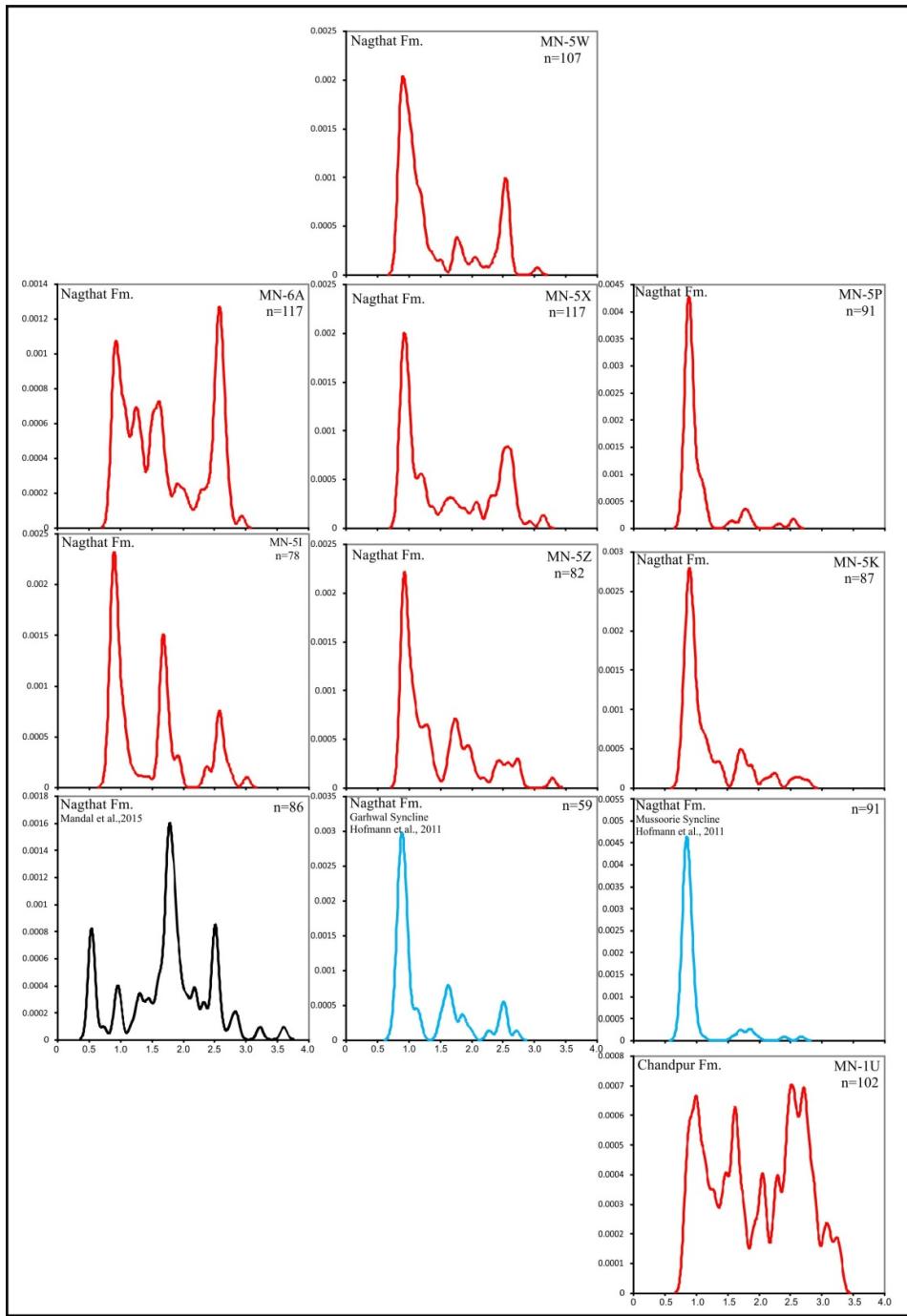
Age (Ga)

Figure 6.4 Detrital zircon age distributions curves of siliciclastic of outer Lesser Himalaya (Garhwal section) and their comparison with the published data of Mandal et al., (2015) and Hofmann et al., (2011). n= number of analysis.

6.3 Comparison of the present study with available data from the Lesser Himalaya

The relative ages of the clastics from the LH and their comparison with the other available data are given in Figure 6.5. The age constraints obtained from this work is useful in describing the chronostratigraphic correlation between inner and outer Lesser Himalaya. Representative siliciclastic samples used for the U–Pb zircon geochronology are dominantly medium to coarse- grained and composed mainly of the quartz.

^{207}Pb/^{206}Pb ages from the Inner Lesser Himalaya siliciclastic samples, MN-4T and MN-6B analysed from the upper Damtha (Rautgara Fm.) of the Garhwal Himalaya. MN-4T Samples of the Rautgara Formation yielding depositional age 1823±40Ma (with two zircon grain yielding 1773±18) and is correlated with the Lower Damtha Group of the Kumaun Lesser Himalaya with 1.8 Ga (McKenzie et al, 2011) depositional age. These grains lack the presence of younger 1.6 Ga detrital zircon grains. Based on this the Late Palaeoproterozoic age is suggested to the Rautgara Formation. Sample MN-6B (Rautgara Formation of Garhwal Lesser Himalaya) is constrained to an approximate deposition age 861± 31Ma. This samples is inconsistent with the age distribution of the Rautgara Formation (1.6 Ga) given by McKenzie et al., 2011 and Mandal et al., 2015, and shows similar distribution of detrital zircon age at 800Ma (sample of Rautgara Formation of Valdiya, (1980). GW18-06 sample of Valdiya is further assigned to be a part of Chandpur Formation (Celerier et al., 2009) because the Rautgara Group is> 970 Ma (Richard et al., 2005). Present study shows that the sample MN-6B showing uncertain detrital zircon age deposition and needs further attention.

The detrital zircon grains from the Inner Lesser Himalaya (Kumaun section), MN-4y and MN-4z (Ghat Gurna) shows that the Rautgara Formation has a Palaeoproterozoic 1600 Ma relative age zircon, similar to the Palaeoproterozoic age from the Rautgara Formation reported by Mandal et al. (2015) and McKenzie et al. (2011).
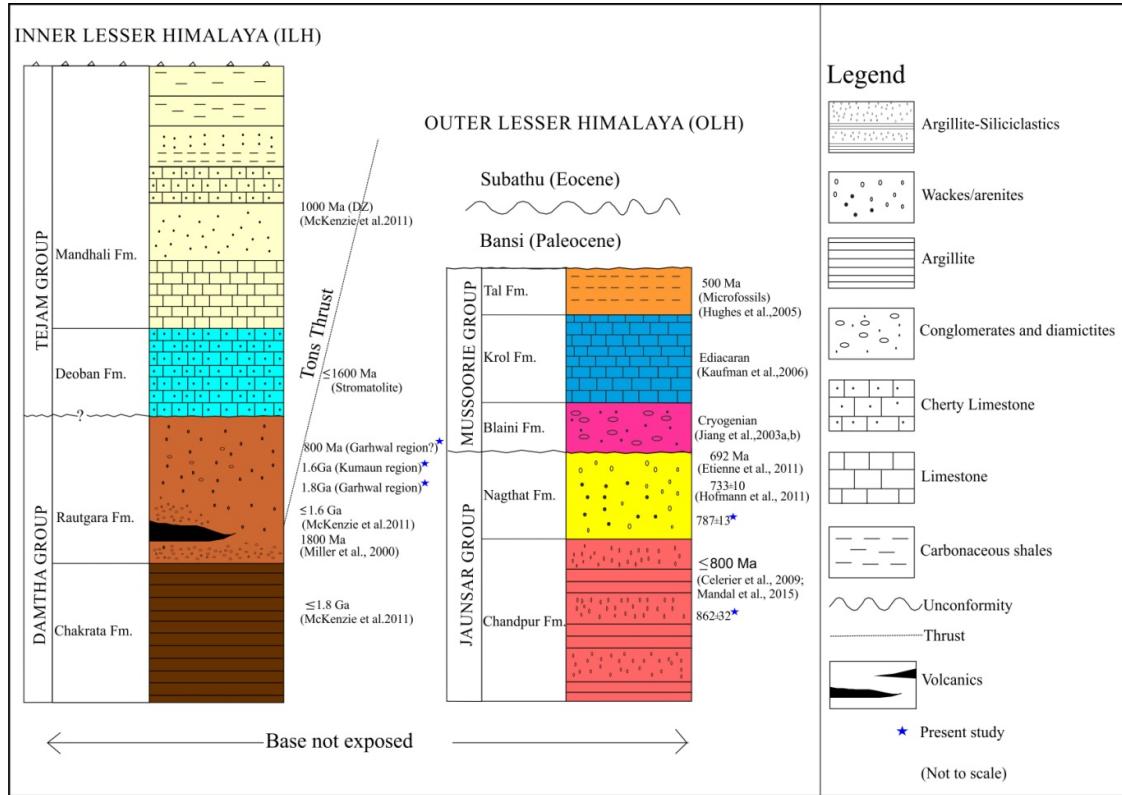
Figure 6.5 Generalized stratigraphy of the Kumaun- Garhwal Lesser Himalaya (modified after Azmi and Paul, 2004; Kohn et al., 2010) with the present geochronological constraints and their comparison with the published data.

From OLH, U-Pb ages from Chandpur formation are dominated by Neoproterozoic population showing $^{207}Pb/^{206}Pb$ age of younger peak at 862±32Ma (n=6). The older ages are mainly spread from 1600-3045 Ma. The age of the Chandpur Formation (present study) is consistent with the detrital zircon ages of the Chandpur Formation (Kumaun region, sample -0602003, GW18-06, GW21-06) mention by Celerier et al (2009) showing the age distribution peak of $^{207}Pb/^{235}U$ between 770 and 3290 Ma. The detrital zircon age from the Nagthat formation of Garhwal region of samples MN-5P (Tons valley); MN-5K (Maldeota); MN-5I (Aglar river); MN-5W, MN-5X, MN-5Z and MN-6A (Saknidhar), yielding zircon age 791 ± 3.9 Ma, 783 ± 18 Ma, 864±20Ma, 868±22 Ma, 873 ±18Ma, 886.95 ±12.3 Ma, 876±20, respectively and assigned to a Neoproterozoic age. The average zircon ages 787±13Ma obtained from the Nagthat Formation is slightly younger than $^{207}Pb/^{206}Pb$ ages obtained from the siliciclastic of the Chandpur Formation. Hofmann et al, (2011) reported the age of the Nagthat Formation as Neoproterozoic, with a minimum age of 733±10 Ma which is consistent with the present data. From the present study, the U-Pb ($^{207}Pb/^{206}Pb$) zircon dating suggesting the Palaeoproterozoic age (1.6-1.8 Ga) to the Garhwal and Kumaun inner Lesser Himalayan sequence (Rautgara Formation) and Neoproterozoic age (862±32Ma and 787±13Ma) to the outer Lesser Himalayan sequence of Garhwal Himalaya (Chandpur and Nagthat formations).
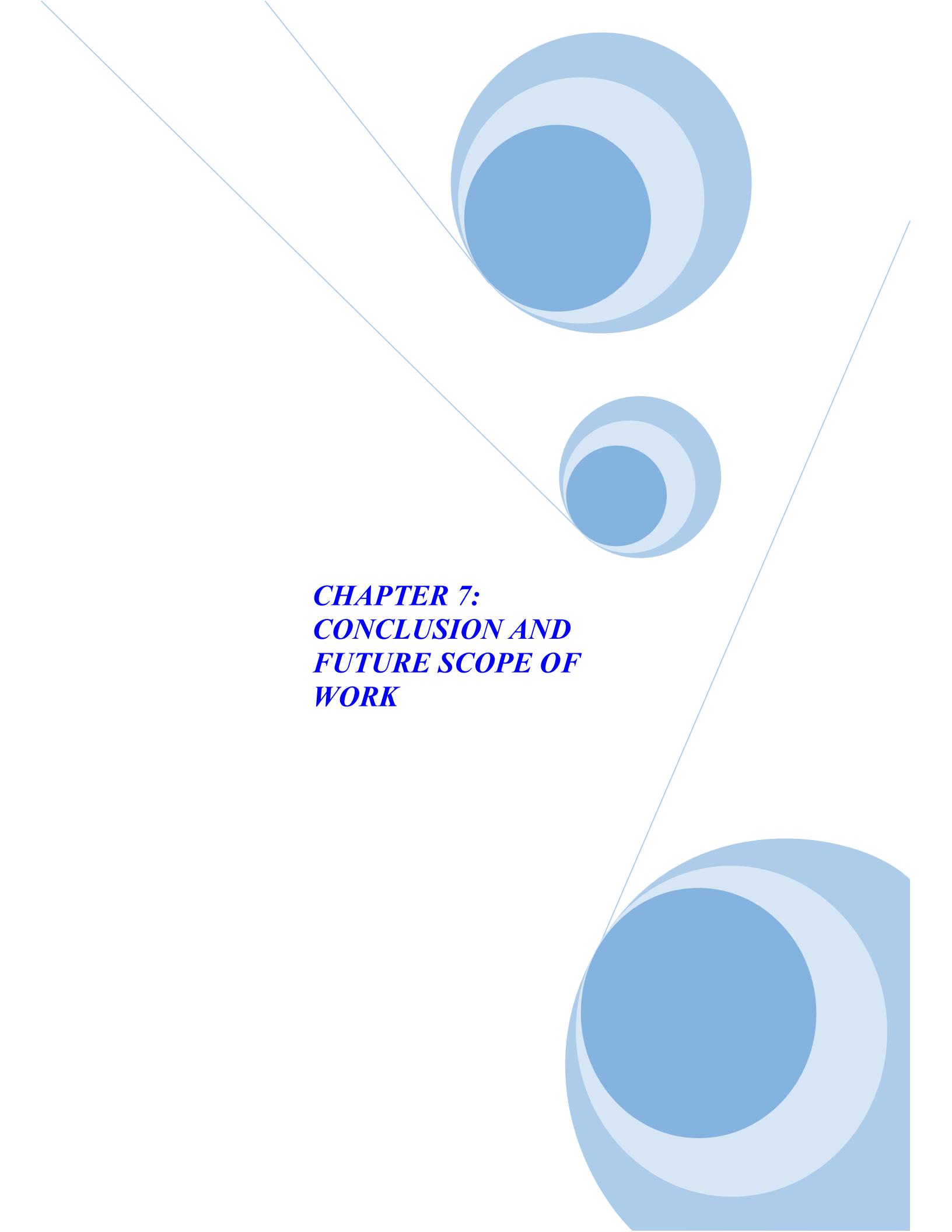
CHAPTER 7:
CONCLUSION AND
FUTURE SCOPE OF
WORK

CHAPTER 7: CONCLUSION AND FUTURE SCOPE OF WORK

7.1 Relevance of the work

The Lesser Himalaya is divided into two major units, along its breadth from north to south, on the basis of lithology, stratigraphy and tectonic settings which are described as the Inner (ILH) and Outer Lesser Himalaya (OLH) (Valdiya, 1980). However, the ages and the relative correlation of the OLH and ILH is still to be understood well and remains a contested issue. Towards this, a new demarcating plane (Tons Thrust) possibly is visualised between the younger (Neoproterozoic-Cambrian age; 800–500Ma) OLH and older (Palaeoproterozoic-Mesoproterozoic; 1900–1600Ma) ILH of the Lesser Himalaya (Ghosh et al, 2016a). The sedimentary succession of the Lesser Himalaya is correlated on the basis of lithofacies and detrital modes and there noted a presence of near shore depositional environment from Late Palaeoproterozoic to Neoproterozoic (Ghosh et al, 2016a).

The siliciclastics of the Lesser Himalayan sedimentary successions are grouped under two major types - i) Siliciclastic (SLC) associated with the autochthon and para- autochthon bodies, which has undergone diagenesis and preserved the sedimentary textures It generally has association with syn-sedimentary basic volcanic rocks, particularly the Rautgara Siliciclastics of Inner Lesser Himalaya (ILH), and ii) Recrystallized Siliciclastic (RSLC)associated mainly with the crystalline sheets (gneissic bodies) and has lost the sedimentary textures and structures due to metamorphism. Compositionally the clastics are arenite and wacke types with detrital proportion of the clastics from the outer and inner Lesser Himalaya are: $Q_{77\pm12}F_{11\pm4}R_{12\pm9}$; $Mx_{9\pm5}$ (n=17) and $Q_{86\pm14}F_{5\pm4}R_{9\pm13}$; $Mx_{10\pm7}$ (n=21), respectively. Quartz grains in the clastics of the Lesser Himalaya are monocrystalline, however polycrystalline quartz are also present. Alkali feldspars are less common than plagioclase that can be related to more

stability of plagioclase bearing rocks at the source area. The rareness of the feldspar in the clastics is mainly due to their alteration into clay minerals during diagenesis. Presence of clay component, siliceous rock fragments and feldspar makes both the clastics of both the OLH and ILH submature. The high components of the quartz in the clastics of the Lesser Himalaya suggest that they are derived from the source region as a recycled material. On the basis of analysis of composition and textural maturity, the clastics are composed predominately of detritus which was derived from coarse grained, granitic or gneissic (felsic) parent rocks The presence of clay minerals is indicative of chemical weathering of the protolith under the influence of warm climate.

Morphological and internal features of the zircon grains from the Proterozoic Lesser Himalayan clastics differ in their response to magmatic and metamorphic processes with respect to crystal morphology and internal structures. The samples were collected from the upper Damtha (Rautgara Fm.) and Jaunsar Group (Chandpur and Nagthat formations of the Lesser Himalaya. They are widely varied in terms of external morphology and internal textures. The separated zircon grains from both the OLH and ILH indicate that they are generally euhedral shape. Dimension wise the OLH zircons are bigger (117μm ± 21 with L/B ratio 1.87 ± 0.11) than the ILH (101 μm ±30 with L/B ratio1.75 ± 0.10). The zircons are irregular and euhedral to anhedral in the ILH domain and prismatic euhedral to anhedral and more elongated in the OLH. The zoning in ILH zircons is faintly visible as compared to OLH. However, zircons from both the belts (OLH and ILH) of the Lesser Himalaya are showing similar internal morphological characteristics, implies that inner and outer zones of the Lesser Himalaya has been sourced from the similar protolith, which had undergone different process of zircon formation as well as the degree of transportation. The resorption features in the grains may be due to the disequilibrium of the zircon grains with the melt during magmatic processes and also can occur due to metamorphic fluid/hydrothermal process due to activity during the Himalayan orogen. Similar inferences has been drawn, based on light mineral detrital modes (quartz, feldspar and rock

fragments), of the OLH and ILH and hints towards derivation from the Aravalli-Bundelkhand craton.

The geochemistry of siliciclastic rocks can be used as a tool for understanding the types and composition of the source rocks. The major and trace element composition shows that clastics from both the OLH and ILH are bearing the similar geochemical attributes. SiO_2 showing negative correlation with Cr, Ni and Nb reflects the quartz dilution effect. Higher SiO_2 content in the clastic sediments implies that the important constituents of their provenance be granites and granitic gneisses. The clastic sediments have high content of SiO_2 suggesting very high quartz content and are present in the form of monocrystalline quartz and polycrystalline quartz as well as quartz overgrowth. CaO and Na_2O were possibly provided by plagioclase and moderate amount of K_2O suggest contribution mainly from K-feldspars and mica. High content of the Al_2O_3 in the sediment indicate the presence of clay minerals (also seen in the petrography) and mica indicative of diagenetic affects. The CIA values of the Lesser Himalaya clastic sediments ranges between 47 and 81 with an average of 70 ± 8 (n=109). The average CIA* of the clastics is 73 ± 7 (n=109), suggest moderate to extreme weathering of the source region. The average PIA and CIW values (81 ± 13; 100, n=109) indicate higher degree of source rock weathering. The A-CN-K plot of the present study indicates that these sediments are derived from a felsic (granitic) source rock and are consistent with the petrographic data.

McLennan et al., (1980) proposed Al_2O_3 wt% versus TiO_2 wt% bivariate discrimination diagram on the basis of significance of Al and Ti in the provenance studies in order to constrain the provenance of clastics rocks. The Lesser Himalayan clastics are ploted along the granite and granodiorite trend (Figure 7.1). Also high Al_2O_3/TiO_2 ratio (>18) of clastics are supporting the granitic source rocks for these sediments.

124
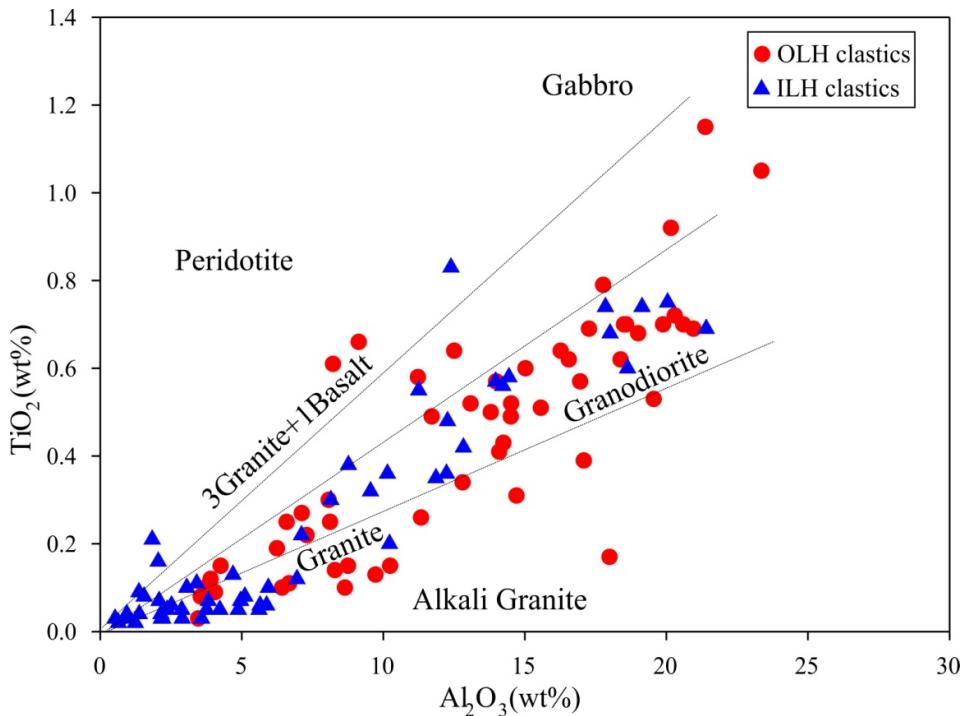
Figure 7.1 TiO$_2$ wt. % versus Al$_2$O$_3$ wt. % bivariate plot (after McLennan et al., 1980). OLH (Chandpur and Nagthat fms.), ILH (Chakrata and Rautgara fms.).

In the bivariate log (Fe$_2$O$_3$/K$_2$O) versus log (SiO$_2$/Al$_2$O$_3$) diagram (after Herron, 1988) the clastics are ploted (Figure 7.2) and are showing similar distribution pattern as compared to QFR diagram Figure 4.4 and thus are classified quartz arenite, arkose, subarkose, litharenite, sub-litharenite and wacke Positive correlations of Ni, Zn and Rb with Al$_2$O$_3$ and K$_2$O and MgO with Ni and Zn suggest that these elements are mainly controlled by clay minerals. The presence of clay mineral is also evident by the petrography and SEM in the form of altered mineral. Therefore on the basis of the geochemical analysis of the clastics it is interpreted that they are dominantly sourced from granitic rock with subordinate mafic component. The HREE depleted, high (La/Yb)$_N$ ratio and negative europium anomaly suggestive of granitic source..Trace elements, LREE enriched, high Th/Sc, La/Sc indicating granitic source rock and High Rb/Sr reflecting recycled sediments.
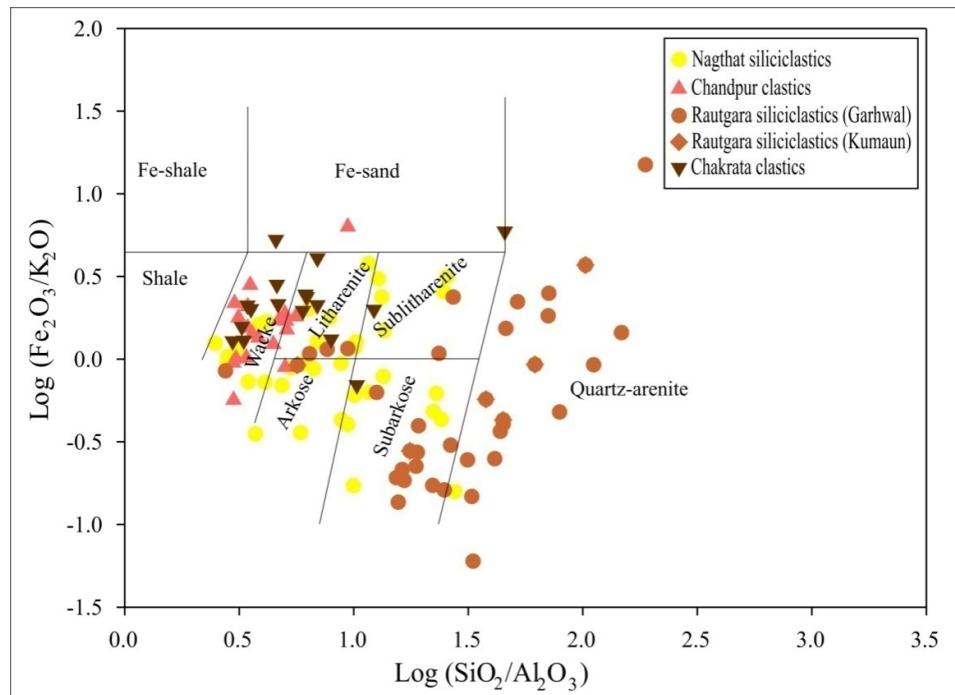
Figure 7.2 Geochemical classification of clastics (Log (Fe$_2$O$_3$/K$_2$O) versus log (SiO$_2$/Al$_2$O$_3$), bivariate diagram (after Herron, 1988).

The average ^{87}Sr/^{86}Sr ratio of the Nagthat and Chandpur Formation of the OLH (Garhwal) are $0.78 \pm 0.02(n = 7)$ and $0.78 \pm 0.05(n = 10)$ and Rautgara Formation of ILH are $0.92 \pm 0.21(n = 15)$ and 0.85 ± 0.10 ($n = 5$) of the Garhwal and Kumaun region, respectively. The ^{87}Sr/^{86}Sr ratio of the Chandpur and Berinag Formation are 0.79±0.03 (n= 6) and 0.88± 0.27(n=3) (Ahmad et al., 2000). This shows that the OLH clastics are less radiogenic than the ILH. Differences in the εNd values has been reported from the lithotectonic units of the Himalaya (DeCelles et al.,2000; Martin et al., 2005; Parrish and Hodges, 1996). In present study sample collected from Jaunsar group (Chandpur and Nagthat fms) yield a εNd value $- 15.4 \pm 4.3(n = 17)$. This value is similar to the reported value -17 of McKenzie et al., 2011 from the Neoproterozoic strata of the Jaunsar group (Kumaun Himalaya). Similar εNd isotopic values -17.9±0.5 (n=6) are reported for the Chandpur Formation by Ahmed et al, (2000).

The εNd values of the present study from the Rautgara Formation of the Garhwal and Kumaun Lesser Himalaya are -25.3 ± 4.2($n = 14$) and − 22.4 ± 4.7($n = 5$) and Chakrata Formation (Garhwal Lesser Himalaya) has εNd values − 22.0 ± 8.0($n = 6$) (present study). Similar inferences (εNd value of - 22) are also drawn by McKenzie et al, (2011).

Siliciclastic samples used for the U–Pb zircon geochronology are dominantly medium- to coarse- grained and composed mainly of the quartz, feldspar and rock fragments of varied proportion. In the OLH, zircons grains of Chandpur formation are dominated by Neoproterozoic population showing $^{207}Pb/^{206}Pb$ age of younger peak at 862±32Ma (n=6). The older ages are mainly spread from 1600-3045 Ma. The age of the Chandpur Formation (present study) is consistent with the detrital zircon ages of the Chandpur Formation (Kumaun region, sample -0602003, GW18-06, GW21-06) of Celerier et al (2009) showing the age distribution peak of $^{207}Pb/^{235}U$ between 770 and 3290 Ma. The detrital zircon age from the Tons valley, Maldeota, Aglar river and Saknidhar area of Nagthat formation (Garhwal region) yielding zircon age 791 ± 3.9 Ma, 783 ± 18 Ma, 864±20Ma, 868±22 Ma, 873 ±18Ma, 886.95 ±12.3 Ma, 876±20 and are assigned to Neoproterozoic age. The average zircon ages 787±13Ma obtained from the Nagthat formation is slightly younger than $^{207}Pb/^{206}Pb$ ages obtained from the siliciclastic of the Chandpur Formation. Hofmann et al. (2011) reported the age of the Nagthat Formation as Neoproterozoic, with a minimum age of 733±10 Ma, which is in closed agreement with present ages with those of the Nagthat Formation.

$^{207}Pb/^{206}Pb$ ages of the siliciclastic samples, from the upper Damtha group (Rautgara Fm.) of the Garhwal Lesser Himalaya yielding depositional age 1823±40Ma (with two zircon grain yielding 1773±18). However, sample MN-6B (Rautgara formation of Garhwal Lesser Himalaya) exhibit a relatively lower age of 861± 31Ma, which requires a suitable explanation as similar observation is also mentioned by Richards et al., (2005).

The detrital zircons recovered from the Kumaun section shows that the Rautgara Formation has a Palaeoproterozoic 1600 Ma depositional age zircon

and corroborates the findings of Mandal et al., (2015) and McKenzie et al., (2011).

7.2 Relationship with the Peninsular Basin

The Indian shield is broadly consists of two Archaean cratonic domains: a northern (Bundelkhand and Aravalli) craton and southern (Bastar, Singhbhum and Dharwar) craton divided by a major tectonic line, the Central Indian Tectonic Zone (CITZ; Radhakrishna 2013) (Figure 7.3). Previous studies identified that the Lesser Himalaya may have been a part of the Paleoproterozoic to Neoproterozoic provenance (Richard et al., 2005; McKenzie et al., 2011). The Proterozoic intracontinental basins were developed over the basement region of Bundelkhand and Bastar cratons. The Vindhyan succession rests unconformably on the Bundelkhand and Aravalli cratons and has close immediacy with the Precambrian stratigraphy of the Lesser Himalayan basin (Ghosh et al 2016a). The Aravalli and Delhi Supergroup (Aravalli craton) comprises of 1.8 and 1.5 Ga (Deb and Sarkar, 1990; Deb et al., 2002; Pradhan et al., 2010) and 1.0 to 0.8 Ga sedimentary successions (Deb et al., 2001; Pradhan et al., 2010)), respectively. The Marwar Supergroup (Aravalli Supergroup) consisting of the Neoproterozoic-cambrian sedimentary successions (Gregory et al., 2009; Malone et al., 2008; Pandit et al., 2001). The detrital zircons age spectra from the sediments of the Aravalli orogen yield ages between 3.35 and 1.75 Ga, with prominent age peaks at ca. 1.85 Ga and ca. 2.5 Ga (Kaur et al., 2013). The Bundelkhand trondhjemite gneiss is characterized by U-Pb zircon age 3551 ± 6 Ma (Kaur et al., 2014). Consequently, it will be proper to consider the Precambrian succession in Himalaya as a part of the Aravalli-Bundelkhand craton. Therefore, provides a basis for correlating the LH strata with age-equivalent Proterozoic successions of the Indian craton (Aravalli- Bundelkhand), situated south of the Himalayan frontal thrust. Sharma (1998), suggested that the Lesser Himalayan gneiss basement represents the northern extension of the Bundelkhand craton and northern Indian shield elements of the Aravalli-Delhi mobile belt (Kumar et al., 2013), and thus inferred that the Lesser Himalayan belt represents the

northern component of the Bundelkhand craton and Aravalli-Delhi mobile belt. Ghosh et al., (2016 b) suggested that Lesser Himalayan basin was formed in a foreland like situation and were sourced from the Aravalli-Delhi Supergroup as recycled material and less commonly the BGC and BG and thus clearly hints towards the near similar source area lithology. The detrital zircon ages of the OLH (Chandpur and Nagthat formation) are equivalent to the ≤850Ma U-Pb age of the Jodhpur Group mentioned by Malone et al (2008) and 771±5 detrital zircon age of Malani igneous suite mentioned by Gregory et al, (2009) from Marwar Supergroup (Aravalli succession). These grains lack the presence of younger 1.6 Ga detrital zircon grains. The distribution from the siliciclastic sample MN-4T of the Rautgara Formation (Garhwal Lesser Himalaya, present study) is equivalent to the $^{207}Pb/^{206}Pb$ 1.8 Ga age of the Semri group of the Rajasthan Vindhyan succession, and further supports the correlation between the Damtha groups (Garhwal Lesser Himalaya) with the Rajasthan Semri group of the lower Vindhyan Supergroup. Also the detrital zircon present in the North Delhi belt (Alwar Group) and Jhamarkotra Formation (Lower Aravalli Supergroup) has $^{207}Pb/^{206}Pb$ depositional age of 1.7 Ga (McKenzie et al., 2013). Age relationship of the Palaeoproterozoic Rautgara Formation of inner Lesser Himalaya reflects those of the Lower Vindhyan (Rajasthan Semri Group) and Aravalli -Delhi Supergroup.

The siliciclastic samples of the Damtha Group (Rautgara formation) from the Kumaun Lesser Himalaya yielding depositional age 1.6 Ga zircon grain. This age is correlated with the 1.6 Ga Semri group of lower Vindhyan succession (Son valley).

Sample collected from Jaunsar group yield a εNd value $-15.4 \pm 4.3 (n = 17)$. The Aravalli craton having εNd value -13.23 ± 9.8 $(n = 15)$. On the basis of isotopic similarities between the OLH and Aravalli craton it is suggested that the OLH received maximum sediments from the Aravalli craton. The εNd values of the Rautgara Formation of the Garhwal and Kumaun Lesser Himalaya are $-24 \pm 5.4 (n = 25)$ (present study). The values of the εNd for the Bundelkhand craton ranges from $-34.95 \pm 7.99 (n = 5)$. The near similar values of the Inner Lesser Himalaya and the Bundelkhand craton are showing the similar εNd isotopic distribution suggestive of the detritus of

Inner Lesser Himalaya sediments are supplied from the Bundelkhand craton. Also the ILH clastics have more negative εNd values than the OLH. The average value of the εNd of Aravalli and Bundelkhand craton is -17±13.3 (n=20). This suggests that Lesser Himalayan clastics have been sourced from the mix sources.
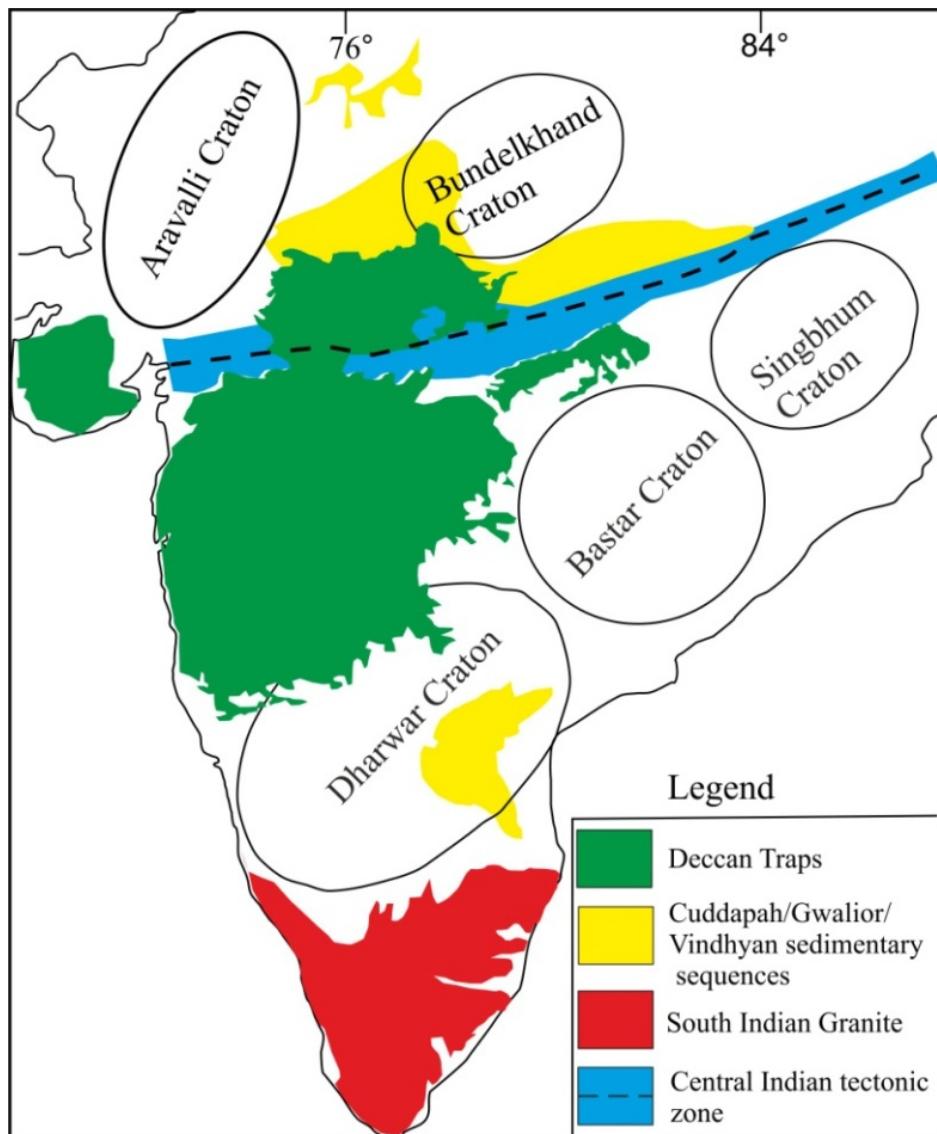
Figure 7.3 Archean cratons of the Indian shield and the surrounding Precambrian sedimentary basins of peninsular region (after Radhakrishna et al., 2013).

7.3 Conclusion

The Proterozoic Lesser Himalayan basin largely consists of thick sequences of siliciclastic, argillite, and limestone deposited under shallow marine shelf set up. The southern and northern parts of the Lesser Himalaya are divided on the basis of lithology, stratigraphy and tectonic settings and grouped as Outer Lesser Himalaya (OLH) and Inner Lesser Himalaya (ILH).

The siliciclastics of OLH and ILH are generally grey, purple, green and dirty white, medium- to fine- grained having sub-angular to well-rounded detritals. Remarkably, the purple, green kinds are common with syn-sedimentary basic volcanics and noticed mainly in ILH and subordinately in OLH (eastern part- Kumaun sector) of the Lesser Himalaya. Compositionally, the siliciclastics are of arenite and wacke types. Arenites includes sublithic arenite, lithic arenite, quartz arenite, and subarkose. Wackes include quartz wacke and lithic greywacke, are abundant in the argillite facies of Chakrata and Chandpur formations. A marginal variation noticed in the detrital proportions of OLH and ILH siliciclastics. The presence of clayey components and moderate amount of siliceous rock fragments and feldspars makes both the siliciclastics compositionally submature. Absence of non-siliceous rock fragments may be because of diagenesis. Texturally, both the siliciclastics are mature as evidenced by an abundance of sub-rounded and rounded detritus and moderate degree of sorting. Feldspar detritus occur as the second most abundant detrital constitute of the clastic having different grain size and types. The most common types are microcline- orthoclase, and rare albite and labradorite - andesine types of plagioclase feldspar. The petrographic studies suggest that the source rocks are mostly granitic (felsic) in composition. The rarity of feldspar and rock fragments in clastics of the OLH and ILH signifies higher mineral maturity and suggest that these sediments are supplied from cratonic sources. The presence of clay minerals is indicative of chemical weathering of the protolith under the influence of warm climate.

Differences in morphological characteristics of different zircons suggest that Damtha and Jaunsar sediments of the Lesser Himalaya are sourced from a protoliths, which underwent different processes of zircon formation as well as

different degree of transportation. The variation in the εNd and ^{87}Sr/^{86}Sr of the Lesser Himalaya sediments suggests that the multiple sources of different ages are the potential sources for these sediments. The U-Pb geochronology age distribution from the ILH and OLH shows Palaeoproterozoic to Neoproterozoic ages, respectively. The ages of the Lesser Himalaya are correlated with the Vindhyan Supergroup, Aravalli craton and Bundelkhand craton. These suggest that Aravalli and Bundelkhand were the possible end members of the Lesser Himalayan clastics.

The similarity of the zircon age distribution from the Lesser Himalayan region and the cratonic succession demonstrate that the LH clastics showing the distal equivalent of the Vindhyan Supergroup and Aravalli cratons. This shows that the LH and the cratonic sedimentary successions are receiving detritus from the similar source (Bundelkhand craton and other Archean Successions).

7.4 Limitations and Future Scope of Work

This work is based on the dating of zircons separated from the siliciclastics which may represent the age of protoliths and hence put a maximum age of these clastic rocks. Therefore, such ages are prone to be overestimated on the counts of recycling process that covers the deposition of clasts followed by subsequent transport and their further deposition in same or different basins. Towards this, it is proposed as a part of future study to identify some secondary minerals like glauconite and fuchsite, chromium rich muscovite mica K (Al, Cr)$_2$(AlSi$_3$O$_{10}$) (OH)$_2$ which can be dated to provide age of deposition for these siliciclastic.

There is a need to add the suitable explanation for abnormally younger ages (0.8 Ga) with the major population particularly in the 1.8 Ga Rautgara Formation.
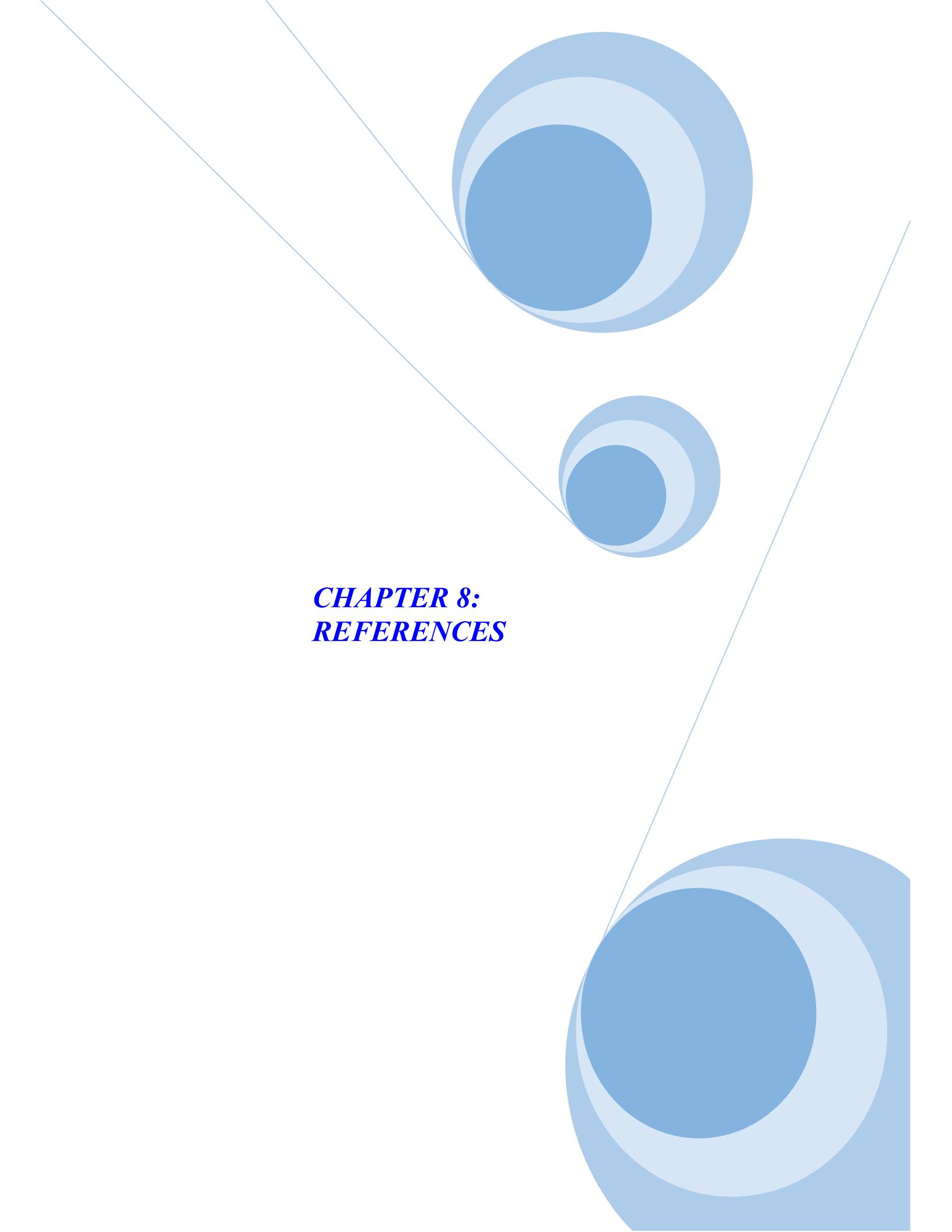
CHAPTER 8: REFERENCES

CHAPTER 8: REFERENCES

Ahmad, T., Harris, N., Bickle, M., Chapman, H., Bunbury, J. and Prince, C. (2000). Isotopic constraints on the structural relationships between the lesser Himalayan series and the high Himalayan crystalline series, Garhwal Himalaya. Geological Society of America Bulletin, Vol. 112, pp. 467-477.

Armstrong-Altrin, J. S., Lee, Y. I., Verma, S. P. and Ramasamy, S. (2004). Geochemistry of sandstones from the upper Miocene Kudankulam Formation, southern India: Implications for provenance, weathering, and tectonic setting. Journal of Sedimentary Research, Vol. 74, pp. 285-297.

Auden, J. B. (1934). The Geology of the Krol belt. Records of Geological Survey of India, Vol. 67, pp. 357-454.

Auden, J. B. (1935). Traverses in the Himalaya. Records of Geological Survey of India, 69, 123-167.

Auden, J. B. (1937). Structure of the Himalaya in Garhwal. Records Geological Survey of India, Vol. 71, pp. 407-433.

Awasthi, N., Ray, E. and Paul, D. (2018). Sr and Nd isotope compositions of alluvial sediments from the Ganga Basin and their use as potential proxies for source identification and apportionment. Chemical Geology, Vol. 476, pp. 327-339.

Azmi, R. J., Joshi, M.N. and Juyal, K.P. (1981). Discovery of the Cambro-Ordovician Conodonts from the Mussoorie Tal Phospholite: Its significant in correlation of the Lesser Himalaya. Contemporary Geoscientific Researches in Himalaya, Vol. 1, pp. 245-250.

Azmi, R. J. and Paul, S. K. (2004). Discovery of Precambrian-Cambrian boundary protoconodonts from the Gangolihat Dolomite of Inner Kumaun Lesser Himalaya: implication on age and correlation. Current Science, Vol. 86, pp. 1653-1660.

Bhargava, O. N. (1976). Geology of the Krol Belt and associated formations: a reappraisal. Geological Survey of India Memoirs, Vol. 106, pp. 167-234.

Bhat, M. I. and Ghosh, S. K. (2001). Geochemistry of the 2.51 Ga old Rampur group pelites, western Himalayas: implications for their provenance and weathering. Precambrian Research, Vol. 108, pp. 1-16.

Bhatt, D. K., Mamgain, V. D., Misra, R. S. and Srivastava, J. P. (1983). Shelly microfossils of Tommotian age (Lower Cambrian) from the Chert-Phosphorite Member of Lower Tal Formation, Maldeota, Dehra Dun District, Uttar Pradesh. Geophytology, Vol. 13, pp. 116-123.

Bhattacharya, A. R. (1983). Record of the stromatolite Plicatina from India. Geological Magazine, Vol. 120, pp. 543-548.

Brasier, M. D. and Singh, P. (1987). Microfossils and Precambrian–Cambrian boundary stratigraphy at Maldeota, Lesser Himalaya. Geological Magazine, Vol. 124, pp. 323-345.

Célérier, J., Harrison, T. M., Webb, A. A. G. and Yin, A. (2009). The Kumaun and Garwhal Lesser Himalaya, India: Part 1. Structure and stratigraphy The Kumaun and Garwhal Lesser Himalaya: Structure and stratigraphy. Geological Society of America Bulletin, Vol. 121, pp. 1262-1280.

Chakrabarti, R., Basu, A. R. and Chakrabarti, A. (2007). Trace element and Nd-isotopic evidence for sediment sources in the mid-Proterozoic Vindhyan Basin, central India. Precambrian Research, Vol. 159, pp. 260-274.

Colin, C., Turpin, L., Bertaux, J., Desprairies, A. and Kissel, C. (1999). Erosional history of the Himalayan and Burman ranges during the last two glacial–interglacial cycles. Earth and Planetary Science Letters, Vol. 171, pp. 647-660.

Condie, K. C. (1993). Chemical composition and evolution of the upper continental crust: contrasting results from surface samples and shales. Chemical Geology, Vol. 104, pp. 1-37.

Corfu, F. and Ayres, L. D. (1984). U-Pb age and genetic significance of heterogeneous zircon populations in rocks from the Favourable Lake

area, northwestern Ontario. Contributions to Mineralogy and Petrology, Vol. 88, pp. 86-101.

Corfu, F., Hanchar, J. M., Hoskin, P. W. andKinny, P. (2003). Atlas of zircon textures. Reviews in Mineralogy and Geochemistry, Vol. 53, pp. 469-500.

Cox, R., Lowe, D. R. and Cullers, R. L. (1995). The influence of sediment recycling and basement composition on evolution of mudrock chemistry in the southwestern United States. Geochimica et Cosmochimica Acta, Vol. 59, pp. 2919-2940.

Cullers, R. L. (2000). The geochemistry of shales, siltstones and sandstones of Pennsylvanian–Permian age, Colorado, USA: implications for provenance and metamorphic studies. Lithos, Vol 51, pp. 181-203.

Dabard, M. P. and Loi, A. (2012). Environmental control on concretion-forming processes: examples from Paleozoic terrigenous sediments of the North Gondwana margin, Armorican Massif (Middle Ordovician and Middle Devonian) and SW Sardinia (Late Ordovician). Sedimentary Geology, Vol. 267, pp. 93-103.

Deb, M. and Sarkar, S. C. (1990). Proterozoic tectonic evolution and metallogenesis in the Aravalli-Delhi orogenic complex, northwestern India. Precambrian Research, Vol. 46, pp. 115-137.

Deb, M., Thorpe, R. I., Krstic, D., Corfu, F. and Davis, D. W. (2001). Zircon U–Pb and galena Pb isotope evidence for an approximate 1.0 Ga terrane constituting the western margin of the Aravalli–Delhi orogenic belt, northwestern India. Precambrian Research, Vol. 108, pp. 195-213.

Deb, M., Thorpe, R. and Krstic, D. (2002). Hindoli Group of Rocks in the Eastern Fringe of the Aravalli-Delhi Orogenic Belt-Archean Secondary Greenstone Belt or Proterozoic SupracrusTals? Gondwana Research, Vol. 5, pp. 879-883.

DeCelles, P. G., Gehrels, G. E., Quade, J., LaReau, B. and Spurlin, M. (2000). Tectonic implications of U-Pb zircon ages of the Himalayan orogenic belt in Nepal. Science, Vol. 288, pp. 497-499.

Dhar, S., Frei, R.,Kramers, J. D., Nagler, T. F. and Kochhar, N. (1996). Sr, Pb and Nd isotope studies and their bearing on the petrogenesis of the Jalor and Siwana complexes, Rajasthan, India. Journal of the Geological Society of India, Vol. 48, pp. 151-160.

Etienne, J. L., Allen, P. A., le Guerroué, E., Heaman, L., Ghosh, S. K. and Islam, R. (2011). The Blaini Formation of the Lesser Himalaya, NW India. Geological Society, London Memoirs, Vol. 36, pp. 347-355.

Fedo, C. M., Wayne Nesbitt, H. and Young, G. M. (1995). Unraveling the effects of potassium metasomatism in sedimentary rocks and paleosols, with implications for paleoweathering conditions and provenance. Geology, Vol. 23, pp. 921-924.

Frank, W., Hoinkes, G., Miller, C., Purtscheller, F., Richter, W.andThöni, M. (1973). Relations between metamorphism and orogeny in a typical section of the Indian Himalayas. Tschermaks mineralogische und petrographische Mitteilungen, Vol. 20, pp. 303-332.

Gansser, A. (1964). Geology of the Himalayas. Wiley Interscience, New York, p. 289.

Garzanti, E., Andò, S., France-Lanord, C., Vezzoli, G., Censi, P., Galy, V. and Najman, Y. (2010). Mineralogical and chemical variability of fluvial sediments: 1. Bedload sand (Ganga–Brahmaputra, Bangladesh). Earth and Planetary Science Letters, Vol. 299, pp. 368-381.

Gehrels, G., Kapp, P., DeCelles, P., Pullen, A., Blakey, R., Weislogel, A., Ding, L., Guynn, J., Martin, A., McQuarrie, N. and Yin, A. (2011). Detrital zircon geochronology of pre-Tertiary strata in the Tibetan-Himalayan orogen. Tectonics, Vol. 30, TC5016, pp. 1-27.

George, B. G. and Ray, J. S. (2017). Provenance of sediments in the Marwar Supergroup, Rajasthan, India: Implications for basin evolution and Neoproterozoic global events. Journal of Asian Earth Sciences, Vol. 147, pp. 254-270.

Ghosh, S. K. (1991). Source rock characteristics of the Late Proterozoic Nagthat Formation, NW Kumaun Lesser Himalaya, India. Journal of the Geological Society of India, 38(5), 485-495.

Ghosh, S. K., Singh, S. S., Ray, Y. and Sinha, S. (2010). Soft-sedimentary deformational structures: seismites or penecontemporaneous, a study from the Palaeoproterozoic Lesser Himalayan succession, India. Current Science, Vol. 98, pp. 247-253.

Ghosh, S. K., Islam, R., Ray, Y. and Sinha, S. (2011). Palaeoproterozoic seismites in Damtha Group, Lesser Himalaya, India. Himalayan Geology, Vol. 32, pp. 43-55.

Ghosh, S. K., Pandey, A. K., Pandey, P., Ray, Y. and Sinha, S. (2012). Soft-sediment deformation structures from the Paleoproterozoic Damtha Group of Garhwal Lesser Himalaya, India. Sedimentary Geology, Vol. 261, pp. 76-89.

Ghosh, S. K., Jalal, P.and Islam, R. (2016a). Sedimentologic attributes of the Proterozoic siliciclastic packages of the Garhwal–Kumaun Lesser Himalaya, India: Implication for their relationship and palaeobasinal conditions. Journal of the Geological Society of India, Vol. 87, pp. 661-678.

Ghosh, S. K., Negi, M., Jalal, P. and Sinha, S. (2016b). Proterozoic sedimentary successions in the Himalayan Orogen: stratigraphy, sedimentology and palaeobasinal conditions. Himalayan Geology, Vol. 37, pp. 121-140.

Gregory, L. C., Meert, J. G., Bingen, B., Pandit, M. K. and Torsvik, T. H. (2009). Paleomagnetism and geochronology of the Malani Igneous Suite, Northwest India: implications for the configuration of Rodiniaand the assembly of Gondwana. Precambrian Research, Vol. 170, pp. 13-26.

Harley, S. L. and Kelly, N. M. (2007). Zircon tiny but timely. Elements, Vol. 3, pp. 13-18.

Harnois, L. (1988). The CIW index: a new chemical index of weathering. Sedimentary Geology, Vol. 55, pp. 319-322.

Hayashi, K. I., Fujisawa, H., Holland, H. D. and Ohmoto, H. (1997). Geochemistry of ~1.9 Ga sedimentary rocks from northeastern Labrador, Canada. Geochimica et Cosmochimica Acta, Vol. 61, pp. 4115-4137.

Heim, A. A. and Gansser, A. (1939). Central Himalaya: Geological observations of the Swiss expedition, Zurich: Gebruder Fretz, Delhi, Hindustan Publishing Corporation (India).Vol. 73, pp.1–246.

Herron, M. M. (1988). Geochemical classification of terrigenous sands and shales from core or log data. Journal of Sedimentary Research, Vol. 58, pp. 820-829.

Hofmann, M., Linnemann, U., Rai, V., Becker, S., Gärtner, A. and Sagawe, A. (2011). The India and South China cratons at the margin of Rodinia—Synchronous Neoproterozoic magmatism revealed by LA-ICP-MS zircon analyses. Lithos, Vol. 123, pp. 176-187.

Holland, T. H. (1908). On the occurrence of striated boulders in the Blaini Formation of Simla, with a discussion of the geological age of the beds. Records of the Geological Survey of India, Vol. 37, pp. 129-135.

Hoskin, P. W. O. and Black, L. P. (2000). Metamorphic zircon formation by solid-state recrystallization of protolith igneous zircon. Journal of Metamorphic Geology, Vol. 18, pp. 423-439.

Hoskin, P. W. O. and Schaltegger, U. (2003). The composition of zircon and igneous and metamorphic petrogenesis. Reviews in Mineralogy and Geochemistry, Vol. 53, pp. 27-62.

Hughes, N. C., Peng, S., Bhargava, O. N., Ahluwalia, A. D., Walia, S., Myrow, P. M. and Parcha, S. K. (2005). Cambrian biostratigraphy of the Tal Group, Lesser Himalaya, India, and early Tsanglangpuan (late early Cambrian) trilobites from the Nigali Dhar syncline. Geological Magazine, Vol. 142, pp. 57-80.

Islam, R., Ghosh, S. K.and Sachan, H. K. (2002). Geochemical characterisation of the Neoproterozoic Nagthat siliciclastics, NW Kumaun Lesser Himalaya: Implications for source rock assessment. Journal of the Geological Society of India, Vol. 60, pp. 91-105.

Jain, A. K. (1972). Overthrusting and emplacement of basic rocks in Lesser Himalaya, Garhwal, UP. Geological Society of India, Vol. 13, pp. 226-237.

Jiang, G., Christie-Blick, N., Kaufman, A. J., Banerjee, D. M. and Rai, V. (2002). Sequence stratigraphy of the Neoproterozoic infra Krol formation and Krol Group, lesser Himalaya, India. Journal of Sedimentary Research, Vol.72, pp. 524-542.

Jiang, G., Christie-Blick, N., Kaufman, A. J., Banerjee, D. M. and Rai, V. (2003a). Carbonate platform growth and cyclicity at a terminal Proterozoic passive margin, Infra Krol Formation and Krol Group, Lesser Himalaya, India. Sedimentology, Vol. 50, pp. 921-952.

Jiang, G., Sohl, L. E. and Christie-Blick, N. (2003b). Neoproterozoic stratigraphic comparison of the Lesser Himalaya (India) and Yangtze block (south China): Paleogeographic implications. Geology, Vol. 31, pp. 917-920.

Jin, Z., Li, F., Cao, J., Wang, S. and Yu, J. (2006). Geochemistry of Daihai Lake sediments, Inner Mongolia, north China: implications for provenance, sedimentary sorting, and catchment weathering. Geomorphology, Vol. 80, pp. 147-163.

Johnsson, M.J. (1993). The system controlling the composition of clastic sediments. In: Johnsson, M.J., Basu, A. (Eds.), Processes Controlling the Composition of Clastic Sediments, Special Papers-Geological Society of America, Vol. 284, pp. 1-19.

Joshi, K. B., Singh, S. K., Lasalle, S., Lancaster, P. J., Storey, C., Fowler, M., Ahmad, T., Halla, J. andRai, V. K. (2016). Archean Crustal Evolution in the Bundelkhand Craton, India: Constraints from Whole Rock Sr-Nd and Zircon U-Pb/Hf Isotopes. In AGU Fall Meeting Abstracts.

Kaufman, A. J., Jiang, G., Christie-Blick, N., Banerjee, D. M. and Rai, V. (2006). Stable isotope record of the terminal Neoproterozoic Krolplatform in the Lesser Himalayas of northern India. Precambrian Research, Vol. 147, pp. 156-185.

Kaur, P., Zeh, A., Chaudhri, N., Gerdes, A. and Okrusch, M. (2013). Nature of magmatism and sedimentation at a Columbia active margin: Insights from combined U–Pb and Lu–Hf isotope data of detrital zircons from NW India. Gondwana Research, Vol. 23, pp. 1040-1052.

Kaur, P., Zeh, A. and Chaudhri, N. (2014). Characterisation and U–Pb–Hf isotope record of the 3.55 Ga felsic crust from the Bundelkhand Craton, northern India. Precambrian Research, Vol. 255, pp. 236-244.

Kessler, L. and Ramasamy, N. (2012). A semi-quantitative assessment of clay content in sedimentary rocks using portable X-ray fluorescence spectrometry. International Journal of Earth Sciences and Engineering, Vol. 5, pp. 363-364.

Khan, T. and Khan, M. S. (2015). Clastic rock geochemistry of Punagarh basin, trans-Aravalli region, NW Indian shield: implications for paleo-weathering, provenance, and tectonic setting. Arabian Journal of Geosciences, Vol. 8, pp. 3621-3644.

Khanna, P. P. (2009). An appraisal of ICP-MS technique for determination of REEs: long term QC assessment of silicate rock analysis. Himalayan Geology, Vol. 30, pp. 95-99.

Kohn, M. J., Paul, S. K. and Corrie, S. L. (2010). The lower Lesser Himalayan sequence: A Paleoproterozoic arc on the northern margin of the Indian plate. Bulletin, Vol. 122, pp. 323-335.

Kumar, M. R., Mishra, D. C., Singh, B., Raju, D. C. V. and Singh, M. (2013). Geodynamics of NW India: subduction, lithospheric flexure, ridges and seismicity. Journal of the Geological Society of India, Vol. 81, pp. 61-78.

Le Fort, P. (1975). Himalayas: the collided range. Present knowledge of the continental arc. American Journal of Science, Vol. 275, pp. 1-44.

Long, S., McQuarrie, N., Tobgay, T., Rose, C., Gehrels, G. and Grujic, D. (2011). Tectonostratigraphy of the Lesser Himalaya of Bhutan: Implications for the along-strike stratigraphic continuity of the northern Indian margin. Bulletin, Vol. 123, pp. 1406-1426.

Mackenzie, F. T. and Garrels, R. M. (1971). Evolution of Sedimentary Rocks. New York: Norton.

Malone, S. J., Meert, J. G., Banerjee, D. M., Pandit, M. K., Tamrat, E., Kamenov, G. D., Pradhan, V. R. and Sohl, L. E. (2008). Paleomagnetism and detrital zircon geochronology of the upper Vindhyan Sequence, Son Valley and Rajasthan, India: A ca. 1000 Ma

closure age for the Purana basins? Precambrian Research, Vol. 164, pp. 137-159.

Mandal, S., Robinson, D. M., Khanal, S., & Das, O. (2015). Redefining the tectonostratigraphic and structural architecture of the Almora klippe and the Ramgarh–Munsiari thrust sheet in NW India. Geological Society, London, Special Publications, 412(1), 247-269.

Martin, A. J., DeCelles, P. G., Gehrels, G. E., Patchett, P. J. and Isachsen, C. (2005). Isotopic and structural constraints on the location of the Main Central thrust in the Annapurna Range, central Nepal Himalaya. Geological Society of America Bulletin, Vol. 117, pp. 926-944.

McCann, T. (1991). Petrological and geochemical determination of provenance in the southern Welsh Basin. Geological Society, London, Special Publications, Vol. 57, pp. 215-230.

McKenzie, N. R., Hughes, N. C., Myrow, P. M., Xiao, S., & Sharma, M. (2011). Correlation of Precambrian–Cambrian sedimentary successions across northern India and the utility of isotopic signatures of Himalayan lithotectonic zones. Earth and Planetary Science Letters, Vol. 312, pp. 471-483.

McKenzie, N. R., Hughes, N. C., Myrow, P. M., Banerjee, D. M., Deb, M. and Planavsky, N. J. (2013). New age constraints for the Proterozoic Aravalli–Delhi successions of India and their implications. Precambrian Research, Vol. 238, pp. 120-128.

McLennan, S. M., Nance, W. B. and Taylor, S. R. (1980). Rare earth element-thorium correlations in sedimentary rocks, and the composition of the continental crust. Geochimica et Cosmochimica Acta, Vol. 44, pp. 1833-1839.

McLennan, S. M., Taylor, S. R. and Eriksson, K. A. (1983). Geochemistry of Archean shales from the Pilbara Supergroup, western Australia. Geochimica et Cosmochimica Acta, Vol. 47, pp. 1211-1222.

McLennan, S. M. (1989). Rare earth elements in sedimentary rocks; influence of provenance and sedimentary processes. Reviews in Mineralogy and Geochemistry, Vol. 21, pp. 169-200.

McLennan, S. M., Hemming, S., McDaniel, D. K. and Hanson, G. N. (1993). Geochemical approaches to sedimentation, provenance, and tectonics. Special Papers-Geological Society of America, Vol. 281, pp. 21-40.

McLennan, S. M. (2001). Relationships between the trace element composition of sedimentary rocks and upper continental crust. Geochemistry, Geophysics, Geosystems, Vol. 2, p. 2000GC000109.

McQuarrie, N., Robinson, D., Long, S., Tobgay, T., Grujic, D., Gehrels, G. and Ducea, M. (2008). Preliminary stratigraphic and structural architecture of Bhutan: Implications for the along strike architecture of the Himalayan system. Earth and Planetary Science Letters, Vol. 272, pp. 105-117.

Medlicott, H. B. (1864). On the geological structure and relations of the southern portion of the Himalayan range between the rivers of the Ganges and Ravee: Geological Survey of India, Vol. 3, pp. 1-86

Miller, C., Klötzli, U., Frank, W., Thöni, M. and Grasemann, B. (2000). Proterozoic crustal evolution in the NW Himalaya (India) as recorded by circa 1.80 Ga mafic and 1.84 Ga granitic magmatism. Precambrian Research, Vol. 103, pp. 191-206.

Mukherjee, P. K., Singhal, S., Adlakha, V., Rai, S. K., Dutt, S., Kharya, A. and Gupta, A. K. (2017). In situ U-Pb zircon micro-geochronology of MCT zone rocks in the Lesser Himalaya using LA-MC-ICPMS technique. Current Science, Vol. 112, pp. 802-810.

Myrow, P. M., Hughes, N. C., Paulsen, T. S., Williams, I. S.,Parcha, S. K., Thompson, K. R., Bowring, S. A., Peng, S.-C. and Ahluwalia, A. D. (2003). Integrated tectonostratigraphic analysis of the Himalaya and implications for its tectonic reconstruction. Earth and Planetary Science Letters, Vol. 212, pp. 433-441.

Myrow, P. M., Hughes, N. C., Goodge, J. W., Fanning, C. M., Williams, I. S., Peng, S., Bhargava, O. N., Parcha, S. K. and Pogue, K. R. (2010). Extraordinary transport and mixing of sediment across Himalayan central Gondwana during the Cambrian–Ordovician. Bulletin, Vol. 122, pp. 1660-1670.

Nagarajan, R., Madhavaraju, J., Nagendra, R., Amstrong-Altrin, J. S., Moutte and J. (2007a). Geochemistry of Neoproterozoic shales of the Rabanpalli Formation, Bhima Basin, Northern Karnataka, southern India: implications for provenance and paleoredox conditions. Revista Mexicana de Ciencias Geológicas, Vol. 24, pp. 150-160.

Nagarajan, R., Armstrong-Altrin, J. S., Nagendra, R., Madhavaraju, J. and Moutte, J. (2007b). Petrography and geochemistry of terrigenous sedimentary rocks in the Neoproterozoic Rabanpalli Formation, Bhima Basin, Southern India: implications for paleoweathering conditions, provenance and source rock composition. Journal Geological Society of India, Vol. 70, pp. 297-312.

Nagarajan, R., Armstrong-Altrin, J. S., Kessler, F. L., Hidalgo-Moral, E. L., Dodge-Wan, D. and Taib, N. I. (2015). Provenance and tectonic setting of Miocene siliciclastic sediments, Sibuti Formation, northwestern Borneo. Arabian Journal of Geosciences, Vol. 8, pp. 8549-8565.

Nagarajan, R., Armstrong-Altrin, J. S., Kessler, F. L. and Jong, J. (2017). Petrological and Geochemical Constraints on Provenance, Paleoweathering, and Tectonic Setting of Clastic Sediments from the Neogene Lambir and Sibuti Formations, Northwest Borneo. In:Sediment Provenance, pp.123-153.

Nath, B. N., Kunzendorf, H. and Pluger, W. L. (2000). Influence of provenance, weathering, and sedimentary processes on the elemental ratios of the fine-grained fraction of the bedload sediments from the Vembanad Lake and the adjoining continental shelf, southwest coast of India. Journal of Sedimentary Research, Vol. 70, pp. 1081-1094.

Negi, M., Rai, K. S, Ghosh, S.K, Bhan, U. and Singhal, S. (2018) Characterization of zircons from the Lesser Himalayan clastics: Implication for provenance appraisal. Himalayan Geology (Communicated).

Nesbitt, H. W., Markovics, G. and Price, R.C. (1980). Chemical processes affecting alkalis and alkaline earths during continental weathering. Geochimica et Cosmochimica Acta, Vol. 44, pp. 1659-1666.

Nesbitt, H. W. and Young, G. M. (1982). Early Proterozoic climates and plate motions inferred from major element chemistry of lutites. Nature, Vol. 299, 715-717.

Nesbitt, H. W. and Young, G. M. (1984). Prediction of some weathering trends of plutonic and volcanic rocks based on thermodynamic and kinetic considerations. Geochimica et Cosmochimica Acta, Vol. 48, pp. 1523-1534.

Nesbitt, H. W. and Young, G. M. (1989). Formation and diagenesis of weathering profiles. The Journal of Geology, Vol. 97, pp. 129-147.

Nesbitt, H. W., Fedo, C. M. and Young, G. M. (1997). Quartz and feldspar stability, steady and non-steady-state weathering, and petrogenesis of siliciclastic sands and muds. The Journal of Geology, Vol. 105, pp. 173-192.

Nyakairu, G. W. and Koeberl, C. (2001). Mineralogical and chemical composition and distribution of rare earth elements in clay-rich sediments from central Uganda. Geochemical Journal, Vol. 35, pp. 13-28.

Oldham, R. D. (1883). Note on the geology of Jaunsar and the Lower Himalayas. Records of the Geological Survey of India, Vol. 16, pp. 193-198.

Oldham, R. D. (1888). The sequence and correlation of the pre-tertiary sedimentary formations of the Simla region of the lower Himalayas. Records of Geological Survey of India, Vol. 21, pp. 130–143.

Osae, S., Asiedu, D. K., Banoeng-Yakubo, B., Koeberl, C. and Dampare, S. B. (2006). Provenance and tectonic setting of Late Proterozoic Buem sandstones of southeastern Ghana: Evidence from geochemistry and detrital modes. Journal of African Earth Sciences, Vol. 44, pp. 85-96.

Pandit, M. K., Sial, A. N., Jamrani, S. S. and Ferreira, V. P. (2001). Carbon isotopic profile across the Bilara group rocks of trans-Aravalli Marwar Supergroup in western India: Implications for Neoproterozoic-Cambrian transition. Gondwana Research, Vol. 4, pp. 387-394.

Pandit, M. K., Carter, L. M., Ashwal, L. D., Tucker, R. D.,Torsvik, T. H., Jamtveit, B. and Bhushan, S. K. (2003). Age, petrogenesis and significance of 1 Ga granitoids and related rocks from the Sendra area, Aravalli Craton, NW India. Journal of Asian Earth Sciences, Vol. 22, pp. 363-381.

Pant, C. C. and Shukla, U. K. (1999). Nagthat Formation: An example of a progradational, tide-dominated Proterozoic succession in Kumaun Lesser Himalaya, India. Journal of Asian Earth Sciences, Vol. 17, pp. 353-368.

Parrish, R. R. and Hodges, V. (1996). Isotopic constraints on the age and provenance of the Lesser and Greater Himalayan sequences, Nepalese Himalaya. Geological Society of America Bulletin, Vol. 108, pp. 904-911.

Pettijohn, F. J., Potter, P. E. and Siever, R. (1987). Sand and Sandstone, New York, Springer, pp. 553.

Pidgeon, R. T. (1992). Recrystallisation of oscillatory zoned zircon: some geochronological and petrological implications. Contributions to Mineralogy and Petrology, Vol. 110, pp. 463-472.

Pidgeon, R. T., Nemchin, A. A. and Hitchen, G. J. (1998). Internal structures of zircons from Archaean granites from the Darling Range batholith: implications for zircon stability and the interpretation of zircon U-Pb ages. Contributions to Mineralogy and Petrology, Vol. 132, pp. 288-299.

Pradhan, V. R., Meert, J. G., Pandit, M. K., Kamenov, G., Gregory, L. C. and Malone, S. J. (2010). India's changing place in global Proterozoic reconstructions: a review of geochronologic constraints and paleomagnetic poles from the Dharwar, Bundelkhand and Marwar cratons. Journal of Geodynamics, Vol. 50, pp. 224-242.

Radhakrishna, T., Krishnendu, N. R. and Balasubramonian, G. (2013). Palaeoproterozoic Indian shield in the global continental assembly: Evidence from the palaeomagnetism of mafic dyke swarms. Earth-Science Reviews, Vol. 126, pp. 370-389.

Raha, P. K., Chandy, M. C. and Balasubrahmanyan, M. N. (1978). Geochronology of the Jammu limestone, Udhampur district, Jammu & Kashmir state, India. Geological Society of India, Vol. 19, pp. 221-223.

Ramachandran, A., Madhavaraju, J., Ramasamy, S., Lee, Y. I., Rao, S., Chawngthu, D. L. andVelmurugan, K. (2016). Geochemistry of Proterozoic clastic rocks of the Kerur Formation of Kaladgi-Badami Basin, North Karnataka, South India: implications for paleoweathering and provenance. Turkish Journal of Earth Sciences, Vol. 25, pp. 126-144.

Rathore, S. S., Venkatesan, T. R. and Srivastava, R. K. (1999). Rb-Sr isotope dating of Neoproterozoic (Malani Group) magmatism from Southwest Rajasthan, India: Evidence of younger Pan-African thermal event by 40Ar-39Ar studies. Gondwana Research, Vol. 2, pp. 271-281.

Richards, A., Argles, T., Harris, N., Parrish, R., Ahmad, T., Darbyshire, F. and Draganits, E. (2005). Himalayan architecture constrained by isotopic tracers from clastic sediments. Earth and Planetary Science Letters, Vol. 236, pp. 773-796.

Rubatto, D. and Hermann, J. (2007). Experimental zircon/melt and zircon/garnet trace element partitioning and implications for the geochronology of crustal rocks. Chemical Geology, Vol. 241, pp. 38-61.

Rupke, J. (1974). Stratigraphic and structural evolution of the Kumaon Lesser Himalaya. Sedimentary Geology, Vol. 11, pp. 81-265.

Saha, D. (2013). Lesser Himalayan sequences in eastern Himalaya and their deformation: Implications for Paleoproterozoic tectonic activity along the northern margin of India. Geoscience Frontiers, Vol. 4, pp. 289-304.

Saini, N. K., Mukherjee, P. K., Rathi, M. S. and Khanna, P. P. (2000). Evaluation of energy-dispersive x-ray fluorescence spectrometry in the rapid analysis of silicate rocks using pressed powder pellets. X-Ray Spectrometry: An International Journal, Vol. 29, pp. 166-172.

Schaltegger, U., Fanning, C. M., Günther, D.,Maurin, J. C., Schulmann, K. and Gebauer, D. (1999). Growth, annealing and recrystallization of zircon and preservation of monazite in high-grade metamorphism: conventional and in-situ U-Pb isotope, cathodoluminescence and microchemical evidence. Contributions to Mineralogy and Petrology, Vol. 134, pp. 186-201.

Sharma, K. K. (1998). Geologic and tectonic evolution of the Himalaya before and after the India-Asia collision. Proceedings of the Indian Academy of Sciences-Earth and Planetary Sciences, Vol. 107, pp. 265-282.

Singh, P. and Rajamani, V. (2001). REE geochemistry of recent clastic sediments from the Kaveri floodplains, southern India: implication to source area weathering and sedimentary processes. Geochimica et Cosmochimica Acta, Vol. 65, pp. 3093-3108.

Singh, P. K. and Khan, M. S. (2017). Geochemistry of Palaeoproterozoic Rocks of Aravalli Supergroup: Implications for Weathering History and Depositional Sequence. International Journal of Geosciences, Vol. 8, pp. 1278-1299.

Singh, S. K., Trivedi, J. R. and Krishnaswami, S. (1999). Re-Os isotope systematics in black shales from the Lesser Himalaya: Their chronology and role in the $187Os/188Os$ evolution of seawater. Geochimica et Cosmochimica Acta, Vol. 63, pp. 2381-2392.

Singh, S. K., Rai, S. K. and Krishnaswami, S. (2008). Sr and Nd isotopes in river sediments from the Ganga Basin: sediment provenance and spatial variability in physical erosion. Journal of Geophysical Research: Earth Surface, Vol. 113, F03006.

Spencer, C. J., Harris, R. A., Sachan, H. K. and Saxena, A. (2011). Depositional provenance of the Greater Himalayan Sequence, Garhwal Himalaya, India: implications for tectonic setting. Journal of Asian Earth Sciences, Vol. 41, pp. 344-354.

Spencer, C. J., Harris, R. A. and Dorais, M. J. (2012). The metamorphism and exhumation of the Himalayan metamorphic core, eastern Garhwal region, India. Tectonics, Vol.31, TC1007, pp. 1-18.

Sugitani, K., Horiuchi, Y., Adachi, M. andSugisaki, R. (1996). Anomalously low Al_2O_3/TiO_2 values for Archean cherts from the Pilbara Block, Western Australia-possible evidence for extensive chemical weathering on the early earth. Precambrian Research, Vol. 80, pp. 49-76.

Sun, S. S. and McDonough, W. S. (1989). Chemical and isotopic systematics of oceanic basalts: implications for mantle composition and processes. Geological Society, London, Special Publications, Vol. 42, pp. 313-345.

Taylor, S. R. and McClennan, S. M. (1985). The Continental Crust; its composition and evolution: Oxford, Blackwell Science Publishers, p. 312.

Tewari, V. C. and Sial, A. N. (2007). Neoproterozoic–Early Cambrian isotopic variation and chemostratigraphy of the Lesser Himalaya, India, Eastern Gondwana. Chemical Geology, Vol. 237, pp. 64-88.

Tiwari, M. and Pant, I. (2009). Microfossils from the Neoproterozoic Gangolihat Formation, Kumaun Lesser Himalaya: their stratigraphic and evolutionary significance. Journal of Asian Earth Sciences, Vol. 35, pp. 137-149.

Valdiya, K. S. (1969). Stromatolites of the Lesser Himalayan carbonate formations and the Vindhyans. Geological Society of India, Vol. 10, pp. 1-25.

Valdiya, K. S. (1970). Simla Slates: The Precambrian flysch of the Lesser Himalaya, its turbidites, sedimentary structures and paleocurrents. Geological Society of America Bulletin, Vol. 81, pp. 451-468.

Valdiya, K. S. (1980). Geology of the Kumaun Lesser Himalaya: Dehra Dun, Wadia Institute of Himalayan Geology, p.291

Valdiya, K. S. (1995). Proterozoic sedimentation and Pan-African geodynamic development in the Himalaya. Precambrian Research, Vol. 74, pp. 35-55.

Vavra, G., Gebauer, D., Schmid, R. and Compston, W. (1996). Multiple zircon growth and recrystallization during polyphase Late Carboniferous to Triassic metamorphism in granulites of the Ivrea Zone (Southern

Alps): an ion microprobe (SHRIMP) study. Contributions to Mineralogy and Petrology, Vol. 122, pp. 337-358.

Verma, P. K. and Greiling, R. O. (1995). Tectonic evolution of the Aravalli orogen (NW India): an inverted Proterozoic rift basin? Geologische Rundschau, Vol. 84, pp. 683-696.

Virdi, N. S. (1988). Pre-Tertiary geotectonic events in the Himalaya. Zeitschrift Fur Geologische Wissenschaften, Vol. 16, pp. 571-585.

Virdi, N. S. (1995). Proterozoic sedimentological cycles and the geotectonic evolution of the southern margin of the proto-tethys: evidence from the western Himalaya. Indian Journal of Petroleum Geology, Vol. 4, pp. 45-73.

Webb, A. A. G., Yin, A., Harrison, T. M., Célérier, J., Gehrels, G. E., Manning, C. E. and Grove, M. (2011). Cenozoic tectonic history of the Himachal Himalaya (northwestern India) and its constraints on the formation mechanism of the Himalayan orogen. Geosphere, Vol. 7, pp. 1013-1061.

Wronkiewicz, D. J. and Condie, K. C. (1987). Geochemistry of Archean shales from the Witwatersrand Supergroup, South Africa: source-area weathering and provenance. Geochimica et Cosmochimica Acta, Vol. 51, pp. 2401-2416.

Wu, Y. and Zheng, Y. (2004). Genesis of zircon and its constraints on interpretation of U-Pb age. Chinese Science Bulletin, Vol. 49, pp. 1554-1569.

Yin, A. (2006). Cenozoic tectonic evolution of the Himalayan orogen as constrained by along-strike variation of structural geometry, exhumation history, and foreland sedimentation. Earth Science Reviews, Vol. 76, pp. 1-131.
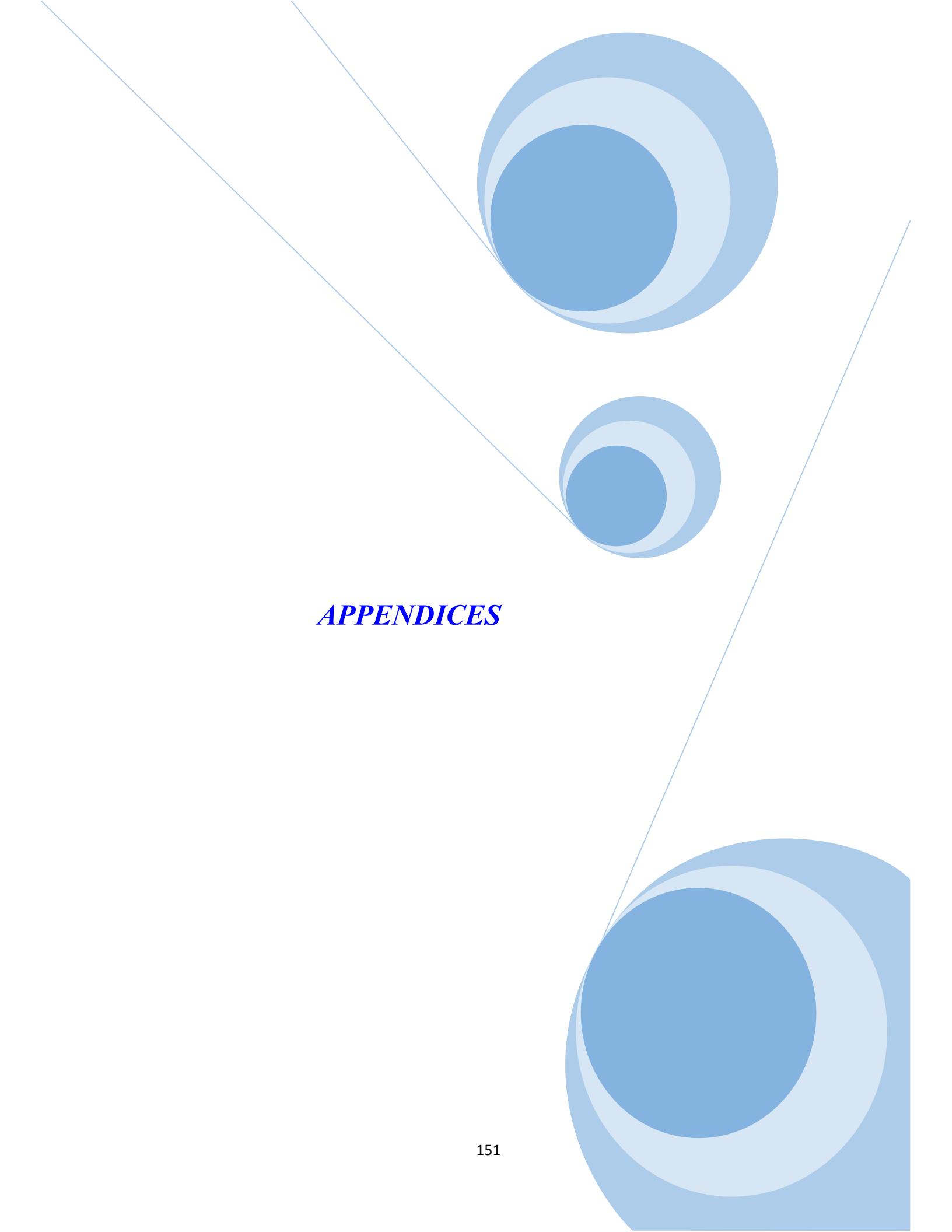
APPENDICES

Table 6.1: U-Pb geochronology of the Nagthat Fm. of outer Lesser Himalaya (Saknidhar, Garhwal section)

Analysis	Isotopic ratio						Apparent age (Ma)						Content (ppm)			
	$^{207}Pb/^{235}U$	2σ	$^{206}Pb/^{238}U$	2σ	$^{207}Pb/^{206}Pb$	2σ	$^{207}Pb/^{235}U$	2σ	$^{206}Pb/^{238}U$	2σ	$^{207}Pb/^{206}Pb$	2σ	U	Th	Pb	U/Th
MN6A-1	4.212	0.039	0.2959	0.003	0.10271	0.0005	1676.0	7.6	1671.0	16.0	1673.2	9.4	196.7	118.7	83.4	1.603
MN6A-2	9.873	0.098	0.4139	0.005	0.17342	0.0005	2424.4	9.9	2232.0	22.0	2590.8	4.8	163.5	98.1	98.0	1.632
MN6A-3	3.424	0.085	0.2457	0.007	0.1005	0.0003	1512.0	18.0	1415.0	34.0	1633.3	6.3	229.0	174.0	99.2	1.342
MN6A-4	1.4	0.023	0.1468	0.003	0.07149	0.0003	888.9	9.7	883.0	17.0	971.2	8.9	271.0	181.0	67.5	1.510
MN6A-5	0.611	0.027	0.0433	0.003	0.1038	0.0013	489.0	19.0	273.0	18.0	1692.0	24.0	1300.0	394.0	66.7	3.430
MN6A-6	0.902	0.035	0.0692	0.002	0.0932	0.0013	652.0	19.0	431.4	9.6	1490.0	27.0	534.0	153.0	47.4	3.533
MN6A-7	1.335	0.032	0.1285	0.004	0.07598	0.0005	861.0	14.0	779.0	21.0	1094.0	14.0	328.0	94.0	14.7	3.750
MN6A-8	0.776	0.067	0.064	0.006	0.08616	0.0006	579.0	38.0	400.0	35.0	1342.0	14.0	902.0	570.0	70.8	1.636
MN6A-9	1.418	0.022	0.1488	0.002	0.06902	0.0007	898.3	8.3	894.0	10.0	898.0	19.0	275.0	144.8	56.0	1.918
MN6A-10	0.67	0.021	0.0699	0.003	0.07052	0.0005	520.0	12.0	435.0	16.0	943.0	15.0	254.5	215.4	46.3	1.192
MN6A-11	11.329	0.098	0.4882	0.006	0.1684	0.0014	2550.3	8.1	2567.0	26.0	2541.0	14.0	91.8	76.3	92.2	1.340
MN6A-12	1.214	0.013	0.1272	0.002	0.06916	0.0003	807.0	5.8	771.7	9.0	903.1	8.9	180.0	104.0	35.1	1.746
MN6A-13	1.116	0.013	0.1173	0.002	0.06932	0.0003	761.0	6.2	714.9	8.4	907.9	8.9	164.0	108.0	33.9	2.180
MN6A-14	2.074	0.046	0.1824	0.004	0.08316	0.0009	1140.0	15.0	1080.0	20.0	1272.0	20.0	233.0	85.0	36.7	2.940
MN6A-15	1.872	0.063	0.1581	0.005	0.08382	0.0004	1070.0	22.0	946.0	29.0	1288.3	8.9	294.0	163.0	67.2	1.818
MN6A-16	5.261	0.094	0.3247	0.004	0.11684	0.0008	1862.0	15.0	1813.0	18.0	1908.0	12.0	140.2	37.0	32.1	3.710
MN6A-17	2.058	0.064	0.1509	0.004	0.10043	0.0009	1133.0	21.0	906.0	24.0	1631.0	16.0	308.8	192.0	72.4	1.617
MN6A-18	1.421	0.029	0.0876	0.002	0.115	0.0011	898.0	12.0	541.2	9.7	1879.0	18.0	471.0	329.0	95.0	1.440
MN6A-19	1.333	0.046	0.104	0.004	0.0947	0.0028	860.0	20.0	638.0	23.0	1519.0	56.0	388.0	195.0	64.1	2.170
MN6A-20	1.271	0.039	0.1106	0.003	0.08236	0.0008	832.0	17.0	676.0	16.0	1253.0	19.0	438.0	439.0	133.0	0.984
MN6A-21	0.848	0.027	0.0737	0.003	0.0839	0.0015	623.0	15.0	458.0	19.0	1290.0	34.0	573.0	360.0	80.0	1.750
MN6A-22	0.902	0.089	0.0605	0.006	0.10828	0.0009	651.0	49.0	379.0	37.0	1771.0	15.0	880.0	760.0	172.0	1.262
MN6A-23	1.084	0.038	0.0769	0.003	0.1013	0.0006	745.0	19.0	483.0	18.0	1648.0	10.0	602.0	536.0	161.3	1.228
MN6A-24	1.093	0.027	0.1055	0.003	0.0756	0.0010	750.0	13.0	647.0	17.0	1083.0	27.0	576.0	243.0	66.0	2.597
MN6A-25	1.0405	0.008	0.10455	0.001	0.07212	0.0004	724.1	3.9	641.0	3.6	989.0	11.0	534.0	271.6	72.4	2.138
MN6A-26	0.679	0.031	0.067	0.003	0.0737	0.0005	526.0	19.0	418.0	19.0	1033.0	13.0	558.0	386.0	50.6	1.598
MN6A-27	4.36	0.140	0.1755	0.006	0.18149	0.0007	1703.0	26.0	1042.0	31.0	2666.5	6.5	704.0	229.0	62.6	3.300
MN6A-28	2.45	0.096	0.1026	0.004	0.17355	0.0004	1256.0	29.0	630.0	23.0	2592.1	4.1	912.0	433.0	67.9	2.370
MN6A-29	4.36	0.180	0.1793	0.007	0.1768	0.0004	1703.0	34.0	1063.0	39.0	2623.0	4.0	463.0	112.4	62.1	4.600
MN6A-30	2.87	0.540	0.1601	0.004	0.129	0.0210	1360.0	140.0	957.0	23.0	2010.0	280.0	103.9	111.0	68.0	1.066
MN6A-31	1.348	0.025	0.1412	0.001	0.0696	0.0011	867.0	11.0	851.6	6.8	915.0	30.0	85.1	106.6	40.8	0.906
MN6A-32	1.4	0.044	0.1263	0.005	0.083	0.0043	888.0	19.0	766.0	28.0	1248.0	93.0	104.0	41.5	15.4	2.914

Continued-

Analysis	Isotopic ratio						Apparent age (Ma)						Content (ppm)			
	$^{207}Pb/^{235}U$	2σ	$^{206}Pb/^{238}U$	2σ	$^{207}Pb/^{206}Pb$	2σ	$^{207}Pb/^{235}U$	2σ	$^{206}Pb/^{238}U$	2σ	$^{207}Pb/^{206}Pb$	2σ	U	Th	Pb	U/Th
MN6A-33	1.262	0.030	0.1245	0.002	0.0737	0.0010	829.0	13.0	757.0	14.0	1040.0	23.0	61.7	26.6	8.8	2.614
MN6A-34	1.211	0.017	0.0946	0.002	0.0936	0.0009	805.5	7.9	582.6	9.5	1500.0	18.0	751.0	148.2	54.7	5.710
MN6A-35	1.323	0.034	0.118	0.003	0.08142	0.0003	859.0	14.0	723.0	17.0	1231.4	7.4	615.0	151.5	46.6	4.622
MN6A-36	1.288	0.015	0.0963	0.002	0.098	0.0017	840.0	6.4	593.0	12.0	1586.0	34.0	781.0	129.8	81.2	7.090
MN6A-37	1.493	0.058	0.1191	0.002	0.0932	0.0031	926.0	24.0	725.0	14.0	1502.0	58.0	221.0	160.0	52.3	1.592
MN6A-38	1.14	0.019	0.0952	0.002	0.08661	0.0007	772.3	8.9	585.9	9.6	1351.0	16.0	216.5	197.9	48.8	1.266
MN6A-39	10.43	0.480	0.441	0.022	0.1728	0.0018	2471.0	43.0	2352.0	99.0	2585.0	17.0	156.0	124.0	124.0	1.496
MN6A-40	5.87	0.160	0.2448	0.006	0.1725	0.0017	1955.0	24.0	1411.0	29.0	2582.0	16.0	226.8	153.6	140.5	1.759
MN6A-41	1.083	0.018	0.0917	0.003	0.0863	0.0029	744.8	8.6	566.0	17.0	1338.0	58.0	603.0	539.0	102.5	1.320
MN6A-42	1.414	0.017	0.125	0.002	0.08237	0.0009	894.9	7.1	759.0	12.0	1254.0	22.0	441.0	419.0	134.4	1.233
MN6A-43	1.207	0.019	0.1259	0.002	0.07	0.0013	803.6	8.6	764.2	8.6	914.0	31.0	271.0	209.0	72.9	1.520
MN6A-44	1.272	0.017	0.1357	0.002	0.06761	0.0007	833.1	7.8	820.0	10.0	856.0	22.0	201.6	176.6	65.1	1.332
MN6A-45	1.22	0.022	0.1242	0.001	0.0715	0.0015	809.0	10.0	754.5	7.7	971.0	41.0	249.3	149.4	54.2	1.954
MN6A-46	1.275	0.015	0.1342	0.001	0.0685	0.0004	834.4	6.9	812.0	7.0	887.0	11.0	144.3	98.2	37.1	1.717
MN6A-47	1.106	0.016	0.1116	0.001	0.07196	0.0008	756.2	7.9	681.9	6.6	984.0	21.0	716.0	988.0	295.0	0.855
MN6A-48	8.484	0.066	0.3513	0.003	0.17533	0.0005	2284.1	7.1	1941.0	13.0	2609.1	5.0	417.3	198.9	158.6	2.415
MN6A-49	7.58	0.120	0.3154	0.004	0.17365	0.0010	2188.0	11.0	1767.0	17.0	2593.1	9.3	371.0	183.1	133.1	2.318
MN6A-50	3.53	0.280	0.148	0.011	0.1733	0.0014	1530.0	60.0	887.0	62.0	2590.0	14.0	560.0	560.0	159.0	1.143
MN6A-51	1.112	0.020	0.0921	0.003	0.088	0.0021	758.8	9.4	568.0	17.0	1379.0	44.0	1074.0	625.0	129.4	2.120
MN6A-52	1.002	0.018	0.0722	0.002	0.0997	0.0019	704.4	9.4	449.0	14.0	1616.0	35.0	809.0	648.0	133.1	1.408
MN6A-53	0.1051	0.006	0.00525	0.000	0.1457	0.0030	101.4	5.7	33.8	1.4	2295.0	35.0	10030.0	9060.0	175.4	1.235
MN6A-54	0.1246	0.004	0.00685	0.000	0.1327	0.0043	119.2	3.3	44.0	1.5	2139.0	58.0	4000.0	3570.0	86.0	1.257
MN6A-55	4.53	0.100	0.2118	0.005	0.15486	0.0005	1735.0	19.0	1238.0	27.0	2400.2	5.5	821.0	491.0	259.3	1.850
MN6A-56	6.38	0.110	0.2788	0.004	0.16578	0.0008	2029.0	16.0	1585.0	20.0	2515.4	7.6	468.0	426.0	271.0	1.198
MN6A-57	4.81	0.490	0.188	0.017	0.1862	0.0039	1778.0	86.0	1107.0	91.0	2708.0	34.0	740.0	474.0	208.0	1.711
MN6A-58	2.27	0.110	0.0926	0.005	0.1775	0.0010	1200.0	34.0	571.0	27.0	2629.3	9.7	1148.0	1271.0	261.0	0.959
MN6A-59	4.41	0.110	0.1746	0.004	0.18315	0.0006	1714.0	20.0	1037.0	22.0	2681.6	5.1	419.0	303.0	85.3	1.410
MN6A-60	0.666	0.011	0.02522	0.000	0.1904	0.0020	518.4	6.5	160.6	2.7	2745.0	17.0	6430.0	3490.0	682.0	1.776
MN6A-61	0.838	0.016	0.0519	0.001	0.11572	0.0010	617.7	9.0	325.9	7.4	1891.0	15.0	3100.0	620.0	256.2	4.820
MN6A-62	0.931	0.013	0.06244	0.001	0.10836	0.0009	668.3	7.1	390.4	4.2	1772.0	15.0	2100.0	317.7	207.3	6.067
MN6A-63	0.987	0.054	0.0747	0.002	0.0966	0.0039	696.0	27.0	465.0	11.0	1554.0	78.0	1226.0	659.0	153.0	1.690
MN6A-64	1.37	0.040	0.1247	0.003	0.07974	0.0004	876.0	17.0	757.0	18.0	1190.0	11.0	1329.0	318.0	150.0	3.660

153

Continued-

Analysis	Isotopic ratio						Apparent age (Ma)						Content (ppm)			
	$^{207}Pb/^{235}U$	2σ	$^{206}Pb/^{238}U$	2σ	$^{207}Pb/^{206}Pb$	2σ	$^{207}Pb/^{235}U$	2σ	$^{206}Pb/^{238}U$	2σ	$^{207}Pb/^{206}Pb$	2σ	U	Th	Pb	U/Th
MN6A-65	1.159	0.019	0.1201	0.002	0.07033	0.0006	781.3	9.0	731.0	13.0	938.0	18.0	839.0	292.0	148.0	2.460
MN6A-66	1.232	0.011	0.1324	0.001	0.06733	0.0002	815.0	5.3	801.7	7.3	847.7	6.1	881.0	542.0	297.0	1.427
MN6A-67	1.716	0.044	0.0699	0.002	0.1764	0.0014	1020.0	18.0	435.0	11.0	2619.0	13.0	2053.0	1173.0	345.0	1.487
MN6A-68	0.898	0.080	0.0376	0.002	0.178	0.0170	648.0	42.0	238.0	13.0	2600.0	150.0	44.0	51.0	5.3	0.710
MN6A-69	2.362	0.057	0.2073	0.005	0.08219	0.0004	1230.0	18.0	1214.0	25.0	1249.9	9.5	315.0	131.0	119.0	2.350
MN6A-70	1.472	0.029	0.1168	0.003	0.09098	0.0004	918.0	12.0	712.0	14.0	1445.9	8.6	834.0	199.9	77.2	3.490
MN6A-71	0.654	0.040	0.0501	0.003	0.0944	0.0012	514.0	24.0	315.0	19.0	1519.0	25.0	2360.0	1640.0	323.0	1.263
MN6A-72	1.148	0.021	0.0821	0.003	0.1002	0.0020	776.4	9.8	509.0	17.0	1626.0	37.0	903.0	646.0	251.2	1.175
MN6A-73	1.626	0.070	0.1458	0.003	0.0811	0.0044	985.0	29.0	877.0	14.0	1210.0	98.0	225.0	95.0	56.3	1.932
MN6A-74	1.269	0.033	0.1275	0.003	0.0725	0.0013	831.0	15.0	773.0	16.0	999.0	35.0	160.6	102.9	48.9	1.313
MN6A-75	1.331	0.018	0.1414	0.002	0.06872	0.0004	860.8	8.4	853.0	11.0	890.0	11.0	515.0	151.9	82.7	2.960
MN6A-76	8.761	0.092	0.3671	0.004	0.1724	0.0002	2314.5	9.2	2018.0	17.0	2581.0	2.1	281.0	167.0	168.0	1.486
MN6A-77	0.4341	0.008	0.02594	0.000	0.12	0.0014	365.9	5.5	165.1	3.0	1954.0	20.0	3430.0	1695.0	242.0	1.743
MN6A-78	1.093	0.023	0.0832	0.002	0.0939	0.0013	750.0	11.0	515.2	9.0	1508.0	25.0	776.0	391.0	166.0	1.890
MN6A-79	4.71	0.060	0.2734	0.003	0.12404	0.0007	1769.0	11.0	1558.0	16.0	2015.0	10.0	119.1	89.9	74.1	1.203
MN6A-80	0.2445	0.004	0.01044	0.000	0.1677	0.0021	222.1	3.2	66.9	1.7	2534.0	21.0	6350.0	2890.0	181.0	2.042
MN6A-81	0.3034	0.007	0.01361	0.000	0.16104	0.0005	269.0	5.2	87.2	2.0	2466.6	4.9	4872.0	2050.0	182.8	2.290
MN6A-82	4.619	0.073	0.1996	0.002	0.16812	0.0004	1752.0	13.0	1173.0	13.0	2539.0	3.5	423.0	146.0	66.7	2.777
MN6A-83	5.304	0.099	0.2291	0.004	0.16723	0.0005	1869.0	16.0	1330.0	23.0	2530.1	5.1	248.0	117.0	80.1	2.020
MN6A-84	12.55	0.210	0.4225	0.007	0.21412	0.0005	2645.0	16.0	2271.0	34.0	2936.9	3.7	127.7	88.3	91.0	1.422
MN6A-85	7.165	0.071	0.3681	0.006	0.1406	0.0010	2133.6	9.4	2020.0	27.0	2234.0	13.0	110.2	44.9	46.1	2.286
MN6A-86	1.646	0.038	0.1476	0.005	0.0802	0.0011	988.0	15.0	887.0	27.0	1201.0	27.0	214.0	158.0	74.4	1.290
MN6A-87	1.846	0.012	0.1749	0.002	0.0756	0.0010	1062.1	4.1	1039.0	13.0	1083.0	26.0	134.7	95.9	51.2	1.337
MN6A-88	1.332	0.026	0.1384	0.003	0.07005	0.0010	861.0	11.0	835.0	19.0	927.0	27.0	47.9	90.0	39.4	0.553
MN6A-89	1.655	0.064	0.1596	0.005	0.07518	0.0007	991.0	24.0	954.0	29.0	1072.0	18.0	77.6	68.2	37.0	1.019
MN6A-90	1.55	0.031	0.1424	0.003	0.0779	0.0007	950.0	13.0	858.0	14.0	1143.0	17.0	136.8	118.0	57.1	1.067
MN6A-91	6.22	0.230	0.25	0.010	0.1803	0.0012	2001.0	33.0	1436.0	53.0	2655.0	11.0	206.0	179.0	114.8	1.081
MN6A-92	1.085	0.038	0.1112	0.004	0.06972	0.0004	744.0	19.0	679.0	25.0	920.0	11.0	234.0	118.5	39.7	1.804
MN6A-93	7.52	0.320	0.329	0.014	0.16488	0.0008	2171.0	39.0	1831.0	69.0	2506.2	8.5	39.9	30.0	12.7	1.187
MN6A-94	10.17	0.340	0.435	0.017	0.1662	0.0011	2431.0	41.0	2321.0	79.0	2519.0	11.0	97.2	39.2	41.3	2.440
MN6A-95	0.261	0.014	0.01158	0.001	0.1642	0.0021	235.0	11.0	74.2	4.5	2497.0	21.0	4610.0	2420.0	123.0	1.493
MN6A-96	1.423	0.022	0.1387	0.002	0.07441	0.0006	898.3	9.4	837.0	13.0	1052.0	15.0	114.9	236.0	108.5	0.383

Continued-

Analysis	Isotopic ratio						Apparent age (Ma)						Content (ppm)			
	$^{207}Pb/^{235}U$	2σ	$^{206}Pb/^{238}U$	2σ	$^{207}Pb/^{206}Pb$	2σ	$^{207}Pb/^{235}U$	2σ	$^{206}Pb/^{238}U$	2σ	$^{207}Pb/^{206}Pb$	2σ	U	Th	Pb	U/Th
MN6A-97	1.352	0.029	0.1369	0.003	0.07122	0.0003	868.0	13.0	827.0	18.0	963.8	7.6	197.0	228.0	102.0	0.704
MN6A-98	10.54	0.550	0.453	0.024	0.16809	0.0005	2490.0	52.0	2430.0	110.0	2538.6	4.5	71.3	54.7	81.0	1.053
MN6A-99	3.794	0.051	0.2689	0.005	0.10242	0.0007	1591.0	11.0	1535.0	27.0	1668.0	13.0	139.4	135.7	111.4	0.841
MN6A-100	1.078	0.019	0.1094	0.002	0.07131	0.0005	742.1	9.2	669.0	14.0	965.0	14.0	227.0	123.4	37.9	1.518
MN6A-101	1.089	0.018	0.1041	0.001	0.0766	0.0012	747.6	8.9	638.2	8.5	1107.0	30.0	120.2	62.7	18.0	1.644
MN6A-102	1.713	0.062	0.0867	0.004	0.1453	0.0025	1014.0	24.0	535.0	21.0	2287.0	30.0	789.0	162.0	82.6	4.210
MN6A-103	0.596	0.019	0.044	0.001	0.0978	0.0014	476.0	12.0	277.3	6.5	1580.0	27.0	718.0	929.0	135.3	0.633
MN6A-104	0.826	0.070	0.0332	0.003	0.1815	0.0017	601.0	40.0	210.0	19.0	2666.0	15.0	1760.0	690.0	118.7	2.250
MN6A-105	1.14	0.012	0.1098	0.001	0.07525	0.0005	772.5	5.7	671.7	7.8	1074.0	14.0	187.7	73.6	30.7	2.111
MN6A-106	1.767	0.042	0.1458	0.003	0.0867	0.0011	1034.0	16.0	877.0	17.0	1351.0	23.0	129.4	78.5	36.5	1.390
MN6A-107	1.174	0.050	0.0568	0.002	0.1506	0.0012	785.0	23.0	356.0	15.0	2352.0	13.0	1032.0	356.0	63.8	2.500
MN6A-108	2.22	0.170	0.1068	0.008	0.1557	0.0012	1192.0	56.0	652.0	48.0	2408.0	13.0	521.0	209.0	43.0	2.210
MN6A-109	0.8282	0.009	0.0641	0.001	0.0937	0.0015	612.4	5.2	400.3	7.8	1498.0	29.0	618.0	349.0	89.9	1.500
MN6A-110	2.84	0.044	0.1609	0.003	0.12786	0.0005	1365.0	12.0	962.0	17.0	2068.6	7.2	349.0	112.5	64.5	2.679
MN6A-111	2.88	0.035	0.2078	0.004	0.10055	0.0006	1376.5	9.1	1217.0	18.0	1634.0	11.0	169.0	151.0	93.6	1.020
MN6A-112	3.791	0.092	0.2803	0.007	0.09789	0.0009	1590.0	19.0	1592.0	35.0	1584.0	17.0	135.7	112.8	98.6	1.071
MN6A-113	1.312	0.015	0.1395	0.002	0.0682	0.0004	850.8	6.6	841.8	9.6	876.0	11.0	98.7	63.2	29.6	1.410
MN6A-114	9.59	0.180	0.4002	0.008	0.17372	0.0003	2399.0	18.0	2169.0	36.0	2593.8	3.2	162.0	107.4	125.7	1.379
MN6A-115	5.531	0.093	0.2341	0.004	0.17104	0.0004	1904.0	15.0	1356.0	21.0	2567.8	4.3	263.0	179.1	118.1	1.357
MN6A-116	2.836	0.045	0.1945	0.003	0.10602	0.0004	1364.0	12.0	1146.0	16.0	1731.9	7.5	172.4	99.9	57.1	1.700
MN6A-117	0.795	0.015	0.0737	0.001	0.0785	0.0011	593.8	8.4	458.4	6.8	1157.0	28.0	388.0	577.0	116.5	0.689

Table 6.2: U-Pb geochronology of the Nagthat Fm. of outer Lesser Himalaya (Saknidhar, Garhwal section)

Analysis	Isotopic ratio						Apparent age (Ma)						Content (ppm)			
	$^{207}Pb/^{235}U$	2σ	$^{206}Pb/^{238}U$	2σ	$^{207}Pb/^{206}Pb$	2σ	$^{207}Pb/^{235}U$	2σ	$^{206}Pb/^{238}U$	2σ	$^{207}Pb/^{206}Pb$	2σ	U	Th	Pb	U/Th
MN5Z-1	4.261	0.099	0.2544	0.0061	0.12134	0.00045	1692	20	1460	31	1975.8	6.6	233	45.5	35.3	5.78
MN5Z-2	1.415	0.05	0.1418	0.0049	0.07152	0.00079	893	21	854	28	971	22	135.6	51.1	25.4	2.95
MN5Z-3	1.862	0.07	0.133	0.0056	0.102	0.0022	1068	25	804	32	1667	42	930	396	172	2.64
MN5Z-4	2.5	0.11	0.12	0.0047	0.1519	0.0013	1265	31	730	27	2367	15	507	76.1	52.8	7.16
MN5Z-5	3.15	0.16	0.1946	0.0085	0.11658	0.00096	1435	41	1144	46	1906	15	248	154	51.9	1.77
MN5Z-6	1.224	0.019	0.1287	0.0017	0.06894	0.00092	811.3	8.7	780.1	9.5	894	26	266	137	53.7	2.132
MN5Z-7	2.489	0.091	0.1831	0.0063	0.09884	0.00055	1264	27	1083	34	1602	10	310	82	49.4	4.49
MN5Z-8	1.159	0.016	0.1199	0.0015	0.07015	0.00026	783.8	6.6	729.8	8.8	932.5	7.5	198	155.2	46.2	1.392
MN5Z-9	1.085	0.01	0.0996	0.0013	0.079	0.00054	745.8	5.1	611.7	7.6	1171	14	396	207	63.5	2.27
MN5Z-10	2.56	0.32	0.12	0.014	0.1611	0.0039	1279	91	722	77	2459	42	630	94	61.7	7.9
MN5Z-11	3.356	0.049	0.22	0.0039	0.10971	0.00053	1493	12	1282	21	1794.2	8.7	400	246	164	1.589
MN5Z-12	3.45	0.11	0.2324	0.0064	0.10729	0.00083	1515	25	1346	34	1753	14	215	329	139.3	0.82
MN5Z-13	11.85	0.39	0.449	0.012	0.1909	0.0015	2590	32	2388	56	2749	13	73.5	48.3	50.3	1.68
MN5Z-14	1.32	0.043	0.1315	0.0047	0.0733	0.0011	853	19	796	27	1018	29	201	145	57	1.421
MN5Z-15	1.367	0.066	0.121	0.0075	0.0825	0.0014	873	29	734	44	1253	33	716	77.9	41.4	10.23
MN5Z-16	1.378	0.07	0.1297	0.0049	0.0746	0.0015	874	30	789	27	1053	39	159	136	69	1.32
MN5Z-17	3.67	0.22	0.231	0.013	0.11427	0.00082	1558	46	1334	69	1870	12	172	67.7	41.3	2.5
MN5Z-18	6.54	0.57	0.301	0.024	0.1552	0.0022	2012	79	1680	120	2401	23	175	25.5	20.8	7.34
MN5Z-19	1.258	0.014	0.112	0.0014	0.08085	0.00036	826.8	6.5	684.4	7.9	1217.6	8.8	568	48.7	21.1	12.41
MN5Z-20	1.529	0.011	0.1603	0.002	0.06902	0.00028	941.9	4.6	958	11	899	8.2	203	45.7	18.4	4.06
MN5Z-21	1.316	0.03	0.1382	0.0019	0.06972	0.00055	852	13	834	11	919	16	201	259	96	0.782
MN5Z-22	4.563	0.099	0.2971	0.0051	0.11188	0.00034	1740	18	1676	26	1830	5.5	111.8	145	119	0.81
MN5Z-23	1.338	0.028	0.1415	0.0033	0.06828	0.00053	861	12	853	18	872	14	175	169	72.1	1.096
MN5Z-24	1.198	0.018	0.1216	0.0014	0.07163	0.0004	799.1	8.2	739.8	7.8	975	11	445	60	19.82	7.15
MN5Z-25	1.369	0.082	0.1373	0.0049	0.0725	0.0016	879	33	833	28	1000	46	237	66.5	26.5	4.01
MN5Z-26	1.234	0.027	0.1243	0.0024	0.07179	0.00044	819	12	755	14	979	12	384	115	41.8	3.5
MN5Z-27	1.144	0.024	0.1158	0.0024	0.07185	0.00058	774	11	706	14	981	16	461	462	147	0.967
MN5Z-28	1.38	0.016	0.1475	0.0011	0.06808	0.00027	880.2	7	886.9	6.2	870.7	8.2	129	155	63.8	0.863
MN5Z-29	1.122	0.02	0.115	0.0025	0.07035	0.0004	763.4	9.6	702	15	938	12	160.1	126	41	1.285
MN5Z-30	1.33	0.023	0.1381	0.0033	0.07009	0.00067	859.9	9.6	833	19	929	19	401	230	88.4	1.75

Continued-

Analysis	Isotopic ratio						Apparent age (Ma)						Content (ppm)			
	$^{207}Pb/^{235}U$	2σ	$^{206}Pb/^{238}U$	2σ	$^{207}Pb/^{206}Pb$	2σ	$^{207}Pb/^{235}U$	2σ	$^{206}Pb/^{238}U$	2σ	$^{207}Pb/^{206}Pb$	2σ	U	Th	Pb	U/Th
MN5Z-31	2.019	0.074	0.1828	0.0043	0.08101	0.0009	1118	24	1082	23	1223	22	303.2	62.4	34	5.04
MN5Z-32	1.315	0.024	0.1386	0.0018	0.06944	0.00041	852	10	837	10	911	12	115.8	85.2	38.6	1.378
MN5Z-33	7.44	0.22	0.3227	0.0099	0.17108	0.00035	2165	27	1802	48	2568.2	3.5	890	103.3	85.7	8.65
MN5Z-34	1.02	0.14	0.0533	0.0085	0.1381	0.0028	714	70	332	51	2198	34	1510	1340	170.2	1.07
MN5Z-35	1.263	0.025	0.1294	0.0014	0.07081	0.0004	828	11	786	8.6	951	11	340	263	93.5	1.338
MN5Z-36	1.25	0.045	0.1056	0.0041	0.0857	0.00081	822	20	647	24	1331	18	738	296	85	3
MN5Z-37	1.535	0.036	0.147	0.0035	0.07489	0.00056	944	14	884	19	1065	15	331	207	81	1.71
MN5Z-38	1.343	0.031	0.141	0.0022	0.06882	0.00039	865	14	850	13	893	12	234	247	98.2	1.073
MN5Z-39	1.279	0.03	0.1306	0.0016	0.0706	0.001	835	13	791.5	9.4	941	28	32.5	59.4	22.3	0.576
MN5Z-40	21.43	0.58	0.58	0.015	0.26741	0.00075	3154	26	2945	61	3290.8	4.4	237	92	116	3.29
MN5Z-41	1.183	0.023	0.124	0.0019	0.07029	0.00054	792	11	754	11	936	15	274	103	30.2	2.73
MN5Z-42	1.585	0.013	0.1628	0.0014	0.07051	0.00037	964.2	5.3	972.1	7.6	943	11	89.4	67.1	32.3	1.408
MN5Z-43	1.592	0.036	0.1537	0.0026	0.07639	0.00069	968	14	922	15	1099	16	355	164	61.7	2.23
MN5Z-44	3.757	0.034	0.2276	0.0018	0.12013	0.00013	1583.2	7.4	1321.8	9.7	1958.1	2	948	152	105.4	6.29
MN5Z-45	4.566	0.062	0.2635	0.0035	0.11869	0.00015	1742	11	1507	18	1936.6	2.2	310.6	50.8	35.9	6.24
MN5Z-46	1.242	0.011	0.1312	0.0015	0.06923	0.00072	819.6	4.8	794.5	8.7	904	21	97.6	80	32.4	1.272
MN5Z-47	1.244	0.019	0.1315	0.0024	0.06874	0.00042	820.1	8.6	796	14	893	12	159.5	80	30.4	2.062
MN5Z-48	4.94	0.22	0.2117	0.0091	0.17236	0.00054	1808	38	1238	48	2580.7	5.3	384	66.5	58.7	5.97
MN5Z-49	1.349	0.05	0.1399	0.0038	0.0697	0.00064	872	23	844	21	918	18	259	56.6	22.3	4.78
MN5Z-50	15.16	0.19	0.5742	0.007	0.19097	0.00037	2825	12	2925	29	2750.5	3.2	133	72	99	2.12
MN5Z-51	5.427	0.077	0.3219	0.005	0.1234	0.0014	1889	12	1799	24	2004	21	242	153.1	165.5	1.544
MN5Z-52	1.506	0.03	0.085	0.0021	0.1283	0.002	933	12	526	13	2073	28	1496	2460	622	0.613
MN5Z-53	1.69	0.1	0.1136	0.0047	0.1095	0.0019	1004	40	693	27	1789	32	673	749	294	0.951
MN5Z-54	2.56	0.35	0.1	0.014	0.1877	0.0015	1250	100	608	83	2721	13	750	760	282	1.002
MN5Z-55	0.69	0.16	0.028	0.0065	0.1788	0.0049	525	95	178	41	2641	45	103	181	10.9	0.576
MN5Z-56	2.245	0.099	0.1912	0.0058	0.0851	0.0013	1193	31	1128	32	1317	30	262	72.4	41.2	3.83
MN5Z-57	1.632	0.038	0.1549	0.0037	0.07617	0.00019	982	15	928	20	1099.5	4.9	269	49	20.2	6.5
MN5Z-58	1.905	0.091	0.1767	0.0077	0.07833	0.00035	1079	32	1048	42	1155.1	8.8	265	96.2	48.1	2.9
MN5Z-59	1.69	0.053	0.1507	0.0047	0.08113	0.00021	1003	21	905	26	1224.6	5.1	391	86.8	40.3	4.83
MN5Z-60	0.943	0.035	0.0754	0.003	0.09088	0.00082	673	17	468	18	1446	17	2060	265	122	7.77

Continued-

Analysis	Isotopic ratio						Apparent age (Ma)						Content (ppm)			
	$^{207}Pb/^{235}U$	2σ	$^{206}Pb/^{238}U$	2σ	$^{207}Pb/^{206}Pb$	2σ	$^{207}Pb/^{235}U$	2σ	$^{206}Pb/^{238}U$	2σ	$^{207}Pb/^{206}Pb$	2σ	U	Th	Pb	U/Th
MN5Z-61	1.323	0.02	0.1301	0.0027	0.07386	0.0007	855.5	8.8	788	15	1036	19	424	39.8	18.42	10.14
MN5Z-62	1.23	0.12	0.108	0.011	0.084	0.0011	806	52	655	64	1290	25	441	133	61.7	3.06
MN5Z-63	2.99	0.11	0.199	0.0074	0.10757	0.00084	1401	27	1173	39	1758	14	524	373	228	1.58
MN5Z-64	1.398	0.029	0.1444	0.0028	0.06981	0.0004	887	12	869	16	922	11	158.7	133.9	53.3	1.32
MN5Z-65	1.519	0.029	0.1415	0.0036	0.07825	0.0008	937	12	853	20	1152	20	349	271	109	1.82
MN5Z-66	1.467	0.028	0.152	0.0032	0.06938	0.00036	916	11	912	18	910	10	164.1	114.3	51.9	1.503
MN5Z-67	1.359	0.038	0.1381	0.0043	0.07142	0.00078	870	17	834	25	968	22	172	146	56.7	1.39
MN5Z-68	3.69	0.12	0.2615	0.0059	0.10215	0.00098	1565	25	1497	30	1659	19	153.5	66.6	50.2	2.65
MN5Z-69	1.894	0.029	0.1857	0.0028	0.07426	0.00052	1078	10	1098	15	1048	14	107.2	67	36.1	1.68
MN5Z-70	4.128	0.056	0.2833	0.0038	0.10519	0.00026	1659	11	1608	19	1717.6	4.5	181.9	146.7	114.5	1.238
MN5Z-71	1.72	0.03	0.1638	0.0028	0.0759	0.0003	1015	11	977	16	1092.1	7.8	151	48.4	21.3	3.19
MN5Z-72	1.375	0.054	0.116	0.0026	0.0853	0.0019	875	22	707	15	1314	41	637	298	128	1.94
MN5Z-73	1.784	0.025	0.1706	0.0026	0.07559	0.00026	1039	9.1	1015	14	1084.2	6.9	178	147	64	2.23
MN5Z-74	4.07	0.083	0.2795	0.0054	0.10522	0.00039	1649	16	1592	28	1718	6.8	183	158	127	1.143
MN5Z-75	1.397	0.03	0.1454	0.0031	0.06939	0.00036	886	13	875	17	910	11	84.2	93	37.3	0.989
MN5Z-76	10.12	0.29	0.45	0.01	0.1618	0.0027	2441	29	2394	45	2476	30	55.2	50.6	63.8	1.165
MN5Z-77	2.23	0.11	0.157	0.01	0.1042	0.0033	1187	34	936	56	1686	57	155	173	62.2	1.11
MN5Z-78	2.753	0.028	0.2262	0.0022	0.08775	0.00042	1342.5	7.5	1315	11	1376.7	9.2	105.6	70.5	44	1.581
MN5Z-79	1.457	0.022	0.1481	0.0022	0.07058	0.00039	912.2	9.1	890	12	945	11	151.2	123.5	55.5	1.251
MN5Z-80	1.456	0.058	0.1254	0.0054	0.08488	0.00088	909	24	760	31	1315	19	250	82.9	27.5	3.2
MN5Z-81	3.527	0.089	0.2383	0.0062	0.10719	0.00034	1531	20	1377	32	1753.5	6.3	375	158.1	122.5	2.41
MN5Z-82	1.23	0.028	0.1205	0.0032	0.07392	0.00066	815	13	733	19	1042	19	267	98.8	33.1	2.61

Table 6.3: U-Pb geochronology of the Nagthat Fm. of outer Lesser Himalaya (Saknidhar, Garhwal section)

Analysis	Isotopic ratio						Apparent age (Ma)						Content (ppm)			
	$^{207}Pb/^{235}U$	2σ	$^{206}Pb/^{238}U$	2σ	$^{207}Pb/^{206}Pb$	2σ	$^{207}Pb/^{235}U$	2σ	$^{206}Pb/^{238}U$	2σ	$^{207}Pb/^{206}Pb$	2σ	U	Th	Pb	U/Th
MN5X-1	17.1	1.2	0.502	0.031	0.2455	0.0023	2926	71	2630	130	3155	15	46.4	76	42.9	0.8
MN5X-2	1.478	0.029	0.1501	0.0032	0.07302	0.00088	921	12	902	18	1014	24	77.1	60.4	24.3	1.37
MN5X-3	1.412	0.018	0.1466	0.001	0.06968	0.00067	893.7	7.6	882	5.9	918	19	85.9	58.3	22.88	1.506
MN5X-4	1.401	0.029	0.1415	0.0014	0.072	0.0013	888	12	852.9	7.9	973	29	75.9	54.8	21.36	1.426
MN5X-5	1.45	0.14	0.0642	0.0059	0.1633	0.0015	888	55	400	35	2489	15	1120	1860	109.1	0.643
MN5X-6	1.341	0.025	0.1402	0.0013	0.0693	0.0011	863	10	845.9	7.3	891	22	27.2	37.8	15.19	0.716
MN5X-7	1.45	0.044	0.1455	0.0013	0.0724	0.0021	908	17	875.6	7.3	972	47	20.66	14.36	5.755	1.492
MN5X-8	1.366	0.021	0.1456	0.0018	0.0683	0.00046	874	9.3	876	10	877	14	90.4	118.9	43.9	0.766
MN5X-9	1.182	0.027	0.1069	0.0033	0.0792	0.0017	795	14	655	19	1174	42	284	177	47.2	1.543
MN5X-10	1.377	0.043	0.1333	0.0034	0.0746	0.0006	877	18	810	20	1053	14	148.2	131	33.2	1.24
MN5X-11	1.134	0.058	0.1073	0.0035	0.0774	0.00036	769	28	657	21	1131.4	9.3	353	418	77.1	0.833
MN5X-12	0.77	0.033	0.0512	0.0017	0.1072	0.001	584	20	322	10	1752	17	849	715	97.3	1.224
MN5X-13	1.535	0.014	0.15644	0.00092	0.07104	0.00045	945.4	5.4	936.9	5.1	958	13	101.3	75.5	30.9	1.342
MN5X-14	5.431	0.092	0.3392	0.0058	0.11531	0.00074	1888	15	1882	28	1884	11	145.9	295	229	0.489
MN5X-15	0.881	0.016	0.0644	0.0017	0.10024	0.00089	641.2	8.7	402	10	1628	17	533	432	84.3	1.25
MN5X-16	1.225	0.051	0.1237	0.0054	0.07027	0.00056	811	24	752	31	936	16	311	378	117.3	0.8245
MN5X-17	0.93	0.032	0.0822	0.0029	0.083	0.0013	669	16	509	17	1265	31	567	586	117.5	0.964
MN5X-18	1.366	0.029	0.1451	0.0033	0.06844	0.00082	873	12	873	19	880	23	131.4	112	41.6	1.213
MN5X-19	1.001	0.041	0.1057	0.004	0.06979	0.00059	703	20	647	23	921	17	150.6	121.6	26.01	1.3
MN5X-20	0.813	0.012	0.0723	0.0013	0.0799	0.0011	604.3	6.9	450	8	1194	26	230.7	237	37.27	0.986
MN5X-21	13.18	0.34	0.4945	0.0094	0.19386	0.0006	2689	25	2589	41	2775.1	5.1	43.7	27.97	27.2	1.58
MN5X-22	1.337	0.017	0.13638	0.00084	0.07122	0.00073	861.4	7.4	824.1	4.7	962	21	54.6	59.7	20.71	0.868
MN5X-23	7.29	0.37	0.29	0.014	0.18083	0.00064	2133	46	1638	70	2660.3	5.8	147.4	146	40.3	1.077
MN5X-24	9.01	0.4	0.367	0.015	0.1782	0.0016	2313	53	2012	74	2635	15	77	75	29.3	1.24
MN5X-25	4.35	0.47	0.19	0.019	0.1639	0.0013	1649	90	1110	100	2499	12	147	246	37.4	0.623
MN5X-26	1.02	0.051	0.106	0.0048	0.0698	0.00033	713	26	649	28	922.1	9.6	293	259	40.3	1.25
MN5X-27	11.35	0.42	0.501	0.016	0.16471	0.00039	2544	34	2614	70	2504.5	4	49.2	33.1	35.5	1.404
MN5X-28	1.206	0.013	0.12958	0.00061	0.06755	0.00048	803.1	5.7	785.4	3.5	854	14	61.5	45.8	15.2	1.345
MN5X-29	1.202	0.011	0.12862	0.00089	0.06806	0.00028	802.4	5.6	781.6	5.9	870.1	8.5	159.2	96.9	33.03	1.623
MN5X-30	4.946	0.099	0.3029	0.0056	0.1186	0.0013	1811	16	1705	28	1933	19	193.8	91	45.5	2.38

Continued-

Analysis	Isotopic ratio						Apparent age (Ma)						Content (ppm)			
	$^{207}Pb/^{235}U$	2σ	$^{206}Pb/^{238}U$	2σ	$^{207}Pb/^{206}Pb$	2σ	$^{207}Pb/^{235}U$	2σ	$^{206}Pb/^{238}U$	2σ	$^{207}Pb/^{206}Pb$	2σ	U	Th	Pb	U/Th
MN5X-31	0.831	0.007	0.08528	0.00076	0.0706	0.00019	614.1	3.9	527.5	4.5	945.9	5.6	516	697	78.5	0.742
MN5X-32	1.25	0.021	0.1303	0.0016	0.06931	0.00034	820.8	9	789.3	9	907.8	9.8	233	137.7	47.9	1.64
MN5X-33	1.62	0.024	0.1648	0.0029	0.0711	0.0003	977.7	9.1	983	16	960.2	8.7	124.3	83	31.1	1.62
MN5X-34	1.36	0.015	0.14521	0.00087	0.06843	0.00028	871.6	6.5	874	4.9	881.4	8.3	84.4	57.9	21.01	1.438
MN5X-35	1.0934	0.0054	0.10987	0.00063	0.07196	0.00025	750.1	2.6	672	3.7	984.7	7.1	235.3	119.4	18.28	1.973
MN5X-36	1.198	0.017	0.1282	0.0014	0.0677	0.00035	799.2	7.7	777.3	7.8	859	11	189	123	38.7	1.54
MN5X-37	1.075	0.017	0.1122	0.0017	0.07001	0.00032	740.9	8.1	685.5	9.8	928.4	9.2	421	372	76.7	1.109
MN5X-38	1.001	0.018	0.0895	0.0018	0.08152	0.00035	704	9	552	11	1233.7	8.4	658	592	117.3	1.087
MN5X-39	1.344	0.019	0.136	0.0018	0.07072	0.00041	864.9	8.3	822	9.9	949	12	245	172.3	55.1	1.41
MN5X-40	1.032	0.015	0.05867	0.00078	0.12834	0.00085	719.6	7.4	367.5	4.8	2075	12	1273	1580	298	0.818
MN5X-41	7	1.1	0.285	0.038	0.177	0.0017	2090	150	1610	190	2625	16	500	410	86	1.3
MN5X-42	8.65	0.24	0.2567	0.0065	0.2418	0.0022	2299	26	1472	33	3134	15	347	557	96.3	0.698
MN5X-43	4.31	0.29	0.182	0.011	0.17087	0.00058	1674	56	1073	60	2566	5.6	412	179	98.8	2.27
MN5X-44	1.67	0.17	0.0892	0.0079	0.1307	0.00058	980	60	556	48	2107.1	7.8	533	758	49.1	0.676
MN5X-45	1.176	0.03	0.1242	0.0029	0.06855	0.00082	788	14	757	17	883	24	150.7	85.1	26.42	1.811
MN5X-46	8.19	0.37	0.338	0.013	0.17433	0.00037	2245	41	1875	65	2599.6	3.6	257	108	88.5	2.4
MN5X-47	4.93	0.4	0.221	0.017	0.1598	0.0015	1775	68	1280	88	2453	15	234	281	67.7	0.96
MN5X-48	0.933	0.02	0.0848	0.0027	0.0806	0.0017	669	11	525	16	1210	42	214	286	41	0.729
MN5X-49	1.012	0.021	0.105	0.0017	0.06908	0.00026	710	10	643	10	901	7.8	257.8	342.1	53.3	0.762
MN5X-50	17.12	0.25	0.5797	0.0066	0.21328	0.00064	2940	14	2947	27	2930.5	4.8	42.6	45.6	59	1.43
MN5X-51	1.134	0.038	0.112	0.0047	0.0735	0.0012	767	18	684	27	1023	33	351	305	70.2	1.38
MN5X-52	0.754	0.016	0.0755	0.0015	0.07288	0.00025	569.7	9.5	469	8.9	1010.4	6.9	369	508	41.8	0.7273
MN5X-53	1.169	0.015	0.1263	0.0013	0.06689	0.00027	784.5	6.5	766.8	7.1	833.9	8.4	161.8	126	48.5	1.213
MN5X-54	1.392	0.069	0.1049	0.0041	0.0957	0.0015	885	29	643	24	1541	30	491	360	70.6	1.5
MN5X-55	1.262	0.016	0.1314	0.0015	0.0705	0.0014	828.4	6.9	795.7	8.4	927	27	154.5	153	50.1	1.057
MN5X-56	0.982	0.025	0.0906	0.0019	0.07882	0.00054	694	13	559	11	1167	14	558	285	38.7	2.38
MN5X-57	0.781	0.022	0.0443	0.0012	0.1276	0.003	586	13	279.6	7.4	2063	41	1392	2480	328	0.577
MN5X-58	0.726	0.033	0.0506	0.0027	0.1043	0.0027	554	20	318	17	1699	48	1130	1810	288	0.651
MN5X-59	0.984	0.031	0.0932	0.0033	0.07674	0.00095	695	16	574	20	1114	25	599	242	47.1	2.77
MN5X-60	0.992	0.019	0.0998	0.0023	0.07215	0.00049	699.5	9.8	613	14	990	14	506	437	54.2	1.192

Continued-

Analysis	Isotopic ratio						Apparent age (Ma)						Content (ppm)			
	$^{207}Pb/^{235}U$	2σ	$^{206}Pb/^{238}U$	2σ	$^{207}Pb/^{206}Pb$	2σ	$^{207}Pb/^{235}U$	2σ	$^{206}Pb/^{238}U$	2σ	$^{207}Pb/^{206}Pb$	2σ	U	Th	Pb	U/Th
MN5X-61	1.015	0.092	0.09	0.0079	0.0818	0.0024	710	47	555	47	1239	57	593	378	72.4	1.612
MN5X-62	2.99	0.084	0.1426	0.0037	0.15154	0.00064	1402	21	859	21	2363.2	7.2	752	321	91.6	2.71
MN5X-63	1.525	0.018	0.1535	0.0019	0.07224	0.0003	940	7.3	920	11	992.5	8.5	78.6	53.5	26.55	1.572
MN5X-64	1.569	0.014	0.1579	0.0014	0.07207	0.00016	957.9	5.5	945	7.8	987.7	4.4	175.5	156.5	72.8	1.125
MN5X-65	1.034	0.058	0.086	0.005	0.0882	0.0015	720	28	532	30	1386	32	924	197	78	4.78
MN5X-66	1.262	0.025	0.1219	0.0023	0.07512	0.00023	828	11	741	13	1071.7	6	470.7	266	55.4	1.89
MN5X-67	2.07	0.062	0.1704	0.005	0.08829	0.0004	1136	20	1014	27	1388.4	8.7	352	393	196	0.931
MN5X-68	6.22	0.12	0.2497	0.0046	0.1804	0.00037	2007	17	1437	24	2656.5	3.5	308	123.2	76.99	2.52
MN5X-69	4.06	0.4	0.17	0.017	0.1777	0.0011	1615	83	1001	91	2631.1	9.8	661	620	243	1.1
MN5X-70	5.46	0.22	0.2228	0.0093	0.17703	0.00059	1886	35	1301	50	2625.1	5.5	410	266	123.6	1.309
MN5X-71	5.75	0.27	0.241	0.011	0.1727	0.00055	1941	41	1390	60	2583.9	5.3	278	320	123	0.862
MN5X-72	2.14	0.14	0.151	0.011	0.1038	0.0014	1159	44	903	62	1692	25	464	339	141	1.335
MN5X-73	1.75	0.18	0.128	0.013	0.09885	0.00038	1012	70	774	77	1602.5	7.2	623	600	141.5	1.15
MN5X-74	3.559	0.048	0.276	0.0036	0.09345	0.00017	1540	11	1571	18	1496.9	3.4	268.1	72.2	67.2	3.632
MN5X-75	0.766	0.036	0.0727	0.0034	0.07633	0.00049	577	21	452	20	1104	13	536	637	118	0.802
MN5X-76	0.8524	0.0076	0.07834	0.00078	0.07844	0.00032	625.9	4.1	486.2	4.7	1157.9	8	531	578	115	0.884
MN5X-77	1.247	0.023	0.0885	0.002	0.1021	0.0011	824.1	9.9	546	12	1661	20	902	376	160.3	2.29
MN5X-78	1.164	0.05	0.0958	0.0045	0.08759	0.00068	783	24	590	26	1373	15	744	374	157.4	1.898
MN5X-79	1.12	0.03	0.1116	0.0031	0.07286	0.00019	764	14	681	18	1009.9	5.4	292	272	56	1.002
MN5X-80	0.884	0.029	0.0451	0.0014	0.14285	0.00092	643	16	284.1	8.4	2262	11	2319	1736	201	1.281
MN5X-81	1.55	0.12	0.0681	0.0051	0.1686	0.0031	949	49	424	31	2541	31	1140	247	155.9	5.52
MN5X-82	2.262	0.097	0.105	0.0045	0.15489	0.00069	1198	31	643	26	2400.5	7.6	1032	1167	199.7	0.873
MN5X-83	1.57	0.21	0.076	0.01	0.1508	0.0011	948	88	469	63	2355	13	910	980	131	0.839
MN5X-84	1.3	0.18	0.0636	0.0084	0.14852	0.00089	834	71	396	50	2329	10	1339	742	164.7	1.775
MN5X-85	0.941	0.027	0.0518	0.0015	0.13157	0.00041	673	14	325.6	9.2	2119	5.5	1059	696	141.8	1.49
MN5X-86	2.513	0.097	0.126	0.0043	0.145	0.002	1281	26	765	24	2287	24	499	390	120.8	1.37
MN5X-87	2.12	0.2	0.106	0.01	0.1447	0.0014	1143	65	650	58	2283	17	447	420	105.7	1.173
MN5X-88	8.44	0.61	0.356	0.024	0.1716	0.0011	2260	69	1950	120	2572	11	180	157	94.4	1.31
MN5X-89	1.386	0.014	0.1499	0.0011	0.0675	0.00028	882.8	6	900.6	6.4	852.9	8.7	91.1	87.8	29.95	1.076
MN5X-90	1.104	0.048	0.1131	0.0054	0.07093	0.00046	754	23	690	31	955	13	360.9	585	115.3	0.649

Continued-

Analysis	Isotopic ratio						Apparent age (Ma)						Content (ppm)			
	$^{207}Pb/^{235}U$	2σ	$^{206}Pb/^{238}U$	2σ	$^{207}Pb/^{206}Pb$	2σ	$^{207}Pb/^{235}U$	2σ	$^{206}Pb/^{238}U$	2σ	$^{207}Pb/^{206}Pb$	2σ	U	Th	Pb	U/Th
MN5X-91	0.579	0.029	0.05	0.0026	0.08297	0.00067	463	19	314	16	1268	16	779	1730	129.2	0.4836
MN5X-92	0.851	0.028	0.0501	0.0019	0.12331	0.00076	624	16	315	12	2006	11	926	182	54.8	5.86
MN5X-93	0.3968	0.0079	0.02941	0.00064	0.09781	0.00053	339.2	5.7	186.9	4	1583	10	2360	2830	138.3	0.894
MN5X-94	0.444	0.016	0.02906	0.00085	0.1106	0.0017	372	11	184.7	5.3	1808	28	1684	1964	102.1	0.917
MN5X-95	3.796	0.071	0.173	0.0031	0.1592	0.0003	1597	15	1028	17	2447.1	3.2	383	105.4	39.9	3.844
MN5X-96	5.33	0.23	0.2292	0.0092	0.16828	0.00049	1869	36	1328	48	2540.5	4.9	332	501	155	0.681
MN5X-97	3.68	0.21	0.1628	0.0089	0.16371	0.00089	1552	47	970	49	2494	9.3	308	551	101.8	0.56
MN5X-98	5.54	0.32	0.24	0.013	0.1666	0.0013	1899	51	1384	69	2529	12	232	154	71.3	1.53
MN5X-99	2.933	0.064	0.1875	0.0047	0.114	0.0012	1390	16	1107	25	1864	18	141	271	58.4	0.576
MN5X-100	1.419	0.059	0.0953	0.0037	0.10758	0.00096	895	25	586	22	1758	16	425	954	161	0.466
MN5X-101	6.356	0.043	0.2811	0.0021	0.16398	0.00045	2026	6	1597	11	2498.6	4.6	156.1	158.4	73.6	1.012
MN5X-102	7.56	0.11	0.3188	0.0043	0.17217	0.0003	2176	15	1783	21	2579.3	3	149.5	144.7	79.33	1.086
MN5X-103	7.576	0.073	0.3086	0.0033	0.17816	0.00032	2181.5	8.5	1734	16	2635.8	3	188	33.9	21.39	5.79
MN5X-104	1.412	0.033	0.1413	0.0033	0.07282	0.00025	895	13	852	18	1008.8	6.8	137.1	140.3	25.3	1.008
MN5X-105	1.26	0.033	0.1314	0.0032	0.06946	0.00024	827	15	795	18	912.2	7.2	93.1	63.2	14.6	1.55
MN5X-106	1.393	0.015	0.1473	0.0015	0.06853	0.0002	885.8	6.2	885.9	8.6	884.4	5.9	212	64	21.53	3.44
MN5X-107	1.719	0.032	0.1747	0.0032	0.07146	0.00024	1015	12	1038	18	970.3	6.9	71	62	23.4	1.304
MN5X-108	1.547	0.023	0.152	0.0026	0.07356	0.00033	949.1	9	912	14	1029.3	9.2	208	135	47.5	1.566
MN5X-109	1.19	0.024	0.1241	0.0025	0.06973	0.00031	796	11	754	14	920.3	9	147	176	52.7	0.844
MN5X-110	1.3865	0.0058	0.1461	0.00056	0.06884	0.00018	883.2	2.5	879	3.2	895.7	5.8	121.6	80.9	28.59	1.524
MN5X-111	1.311	0.021	0.1371	0.0024	0.06975	0.00035	850	9.3	828	13	920	10	226	266	91.5	0.826
MN5X-112	11.7	0.47	0.461	0.018	0.18352	0.00096	2571	38	2439	78	2684.6	8.5	67.8	38.2	32.8	1.83
MN5X-113	10.23	0.39	0.4	0.016	0.1846	0.0013	2447	37	2164	73	2694	12	111.3	41.6	37.2	3.19
MN5X-114	1.288	0.013	0.1363	0.0015	0.06857	0.00025	840.2	5.7	823.6	8.6	885.6	7.5	219.3	269	96.2	0.8
MN5X-115	0.954	0.026	0.0995	0.003	0.07015	0.00037	680	13	611	18	933	11	342	213	37	1.64
MN5X-116	1.4	0.051	0.1238	0.0044	0.08215	0.00031	887	22	752	25	1248.8	7.3	334	355	103.4	0.939
MN5X-117	7.65	0.3	0.34	0.013	0.16291	0.00035	2196	37	1896	66	2486	3.6	145.4	236	230.3	0.6164

Table 6.4: U-Pb geochronology of the Nagthat Fm. of outer Lesser Himalaya (Saknidhar, Garhwal section)

Analysis	Isotopic ratio						Apparent age (Ma)						Content (ppm)			
	$^{207}Pb/^{235}U$	2σ	$^{206}Pb/^{238}U$	2σ	$^{207}Pb/^{206}Pb$	2σ	$^{207}Pb/^{235}U$	2σ	$^{206}Pb/^{238}U$	2σ	$^{207}Pb/^{206}Pb$	2σ	U	Th	Pb	U/Th
MN5W-1	0.398	0.041	0.0424	0.0048	0.075	0.0015	352	37	268	30	1068	41	1390	12400	430	0.099
MN5W-2	0.9545	0.0079	0.0898	0.0013	0.08123	0.00076	680.4	4.1	554.1	7.8	1226	18	633	831	165.4	0.745
MN5W-3	0.657	0.026	0.0612	0.0023	0.0816	0.001	512	16	383	14	1236	24	671	960	80	0.665
MN5W-4	2.13	0.12	0.169	0.0043	0.0942	0.0039	1153	37	1006	23	1499	73	6.82	2.3	1.99	2.93
MN5W-5	1.115	0.017	0.1145	0.0016	0.07407	0.00036	760.5	7.9	698.8	9	1043.3	9.9	341.6	287.8	77.8	1.148
MN5W-6	1.465	0.035	0.1376	0.0026	0.0773	0.00029	915	14	831	15	1128.8	7.4	551	172	64.1	3.13
MN5W-7	1.1731	0.0076	0.12923	0.00067	0.06888	0.00026	788.1	3.5	783.4	3.9	895	7.8	265.7	169.6	67.17	1.546
MN5W-8	1.275	0.018	0.117	0.0023	0.0783	0.0018	834.4	8.2	713	13	1153	45	68.9	92.8	16.1	0.742
MN5W-9	1.453	0.024	0.1537	0.0033	0.06857	0.00044	911	10	921	18	885	13	60.7	16.8	8.2	3.69
MN5W-10	6.67	0.12	0.3822	0.0061	0.13131	0.00063	2068	16	2086	28	2115.5	8.4	199.8	82.3	94.6	2.423
MN5W-11	1.351	0.03	0.1428	0.0022	0.06823	0.00038	867	13	860	12	875	12	105.2	96	38.2	1.047
MN5W-12	1.363	0.013	0.145	0.0011	0.06849	0.00044	873	5.4	873	6	883	13	255	236	95.4	1.14
MN5W-13	1.3666	0.0097	0.1476	0.0014	0.0676	0.00029	874.6	4.2	887.7	8.1	856	8.9	173.5	181.4	75.5	1.011
MN5W-14	1.428	0.011	0.1527	0.0013	0.06757	0.0004	900.8	4.7	916.1	7.4	855	12	141.8	10.2	5.09	14.9
MN5W-15	1.675	0.023	0.1633	0.0016	0.0747	0.00042	998.6	8.8	975	9	1060	11	124.5	172	64.8	0.802
MN5W-16	3.388	0.058	0.2318	0.0036	0.10948	0.00098	1501	14	1344	19	1790	16	340	234	144	1.513
MN5W-17	6.3	0.16	0.2905	0.0066	0.16396	0.00051	2017	22	1644	33	2496.8	5.3	242	255	122.7	0.99
MN5W-18	4.58	0.11	0.2187	0.0049	0.15814	0.00043	1745	20	1275	26	2435.9	4.6	409.1	503	184.2	0.85
MN5W-19	0.751	0.019	0.05055	0.00085	0.112	0.0027	569	11	317.9	5.2	1837	45	1026	1870	168.1	0.69
MN5W-20	1.195	0.021	0.1262	0.0027	0.07159	0.00062	798.1	9.8	766	16	974	18	378	250	69.4	1.589
MN5W-21	1.28	0.012	0.1361	0.00067	0.06827	0.00042	836.6	5.4	822.5	3.8	876	13	64.4	46.5	20.3	1.514
MN5W-22	1.248	0.019	0.13559	0.00091	0.06714	0.00046	822	8.5	819.7	5.1	841	14	59.15	38.5	16.52	1.61
MN5W-23	1.18	0.043	0.1294	0.0051	0.06996	0.00027	789	21	784	29	927	7.8	160.5	127.3	59.8	1.348
MN5W-24	1.247	0.015	0.13593	0.00097	0.06771	0.00021	821.9	6.7	821.6	5.5	859.6	6.3	205	114	50.6	1.852
MN5W-25	8.11	0.22	0.378	0.012	0.16569	0.00085	2240	24	2065	55	2515.6	8.8	166.9	131.9	126.8	1.33
MN5W-26	1.108	0.033	0.1282	0.0037	0.06754	0.0003	758	15	777	21	854.3	9.1	149	115.4	57	1.242
MN5W-27	10.52	0.27	0.4637	0.0079	0.1686	0.00095	2478	24	2455	35	2543.4	9.4	135.5	70.6	72.8	2.037
MN5W-28	1.273	0.021	0.1397	0.0016	0.06766	0.00073	833	9.7	844.3	8.8	856	22	37.4	37.7	17.15	1.043
MN5W-29	1.109	0.018	0.1266	0.0023	0.06818	0.0002	757.2	8.7	768	13	874	6.1	269.9	143.5	65.5	1.946
MN5W-30	1.192	0.014	0.1322	0.0016	0.06792	0.00057	796.7	6.6	800.2	8.9	865	17	70.7	54	20.1	1.347

Continued-

Analysis	Isotopic ratio						Apparent age (Ma)						Content (ppm)			
	$^{207}Pb/^{235}U$	2σ	$^{206}Pb/^{238}U$	2σ	$^{207}Pb/^{206}Pb$	2σ	$^{207}Pb/^{235}U$	2σ	$^{206}Pb/^{238}U$	2σ	$^{207}Pb/^{206}Pb$	2σ	U	Th	Pb	U/Th
MN5W-31	1.169	0.022	0.1275	0.0017	0.06826	0.00036	785	10	773.3	9.4	876	11	116.4	104.4	39.7	1.083
MN5W-32	1.054	0.011	0.115	0.0012	0.07163	0.00032	730.8	5.2	701.8	7	975.2	9.2	235.6	423	115.2	0.584
MN5W-33	1.255	0.032	0.135	0.0028	0.069	0.00034	824	15	816	16	898	10	153.3	161	61.4	0.968
MN5W-34	5.48	0.12	0.3357	0.0074	0.12655	0.00042	1898	18	1865	36	2050.4	5.9	129.5	115	128.8	1.167
MN5W-35	0.742	0.021	0.0533	0.0016	0.10591	0.00093	563	12	335	10	1730	16	1603	1138	184	1.345
MN5W-36	0.776	0.013	0.06256	0.00061	0.09444	0.00052	586.7	5.7	391.2	3.7	1517	10	897	746	145.7	1.151
MN5W-37	1.219	0.036	0.1213	0.0016	0.07144	0.00076	808	16	738.1	9.4	969	21	282	222.1	56.1	1.178
MN5W-38	1.688	0.056	0.1416	0.0033	0.0838	0.0015	1004	21	854	18	1286	36	116.1	314.5	92.8	0.3378
MN5W-39	1.129	0.02	0.1104	0.0014	0.07359	0.00076	767.3	9.4	674.8	8.1	1030	21	142.2	437.2	126	0.2999
MN5W-40	1.079	0.025	0.094	0.0011	0.07977	0.00091	743	12	579.4	6.4	1190	22	514	812	98.2	0.589
MN5W-41	1.301	0.025	0.1253	0.0025	0.07542	0.00042	846	11	761	14	1079	11	542	160.7	59.3	3.06
MN5W-42	1.421	0.066	0.1351	0.0059	0.07558	0.00072	897	27	817	33	1084	19	470	106.7	35.5	4.17
MN5W-43	1.408	0.026	0.128	0.0026	0.07875	0.00031	892	11	777	15	1165.9	7.8	357	182.9	49.8	1.74
MN5W-44	1.476	0.084	0.126	0.0068	0.079	0.00041	919	35	765	39	1172	10	560	246	73.2	2.23
MN5W-45	1.304	0.018	0.1187	0.0026	0.0763	0.0015	847.5	8.1	723	15	1101	40	289	171	35.6	1.543
MN5W-46	5.37	0.35	0.233	0.014	0.1616	0.0011	1862	56	1345	74	2472	12	418	438	128	0.941
MN5W-47	1.548	0.034	0.1378	0.0019	0.0737	0.001	949	14	832	11	1031	27	273.1	188.9	49.68	1.328
MN5W-48	1.288	0.012	0.12313	0.00072	0.0715	0.00043	840.1	5.4	748.6	4.1	972	12	165.1	136.9	35.76	1.119
MN5W-49	1.367	0.021	0.1478	0.0019	0.06978	0.00044	874.5	9.1	891	11	921	13	100	146	59.2	0.659
MN5W-50	1.524	0.026	0.163	0.0027	0.06966	0.00022	939	11	973	15	918.4	6.4	195.7	63.3	25.51	3.07
MN5W-51	6.02	0.076	0.3	0.0036	0.15098	0.00095	1978	11	1691	18	2357	11	188.7	126.7	57.3	1.497
MN5W-52	6.93	0.18	0.3367	0.0095	0.15256	0.00032	2100	25	1870	47	2374.8	3.6	196.2	81	31.4	2.43
MN5W-53	5.14	0.17	0.2723	0.0068	0.1404	0.0016	1842	28	1552	35	2232	20	428	143	25.6	3.06
MN5W-54	1.202	0.023	0.1259	0.0018	0.07155	0.00063	801	10	764	10	972	18	95	119	28.2	0.845
MN5W-55	1.182	0.033	0.128	0.0033	0.06948	0.0004	791	15	776	19	912	12	135	93.7	34.7	1.472
MN5W-56	1.237	0.038	0.1276	0.0045	0.07225	0.00042	816	17	774	26	993	12	129.4	112.6	33	1.218
MN5W-57	1.14	0.018	0.1152	0.0017	0.07424	0.00022	773.5	8.8	702.9	9.8	1048	6	269.1	278	54.8	0.99
MN5W-58	1.131	0.019	0.1223	0.0026	0.06982	0.00065	769.8	8.8	744	15	922	19	70.5	68.9	22.83	1.053
MN5W-59	0.721	0.016	0.0716	0.0015	0.07443	0.00072	553.3	8.3	445.8	8.8	1052	19	252	449	84	0.65
MN5W-60	1.092	0.016	0.1015	0.0027	0.0802	0.0012	749.4	7.7	623	16	1200	29	306	774	192	0.407

Continued-

Analysis	Isotopic ratio						Apparent age (Ma)						Content (ppm)			
	$^{207}Pb/^{235}U$	2σ	$^{206}Pb/^{238}U$	2σ	$^{207}Pb/^{206}Pb$	2σ	$^{207}Pb/^{235}U$	2σ	$^{206}Pb/^{238}U$	2σ	$^{207}Pb/^{206}Pb$	2σ	U	Th	Pb	U/Th
MN5W-61	1.255	0.045	0.1335	0.0064	0.0721	0.002	825	21	808	36	984	53	206	140	29.3	2.58
MN5W-62	0.902	0.018	0.0755	0.0026	0.0885	0.0016	652.6	9.5	469	16	1391	33	393	860	114.6	0.482
MN5W-63	1.292	0.073	0.1167	0.0024	0.0868	0.0069	837	30	711	14	1230	110	114	121	27.7	0.96
MN5W-64	1.345	0.018	0.1436	0.0018	0.07059	0.00069	865.1	7.8	864.9	9.9	944	20	55.2	39.3	13.7	1.457
MN5W-65	10.28	0.15	0.4699	0.0078	0.16272	0.00052	2459	14	2488	35	2484	5.3	25.8	35.9	44.7	0.722
MN5W-66	1.295	0.042	0.1341	0.0035	0.07141	0.00076	842	19	811	20	968	21	166	215	75.4	0.851
MN5W-67	1.024	0.012	0.1062	0.0016	0.07114	0.00049	715.9	6	650.8	9.4	961	14	232	484	99	0.504
MN5W-68	1.254	0.014	0.136	0.0012	0.06832	0.00057	825.1	6.3	822.1	7.1	880	18	41.8	111.8	41.8	0.378
MN5W-69	1.226	0.011	0.1358	0.001	0.06692	0.00043	812.4	5.1	821	5.8	835	13	46.6	79.8	30.5	0.599
MN5W-70	10.011	0.083	0.4348	0.0044	0.16982	0.00069	2435.4	7.7	2331	19	2557	6.3	86.9	90	95.2	1.016
MN5W-71	1.501	0.05	0.1426	0.0058	0.07894	0.00096	931	21	863	32	1172	25	243	111	31.3	2.5
MN5W-72	1.483	0.013	0.141	0.0014	0.07755	0.00073	923.4	5.2	850.5	7.7	1134	19	251.3	162	43.7	1.72
MN5W-73	10.73	0.12	0.4798	0.0049	0.16593	0.00067	2499	10	2526	21	2516.8	6.7	17.3	23.8	31.4	0.769
MN5W-74	11.96	0.21	0.534	0.011	0.16526	0.00064	2602	18	2757	47	2510.1	6.4	36.1	30.8	41.3	1.171
MN5W-75	1.07	0.021	0.1138	0.0023	0.06891	0.00033	738	11	695	13	895.7	9.9	207	312	101	0.94
MN5W-76	0.628	0.019	0.0689	0.0018	0.06631	0.00066	494	12	430	11	816	21	507	1990	130	0.295
MN5W-77	1.217	0.054	0.1293	0.0041	0.0694	0.0012	804	24	783	24	895	24	96	113	41.9	0.83
MN5W-78	3.79	0.4	0.16	0.016	0.1712	0.0021	1583	85	974	87	2567	21	285	338	98	0.939
MN5W-79	4.63	0.12	0.1999	0.0053	0.1697	0.0013	1752	22	1174	28	2554	13	315	410	150	0.846
MN5W-80	1.018	0.061	0.0655	0.0035	0.11264	0.00083	706	31	409	21	1842	13	780	74.6	14.32	11.8
MN5W-81	11.38	0.11	0.4761	0.0056	0.17335	0.00081	2554.6	9.1	2510	25	2591.4	7.5	78.5	68.3	79.7	1.217
MN5W-82	9.45	0.17	0.4061	0.0084	0.16896	0.00099	2381	17	2196	38	2546.9	9.8	99.6	64.2	61.7	1.71
MN5W-83	0.89	0.051	0.0779	0.0072	0.0874	0.004	641	28	482	43	1335	87	431	436	85	1.012
MN5W-84	1.57	0.024	0.1588	0.0024	0.07157	0.00031	957.7	9.8	950	14	973.5	8.9	97.9	54.9	25.41	1.909
MN5W-85	1.63	0.055	0.1626	0.0064	0.07164	0.00046	979	22	975	35	975	13	114	49	24.1	2.24
MN5W-86	11.15	0.21	0.4674	0.009	0.1714	0.0016	2539	16	2482	34	2571	15	76.6	22.7	24	3.53
MN5W-87	1.355	0.026	0.0697	0.0016	0.1254	0.0025	870	11	434.3	9.9	2033	36	1016	374	113.6	2.65
MN5W-88	1.572	0.029	0.1376	0.0033	0.07835	0.00088	959	12	831	19	1155	22	339.4	599	108.1	0.566
MN5W-89	1.342	0.03	0.1335	0.0033	0.07032	0.00028	863	13	807	19	938.9	7.9	157	63.6	18.5	2.61
MN5W-90	6.96	0.15	0.2912	0.0062	0.16381	0.00079	2109	20	1647	31	2496.8	7.7	283	224	152	1.327

Continued-

Analysis	Isotopic ratio						Apparent age (Ma)						Content (ppm)			
	$^{207}Pb/^{235}U$	2σ	$^{206}Pb/^{238}U$	2σ	$^{207}Pb/^{206}Pb$	2σ	$^{207}Pb/^{235}U$	2σ	$^{206}Pb/^{238}U$	2σ	$^{207}Pb/^{206}Pb$	2σ	U	Th	Pb	U/Th
MN5W-91	2.278	0.027	0.2118	0.0024	0.07335	0.00029	1205.2	8.4	1238	13	1023.5	7.9	98.5	56.4	30	1.826
MN5W-92	11.47	0.24	0.475	0.011	0.17364	0.00098	2560	19	2502	48	2592.7	9.3	139	133	122	1.152
MN5W-93	11.89	0.37	0.504	0.018	0.17164	0.00094	2590	29	2625	77	2573.4	9.1	116.1	76.9	103.5	1.696
MN5W-94	5.23	0.19	0.326	0.012	0.11798	0.00039	1854	31	1818	60	1925.7	5.8	246	101	64	2.9
MN5W-95	1.85	0.017	0.1791	0.0012	0.07337	0.00044	1063.2	5.9	1062.2	6.3	1024	12	80.6	49.9	22.93	1.783
MN5W-96	3.2	0.14	0.218	0.012	0.10623	0.00088	1457	31	1277	60	1738	16	387	790	187	0.641
MN5W-97	1.383	0.028	0.1395	0.0025	0.07516	0.00037	881	12	842	14	1072.4	9.8	341	276	69	1.58
MN5W-98	3.28	0.11	0.2201	0.0048	0.10677	0.00054	1472	26	1282	25	1744.8	9.3	326	428	165	0.99
MN5W-99	2.06	0.12	0.1438	0.0095	0.1083	0.0016	1134	39	865	54	1769	27	529	1250	292	0.5
MN5W-100	1.122	0.029	0.1271	0.0037	0.0679	0.00029	763	14	771	21	865.4	8.8	150	175	70.3	1.13
MN5W-101	1.261	0.021	0.1319	0.002	0.07379	0.00035	828	9.3	799	11	1035.5	9.6	244.4	343.6	122.5	0.844
MN5W-102	1.895	0.024	0.1746	0.0021	0.08073	0.00033	1079	8.5	1037	12	1214.5	8	114.3	143.3	53.4	0.943
MN5W-103	1.389	0.026	0.1494	0.0016	0.07017	0.00055	885	11	897.7	8.9	932	16	155.1	95.7	38.4	1.927
MN5W-104	0.771	0.027	0.0815	0.0043	0.0741	0.0012	580	16	505	26	1043	31	279	362	41.7	0.889
MN5W-105	0.912	0.033	0.0826	0.0026	0.08751	0.0006	658	18	512	16	1372	13	399	589	90.2	0.791
MN5W-106	11.42	0.34	0.4891	0.0099	0.1726	0.0033	2566	32	2566	43	2581	31	82.3	44.9	65	2.31
MN5W-107	16.26	0.48	0.5487	0.0091	0.2285	0.0036	2890	28	2819	38	3046	27	33.2	50.8	92.7	0.798

Table 6.5: U-Pb geochronology of the Nagthat Fm. of outer Lesser Himalaya (Tons Valley, Garhwal section)

Analysis	Isotopic ratio						Apparent age (Ma)						Content (ppm)			
	$^{207}Pb/^{235}U$	2σ	$^{206}Pb/^{238}U$	2σ	$^{207}Pb/^{206}Pb$	2σ	$^{207}Pb/^{235}U$	2σ	$^{206}Pb/^{238}U$	2σ	$^{207}Pb/^{206}Pb$	2σ	U	Th	Pb	U/Th
MN5P-1	1.375	0.019	0.1465	0.0017	0.06824	0.00043	879.9	7.2	881.2	9.8	875	13	81.4	44.4	21.5	2.17
MN5P-2	1.281	0.015	0.1387	0.0013	0.06726	0.00034	837.1	6.4	837.4	7.4	845	11	53.9	20.1	9.23	3.19
MN5P-3	2.079	0.038	0.1951	0.0025	0.07772	0.00049	1141	13	1149	14	1139	12	69.9	62.2	39.6	1.344
MN5P-4	1.232	0.012	0.1366	0.0014	0.06565	0.00033	815.2	5.5	825.2	7.7	795	11	46.6	40.6	17	1.8
MN5P-5	1.213	0.012	0.1344	0.0011	0.06562	0.00031	807.2	5.1	812.9	6.5	793.8	9.8	62.8	41.5	18.4	2.2
MN5P-6	1.2316	0.0086	0.13692	0.00079	0.06539	0.00026	815	3.9	827.2	4.5	786.5	8.2	57.4	31.8	14.2	2.22
MN5P-7	1.367	0.017	0.1459	0.0017	0.06783	0.00027	874.7	7.4	877.9	9.7	863.1	8.2	91.4	48.8	23	2.55
MN5P-8	1.484	0.021	0.1517	0.0018	0.07128	0.00049	923.3	8.6	910.5	9.8	965	14	42	18.4	9.07	2.87
MN5P-9	1.207	0.026	0.1273	0.0027	0.06912	0.00036	803	12	772	15	902	11	51.6	32.9	10.66	2.129
MN5P-10	1.434	0.027	0.1497	0.0032	0.06957	0.0003	903	11	902	19	915.3	8.9	184.2	120	55.2	2.38
MN5P-11	1.206	0.016	0.1268	0.0016	0.06903	0.00024	803.1	7.2	769.6	9.3	899.4	7.2	277.2	54.4	17.01	6.599
MN5P-12	1.632	0.046	0.1574	0.0032	0.07477	0.00088	982	18	942	18	1062	24	53	40	17.6	1.309
MN5P-13	1.301	0.023	0.1368	0.0022	0.06841	0.0004	847	10	827	13	880	12	189	382	151	0.489
MN5P-14	1.532	0.017	0.0997	0.0015	0.11162	0.00089	943.3	6.7	612.8	8.5	1826	14	1716	1790	557	0.968
MN5P-15	0.912	0.029	0.0669	0.0019	0.09862	0.00054	657	16	417	11	1598	10	1220	2320	356	0.521
MN5P-16	1.31	0.015	0.1403	0.0015	0.06771	0.00028	849.8	6.8	846.1	8.7	859.5	8.6	72.8	41.2	16.44	1.676
MN5P-17	1.478	0.026	0.0979	0.0019	0.1098	0.0013	921	11	602	11	1796	22	1802	2480	616	0.708
MN5P-18	1.179	0.067	0.0799	0.0043	0.1064	0.0013	789	32	495	26	1737	22	1020	2270	439	0.454
MN5P-19	2.11	0.15	0.1299	0.0038	0.1145	0.003	1165	53	787	22	1870	48	888	1273	366	0.677
MN5P-20	1.507	0.041	0.1032	0.002	0.106	0.0022	932	17	633	12	1729	37	611	1083	236	0.57
MN5P-21	1.388	0.025	0.1453	0.0021	0.06901	0.00045	883	10	874	12	898	13	105.6	61.7	26.3	1.697
MN5P-22	1.1337	0.0069	0.11868	0.00063	0.06908	0.00037	769.5	3.3	723	3.6	901	11	74.7	42.2	15.9	1.709
MN5P-23	1.269	0.013	0.1273	0.0011	0.07191	0.00069	831.9	5.8	772.2	6	983	19	25.7	13.5	5.96	1.799
MN5P-24	1.0947	0.0069	0.12117	0.00084	0.06547	0.00019	750.7	3.3	737.3	4.8	789.4	6.1	71.7	36.1	12.52	1.897
MN5P-25	1.266	0.013	0.132	0.0011	0.0693	0.00035	829.4	6	799.4	6.3	907	10	213	298.8	113.2	0.701
MN5P-26	1.335	0.024	0.1422	0.002	0.06827	0.0004	860	10	857	12	876	12	179.5	85.9	34.7	2.069
MN5P-27	1.349	0.023	0.1427	0.0024	0.06801	0.00027	866	10	860	13	868.5	8	154.8	84	36.1	2.27
MN5P-28	1.447	0.044	0.1493	0.0051	0.07036	0.00073	906	18	896	28	937	21	203	174	64.3	1.3
MN5P-29	1.372	0.027	0.1454	0.0025	0.06824	0.00058	878	11	875	14	875	17	130.4	151.8	59.1	0.891
MN5P-30	1.293	0.016	0.1396	0.0018	0.06705	0.00019	842.4	7.2	844	11	839.1	5.8	185.6	108.9	40.4	1.794

Continued-

Analysis	Isotopic ratio						Apparent age (Ma)						Content (ppm)			
	$^{207}Pb/^{235}U$	2σ	$^{206}Pb/^{238}U$	2σ	$^{207}Pb/^{206}Pb$	2σ	$^{207}Pb/^{235}U$	2σ	$^{206}Pb/^{238}U$	2σ	$^{207}Pb/^{206}Pb$	2σ	U	Th	Pb	U/Th
MN5P-31	1.176	0.013	0.1284	0.0013	0.06628	0.00039	789.1	6.3	780.1	7.5	815	12	212	122.9	41	1.69
MN5P-32	1.232	0.026	0.1318	0.0025	0.06779	0.00048	814	12	798	14	861	14	226	149.4	51.8	1.497
MN5P-33	1.502	0.03	0.1563	0.0034	0.06921	0.00038	933	12	936	19	905	11	162	59	27.5	2.76
MN5P-34	1.221	0.022	0.1317	0.0022	0.06699	0.00021	811.3	9.6	798	13	837.2	6.5	104.9	88.5	34.1	1.26
MN5P-35	1.328	0.041	0.1378	0.0069	0.06896	0.00091	858	18	832	39	897	27	160	52.2	22.3	3.09
MN5P-36	1.285	0.04	0.1313	0.004	0.0696	0.0011	838	18	795	22	914	33	159	63.6	26.3	2.553
MN5P-37	1.169	0.027	0.1261	0.0031	0.06702	0.00014	787	13	765	18	838.2	4.4	220	71.9	25.5	3.15
MN5P-38	1.293	0.017	0.1362	0.0012	0.06877	0.00054	842.4	7.5	823.2	6.8	891	16	45.3	17.94	8.13	2.41
MN5P-39	1.442	0.031	0.1483	0.0037	0.07059	0.0004	906	13	891	21	945	12	243	97	36	2.97
MN5P-40	1.605	0.021	0.1062	0.0013	0.1087	0.0011	971.9	8.1	650.7	7.4	1775	19	1510	990	495	1.488
MN5P-41	1.416	0.058	0.1343	0.0028	0.0757	0.0023	895	24	812	16	1082	60	197	148.2	55.5	1.4
MN5P-42	1.372	0.03	0.1479	0.0031	0.0673	0.00053	876	13	889	17	846	16	48.8	67.9	28.6	0.753
MN5P-43	1.281	0.067	0.1212	0.0019	0.0767	0.0036	835	27	737	11	1101	78	604	385	128	1.98
MN5P-44	1.038	0.018	0.1008	0.0015	0.07463	0.00067	722.7	8.9	619.2	9.1	1058	18	466	600	148	0.85
MN5P-45	1.349	0.06	0.1308	0.0017	0.0753	0.0039	866	26	792.4	9.7	1070	100	224	560	152	0.48
MN5P-46	1.479	0.052	0.1464	0.0056	0.0723	0.0013	921	21	880	32	991	37	181	472	144	0.383
MN5P-47	1.226	0.018	0.1306	0.0013	0.06799	0.00046	812.6	8.1	791.2	7.6	868	14	204.8	544	137.5	0.383
MN5P-48	1.386	0.024	0.1315	0.0036	0.0767	0.0012	882	10	796	21	1108	31	569	164	52.4	4.68
MN5P-49	1.413	0.027	0.1454	0.0031	0.07054	0.0008	893	11	875	17	942	23	193	140	60.4	1.47
MN5P-50	1.241	0.034	0.11404	0.00078	0.0788	0.0019	818	15	696.2	4.5	1162	45	715	318	115	2.43
MN5P-51	1.162	0.047	0.1205	0.0047	0.06974	0.00066	782	23	733	27	920	19	300	117	42.4	2.74
MN5P-52	1.368	0.032	0.1306	0.0019	0.075	0.0015	878	15	791	11	1064	38	531	303	113	1.94
MN5P-53	0.67	0.14	0.063	0.014	0.0772	0.0013	513	85	394	84	1126	33	770	2120	203	0.49
MN5P-54	1.426	0.013	0.1411	0.001	0.07294	0.00051	899.6	5.5	850.9	5.7	1012	14	268	109	45.6	3.12
MN5P-55	1.246	0.042	0.1291	0.0044	0.06966	0.00041	821	19	783	25	918	12	164.8	87	23.2	2.01
MN5P-56	1.406	0.015	0.1495	0.0019	0.06882	0.00017	891.3	6.2	898	11	893.3	5.1	308	199	84	1.607
MN5P-57	1.212	0.017	0.1337	0.0019	0.06667	0.00015	805.9	7.6	809	11	827.4	4.7	222.6	141.3	52.9	1.665
MN5P-58	1.381	0.017	0.1422	0.0013	0.07169	0.00043	880.8	7.3	856.8	7.2	977	12	412	297	54.2	1.54
MN5P-59	1.497	0.023	0.1591	0.0024	0.06923	0.00049	928.7	9.5	952	13	905	15	45.7	19.9	9.37	2.3
MN5P-60	1.455	0.016	0.1524	0.0013	0.06995	0.00038	911.5	6.5	914.5	7.4	927	11	58.1	37.8	16.64	1.56

Continued-

Analysis	Isotopic ratio						Apparent age (Ma)						Content (ppm)			
	$^{207}Pb/^{235}U$	2σ	$^{206}Pb/^{238}U$	2σ	$^{207}Pb/^{206}Pb$	2σ	$^{207}Pb/^{235}U$	2σ	$^{206}Pb/^{238}U$	2σ	$^{207}Pb/^{206}Pb$	2σ	U	Th	Pb	U/Th
MN5P-61	1.308	0.011	0.13983	0.00088	0.06844	0.00032	849.3	4.6	843.7	4.9	881.5	9.7	74	30	13.55	2.398
MN5P-62	1.537	0.021	0.1637	0.0021	0.06868	0.00027	945.1	8.4	977	12	888.8	8	91.4	156.5	68	0.602
MN5P-63	1.257	0.016	0.1368	0.0013	0.06733	0.00042	826.5	7.1	826.3	7.5	847	13	126.1	240	103.4	0.524
MN5P-64	1.219	0.011	0.1349	0.0014	0.06615	0.00017	809.4	5.2	815.9	8.2	811	5.5	259.4	31.7	15	8.4
MN5P-65	1.307	0.011	0.1426	0.0016	0.06724	0.00021	848.6	4.9	859.2	8.8	844.9	6.4	215.1	143.5	62.1	1.62
MN5P-66	1.353	0.012	0.1475	0.0011	0.06731	0.00023	868.5	5.2	887.1	6.1	847.1	7.2	171.2	122.9	54.4	1.459
MN5P-67	1.47	0.027	0.1557	0.0027	0.06906	0.00039	917	11	933	15	900	11	211.2	47.5	25.7	4.52
MN5P-68	1.224	0.012	0.13285	0.0009	0.06701	0.00034	811.3	5.3	804.1	5.1	838	11	96	52.3	23.2	1.912
MN5P-69	6.83	0.12	0.2953	0.0035	0.16919	0.00099	2088	16	1668	18	2546	12	296.2	123	100.6	2.55
MN5P-70	1.366	0.03	0.1468	0.0029	0.06867	0.00028	878	13	883	17	888.5	8.3	239	197	89.8	1.297
MN5P-71	1.411	0.026	0.15	0.003	0.06841	0.00032	895	11	901	17	880.5	9.5	197	166	73	1.195
MN5P-72	1.289	0.015	0.1375	0.0017	0.06833	0.00021	840.8	6.7	830.4	9.4	878.4	6.2	125	93	35.1	1.431
MN5P-73	1.452	0.058	0.1104	0.0011	0.0951	0.0017	900	13	674.7	6.6	1526	30	1787	988	376	1.743
MN5P-74	1.563	0.016	0.1528	0.0018	0.07488	0.00023	955.5	6.4	916.4	9.8	1065	6	354	216	82.9	1.613
MN5P-75	1.6393	0.0099	0.1652	0.0011	0.07214	0.00021	985.4	3.8	985.7	6.3	989.6	5.9	248	153	76.8	1.71
MN5P-76	1.2242	0.009	0.13343	0.00077	0.06669	0.00034	811.6	4.1	807.4	4.4	828	10	56.2	21.75	9.32	3.37
MN5P-77	1.253	0.014	0.1346	0.0017	0.06729	0.00024	824.7	6.5	814.2	9.7	846.5	7.4	98.5	35.5	15.1	3.58
MN5P-78	1.197	0.019	0.1286	0.0015	0.06722	0.00053	798.7	8.8	779.7	8.5	843	16	41.3	26.4	11.2	1.97
MN5P-79	1.221	0.012	0.1319	0.0013	0.06714	0.00036	809.9	5.5	798.7	7.5	842	11	28.1	18.52	7.82	1.95
MN5P-80	9.16	0.24	0.396	0.01	0.16868	0.00092	2353	24	2152	48	2544.4	9.2	50.6	13.2	18	4.72
MN5P-81	6.849	0.09	0.3376	0.0042	0.14732	0.00045	2092	12	1875	20	2315	5.3	72.1	70.9	64.5	1.232
MN5P-82	1.2464	0.0078	0.13099	0.00069	0.0693	0.00024	821.7	3.5	793.5	3.9	907.4	7.3	96.7	94.5	41.39	1.255
MN5P-83	1.346	0.028	0.1449	0.0028	0.06709	0.00028	865	12	872	16	840.1	8.7	83.3	98	43.5	1.05
MN5P-84	1.546	0.027	0.1608	0.0029	0.0697	0.00025	948	11	961	16	919.4	7.3	80.2	29	14.8	3.25
MN5P-85	1.516	0.012	0.1567	0.0016	0.06995	0.00024	936.9	5	938.1	8.7	926.6	7.1	114.6	19.3	8.27	6.86
MN5P-86	1.324	0.015	0.1405	0.0015	0.06844	0.0003	856.2	6.6	847.5	8.7	881.7	9	62.2	34.4	14.71	2.07
MN5P-87	1.375	0.02	0.1366	0.0018	0.07212	0.00065	877.8	8.4	830	12	988	18	245	27	12.48	9.53
MN5P-88	1.262	0.033	0.1397	0.0035	0.06589	0.00059	828	15	843	20	802	18	25.4	8.2	3.53	3.42
MN5P-89	1.26	0.038	0.1342	0.0013	0.068	0.0018	826	16	813.1	7.4	858	52	9.78	5.48	2.47	1.92
MN5P-90	1.499	0.029	0.1591	0.0034	0.06851	0.00026	929	12	951	19	883.8	7.8	98	46.9	22.4	2.52

Continued-

Analysis	Isotopic ratio						Apparent age (Ma)						Content (ppm)			
	$^{207}Pb/^{235}U$	2σ	$^{206}Pb/^{238}U$	2σ	$^{207}Pb/^{206}Pb$	2σ	$^{207}Pb/^{235}U$	2σ	$^{206}Pb/^{238}U$	2σ	$^{207}Pb/^{206}Pb$	2σ	U	Th	Pb	U/Th
MN5P-91	1.423	0.019	0.1505	0.0021	0.06868	0.00029	898.3	8	904	12	890.3	9	91.2	50.1	23.5	1.78

Table 6.6: U-Pb geochronology of the Nagthat Fm. of outer Lesser Himalaya (Maldeota, Garhwal section)

Analysis	Isotopic ratio						Apparent age (Ma)						Content (ppm)			
	$^{207}Pb/^{235}U$	2σ	$^{206}Pb/^{238}U$	2σ	$^{207}Pb/^{206}Pb$	2σ	$^{207}Pb/^{235}U$	2σ	$^{206}Pb/^{238}U$	2σ	$^{207}Pb/^{206}Pb$	2σ	U	Th	Pb	U/Pb
MN5K-1	4.371	0.039	0.3019	0.0018	0.10526	0.0003	1706.6	7.4	1700.6	9.1	1718.7	5.1	52.3	107.1	84.1	0.494
MN5K-2	6.3	0.35	0.3187	0.0037	0.1445	0.0067	2016	49	1783	18	2276	80	34	54.7	58.4	0.632
MN5K-3	4.684	0.065	0.294	0.0014	0.1146	0.0012	1764	12	1661.5	6.8	1873	19	30.47	76.9	62	0.4071
MN5K-4	1.198	0.013	0.13083	0.00077	0.06641	0.00023	799.3	5.9	792.6	4.4	819.2	7.4	185.5	125.2	44.7	1.512
MN5K-5	1.174	0.01	0.12884	0.00095	0.06658	0.0002	788.6	4.8	781.2	5.4	824.4	6.1	160.3	80.39	28.04	2.011
MN5K-6	1.344	0.02	0.1415	0.0021	0.06852	0.00031	864.5	8.7	853	12	883.9	9.2	284	126	45.7	2.49
MN5K-7	4.627	0.073	0.3111	0.0054	0.10742	0.00071	1755	13	1750	26	1753	11	159	77.8	64.6	2.065
MN5K-8	1.222	0.035	0.1269	0.0026	0.07024	0.00094	809	16	770	15	933	26	362	173	43.6	2.56
MN5K-9	1.227	0.017	0.1325	0.0016	0.06741	0.00047	812.6	8	803.4	8.8	850	14	69	102	36.3	0.716
MN5K-10	1.427	0.035	0.1461	0.0027	0.07082	0.00044	899	14	879	15	952	13	53.5	23.2	9.84	2.41
MN5K-11	0.974	0.036	0.0993	0.0035	0.07145	0.00072	702	23	610	21	969	20	503	212	52.4	2.53
MN5K-12	1.408	0.058	0.1464	0.0064	0.06939	0.00068	888	25	879	36	905	19	158	81.7	37.7	1.972
MN5K-13	1.282	0.022	0.1307	0.0021	0.07023	0.00056	837.3	9.7	792	12	934	16	297	92.2	38.5	3.34
MN5K-14	10.54	0.099	0.4352	0.0042	0.17467	0.00044	2483	8.7	2329	19	2602.8	4.2	90.7	75.4	89.7	1.313
MN5K-15	1.315	0.025	0.14	0.0028	0.06749	0.00036	852	11	844	16	855	12	118.5	80.7	35.5	1.66
MN5K-16	1.268	0.094	0.0706	0.0077	0.136	0.012	823	40	438	46	2080	160	35.2	77	18.5	0.521
MN5K-17	1.262	0.016	0.1365	0.0015	0.06713	0.00028	828.6	7.1	824.9	8.5	843	8.5	70.8	38.2	16.68	2.028
MN5K-18	1.346	0.038	0.1426	0.0042	0.06863	0.00027	864	16	859	23	887.3	8.1	91.3	37.4	18.7	2.89
MN5K-19	1.515	0.016	0.1597	0.0013	0.0684	0.00044	936.3	6.5	954.9	7.1	880	13	33.2	24.8	12.53	1.464
MN5K-20	1.693	0.068	0.1636	0.0045	0.0763	0.0013	1006	26	976	25	1098	32	137	92	51.9	1.689
MN5K-21	2.163	0.052	0.1943	0.0051	0.08066	0.00055	1173	16	1144	28	1212	13	169.9	138.8	82.4	1.479
MN5K-22	1.267	0.033	0.1338	0.0036	0.06775	0.00048	830	15	809	20	860	15	48	45.2	20.17	1.267
MN5K-23	3.136	0.068	0.223	0.0054	0.10074	0.00041	1442	16	1297	28	1637.6	7.6	132.1	86.1	60.3	1.95

Continued-

Analysis	Isotopic ratio						Apparent age (Ma)						Content (ppm)			
	$^{207}Pb/^{235}U$	2σ	$^{206}Pb/^{238}U$	2σ	$^{207}Pb/^{206}Pb$	2σ	$^{207}Pb/^{235}U$	2σ	$^{206}Pb/^{238}U$	2σ	$^{207}Pb/^{206}Pb$	2σ	U	Th	Pb	U/Th
MN5K-24	1.167	0.027	0.1265	0.0032	0.06676	0.00026	790	13	767	19	830.2	7.9	221.2	136.6	57.7	1.931
MN5K-25	1.302	0.042	0.1375	0.005	0.06829	0.0008	844	19	830	28	875	23	146	46.5	21.3	3.95
MN5K-26	1.029	0.02	0.1115	0.0022	0.06673	0.00058	717.9	9.9	681	13	828	18	203.9	148	59	1.74
MN5K-27	1.591	0.064	0.1445	0.0058	0.07894	0.0002	962	26	869	33	1170.6	5	297	259	112	1.267
MN5K-28	1.089	0.04	0.1232	0.0043	0.06431	0.00038	752	18	748	24	751	12	59.7	36.9	16.3	1.86
MN5K-29	1.288	0.058	0.1192	0.0052	0.0776	0.001	838	26	725	30	1134	25	290	804	291	0.425
MN5K-30	1.535	0.037	0.1297	0.0019	0.0875	0.0026	946	16	786	11	1360	54	170	168	75.6	1.58
MN5K-31	1.397	0.052	0.1458	0.0056	0.06931	0.00035	888	22	881	31	908	10	148	91.3	42.9	2.07
MN5K-32	2.798	0.057	0.2268	0.0054	0.08959	0.00058	1356	15	1317	28	1416	12	173.2	33.2	23.3	8.1
MN5K-33	11.76	0.24	0.466	0.012	0.18323	0.00088	2583	19	2471	52	2682	7.9	91.9	41.2	51.3	2.65
MN5K-34	7.74	0.21	0.2898	0.0044	0.1959	0.0042	2202	23	1640	22	2788	33	171	137.3	62	1.48
MN5K-35	1.164	0.05	0.1072	0.0039	0.0817	0.0027	781	23	656	23	1226	63	227	281	37.1	0.93
MN5K-36	1.528	0.018	0.1567	0.0014	0.07076	0.00043	941.5	7.3	938.4	7.5	952	12	29	14.25	7.07	2.35
MN5K-37	1.741	0.076	0.162	0.003	0.0785	0.0029	1020	24	968	17	1125	43	225	60.9	31.6	4.09
MN5K-38	1.209	0.09	0.1067	0.0092	0.0823	0.0024	799	44	651	54	1241	54	660	1100	157	2.37
MN5K-39	1.622	0.051	0.1607	0.0053	0.07283	0.00035	976	20	960	30	1008.7	9.8	93	90	46.4	1.23
MN5K-40	1.605	0.064	0.1587	0.0066	0.0727	0.00032	968	25	948	37	1005.4	8.9	66.1	47.15	24.36	1.564
MN5K-41	4.84	0.3	0.301	0.021	0.11654	0.00097	1774	53	1690	100	1903	15	257	55.6	38.5	4.06
MN5K-42	1.375	0.037	0.1401	0.0045	0.0717	0.0014	880	15	845	25	971	37	86.5	83.4	34	1.098
MN5K-43	1.322	0.028	0.1339	0.0048	0.07044	0.00089	855	12	809	27	939	24	156.6	80.3	34.93	2.135
MN5K-44	1.339	0.056	0.1408	0.0061	0.06849	0.00022	863	24	848	34	883.2	6.8	189	79.6	35.2	2.483
MN5K-45	1.219	0.019	0.1348	0.0017	0.06568	0.00042	809	8.6	815	9.6	796	13	67.2	79.3	31.4	0.98
MN5K-46	1.077	0.07	0.1122	0.0074	0.06938	0.00065	734	36	683	44	909	19	244	113	18.8	5.8
MN5K-47	1.321	0.035	0.1398	0.0039	0.06818	0.00046	853	16	843	22	873	14	179	22.3	9.61	8.05
MN5K-48	1.358	0.014	0.1381	0.0014	0.07083	0.00038	870.6	5.8	833.7	7.7	952	11	249.6	215	89.6	1.197
MN5K-49	1.172	0.06	0.1097	0.005	0.0772	0.0015	782	29	670	29	1120	35	383	231	33	2.11
MN5K-50	1.08	0.02	0.1211	0.0016	0.06498	0.00028	744.5	9.9	737.1	9.1	774.8	8.8	103.2	133	56.9	0.782
MN5K-51	1.099	0.013	0.12264	0.00096	0.06534	0.00037	754	5.8	745.7	5.5	785	12	184.4	111.7	41.7	1.77
MN5K-52	1.139	0.021	0.1259	0.0017	0.06562	0.00035	773	10	764.5	9.6	794	11	166.9	152	58.5	1.25
MN5K-53	1.378	0.026	0.1452	0.002	0.06928	0.00027	879	11	874	11	906.8	8	115.7	62.9	27.5	2.03

Continued-

Analysis	Isotopic ratio						Apparent age (Ma)						Content (ppm)			
	$^{207}Pb/^{235}U$	2σ	$^{206}Pb/^{238}U$	2σ	$^{207}Pb/^{206}Pb$	2σ	$^{207}Pb/^{235}U$	2σ	$^{206}Pb/^{238}U$	2σ	$^{207}Pb/^{206}Pb$	2σ	U	Th	Pb	U/Th
MN5K-54	4.045	0.054	0.2811	0.0038	0.10336	0.00067	1643	11	1596	19	1685	12	125.2	76.1	63.8	1.682
MN5K-55	1.309	0.02	0.1382	0.0018	0.06888	0.00067	851	8.4	834	10	893	20	159.9	149.6	65.1	1.16
MN5K-56	7.179	0.057	0.3646	0.0037	0.14246	0.00052	2133.6	7.1	2004	17	2257.2	6.2	155.1	73.4	70.7	2.188
MN5K-57	1.448	0.015	0.146	0.0018	0.07224	0.00017	909	6	879	10	992.7	4.8	188	128	54.5	1.6
MN5K-58	1.331	0.016	0.141	0.0015	0.06866	0.00023	860.7	7.5	850.3	8.5	888.4	6.9	168	191	79.5	0.874
MN5K-59	4.165	0.066	0.2889	0.0038	0.10467	0.00047	1666	13	1636	19	1708.2	8.2	161.6	49.2	37.5	3.5
MN5K-60	1.494	0.025	0.1505	0.0021	0.0729	0.00037	927	10	903	12	1011	10	298.3	246	103.1	1.232
MN5K-61	1.348	0.036	0.1334	0.0012	0.074	0.002	865	15	807.2	6.6	1038	54	128.6	66.2	29.4	2.07
MN5K-62	4.34	0.055	0.2856	0.0035	0.10899	0.00091	1700	12	1619	17	1782	15	143.7	96.9	82.2	1.527
MN5K-63	1.622	0.027	0.1564	0.0024	0.0747	0.00045	978	10	937	13	1060	12	226.3	57.5	29.6	4
MN5K-64	1.245	0.03	0.1174	0.0021	0.0762	0.0007	820	14	715	12	1099	18	498	84	20.6	6.66
MN5K-65	2.261	0.061	0.1921	0.005	0.08494	0.00056	1198	19	1132	27	1314	13	170	23.7	17.1	12.5
MN5K-66	1.097	0.016	0.1209	0.0015	0.06572	0.00051	751.5	7.5	735.9	8.8	797	16	264	285	101.5	0.963
MN5K-67	1.226	0.016	0.13173	0.00088	0.06743	0.0002	812.4	7.1	797.7	5	850.9	6.2	146.9	71.3	26.8	2.088
MN5K-68	4.385	0.058	0.294	0.0029	0.10857	0.00024	1709	11	1661	15	1774.4	3.5	166.2	87.6	65.3	1.946
MN5K-69	4.239	0.038	0.2659	0.0019	0.1158	0.0013	1681.2	7.4	1520	9.7	1890	20	134.6	64.9	49.6	2.169
MN5K-70	1.284	0.027	0.1369	0.0025	0.06808	0.00055	838	12	827	14	870	17	65.1	92.2	33.1	0.685
MN5K-71	1.377	0.035	0.1434	0.0019	0.0707	0.0015	878	14	864	11	928	25	226	39.1	15.3	6.16
MN5K-72	2.55	0.21	0.1992	0.0042	0.0923	0.0054	1272	44	1171	22	1411	56	243.3	97	58	2.84
MN5K-73	1.25	0.023	0.1327	0.0025	0.06871	0.00034	823	11	803	14	890	10	308	92	30.6	3.97
MN5K-74	1.41	0.052	0.1285	0.0061	0.0786	0.0012	892	22	779	35	1162	30	580	226	86	2.86
MN5K-75	10.01	0.14	0.437	0.0062	0.16599	0.00089	2439	14	2336	28	2517.3	9	122.1	85.5	91.8	1.456
MN5K-76	1.247	0.03	0.132	0.003	0.06916	0.00058	821	14	799	17	903	17	413	82.1	30.3	5.28
MN5K-77	3.684	0.083	0.2595	0.0019	0.1022	0.0013	1566	17	1487.2	9.6	1663	23	121.7	91.6	66.4	1.396
MN5K-78	1.418	0.019	0.1492	0.0027	0.069	0.0005	897.3	8.3	896	15	898	15	218	58.6	23.2	4.04
MN5K-79	1.113	0.015	0.1217	0.0013	0.06622	0.00029	759.2	7.3	740.2	7.2	812.9	9.2	165.6	152.6	51.8	1.145
MN5K-80	4.01	0.087	0.2154	0.0031	0.13546	0.00086	1634	18	1257	16	2169	11	776	704	363	1.1184
MN5K-81	1.274	0.024	0.1339	0.0025	0.06866	0.00033	834	11	812	14	888.2	9.8	282	213	80.3	1.394
MN5K-82	1.334	0.031	0.1313	0.0019	0.0741	0.0013	860	14	795	11	1040	35	316	213	73.9	1.69
MN5K-83	1.465	0.019	0.1504	0.0021	0.07072	0.00024	915.7	7.7	903	12	949	7	158.1	127.1	53.8	1.265

172

Continued-

Analysis	Isotopic ratio						Apparent age (Ma)						Content (ppm)			
	$^{207}Pb/^{235}U$	2σ	$^{206}Pb/^{238}U$	2σ	$^{207}Pb/^{206}Pb$	2σ	$^{207}Pb/^{235}U$	2σ	$^{206}Pb/^{238}U$	2σ	$^{207}Pb/^{206}Pb$	2σ	U	Th	Pb	U/Th
MN5K-84	1.378	0.04	0.1165	0.0012	0.0858	0.0022	878	17	710.5	7	1328	48	24.99	18.58	7.6	1.383
MN5K-85	1.364	0.018	0.1403	0.0016	0.07051	0.00046	873.2	7.8	846.4	9	939	11	163	52	21.3	3.11
MN5K-86	1.309	0.015	0.1337	0.0012	0.07103	0.00061	849.6	6.5	808.9	7	957	17	267	64.2	24.2	4.66
MN5K-87	1.316	0.011	0.13767	0.00075	0.06972	0.00045	852.8	5	831.4	4.2	915	10	252.9	147.2	58.6	1.733

Table 6.7: U-Pb geochronology of the Nagthat Fm. of outer Lesser Himalaya (Aglar river, Garhwal section)

Analysis	Isotopic ratio						Apparent age (Ma)						Content (ppm)			
	$^{207}Pb/^{235}U$	2σ	$^{206}Pb/^{238}U$	2σ	$^{207}Pb/^{206}Pb$	2σ	$^{207}Pb/^{235}U$	2σ	$^{206}Pb/^{238}U$	2σ	$^{207}Pb/^{206}Pb$	2σ	U	Th	Pb	U/Th
MN5I-1	2.702	0.014	0.21523	0.00096	0.09059	0.00017	1329	3.9	1256.6	5.1	1438	3.5	272.2	94.7	59.3	2.89
MN5I-2	1.349	0.02	0.1422	0.0026	0.06862	0.00026	866.6	8.7	857	15	887.1	7.7	301	258	104.9	1.139
MN5I-3	1.502	0.02	0.1451	0.0015	0.07433	0.00047	930.9	8.1	873.4	8.5	1050	13	433	374	141.3	1.12
MN5I-4	1.33	0.05	0.1272	0.0023	0.0731	0.0018	856	21	772	13	1018	50	400	230	93.1	1.71
MN5I-5	1.032	0.012	0.103	0.0014	0.07233	0.00065	719.8	5.8	631.6	8.4	994	18	604	1021	312	0.58
MN5I-6	1.338	0.014	0.1409	0.0019	0.06873	0.00034	862.4	5.9	850	11	890	10	303	172	75.9	1.694
MN5I-7	4.505	0.072	0.3015	0.0067	0.10714	0.00079	1731	13	1698	33	1751	13	145.3	88.1	74.7	1.682
MN5I-8	3.995	0.061	0.2819	0.005	0.10243	0.00069	1634	13	1609	27	1668	12	209	137.2	110.4	1.539
MN5I-9	12.46	0.45	0.4	0.011	0.2244	0.0023	2632	34	2168	49	3013	16	600.2	154	122.1	4.18
MN5I-10	1.3119	0.0096	0.1396	0.0011	0.06789	0.00025	850.8	4.2	842.5	6	864.9	7.7	215.9	156.2	66.8	1.427
MN5I-11	1.326	0.019	0.1391	0.0028	0.06858	0.00038	856.8	8.5	839	16	886	11	287	344	141	0.914
MN5I-12	3.555	0.031	0.2454	0.0016	0.10415	0.00031	1539.2	6.9	1414.9	8.1	1699.2	5.5	254	185.7	138.5	1.36
MN5I-13	10.65	0.18	0.453	0.0085	0.17011	0.00089	2499	15	2413	39	2558.4	8.7	113.1	91.4	118.7	1.231
MN5I-14	3.951	0.046	0.2831	0.0026	0.10148	0.00049	1623.6	9.5	1607	13	1651	8.7	147.7	241.2	185	0.612
MN5I-15	3.688	0.06	0.2622	0.0042	0.10172	0.00043	1568	13	1501	21	1655.4	7.8	207	150	109.3	1.426
MN5I-16	1.9615	0.0082	0.17591	0.00089	0.08068	0.0002	1102.4	2.8	1044.6	4.9	1213.7	4.9	354	182.3	90.6	1.912
MN5I-17	3.61	0.03	0.2679	0.0029	0.09783	0.00032	1551.6	6.7	1530	15	1583.1	6.2	109.8	55.2	44.6	2.08
MN5I-18	13.06	0.12	0.5125	0.0055	0.1851	0.00038	2683.7	8.7	2667	23	2699.1	3.4	49.3	38.9	53.3	1.234
MN5I-19	7.6	0.15	0.3354	0.0063	0.16443	0.00045	2187	17	1864	31	2501.7	4.6	482	234.3	187.4	2.079
MN5I-20	1.2941	0.0068	0.13769	0.00057	0.0682	0.00026	843.1	3	831.6	3.2	874.4	8	115.4	69.9	31.6	1.659

Continued-

Analysis	Isotopic ratio						Apparent age (Ma)						Content (ppm)			
	$^{207}Pb/^{235}U$	2σ	$^{206}Pb/^{238}U$	2σ	$^{207}Pb/^{206}Pb$	2σ	$^{207}Pb/^{235}U$	2σ	$^{206}Pb/^{238}U$	2σ	$^{207}Pb/^{206}Pb$	2σ	U	Th	Pb	U/Th
MN5I-21	1.14	0.011	0.12379	0.00099	0.06556	0.0003	772.5	5.1	752.3	5.7	792.1	9.5	109.6	141	53	0.867
MN5I-22	1.41	0.1	0.1311	0.0012	0.0765	0.0048	883	39	794.2	6.7	1060	110	27.8	17.51	8.19	1.544
MN5I-23	1.378	0.019	0.1416	0.0018	0.06977	0.00024	879.4	7.9	854	10	921.5	7	172.6	116.2	53.1	1.52
MN5I-24	11.259	0.085	0.4692	0.004	0.1727	0.00048	2544.6	7.1	2480	18	2583.9	4.6	92.1	44.8	56.2	2.17
MN5I-25	4.038	0.019	0.2789	0.0018	0.10409	0.00026	1641.7	3.8	1585.9	9.3	1698.3	4.6	156	78.7	64.08	1.941
MN5I-26	5.3	0.048	0.3256	0.0028	0.11728	0.00064	1868.5	7.8	1817	13	1914.7	9.6	148.2	65.3	58	2.195
MN5I-27	6.9	0.12	0.3269	0.004	0.1515	0.0013	2098	15	1823	20	2362	14	549	282	200.2	1.97
MN5I-28	1.293	0.039	0.11944	0.00073	0.0784	0.0025	843	17	727.4	4.2	1150	62	563	134.3	52.4	4.21
MN5I-29	1.184	0.011	0.1221	0.0011	0.06957	0.00024	792.9	5.2	742.6	6.2	915.4	6.9	472	95	27.86	4.85
MN5I-30	4.989	0.087	0.3078	0.0057	0.11717	0.0008	1819	14	1729	28	1909	9	301	163	139.4	1.781
MN5I-31	1.196	0.011	0.1227	0.001	0.06986	0.0002	798.7	5.1	746	5.7	924.2	5.8	417	38.8	9.92	11.9
MN5I-32	10.903	0.091	0.4523	0.0032	0.17314	0.00079	2514.7	7.8	2410	11	2588.1	7.6	84.5	40.2	55.7	2.083
MN5I-33	7.94	0.21	0.3727	0.0067	0.1532	0.002	2223	24	2042	32	2382	23	109.2	50.7	50.6	2.133
MN5I-34	1.4828	0.0089	0.1438	0.0011	0.07374	0.00048	923.3	3.6	866.3	6.3	1034	13	319.9	110	50.7	2.75
MN5I-35	1.552	0.027	0.1555	0.0027	0.0718	0.00023	951	11	932	15	980.2	6.7	83.7	72.9	37.5	1.192
MN5I-36	1.413	0.015	0.1499	0.0015	0.06777	0.0003	894.3	6.5	900.3	8.1	861.2	9.3	95.1	55.8	27	1.756
MN5I-37	1.384	0.012	0.1472	0.0015	0.06767	0.00019	882.8	4.8	885	8.5	858.2	5.9	239.7	210.8	98.7	1.171
MN5I-38	3.465	0.036	0.2427	0.0018	0.10256	0.0004	1518.8	8	1400.7	9.2	1671.9	7.1	210.7	151.2	93.8	1.42
MN5I-39	3.612	0.048	0.2429	0.0033	0.10775	0.00089	1552	11	1402	17	1761	15	275.1	67	47.36	4.13
MN5I-40	11.109	0.056	0.4607	0.0033	0.17358	0.00041	2532.2	4.7	2443	15	2592.4	3.9	178.7	76.6	98.2	2.261
MN5I-41	1.245	0.022	0.1353	0.0022	0.06657	0.00041	822.1	9.4	818	12	824	13	53	47.6	21.9	1.082
MN5I-42	1.147	0.017	0.12233	0.00097	0.06748	0.00044	775.4	8	743.9	5.6	852	13	229.9	55.7	21.1	4.22
MN5I-43	1.3758	0.0078	0.14275	0.00052	0.06913	0.00034	878.6	3.4	860.2	2.9	902	10	62.1	25.2	11.94	2.39
MN5I-44	1.364	0.022	0.1447	0.0024	0.06782	0.0002	873	9.6	871	13	862.8	6	199.5	75.9	39.1	2.78
MN5I-45	1.65	0.021	0.1672	0.0023	0.07093	0.00022	989.2	8.1	996	13	955.3	6.4	199.1	221	114.4	0.924
MN5I-46	1.424	0.017	0.1488	0.0015	0.06859	0.00027	898.6	6.9	894	8.6	886.3	8	167.7	78.3	37.1	2.28
MN5I-47	3.87	0.031	0.2664	0.0025	0.10448	0.00022	1607.1	6.5	1522	13	1705.1	3.8	350.2	277	213.6	1.285
MN5I-48	4.046	0.03	0.2785	0.0028	0.10439	0.00031	1643.4	6	1584	14	1703.5	5.5	313	123.2	98.9	2.395
MN5I-49	1.326	0.02	0.1368	0.0025	0.06951	0.00042	856.6	8.8	826	14	913	12	294	240	105.3	1.287
MN5I-50	1.2581	0.0059	0.12893	0.00079	0.07045	0.00026	827	2.7	781.7	4.5	941.4	7.4	416	154.8	65	2.569

Continued-

Analysis	Isotopic ratio						Apparent age (Ma)						Content (ppm)			
	$^{207}Pb/^{235}U$	2σ	$^{206}Pb/^{238}U$	2σ	$^{207}Pb/^{206}Pb$	2σ	$^{207}Pb/^{235}U$	2σ	$^{206}Pb/^{238}U$	2σ	$^{207}Pb/^{206}Pb$	2σ	U	Th	Pb	U/Th
MN5I-51	1.551	0.021	0.1465	0.0015	0.07599	0.0006	950.3	8.4	881.2	8.5	1094	15	301	136.8	57.5	2.11
MN5I-52	1.5221	0.0071	0.14731	0.00069	0.07448	0.00024	939.3	2.8	885.8	3.9	1055.6	6.7	401	61	27.5	6.57
MN5I-53	3.708	0.036	0.2553	0.002	0.10448	0.00038	1572.7	7.8	1466	10	1705.1	6.7	318.8	163.7	121.1	2.09
MN5I-54	4.203	0.022	0.2761	0.0016	0.11005	0.00017	1674.5	4.2	1571.8	7.9	1800.2	2.9	248.4	125.2	100.8	2.01
MN5I-55	9.186	0.09	0.3693	0.0054	0.1803	0.0021	2356.7	9	2026	25	2656	20	364	413	575	0.87
MN5I-56	5.14	0.54	0.22	0.01	0.174	0.014	1823	80	1280	53	2560	120	695	1190	820	0.578
MN5I-57	2.33	0.53	0.1203	0.0053	0.133	0.023	1150	140	732	30	1930	280	502	502	212	0.981
MN5I-58	3.776	0.029	0.2665	0.0024	0.10238	0.00048	1587.4	6.2	1523	12	1667.5	8.6	203.9	179.1	133	1.1311
MN5I-59	3.778	0.024	0.2648	0.0017	0.1033	0.00039	1587.9	5	1514.1	8.4	1684.1	7	210	192.8	137.9	1.102
MN5I-60	3.866	0.047	0.2744	0.0034	0.10173	0.00044	1606.1	9.8	1563	17	1655.6	8.1	190.8	162.3	122.9	1.156
MN5I-61	3.709	0.025	0.2612	0.0018	0.10285	0.00025	1573.2	5.3	1495.7	9.1	1676.2	4.5	191.3	150.3	102.6	1.246
MN5I-62	3.131	0.059	0.221	0.0042	0.10295	0.00018	1439	15	1287	22	1677.9	3.3	451	304	148	1.476
MN5I-63	1.318	0.016	0.1365	0.0014	0.07009	0.00034	853.2	7.1	824.7	7.8	930.6	9.9	329	165	67.4	2.066
MN5I-64	1.267	0.012	0.1363	0.0014	0.06781	0.00017	830.9	5.3	823.6	7.9	862.7	5.1	253	178.8	73.5	1.443
MN5I-65	1.2513	0.0068	0.13444	0.00056	0.06772	0.00016	823.9	3	813.2	3.2	860.8	5.3	254.9	229.1	88.2	1.111
MN5I-66	1.3065	0.0088	0.14001	0.00094	0.06789	0.00022	848.5	3.8	844.7	5.3	865	6.6	215.9	139.2	56.5	1.583
MN5I-67	10.08	0.25	0.4262	0.0032	0.1722	0.0033	2439	18	2288	14	2562.7	3.8	130.5	179.6	172.4	0.738
MN5I-68	10.23	0.15	0.436	0.0048	0.1704	0.0011	2455	13	2332	22	2561	10	128.8	135.1	149	0.937
MN5I-69	1.1777	0.0067	0.12924	0.00076	0.06655	0.00019	790.2	3.1	783.5	4.3	824.5	6.2	177.5	214	79.7	0.868
MN5I-70	1.277	0.051	0.1296	0.0011	0.0717	0.0026	833	22	785.6	6.3	959	68	193.7	300	114.7	0.669
MN5I-71	1.368	0.014	0.14306	0.00061	0.06978	0.00067	875.2	6	861.9	3.4	913	12	49.3	35.4	14.77	1.382
MN5I-72	1.332	0.0078	0.1405	0.00052	0.0692	0.00032	859.7	3.4	847.5	2.9	905.8	9.7	70.3	44.86	18.16	1.533
MN5I-73	4.365	0.063	0.2907	0.0048	0.10941	0.0005	1705	12	1644	24	1789.3	8.2	181.2	134.4	104.4	1.361
MN5I-74	1.511	0.029	0.1296	0.0018	0.08531	0.00066	936	12	785	10	1322	15	679	747	261.1	0.932
MN5I-75	11.77	0.11	0.4491	0.0043	0.19202	0.00032	2586.1	8.6	2391	19	2759.5	2.8	200.4	131.7	134.1	1.548
MN5I-76	2.947	0.027	0.2143	0.0016	0.10091	0.00028	1393.9	7	1251.5	8.5	1640.9	5.2	350	297.7	144.7	1.21
MN5I-77	1.331	0.014	0.13715	0.00093	0.07059	0.00043	859.1	5.9	828.5	5.3	945	12	121.1	65.44	27.18	1.836
MN5I-78	1.286	0.011	0.1334	0.0016	0.07044	0.00048	839.6	4.9	807	9.1	940	14	406	247	92.6	1.681

Table 6.8: U-Pb geochronology of the Nagthat Fm. of outer Lesser Himalaya (Shivpuri-Timli road, Garhwal section)

Analysis	Isotopic ratio						Apparent age (Ma)						Content (ppm)			
	$^{207}Pb/^{235}U$	2σ	$^{206}Pb/^{238}U$	2σ	$^{207}Pb/^{206}Pb$	2σ	$^{207}Pb/^{235}U$	2σ	$^{206}Pb/^{238}U$	2σ	$^{207}Pb/^{206}Pb$	2σ	U	Th	Pb	U/Th
MN1U-1	2.719	0.071	0.1841	0.0027	0.1062	0.0013	1333	20	1089	15	1735	23	209	391	130.9	0.5502
MN1U-2	1.195	0.022	0.0768	0.0021	0.1208	0.0024	798	10	477	13	1965	36	885	506	182	1.85
MN1U-3	1.085	0.033	0.1105	0.0019	0.07223	0.00082	745	16	676	11	991	23	283	201.8	32.7	1.418
MN1U-4	0.931	0.011	0.0979	0.0016	0.07213	0.00092	668	5.9	602.3	9.5	989	26	293	181.6	26.35	1.652
MN1U-5	0.896	0.039	0.0695	0.0039	0.0989	0.0014	649	21	433	23	1603	26	409	430	133	1.02
MN1U-6	0.702	0.023	0.03441	0.00062	0.1572	0.0037	540	14	218.1	3.9	2424	40	825	1896	210.4	0.4403
MN1U-7	8.49	0.3	0.364	0.015	0.1745	0.0012	2291	30	2001	71	2601	12	252	225	208	1.093
MN1U-8	4.2	0.35	0.172	0.016	0.1869	0.0042	1669	71	1019	89	2714	37	482	407	179.8	1.141
MN1U-9	0.855	0.019	0.0353	0.0012	0.1866	0.0058	627	11	223.7	7.5	2710	52	1240	2130	235	0.612
MN1U-10	1.824	0.039	0.1703	0.0041	0.0835	0.00044	1053	14	1013	23	1281	10	331	274.1	147.7	1.206
MN1U-11	1.194	0.017	0.1099	0.0032	0.0848	0.0018	797.3	7.9	672	19	1306	40	368	215.3	54.7	1.723
MN1U-12	4.34	0.19	0.212	0.012	0.1489	0.0046	1699	37	1256	69	2330	54	460	261	180	1.85
MN1U-13	3.07	0.16	0.138	0.0095	0.169	0.0039	1422	39	832	53	2545	39	696	521	265	1.317
MN1U-14	0.908	0.023	0.031	0.00081	0.2268	0.0015	655	12	196.8	5.1	3029	11	2200	1530	293	1.44
MN1U-15	1.279	0.033	0.1205	0.0018	0.0819	0.0012	836	14	733	10	1241	28	298.3	248	99.6	1.202
MN1U-16	1.137	0.034	0.13	0.0042	0.06787	0.00036	769	16	787	24	864	11	247	144.9	60.4	1.66
MN1U-17	1.237	0.028	0.1363	0.003	0.07055	0.00028	816	13	823	17	944.2	8	119.7	93	37.5	1.57
MN1U-18	3.347	0.05	0.2476	0.003	0.10543	0.00035	1492	12	1426	15	1721.8	6.1	219	532	401	0.3922
MN1U-19	3.027	0.069	0.2182	0.004	0.10776	0.0008	1414	17	1272	21	1762	13	160.1	207.2	154.4	0.734
MN1U-20	1.153	0.017	0.0965	0.0015	0.0935	0.0013	778.5	8.1	594.1	8.7	1502	24	539	375	129.7	1.3799
MN1U-21	1.252	0.015	0.1229	0.0017	0.07934	0.00051	824.1	7	747	10	1180	13	206.2	289.7	94.7	0.682
MN1U-22	1.358	0.057	0.1353	0.0031	0.0739	0.002	867	25	818	18	1026	53	60.8	61	23	1.23
MN1U-23	1.159	0.018	0.0979	0.0023	0.0922	0.0026	781.2	8.4	602	14	1469	53	408	224.2	74.4	1.74
MN1U-24	1.317	0.05	0.1027	0.0029	0.0988	0.0045	852	23	630	17	1584	85	401	278	112	1.38
MN1U-25	1.099	0.028	0.1242	0.0028	0.06894	0.00043	752	14	754	16	896	13	241	270	112	0.925
MN1U-26	1.749	0.023	0.1708	0.0024	0.07621	0.00079	1026.4	8.5	1016	13	1099	21	174.7	40.9	22	4.02
MN1U-27	3.639	0.054	0.2754	0.0031	0.09704	0.00031	1557	12	1568	15	1567.8	5.9	151.3	146	108.5	0.962
MN1U-28	1.836	0.075	0.1505	0.0088	0.0917	0.0015	1056	27	903	49	1461	31	479	182	66.8	2.56
MN1U-29	10.68	0.26	0.456	0.0078	0.18	0.0023	2495	23	2422	35	2652	22	100.1	80.4	97.2	1.18
MN1U-30	1.119	0.012	0.09135	0.00092	0.09042	0.00069	762.4	5.6	564.7	5.9	1437	16	408	424.9	88	0.9556

176

Continued-

Analysis	Isotopic ratio						Apparent age (Ma)						Content (ppm)			
	$^{207}Pb/^{235}U$	2σ	$^{206}Pb/^{238}U$	2σ	$^{207}Pb/^{206}Pb$	2σ	$^{207}Pb/^{235}U$	2σ	$^{206}Pb/^{238}U$	2σ	$^{207}Pb/^{206}Pb$	2σ	U	Th	Pb	U/Th
MN1U-31	1.547	0.051	0.1525	0.0028	0.0758	0.0016	948	21	915	16	1088	42	354.2	106	50.7	3.59
MN1U-32	1.442	0.024	0.0894	0.0025	0.124	0.0024	911	13	552	15	2013	34	796	374	183.1	2.118
MN1U-33	1.227	0.051	0.1107	0.0018	0.0844	0.0032	817	23	677	10	1280	73	195.1	168	59.1	1.23
MN1U-34	9.36	0.11	0.4251	0.0038	0.16073	0.00086	2373	11	2283	17	2463.1	8.9	159.5	98.6	71.5	1.624
MN1U-35	1.059	0.02	0.0913	0.0022	0.08737	0.00068	733	10	563	13	1368	15	638	325	109	2.05
MN1U-36	1.142	0.021	0.0864	0.0018	0.10082	0.0008	773	10	534	11	1639	15	366.7	355	59.8	1.033
MN1U-37	1.419	0.025	0.1473	0.0029	0.07015	0.00053	896	11	885	16	932	15	202	140	53.4	1.395
MN1U-38	1.415	0.023	0.1555	0.0018	0.06682	0.00044	896.9	8.8	931	10	832	13	159.9	42.3	18.5	4.1
MN1U-39	1.378	0.029	0.1473	0.0012	0.06818	0.00086	879	12	885.6	7	872	25	146	37.1	14.7	4.017
MN1U-40	3.68	0.28	0.1464	0.0032	0.1762	0.0086	1562	59	881	18	2610	79	352	296	169.6	1.188
MN1U-41	1.47	0.11	0.1062	0.0021	0.1015	0.0058	914	44	651	12	1642	98	364.9	501	100.6	0.7296
MN1U-42	1.113	0.021	0.0761	0.0019	0.1094	0.0017	759	10	473	11	1789	28	363	831	90.8	0.442
MN1U-43	1.294	0.032	0.1346	0.0017	0.06955	0.00083	842	14	815.8	9.2	913	24	254.9	329.3	113	0.78
MN1U-44	2.962	0.076	0.2321	0.0056	0.0931	0.00056	1396	19	1345	29	1489	11	108.7	99.9	49.9	1.126
MN1U-45	2.213	0.087	0.0794	0.0033	0.2045	0.0014	1183	28	493	20	2862	11	1210	1080	199	1.123
MN1U-46	2.941	0.092	0.1152	0.0038	0.19115	0.00093	1392	24	703	22	2752	8	1044	430	215.4	2.401
MN1U-47	4.774	0.089	0.2144	0.0039	0.166	0.0012	1781	15	1252	21	2517	12	378	310	166.5	1.255
MN1U-48	1.371	0.03	0.12925	0.00065	0.077	0.0012	876	13	783.6	3.7	1118	31	211.9	167.5	49.8	1.282
MN1U-49	1.084	0.025	0.1112	0.0013	0.07303	0.00081	745	12	679.6	7.7	1014	22	187.5	189.7	47.4	1.013
MN1U-50	2.162	0.099	0.0883	0.0059	0.185	0.0052	1168	32	545	35	2696	45	533	1800	234.2	0.307
MN1U-51	6.67	0.21	0.351	0.014	0.1465	0.0014	2066	28	1938	68	2305	16	118.1	193	182.1	0.619
MN1U-52	9.88	0.25	0.4335	0.0089	0.1636	0.0013	2422	23	2321	40	2493	14	160	121.3	103.4	1.42
MN1U-53	8.012	0.058	0.3724	0.003	0.16091	0.00044	2232.3	6.5	2041	14	2465.2	4.6	91	145.6	112.4	0.643
MN1U-54	4.55	0.18	0.254	0.012	0.1292	0.0024	1738	33	1460	60	2086	32	94.6	83	46.8	1.153
MN1U-55	2.68	0.15	0.1604	0.008	0.12764	0.00074	1329	39	958	45	2066	10	69.9	116	22.7	0.62
MN1U-56	1.128	0.03	0.1272	0.0045	0.06879	0.00081	766	14	772	26	892	24	252	216	95.4	1.197
MN1U-57	1.331	0.018	0.1549	0.0021	0.06627	0.00034	859.2	7.9	928	12	815	11	157.6	137.7	63.6	1.157
MN1U-58	14.86	0.43	0.412	0.018	0.2606	0.0035	2805	28	2222	81	3250	21	246.6	94.7	33	2.53
MN1U-59	5.86	0.31	0.177	0.01	0.2384	0.0021	1950	46	1052	55	3112	15	57	89	8.8	0.572
MN1U-60	1.177	0.023	0.1069	0.0034	0.0804	0.0018	789	11	655	20	1200	39	197.2	177.4	41.67	1.026

Continued-

Analysis	Isotopic ratio						Apparent age (Ma)						Content (ppm)			
	$^{207}Pb/^{235}U$	2σ	$^{206}Pb/^{238}U$	2σ	$^{207}Pb/^{206}Pb$	2σ	$^{207}Pb/^{235}U$	2σ	$^{206}Pb/^{238}U$	2σ	$^{207}Pb/^{206}Pb$	2σ	U	Th	Pb	U/Th
MN1U-61	1.228	0.026	0.1215	0.0034	0.0731	0.0012	813	12	739	20	1013	34	67	126	20.6	0.492
MN1U-62	6.824	0.083	0.2877	0.0049	0.171	0.001	2090	10	1629	24	2566.8	9.7	114.7	170.7	71.2	0.634
MN1U-63	1.74	0.065	0.1077	0.0061	0.1175	0.0036	1020	24	658	36	1907	52	233	231	55.9	0.859
MN1U-64	0.872	0.043	0.0272	0.0016	0.2301	0.004	633	23	175	10	3049	28	1250	910	147	1.175
MN1U-65	1.172	0.019	0.1167	0.0019	0.07276	0.0006	787.3	8.6	711	11	1006	17	169.5	139	23.2	1.23
MN1U-66	1.563	0.051	0.1451	0.0061	0.0782	0.0017	954	20	873	34	1147	42	48.7	47.3	17.2	1
MN1U-67	1.064	0.048	0.0767	0.0043	0.0998	0.0037	734	23	476	26	1612	69	51.1	95	9.08	0.502
MN1U-68	6.27	0.14	0.2424	0.0057	0.18694	0.00081	2013	20	1399	30	2715.4	7.2	349	280	89.9	1.134
MN1U-69	4.52	0.11	0.167	0.0042	0.196	0.0011	1733	20	996	23	2792.7	9.2	307	301	68.6	0.896
MN1U-70	7.07	0.19	0.2992	0.0051	0.1705	0.002	2119	24	1687	25	2561	20	138.5	209	45.5	0.632
MN1U-71	1.066	0.021	0.099	0.0026	0.07731	0.00084	736	10	608	15	1128	21	198	98	25.6	1.86
MN1U-72	5.23	0.26	0.2003	0.0089	0.1868	0.0022	1847	43	1182	49	2715	19	173	233	44.9	0.732
MN1U-73	0.935	0.018	0.0519	0.0019	0.1268	0.0025	669.9	9.6	326	12	2049	35	649	429	105.2	1.367
MN1U-74	2.682	0.076	0.1413	0.0037	0.1398	0.002	1321	21	852	21	2216	21	287	279	33.1	0.872
MN1U-75	2.392	0.092	0.1363	0.0055	0.1272	0.00091	1236	27	823	31	2059	13	227	191	23.6	0.93
MN1U-76	1.024	0.024	0.0843	0.0024	0.088	0.0011	715	12	522	14	1381	24	157.1	275	77.5	0.491
MN1U-77	7.26	0.16	0.2711	0.0053	0.19539	0.0009	2144	19	1546	27	2788	7.6	117.4	124	62.4	0.834
MN1U-78	1.1838	0.0088	0.1164	0.0011	0.0736	0.00067	793	4.1	709.9	6.2	1030	18	198.4	202	63.2	0.888
MN1U-79	3.87	0.059	0.1438	0.0025	0.1958	0.0018	1607	12	866	14	2791	15	328	241	93	1.22
MN1U-80	1.444	0.085	0.1065	0.0069	0.0987	0.0011	906	36	652	40	1607	18	390	221	73.5	1.634
MN1U-81	0.805	0.017	0.0408	0.0015	0.1425	0.0029	599.3	9.8	257.6	9.2	2253	36	798	451	89.9	1.471
MN1U-82	1.151	0.036	0.0537	0.0022	0.1529	0.0039	776	17	337	13	2378	45	688	525	148.3	1.236
MN1U-83	0.585	0.023	0.01671	0.00071	0.2532	0.0034	467	15	106.8	4.5	3209	19	2280	1960	193	1.045
MN1U-84	0.873	0.022	0.0552	0.0023	0.1169	0.0027	636	12	346	14	1907	42	620	670	94	0.952
MN1U-85	2.959	0.053	0.1032	0.0021	0.2074	0.0019	1397	14	633	12	2885	15	466	350	89.9	1.152
MN1U-86	2.612	0.086	0.0795	0.0019	0.24	0.0028	1303	24	493	11	3120	19	964	533	194.4	1.75
MN1U-87	5.2	0.12	0.2109	0.0057	0.1791	0.0015	1851	21	1233	30	2645	13	184	281	77.3	0.594
MN1U-88	1.712	0.027	0.0629	0.0018	0.1994	0.0032	1013	10	393	11	2819	26	790	596	137.2	1.212
MN1U-89	1.419	0.058	0.0619	0.0023	0.1683	0.0027	900	23	387	14	2539	28	82	144	11.7	0.456
MN1U-90	0.425	0.054	0.0144	0.0017	0.212	0.0036	355	38	92	11	2919	28	2350	2820	173	0.867

Continued-

Analysis	Isotopic ratio						Apparent age (Ma)						Content (ppm)			
	$^{207}Pb/^{235}U$	2σ	$^{206}Pb/^{238}U$	2σ	$^{207}Pb/^{206}Pb$	2σ	$^{207}Pb/^{235}U$	2σ	$^{206}Pb/^{238}U$	2σ	$^{207}Pb/^{206}Pb$	2σ	U	Th	Pb	U/Th
MN1U-91	0.305	0.028	0.01375	0.00099	0.1645	0.006	270	22	88	6.3	2499	61	15.6	36.5	0.92	0.4176
MN1U-92	1.355	0.086	0.0698	0.0047	0.147	0.0068	864	37	434	29	2294	80	286	251	63	0.92
MN1U-93	1.93	0.12	0.1409	0.0061	0.102	0.0036	1090	41	850	34	1658	66	79	77	15.5	1.022
MN1U-94	3.96	0.47	0.1106	0.0047	0.271	0.021	1616	93	676	28	3300	120	201	288	95.3	0.717
MN1U-95	1.68	0.12	0.0609	0.0022	0.21	0.01	998	45	381	13	2898	78	457	730	91	0.65
MN1U-96	2.21	0.1	0.1626	0.0046	0.1032	0.0062	1180	31	971	25	1650	110	53	39	8.2	1.309
MN1U-97	1.161	0.036	0.0627	0.0036	0.148	0.0082	783	17	392	22	2286	88	1008	586	172	1.81
MN1U-98	2.75	0.11	0.1106	0.0054	0.186	0.0017	1336	31	675	31	2706	15	706	923	240	0.785
MN1U-99	0.958	0.023	0.0424	0.0026	0.1709	0.0084	682	12	268	16	2592	77	1240	1130	238	1.093
MN1U-100	1.288	0.021	0.0743	0.0042	0.133	0.0063	840	9.3	461	25	2121	87	578	549	153	0.963
MN1U-101	3.85	0.093	0.1717	0.0038	0.158	0.0048	1603	20	1022	21	2431	52	178	384	60.5	0.465
MN1U-102	3.283	0.079	0.1501	0.0036	0.1618	0.0021	1476	19	901	20	2475	22	69	205	23.85	0.3465

Table 6.9: U-Pb geochronology of the Nagthat Fm. of outer Lesser Himalaya (Kaliasaur, Garhwal section)

Analysis	Isotopic ratio						Apparent age (Ma)						Content (ppm)			
	$^{207}Pb/^{235}U$	2σ	$^{206}Pb/^{238}U$	2σ	$^{207}Pb/^{206}Pb$	2σ	$^{207}Pb/^{235}U$	2σ	$^{206}Pb/^{238}U$	2σ	$^{207}Pb/^{206}Pb$	2σ	U	Th	Pb	U/Th
MN4T-1	5.41	0.18	0.323	0.01	0.11312	0.00023	1891	27	1800	50	1850	3.7	160	168	150	0.988
MN4T-2	8.753	0.073	0.3884	0.0033	0.14323	0.00022	2312.3	7.5	2115	16	2266.6	2.7	255	214.5	165.2	1.219
MN4T-3	8.06	0.23	0.386	0.011	0.13661	0.00038	2238	26	2100	54	2184.5	4.8	160.6	200.2	210.9	0.866
MN4T-4	14.36	0.41	0.496	0.017	0.1883	0.0012	2769	28	2592	74	2727	10	105.7	112.3	151.3	1.04
MN4T-5	8.29	0.13	0.3934	0.0072	0.13634	0.0003	2262	15	2138	34	2181.1	3.8	71.6	35.66	38.68	2.12
MN4T-6	7.29	0.24	0.376	0.014	0.12643	0.00051	2142	31	2053	64	2048.7	7.1	143.1	49.2	49.6	3.01
MN4T-7	8.97	0.29	0.3561	0.0086	0.1574	0.00085	2334	30	1962	41	2428.9	8.9	273	23.9	18.38	13
MN4T-8	4.08	0.13	0.1994	0.0061	0.12892	0.00029	1650	26	1171	33	2083.2	4	268	406	173.7	0.69
MN4T-9	7.17	0.47	0.327	0.018	0.14016	0.00065	2120	58	1816	87	2228.9	7.9	263	157	56.9	1.92
MN4T-10	4.904	0.092	0.2675	0.0036	0.12055	0.00058	1804	15	1528	18	1964	8.5	247	184.7	75.7	1.376
MN4T-11	7.57	0.3	0.381	0.016	0.13172	0.0002	2189	33	2076	78	2121	2.6	225	116	84.6	2.19

Continued-

Analysis	Isotopic ratio						Apparent age (Ma)						Content (ppm)			
	$^{207}Pb/^{235}U$	2σ	$^{206}Pb/^{238}U$	2σ	$^{207}Pb/^{206}Pb$	2σ	$^{207}Pb/^{235}U$	2σ	$^{206}Pb/^{238}U$	2σ	$^{207}Pb/^{206}Pb$	2σ	U	Th	Pb	U/Th
MN4T-12	4.65	0.67	0.218	0.029	0.14149	0.00048	1670	120	1250	150	2245.3	5.9	444	357	96.8	1.75
MN4T-13	3.086	0.084	0.1584	0.0043	0.13343	0.00068	1427	20	948	24	2144.4	8.8	592	112.1	48.7	5.53
MN4T-14	2	0.3	0.105	0.016	0.1386	0.001	1053	99	633	92	2209	13	830	1240	143	0.705
MN4T-15	8.04	0.27	0.414	0.014	0.1442	0.00032	2244	29	2228	66	2278.1	3.9	105	67.4	79.8	1.541
MN4T-16	6.43	0.18	0.337	0.011	0.14165	0.00066	2037	25	1879	51	2247.3	8	158	156.5	113.3	1.015
MN4T-17	2.404	0.043	0.1117	0.0025	0.1618	0.0014	1243	13	683	14	2474	14	820	778	110.6	1.041
MN4T-18	6.89	0.51	0.273	0.018	0.18726	0.00098	2071	64	1547	93	2717.9	8.5	236	329	54.4	0.711
MN4T-19	1.53	0.15	0.0804	0.0074	0.14204	0.00026	929	59	496	44	2252.1	3.1	1170	953	129.3	1.196
MN4T-20	6.65	0.23	0.3135	0.0087	0.1579	0.0014	2064	30	1757	43	2433	15	327	319.1	227.1	1.023
MN4T-21	3.72	0.17	0.216	0.011	0.13227	0.00095	1574	36	1260	56	2128	12	270	229	129.5	1.169
MN4T-22	2.82	0.3	0.166	0.017	0.12918	0.00095	1334	77	985	92	2086	13	414	329	52.1	1.263
MN4T-23	7.05	0.33	0.283	0.013	0.19051	0.00091	2107	44	1615	63	2746.3	7.9	338	338	98.8	1.036
MN4T-24	4.32	0.24	0.259	0.012	0.12743	0.00085	1685	45	1480	60	2062	11	300.2	309	113.9	0.981
MN4T-25	2.98	0.4	0.173	0.019	0.1308	0.0026	1345	98	1020	100	2095	27	17.5	30	5.9	0.558
MN4T-26	4.61	0.12	0.3137	0.0057	0.11349	0.0003	1753	21	1758	28	1856	4.7	147.7	147.6	58.5	1.021
MN4T-27	5.37	0.29	0.315	0.015	0.13127	0.00051	1875	46	1762	71	2114.8	6.8	339	139.1	73.7	2.469
MN4T-28	5.6	0.69	0.321	0.037	0.1324	0.0013	1890	110	1800	180	2134	16	27.4	35.3	15.4	0.784
MN4T-29	3.73	0.11	0.2584	0.0079	0.10918	0.00063	1578	25	1481	41	1786	11	149.5	132.5	36.2	1.122
MN4T-30	1.77	0.13	0.1173	0.0093	0.11699	0.0007	1029	49	714	54	1911	11	125	77	19.8	1.66
MN4T-31	9.4	1.1	0.511	0.053	0.1412	0.0056	2400	110	2640	230	2234	68	1.85	4.7	1.62	0.385
MN4T-32	6.32	0.34	0.385	0.019	0.1251	0.0019	2011	50	2113	94	2027	27	19.8	24.5	11.9	0.72
MN4T-33	1.87	0.098	0.1157	0.0055	0.1252	0.0004	1067	35	705	32	2031.6	5.7	609	216	38.9	2.9
MN4T-34	8.51	0.52	0.296	0.017	0.22104	0.0005	2276	55	1670	84	2988.2	3.6	368	299	119.2	1.255
MN4T-35	13.35	0.94	0.556	0.036	0.1822	0.0013	2688	70	2830	150	2672	12	11.3	21.4	7.7	0.55
MN4T-36	3.5	0.21	0.196	0.013	0.13654	0.00049	1526	48	1158	73	2183.6	6.3	453	536	169.3	0.846
MN4T-37	7.9	0.24	0.3776	0.0096	0.15838	0.00038	2223	29	2063	45	2438.4	4.1	119.6	182	49.3	0.678
MN4T-38	4.86	0.18	0.2414	0.009	0.15753	0.00036	1794	32	1392	47	2429.3	3.9	212.5	267	57.8	0.835
MN4T-39	4.63	0.17	0.2674	0.008	0.12827	0.0004	1753	31	1526	40	2075.3	5.8	371	175	41.5	2.1
MN4T-40	9.29	0.11	0.3967	0.005	0.18117	0.00043	2368	15	2159	31	2663.5	3.9	115.5	175	77.9	0.673
MN4T-41	5.4	0.21	0.315	0.013	0.12526	0.00049	1879	35	1763	62	2032.3	6.8	160	224	59	0.83

Continued-

Analysis	Isotopic ratio						Apparent age (Ma)						Content (ppm)			
	$^{207}Pb/^{235}U$	2σ	$^{206}Pb/^{238}U$	2σ	$^{207}Pb/^{206}Pb$	2σ	$^{207}Pb/^{235}U$	2σ	$^{206}Pb/^{238}U$	2σ	$^{207}Pb/^{206}Pb$	2σ	U	Th	Pb	U/Th
MN4T-42	4	0.12	0.2736	0.0058	0.10767	0.00026	1635	23	1563	28	1760.2	4.3	318.7	239	108.6	1.354
MN4T-43	4.04	0.22	0.259	0.015	0.1125	0.0011	1632	45	1478	77	1838	18	70	166	31.8	0.371
MN4T-44	4.553	0.092	0.2397	0.0039	0.13998	0.00071	1742	18	1385	20	2226.6	8.7	480	179	95.4	2.68
MN4T-45	3.49	0.11	0.2146	0.007	0.12324	0.00042	1520	27	1252	38	2003.5	6.1	287	490	148	0.617
MN4T-46	6.29	0.23	0.2812	0.0099	0.16275	0.00032	2010	31	1595	49	2484.4	3.3	381	376	155	1.045
MN4T-47	2.761	0.061	0.1851	0.0044	0.11282	0.00074	1343	17	1094	24	1845	12	392	339	125.1	1.182
MN4T-48	5.87	0.39	0.338	0.023	0.1255	0.0022	1940	61	1890	110	2033	30	10.2	43	5.7	0.22
MN4T-49	11.07	0.22	0.4162	0.0086	0.1902	0.0014	2527	19	2248	38	2743	12	231.6	99.1	57.8	2.306
MN4T-50	0.504	0.022	0.0308	0.0014	0.12347	0.00086	416	16	195.6	8.7	2006	13	2350	2810	80.2	0.827
MN4T-51	2.51	0.17	0.146	0.01	0.13074	0.00043	1259	54	873	58	2107.7	5.7	607	242	94	2.53
MN4T-52	2.673	0.092	0.1363	0.0043	0.14225	0.00089	1317	25	823	24	2254	11	727	497	101	1.57
MN4T-53	2.76	0.32	0.151	0.019	0.1345	0.0014	1289	97	900	110	2160	18	760	1100	96.8	0.773
MN4T-54	2.62	0.15	0.1562	0.0064	0.1209	0.0013	1298	40	945	37	1968	18	639	303	97.4	2.2
MN4T-55	1.6	0.24	0.094	0.015	0.1346	0.0039	900	110	572	87	2149	47	1160	1460	168	0.733
MN4T-56	1.94	0.16	0.1124	0.0094	0.1259	0.0011	1079	53	684	54	2040	15	801	1150	130.4	0.732
MN4T-57	3.31	0.22	0.19	0.011	0.1252	0.0017	1467	51	1118	59	2029	24	569	170	45	3.5
MN4T-58	1.178	0.057	0.0564	0.0029	0.1502	0.001	790	26	356	18	2348	11	1570	1800	129.8	0.936
MN4T-59	11.45	0.31	0.4662	0.009	0.17963	0.00096	2561	24	2466	39	2649.1	8.8	179.6	245	206.5	0.722
MN4T-60	3.834	0.075	0.2158	0.0042	0.12883	0.00031	1601	15	1259	22	2082	4.3	514	180.1	99.2	2.79
MN4T-61	8.88	0.1	0.4005	0.0043	0.16075	0.00036	2325	10	2171	20	2463.5	3.7	332	70.5	79.4	4.73
MN4T-62	6.167	0.042	0.3351	0.0027	0.13369	0.00027	1999.5	5.9	1863	13	2146.9	3.5	140.8	65.2	60.2	2.21
MN4T-63	4.774	0.04	0.2705	0.0016	0.12728	0.00046	1779.9	7	1543.1	8	2060.6	6.4	96.4	95.3	50.2	1.028
MN4T-64	6.77	0.31	0.288	0.012	0.17337	0.00055	2079	40	1633	61	2590.4	5.3	313	398	330	0.794
MN4T-65	7.44	0.14	0.3178	0.0056	0.16775	0.00047	2164	17	1778	28	2535.3	4.7	109.7	136	87.9	0.817
MN4T-66	6.73	0.079	0.3671	0.0043	0.13302	0.00018	2076	10	2015	20	2138.2	2.4	202.9	61	54.9	3.372
MN4T-67	10.1	0.066	0.4244	0.0033	0.17263	0.00034	2443.8	6	2280	15	2583.3	3.3	94.4	51.8	57.5	1.823
MN4T-68	5.66	0.21	0.309	0.012	0.13293	0.00022	1920	37	1736	62	2137	2.8	165	185	123	1.008
MN4T-69	2.766	0.067	0.153	0.0041	0.13136	0.00019	1348	17	917	23	2116.1	2.5	535	320	80.1	1.8
MN4T-70	8.18	0.088	0.3873	0.0039	0.15306	0.00058	2250.5	9.8	2110	18	2380.2	6.4	188.7	15	13.7	13
MN4T-71	6.584	0.091	0.3622	0.004	0.13148	0.00075	2056	12	1992	19	2117	10	111.7	26.1	25.4	4.24

Continued-

Analysis	Isotopic ratio						Apparent age (Ma)						Content (ppm)			
	$^{207}Pb/^{235}U$	2σ	$^{206}Pb/^{238}U$	2σ	$^{207}Pb/^{206}Pb$	2σ	$^{207}Pb/^{235}U$	2σ	$^{206}Pb/^{238}U$	2σ	$^{207}Pb/^{206}Pb$	2σ	U	Th	Pb	U/Th
MN4T-72	6.35	0.063	0.3526	0.0033	0.13027	0.00037	2024.9	8.7	1947	16	2101.4	5	144.5	2.55	1.601	55.8
MN4T-73	6.401	0.061	0.3563	0.0035	0.1299	0.00033	2032	8.3	1964	17	2096.5	4.4	84.8	30.6	29.3	3.05
MN4T-74	9.5	0.14	0.4063	0.0068	0.17028	0.00033	2389	15	2197	31	2560.3	3.2	121.5	78.4	72.7	1.514
MN4T-75	8.98	0.21	0.3947	0.0096	0.16623	0.00064	2336	22	2143	44	2519.8	6.5	114.4	98.8	79.8	1.195
MN4T-76	7.24	0.073	0.3737	0.0033	0.14174	0.0005	2141.3	8.9	2050	17	2248.5	6	169	26.9	24	7.2
MN4T-77	8.723	0.073	0.462	0.0034	0.13457	0.00037	2309.4	7.7	2448	15	2159.5	4.5	69.8	31.84	33.4	2.209
MN4T-78	15.13	0.31	0.503	0.01	0.21861	0.00079	2824	20	2631	42	2970.3	5.8	81.7	75.2	90.1	1.088
MN4T-79	6.432	0.06	0.3543	0.0038	0.13165	0.00054	2036.2	8.1	1955	18	2119.9	7.1	41	21.04	20.71	2.008
MN4T-80	5.12	0.1	0.2944	0.005	0.12618	0.0005	1840	17	1663	25	2045.2	6.9	122	96.6	39.5	1.296
MN4T-81	6.34	0.23	0.2912	0.0088	0.15847	0.0007	2027	32	1646	44	2439.1	7.4	333	518	334	0.632
MN4T-82	5.91	0.17	0.3126	0.0098	0.13646	0.00079	1959	25	1751	48	2182	10	117	118	58.8	1.105
MN4T-83	6.229	0.095	0.3487	0.0052	0.12908	0.00057	2010	14	1933	26	2085.3	7.6	100.5	31.5	30.4	3.18
MN4T-84	6.385	0.062	0.3508	0.0026	0.13149	0.00061	2029.7	8.5	1938	13	2117.7	8.2	132.3	46.8	41.2	2.791
MN4T-85	6.735	0.061	0.3652	0.0026	0.13372	0.00029	2076.8	8.1	2007	12	2147.3	3.7	130.5	68.1	60.6	1.88
MN4T-86	2.398	0.037	0.1413	0.002	0.12237	0.00051	1241	11	852	11	1990.9	7.3	662	225.9	102.5	2.77
MN4T-87	10.91	0.12	0.4768	0.0049	0.16486	0.00076	2515	10	2513	22	2505.9	7.6	50.2	32.7	39.6	1.446
MN4T-88	1.932	0.073	0.089	0.0026	0.1572	0.0015	1089	24	550	15	2424	15	925	442	99.6	2.16
MN4T-89	8.07	0.11	0.3396	0.004	0.17191	0.00046	2240	14	1884	19	2576.2	4.4	259.1	494	340	0.515
MN4T-90	5.235	0.056	0.2942	0.0048	0.13079	0.00067	1858	9.2	1662	24	2108.4	9	285	123	63.2	2.41
MN4T-91	6.28	0.13	0.3235	0.0049	0.13933	0.00035	2014	19	1806	24	2218.8	4.3	135.5	77.8	51.61	1.75
MN4T-92	1.03	0.078	0.0582	0.0048	0.1246	0.00089	715	38	364	29	2023	13	1020	421	55.6	2.36

Table 6.10: U-Pb geochronology of the Nagthat Fm. of outer Lesser Himalaya (Kaliasaur, Garhwal section)

Analysis	Isotopic ratio						Apparent age (Ma)						Content (ppm)			
	$^{207}Pb/^{235}U$	2σ	$^{206}Pb/^{238}U$	2σ	$^{207}Pb/^{206}Pb$	2σ	$^{207}Pb/^{235}U$	2σ	$^{206}Pb/^{238}U$	2σ	$^{207}Pb/^{206}Pb$	2σ	U	Th	Pb	U/Th
MN6B-1	2.78	0.054	0.1732	0.0032	0.11714	0.00051	1350	14	1030	18	1913	7.8	411.3	229	118.5	1.854
MN6B-2	3.054	0.036	0.1768	0.0016	0.1254	0.00047	1421.2	9.1	1049.3	8.7	2034.4	6.6	341.6	271.1	130.2	1.297
MN6B-3	3.031	0.043	0.1798	0.0021	0.122	0.0013	1415	11	1066	12	1985	18	286	221	111.8	1.3306
MN6B-4	4.93	0.13	0.305	0.011	0.1166	0.0013	1806	22	1714	56	1904	20	170	51.5	37.8	3.52
MN6B-5	4.17	0.35	0.252	0.022	0.1201	0.001	1664	69	1450	110	1957	15	216	40.1	28.3	5.6
MN6B-6	5.76	0.08	0.3657	0.0052	0.11424	0.00031	1940	12	2009	24	1867.8	5	119	36.2	35.9	3.36
MN6B-7	3.19	0.16	0.19	0.011	0.1229	0.0014	1454	39	1121	60	1998	20	371	100.1	34.67	3.87
MN6B-8	2.975	0.035	0.1728	0.0017	0.12533	0.00043	1401	9	1027.2	9.3	2033.5	6	364	135.8	44.6	2.774
MN6B-9	3.34	0.07	0.2037	0.005	0.11907	0.00088	1490	16	1195	27	1942	13	253	97.3	29.7	2.75
MN6B-10	1.19	0.016	0.1294	0.00087	0.06649	0.00068	796	7.5	784.4	4.9	821	21	38.8	16.11	7.04	2.47
MN6B-11	1.218	0.02	0.135	0.0011	0.0653	0.00092	808.6	9	816.2	6.5	783	30	29	14.94	6.02	2.067
MN6B-12	2.154	0.025	0.2014	0.0019	0.07795	0.00046	1166.1	8	1182.6	9.9	1145	12	57.6	24.17	15.15	2.61
MN6B-13	2.298	0.026	0.2104	0.0015	0.07907	0.00055	1211.4	8.1	1230.8	7.9	1174	14	41.2	22.44	13.93	1.965
MN6B-14	3.83	0.12	0.2251	0.0067	0.12458	0.00082	1604	23	1308	35	2023	12	280	269	42.6	1.144
MN6B-15	3.613	0.094	0.2077	0.005	0.1263	0.0011	1552	21	1216	26	2047	15	313	379	53.9	0.9
MN6B-16	4.904	0.044	0.2298	0.0012	0.1554	0.0016	1802.9	7.6	1333.4	6.4	2406	17	156.6	48.5	47.4	3.71
MN6B-17	3.96	0.12	0.208	0.0067	0.13906	0.00057	1635	24	1218	36	2215.5	7	219.8	120.1	83.7	2.065
MN6B-18	4.033	0.038	0.1994	0.0044	0.1457	0.0017	1640.8	7.8	1172	24	2296	21	210	127.6	92.8	1.818
MN6B-19	5.07	0.13	0.3054	0.0082	0.1217	0.0011	1831	23	1718	41	1981	16	178	18.3	15.34	10.9
MN6B-20	4.52	0.18	0.306	0.015	0.1078	0.0015	1733	33	1720	73	1763	26	110	157	153	0.812
MN6B-21	4.745	0.071	0.3276	0.0041	0.10487	0.00023	1775	12	1833	23	1712.1	4.1	99.8	182	166	0.62
MN6B-22	4.642	0.03	0.3217	0.002	0.10474	0.0003	1756.9	5.4	1798	9.7	1709.8	5.3	104.9	208.2	188.1	0.5762
MN6B-23	1.389	0.035	0.1415	0.0035	0.07174	0.00085	884	15	853	20	978	24	283.4	15.3	6.72	22.5
MN6B-24	1.44	0.032	0.1552	0.0033	0.06769	0.00019	908	12	930	19	859.1	5.8	376	28.2	12.7	15.7
MN6B-25	1.472	0.043	0.158	0.0047	0.06751	0.00017	919	18	946	26	853.5	5.2	336	29.5	13.17	13.14
MN6B-26	4.784	0.052	0.3038	0.0036	0.11352	0.00024	1781.5	9.4	1710	18	1856.5	3.8	154.1	62.7	48.6	2.77
MN6B-27	1.309	0.011	0.1375	0.0012	0.06868	0.00014	849.5	5	830.2	6.7	889.1	4.1	285	259	96.7	1.224
MN6B-28	1.331	0.018	0.1352	0.0019	0.0709	0.00029	859	7.9	817	11	954.1	8.3	301	310	107.4	1.109
MN6B-29	3.625	0.025	0.2633	0.0017	0.09918	0.00026	1554.8	5.5	1506.5	8.8	1608.7	4.8	54.2	45.9	30.9	1.364
MN6B-30	3.423	0.03	0.246	0.0021	0.1002	0.00021	1509.4	6.7	1417	11	1627.7	3.9	106.8	111.4	69.6	1.121

Continued-

Analysis	Isotopic ratio						Apparent age (Ma)						Content (ppm)			
	$^{207}Pb/^{235}U$	2σ	$^{206}Pb/^{238}U$	2σ	$^{207}Pb/^{206}Pb$	2σ	$^{207}Pb/^{235}U$	2σ	$^{206}Pb/^{238}U$	2σ	$^{207}Pb/^{206}Pb$	2σ	U	Th	Pb	U/Th
MN6B-31	3.481	0.033	0.2359	0.0011	0.1069	0.00067	1522.9	7.4	1365.4	5.6	1747	11	192.6	245.9	127.1	0.92
MN6B-32	3.33	0.21	0.2174	0.0057	0.1105	0.0054	1482	47	1268	30	1793	81	169	268	138	0.755
MN6B-33	5.4	0.13	0.3407	0.0089	0.11397	0.00047	1884	21	1889	43	1863.5	7.4	119	64.6	54.1	2.219
MN6B-34	2.01	0.025	0.12052	0.00093	0.12068	0.00091	1118.5	8.6	733.5	5.3	1965	14	363	159.3	30.76	2.789
MN6B-35	4.316	0.028	0.2714	0.0015	0.11469	0.00028	1696.3	5.3	1547.9	7.5	1874.9	4.4	44.51	55.15	33.04	0.958
MN6B-36	3.767	0.025	0.236	0.0019	0.11551	0.00049	1585.7	5.3	1366	10	1887.8	7.6	41.5	68.8	31.21	0.723
MN6B-37	5.127	0.039	0.3257	0.0026	0.11372	0.0002	1840.3	6.6	1817	13	1859.6	3.1	96.4	37.2	29.9	3.14
MN6B-38	4.918	0.031	0.2986	0.0019	0.11907	0.00029	1805.2	5.4	1684.3	9.5	1942.2	4.3	115.5	67.4	48.6	2.015
MN6B-39	1.292	0.036	0.1376	0.0043	0.06827	0.00035	845	17	831	24	876	11	231	321	100	0.92
MN6B-40	1.22	0.041	0.1106	0.003	0.0793	0.0025	809	18	676	17	1175	57	148	518	102	0.337
MN6B-41	1.3151	0.007	0.13964	0.00062	0.06795	0.00019	852.3	3.1	842.6	3.5	866.9	5.8	102.1	84.7	30.61	1.448
MN6B-42	1.423	0.079	0.1322	0.0046	0.0756	0.0013	897	32	800	26	1084	33	242	264	71.1	1.075
MN6B-43	0.923	0.03	0.0898	0.0019	0.0766	0.0039	663	16	554	12	1095	81	399	472	86.7	1.015
MN6B-44	1.3394	0.0088	0.14193	0.00053	0.06816	0.00027	862.9	3.8	855.5	3	873.2	8.1	111.1	72.8	28.26	1.743
MN6B-45	10.937	0.093	0.4567	0.0048	0.17243	0.00052	2514.8	9.3	2424	21	2581.2	5.1	90.5	51.6	60.1	1.954
MN6B-46	3.49	0.11	0.2441	0.0073	0.10357	0.00072	1524	25	1408	38	1689	13	127.4	48.6	23.8	3.104
MN6B-47	3.39	0.16	0.2348	0.0095	0.1045	0.0019	1498	37	1359	50	1703	35	157	101	49.3	1.84
MN6B-48	6.484	0.094	0.3595	0.0068	0.1306	0.0011	2043	13	1980	32	2105	14	96.5	21.9	21.9	5.34
MN6B-49	6.518	0.04	0.382	0.0025	0.12355	0.0003	2048.3	5.4	2086	12	2008	4.3	94.9	22.9	23.7	4.79
MN6B-50	11.021	0.051	0.4591	0.0023	0.17313	0.00039	2524.8	4.4	2435	10	2588.1	3.8	87.1	119.4	136.6	0.811
MN6B-51	11.178	0.052	0.4659	0.0023	0.17316	0.00033	2538	4.4	2466	10	2588.4	3.2	88.5	112.6	128.9	0.862
MN6B-52	1.191	0.021	0.1262	0.0022	0.06846	0.00055	796	10	766	12	882	16	78.4	42	13.59	2.066
MN6B-53	1.025	0.017	0.1059	0.0017	0.06982	0.00055	716.4	8.4	649.1	9.7	923	16	49.5	39.4	7.38	1.354
MN6B-54	1.298	0.014	0.1354	0.0015	0.0689	0.00039	844.7	6.3	818.4	8.7	895	11	63.9	63.4	23.1	1.184
MN6B-55	1.2656	0.0098	0.134	0.0015	0.06843	0.00038	830.3	4.4	810.6	8.5	881	12	136.3	87.3	32.54	1.71
MN6B-56	1.045	0.018	0.1074	0.0015	0.07047	0.00065	726.3	8.8	657.6	8.7	942	19	58.2	61.3	16.15	1.038
MN6B-57	1.2053	0.0058	0.13052	0.00055	0.06678	0.00019	803	2.7	790.8	3.1	830.7	5.8	175	123.3	45.3	1.503
MN6B-58	1.415	0.018	0.1495	0.0021	0.06821	0.00018	894.7	7.7	898	12	874.7	5.4	317	231	96.7	1.442
MN6B-59	1.306	0.025	0.1362	0.0028	0.06923	0.00038	847	11	823	16	905	11	398	347	125	1.182
MN6B-60	1.439	0.02	0.1477	0.0013	0.07053	0.00052	904.9	8.2	887.9	7.3	943	15	63.9	42.1	17.6	1.518

Continued-

Analysis	Isotopic ratio						Apparent age (Ma)						Content (ppm)			
	$^{207}Pb/^{235}U$	2σ	$^{206}Pb/^{238}U$	2σ	$^{207}Pb/^{206}Pb$	2σ	$^{207}Pb/^{235}U$	2σ	$^{206}Pb/^{238}U$	2σ	$^{207}Pb/^{206}Pb$	2σ	U	Th	Pb	U/Th
MN6B-61	1.511	0.034	0.1497	0.0024	0.07278	0.00074	934	14	899	13	1009	21	178	119	53.8	1.419
MN6B-62	1.72	0.23	0.1345	0.0037	0.095	0.011	998	79	813	21	1450	190	319	321	118	1.016
MN6B-63	2.701	0.083	0.1652	0.0049	0.11811	0.00098	1333	24	985	27	1927	15	369	182	57.1	1.959
MN6B-64	3.36	0.095	0.2012	0.0055	0.12005	0.0008	1492	22	1181	30	1956	12	371	73.2	27.5	4.6
MN6B-65	5.154	0.062	0.3169	0.0054	0.1175	0.001	1844	10	1774	26	1917	15	196.1	64.3	53.4	2.801
MN6B-66	2.01	0.22	0.1664	0.0042	0.0856	0.0066	1092	61	992	23	1230	110	54.3	134.7	77	0.394
MN6B-67	3.37	0.11	0.197	0.0056	0.12274	0.00084	1496	26	1158	30	1996	12	275	228	94.7	1.112
MN6B-68	1.203	0.011	0.1286	0.0013	0.06786	0.00015	801.7	5.1	779.8	7.4	864.3	4.5	270.8	198.3	75.3	1.288
MN6B-69	1.144	0.032	0.1164	0.0032	0.07122	0.0004	773	15	712	18	963	11	471	356	93.6	1.42
MN6B-70	1.85	0.19	0.1159	0.0041	0.1116	0.0073	1037	63	706	23	1770	120	516	331	100.7	1.455
MN6B-71	1.248	0.017	0.1316	0.0023	0.06889	0.00039	822.1	7.6	797	13	895	11	191.4	88.9	33.09	2.038
MN6B-72	4.707	0.063	0.3138	0.0045	0.10822	0.00032	1768	11	1759	22	1769.6	5.3	137.6	68.9	54.8	1.919
MN6B-73	1.292	0.014	0.1403	0.001	0.06663	0.00039	842.2	6	846.2	5.9	826	12	79.3	83.2	29.5	0.929
MN6B-74	1.221	0.02	0.1283	0.0018	0.06891	0.00028	809.5	9.1	778	10	895.9	8.3	200	71.5	30.74	2.73
MN6B-75	1.444	0.017	0.1383	0.0014	0.0756	0.00024	907.2	7.1	835	7.9	1084.4	6.3	470	42.4	17.3	10.67
MN6B-76	3.35	0.1	0.2045	0.0059	0.11946	0.00058	1492	25	1198	32	1947.9	8.6	333	230	109.2	1.46
MN6B-77	11.83	0.16	0.5005	0.005	0.17282	0.00094	2591	13	2616	22	2585	9	104	72.1	85.9	1.519
MN6B-78	11.58	0.14	0.488	0.0057	0.171	0.00033	2571	11	2562	25	2567.4	3.2	94.6	95.4	109.5	1.051
MN6B-79	10.804	0.074	0.451	0.003	0.17272	0.00037	2506.1	6.3	2399	13	2584.1	3.6	115.1	82.6	86.7	1.449
MN6B-80	1.535	0.011	0.15659	0.0009	0.07075	0.00037	944.5	4.5	937.8	5	950	11	52.4	59.1	26.29	0.926
MN6B-81	1.359	0.028	0.1328	0.0018	0.07364	0.00076	874	13	804	10	1031	21	214	208	56.3	1.088
MN6B-82	1.131	0.015	0.1132	0.0014	0.07207	0.00031	768	7.3	691.5	7.9	987.7	8.7	160.9	200.2	47.5	0.864
MN6B-83	1.481	0.02	0.0745	0.0015	0.144	0.0019	922.7	8.3	463.1	9.3	2276	23	964	501	80.6	2.045
MN6B-84	1.781	0.059	0.0999	0.0041	0.1275	0.0021	1037	21	614	24	2062	29	528	183	47.2	3.62
MN6B-85	2.4	0.11	0.1435	0.0057	0.12062	0.00089	1242	32	864	32	1965	13	289	76	29.8	4.18
MN6B-86	3.116	0.054	0.1912	0.0027	0.11619	0.00098	1436	14	1130	15	1898	15	240.9	92	49.3	3.91
MN6B-87	5.114	0.083	0.3224	0.0055	0.11401	0.00029	1837	14	1801	27	1864.2	4.5	118	73.7	61.2	1.658
MN6B-88	4.48	0.11	0.2625	0.0071	0.12345	0.00054	1726	21	1502	36	2006.6	7.7	210.3	71.4	19.26	3.08
MN6B-89	3.839	0.059	0.2235	0.0039	0.12371	0.00047	1601	12	1300	21	2010.4	6.7	192.4	152.2	21.9	1.29
MN6B-90	4.318	0.056	0.256	0.0047	0.12163	0.00084	1697	11	1469	24	1980	12	162.3	98.6	23.15	1.633

Continued-

Analysis	Isotopic ratio						Apparent age (Ma)						Content (ppm)			
	$^{207}Pb/^{235}U$	2σ	$^{206}Pb/^{238}U$	2σ	$^{207}Pb/^{206}Pb$	2σ	$^{207}Pb/^{235}U$	2σ	$^{206}Pb/^{238}U$	2σ	$^{207}Pb/^{206}Pb$	2σ	U	Th	Pb	U/Th
MN6B-91	4.871	0.078	0.2869	0.0062	0.1244	0.0023	1797	13	1625	31	2019	31	144	47.5	33.2	3.12
MN6B-92	3.096	0.094	0.1876	0.005	0.11885	0.00098	1430	23	1108	27	1939	15	244.4	115	21.67	2.2
MN6B-93	4.845	0.043	0.292	0.0031	0.12043	0.00053	1792.6	7.5	1651	16	1962.5	7.9	203	21.78	15.83	9.31
MN6B-94	5.45	0.13	0.3378	0.0091	0.11619	0.00054	1892	21	1875	44	1898.2	8.4	141	25.2	20.2	5.647
MN6B-95	3.825	0.034	0.2251	0.0022	0.1232	0.0013	1598	7.1	1308	11	2002	18	256	166.5	87.3	1.513
MN6B-96	4.59	0.21	0.288	0.014	0.11498	0.00052	1745	38	1630	68	1879.4	8.2	194	141	101.4	1.353
MN6B-97	10.63	0.12	0.436	0.0044	0.1746	0.00062	2491	10	2332	20	2602.1	5.8	176.3	162	165	1.109
MN6B-98	5.28	0.15	0.326	0.011	0.11653	0.00081	1869	26	1831	59	1903	12	149.8	62.4	49.4	2.257
MN6B-99	2.86	0.1	0.2345	0.0075	0.088	0.00079	1369	26	1357	39	1382	17	249	129	83.3	1.818
MN6B-100	3.38	0.18	0.244	0.015	0.0994	0.0012	1494	44	1403	78	1612	21	247	183	91.8	1.212
MN6B-101	3.758	0.056	0.2185	0.0045	0.1243	0.0014	1583	12	1274	24	2018	20	262	172	59	1.39
MN6B-102	2.86	0.15	0.149	0.01	0.1372	0.0041	1367	40	895	58	2188	50	407	97	87	3.785
MN6B-103	6.48	0.22	0.2732	0.0077	0.1713	0.0014	2042	29	1556	39	2570	14	715	231	101.8	2.8
MN6B-104	12.11	0.36	0.459	0.011	0.1892	0.0011	2611	28	2435	48	2735	9.6	262	125	138	1.86
MN6B-105	1.721	0.062	0.0789	0.0045	0.1548	0.0035	1015	23	489	27	2397	39	1220	424	168.8	2.46
MN6B-106	2.4	0.15	0.1376	0.0078	0.12581	0.00065	1238	44	830	44	2040.1	9.2	485	200	99.5	2.08
MN6B-107	5.49	0.26	0.271	0.013	0.1426	0.0013	1897	41	1548	64	2259	16	208	95	115	1.923
MN6B-108	4.61	0.2	0.2763	0.0084	0.1181	0.0038	1750	36	1573	42	1924	58	242	138	118	1.549
MN6B-109	4.1	0.15	0.291	0.011	0.10135	0.00057	1654	30	1648	54	1649	10	264	145	111.8	1.584
MN6B-110	3.38	0.11	0.1892	0.0069	0.1301	0.0066	1500	26	1117	37	2097	89	424	82	56.2	4.62
MN6B-111	4.125	0.068	0.2505	0.0044	0.11798	0.00083	1659	13	1441	23	1925	13	270	69.1	44.1	3.29
MN6B-112	3.847	0.053	0.2379	0.0028	0.11674	0.00046	1602	11	1376	15	1906.9	7	474	82.8	58.6	4.99
MN6B-113	4.425	0.046	0.2737	0.0025	0.11678	0.00031	1716.9	8.6	1559	13	1907.4	4.8	277.7	59.3	46.8	4.044
MN6B-114	5.032	0.041	0.3179	0.0028	0.11383	0.0002	1824.7	6.9	1783	13	1861.4	3.2	208.9	84.1	71.1	2.137
MN6B-115	5.567	0.052	0.3524	0.0035	0.11378	0.00024	1910.9	8	1946	17	1860.7	3.8	135.3	63.5	58.1	1.85
MN6B-116	5.088	0.039	0.3053	0.0017	0.1202	0.00043	1834	6.5	1717.4	8.6	1959.1	6.4	248.9	63.8	50.5	3.44
MN6B-117	5.61	0.2	0.347	0.014	0.11672	0.00089	1924	29	1917	67	1906	14	206	66.3	60.6	2.729
MN6B-118	4.628	0.099	0.2755	0.006	0.12059	0.00063	1759	19	1568	30	1964.6	9.3	228	123.5	84.9	1.736
MN6B-119	4.27	0.06	0.2463	0.0019	0.1259	0.0012	1687	12	1419.3	9.7	2042	17	349	83	63	4.02
MN6B-120	3.802	0.07	0.1923	0.003	0.1404	0.0022	1592	14	1134	16	2230	27	225.6	243.6	119.1	0.856

Continued-

Analysis	Isotopic ratio						Apparent age (Ma)						Content (ppm)			
	$^{207}Pb/^{235}U$	2σ	$^{206}Pb/^{238}U$	2σ	$^{207}Pb/^{206}Pb$	2σ	$^{207}Pb/^{235}U$	2σ	$^{206}Pb/^{238}U$	2σ	$^{207}Pb/^{206}Pb$	2σ	U	Th	Pb	U/Th
MN6B-121	3.684	0.041	0.2659	0.0028	0.10008	0.00062	1567.9	8.9	1520	14	1625	12	110.2	80.4	63.6	1.314
MN6B-122	3.946	0.029	0.2841	0.0019	0.10001	0.00043	1623.1	6	1611.9	9.5	1624.2	8	66.8	50.1	40.6	1.279

Table 6.11: U-Pb geochronology of the Nagthat Fm. of outer Lesser Himalaya (Ghat-Gurna, Kumaun section)

Analysis	Isotopic ratio						Apparent age (Ma)						Content (ppm)			
	$^{207}Pb/^{235}U$	2σ	$^{206}Pb/^{238}U$	2σ	$^{207}Pb/^{206}Pb$	2σ	$^{207}Pb/^{235}U$	2σ	$^{206}Pb/^{238}U$	2σ	$^{207}Pb/^{206}Pb$	2σ	U	Th	Pb	U/Th
MN4Y-1	3.859	0.06	0.2043	0.0033	0.1381	0.0026	1607	13	1198	18	2200	33	290	190.4	90.5	1.56
MN4Y-2	4.611	0.055	0.2808	0.0039	0.11966	0.00031	1751	10	1595	20	1951.1	4.6	207	143.2	85.1	1.552
MN4Y-3	3.81	0.11	0.2272	0.0062	0.12165	0.00063	1593	24	1319	33	1980.4	9.2	192.2	81.7	63.8	2.53
MN4Y-4	4.58	0.17	0.2412	0.0073	0.1379	0.0017	1743	30	1401	41	2200	20	159	148	88.7	1.139
MN4Y-5	2.04	0.11	0.0923	0.0044	0.1583	0.0014	1124	35	569	26	2437	15	790	432	139	1.893
MN4Y-6	3.54	0.11	0.2066	0.0063	0.12418	0.00029	1533	24	1210	34	2017.1	4.1	212	282	67.8	0.807
MN4Y-7	4.918	0.074	0.3196	0.006	0.11169	0.00063	1804	13	1787	29	1827	10	122.8	74.6	63	1.75
MN4Y-8	2.2	0.11	0.0994	0.0052	0.1607	0.0013	1179	35	610	30	2462	14	657	488	214.2	1.397
MN4Y-9	3.08	0.15	0.181	0.011	0.1206	0.0015	1420	39	1068	60	1963	22	264	134	64.8	2.08
MN4Y-10	3.05	0.4	0.1769	0.006	0.124	0.012	1406	87	1050	33	1980	140	225.2	225	85	1.048
MN4Y-11	3.3	0.18	0.224	0.013	0.10695	0.00054	1479	44	1303	69	1748	9.2	186	183	76	1.031
MN4Y-12	3.629	0.079	0.2237	0.0045	0.11762	0.00044	1555	18	1301	24	1920.3	6.8	201	184.4	100.9	1.114
MN4Y-13	0.972	0.027	0.0504	0.0013	0.1391	0.00098	689	14	317.2	8.3	2216	12	1139	636	113	1.82
MN4Y-14	3.219	0.07	0.1788	0.0032	0.12992	0.00091	1460	17	1063	17	2096	12	322	300	140	1.114
MN4Y-15	2.581	0.084	0.1457	0.0043	0.12904	0.0008	1300	25	876	24	2084	11	622	412	103	1.58
MN4Y-16	2.539	0.095	0.1556	0.0054	0.11759	0.00044	1281	27	932	30	1919.9	6.7	292.3	342	83.1	0.902
MN4Y-17	1.687	0.095	0.096	0.0057	0.1286	0.0016	998	36	590	33	2078	22	549	416	115.6	1.337
MN4Y-18	1.81	0.12	0.1178	0.0075	0.11105	0.00074	1050	42	729	45	1816	12	534	303	100.9	1.74
MN4Y-19	4.745	0.036	0.318	0.0024	0.10818	0.00025	1776.3	6.6	1780	12	1768.9	4.2	97.7	75.4	62.4	1.361
MN4Y-20	2.52	0.1	0.1572	0.0069	0.11603	0.00066	1275	30	941	38	1896	10	379	279	94.7	1.45
MN4Y-21	1.25	0.1	0.0682	0.0049	0.1356	0.007	818	42	425	30	2153	81	837	748	161	1.152
MN4Y-22	3.004	0.07	0.1971	0.0039	0.10929	0.00083	1408	18	1160	21	1787	14	492	85	53.1	6.4

Continued-

Analysis	Isotopic ratio						Apparent age (Ma)						Content (ppm)			
	$^{207}Pb/^{235}U$	2σ	$^{206}Pb/^{238}U$	2σ	$^{207}Pb/^{206}Pb$	2σ	$^{207}Pb/^{235}U$	2σ	$^{206}Pb/^{238}U$	2σ	$^{207}Pb/^{206}Pb$	2σ	U	Th	Pb	U/Th
MN4Y-23	2.253	0.087	0.1403	0.0011	0.1165	0.0051	1196	27	846.3	6.1	1894	80	485	259	44.7	3.5
MN4Y-24	2.968	0.084	0.1718	0.006	0.1244	0.0013	1398	21	1022	33	2020	18	281.4	172.1	93.3	1.681
MN4Y-25	4.431	0.064	0.2795	0.0044	0.11479	0.00061	1720	13	1588	22	1876.3	9.5	122.3	108	70.7	1.185
MN4Y-26	3.906	0.084	0.2349	0.0057	0.11984	0.00044	1614	18	1360	30	1953.8	6.5	318	156.1	98.9	2.03
MN4Y-27	2.224	0.071	0.1257	0.0041	0.12809	0.00063	1188	23	763	23	2071.9	8.7	373	363	90.8	1.039
MN4Y-28	4.827	0.048	0.3181	0.0043	0.10897	0.00045	1789.3	8.3	1780	21	1782	7.4	120.4	66.4	63.6	1.859
MN4Y-29	8.67	0.3	0.344	0.011	0.1818	0.0011	2302	32	1907	53	2669	10	132.2	157	65.1	0.876
MN4Y-30	3.584	0.09	0.23	0.0064	0.11204	0.00027	1545	20	1334	33	1832.7	4.3	286	81	43	3.649
MN4Y-31	3.9	0.18	0.25	0.01	0.11288	0.00083	1611	38	1436	54	1846	13	227.8	70.8	44.88	3.31
MN4Y-32	1.904	0.066	0.1092	0.0041	0.1262	0.002	1079	23	668	24	2043	27	766	825	152.6	0.873
MN4Y-33	3.29	0.14	0.2046	0.0082	0.116	0.0011	1477	33	1205	43	1894	17	262	93.4	72.1	2.85
MN4Y-34	4.048	0.072	0.2602	0.0039	0.11152	0.00048	1643	15	1490	20	1824.2	7.8	181.1	271	175	0.699
MN4Y-35	9.858	0.067	0.4284	0.0026	0.16533	0.00047	2421.4	6.3	2298	12	2510.8	4.7	124.1	121	127	1.11
MN4Y-36	2.326	0.048	0.1061	0.0024	0.157	0.001	1219	15	652	14	2423	11	1001	984	177	1.115
MN4Y-37	2.317	0.076	0.1318	0.0047	0.12657	0.00072	1214	23	797	27	2050	10	492	509	127.8	0.975
MN4Y-38	1.443	0.043	0.0823	0.0026	0.12565	0.00077	908	17	510	15	2037	11	679.4	197.7	94.7	3.53
MN4Y-39	4.251	0.042	0.1995	0.0025	0.15353	0.00086	1683.7	8.1	1173	13	2385.3	9.4	573	272.6	121.4	2.16
MN4Y-40	1.102	0.022	0.0588	0.0011	0.1353	0.0011	757.3	9.9	368.1	6.7	2167	14	841	1074	166.5	0.801
MN4Y-41	5.569	0.093	0.2264	0.0057	0.1765	0.0014	1911	14	1315	30	2620	13	361	277	78.4	1.313
MN4Y-42	3.53	0.029	0.2552	0.0029	0.09907	0.00038	1533.7	6.5	1465	15	1606.6	7.1	177.6	77.8	51.5	2.4
MN4Y-43	3.63	0.26	0.195	0.012	0.1325	0.0026	1569	47	1149	63	2139	37	284	308	135	0.947
MN4Y-44	1.477	0.044	0.0707	0.0019	0.15	0.0018	920	18	440	12	2345	20	898	756	170.7	1.198
MN4Y-45	4.64	0.18	0.29	0.0092	0.1149	0.0016	1760	35	1640	46	1878	25	179.8	62.3	56.2	2.882
MN4Y-46	4.16	0.21	0.205	0.0083	0.1453	0.002	1661	42	1201	45	2290	23	475	609	197	0.792
MN4Y-47	4.058	0.096	0.2303	0.0051	0.12665	0.00034	1644	20	1336	27	2051.9	4.8	310.7	69.1	42.8	4.84
MN4Y-48	4.28	0.15	0.263	0.011	0.11666	0.00081	1686	29	1503	55	1905	12	143	129	72.3	1.119
MN4Y-49	1.73	0.16	0.107	0.01	0.1214	0.0011	1025	57	649	61	1979	16	617	268	93	2.45
MN4Y-50	3.09	0.13	0.1654	0.0047	0.1375	0.0045	1425	32	990	27	2191	57	241	366	83	0.715
MN4Y-51	4.07	0.08	0.251	0.0041	0.1199	0.0011	1647	17	1443	22	1953	15	241.4	78.2	41.7	3.14
MN4Y-52	3.635	0.083	0.2572	0.0069	0.10514	0.00054	1555	19	1474	36	1716.4	9.2	210.6	204	140	1.073

Continued-

Analysis	Isotopic ratio						Apparent age (Ma)						Content (ppm)			
	$^{207}Pb/^{235}U$	2σ	$^{206}Pb/^{238}U$	2σ	$^{207}Pb/^{206}Pb$	2σ	$^{207}Pb/^{235}U$	2σ	$^{206}Pb/^{238}U$	2σ	$^{207}Pb/^{206}Pb$	2σ	U	Th	Pb	U/Th
MN4Y-53	1.669	0.067	0.0842	0.0036	0.14715	0.0007	995	26	521	22	2312.9	8.1	958	778	132.1	1.282
MN4Y-54	6.02	0.2	0.2189	0.007	0.2039	0.0014	1978	30	1276	37	2858	11	469	162.3	65.4	2.92
MN4Y-55	4.5	0.15	0.1637	0.0038	0.2061	0.0018	1729	28	977	21	2875	15	526	228	75.5	2.35
MN4Y-56	2.41	0.14	0.1084	0.0048	0.1686	0.0053	1249	42	663	28	2533	54	538	266	185	2.147
MN4Y-57	1.61	0.1	0.0903	0.0077	0.1276	0.0024	971	40	563	47	2062	32	653	802	92.5	0.832
MN4Y-58	2.857	0.086	0.1637	0.0052	0.12914	0.00059	1370	23	977	29	2086.2	8.1	455	503	135.8	0.9
MN4Y-59	5.15	0.26	0.297	0.016	0.12906	0.00063	1848	40	1675	78	2085.1	8.6	202	188	84.7	1.06
MN4Y-60	10.52	0.55	0.4593	0.0077	0.1705	0.0054	2471	43	2436	34	2553	46	78.5	64.4	63.3	1.26
MN4Y-61	1.22	0.022	0.05788	0.00086	0.1586	0.0021	809	10	362.7	5.3	2439	23	1143	1345	108.3	0.865
MN4Y-62	3.195	0.063	0.1821	0.003	0.1301	0.0012	1455	16	1078	16	2099	16	303	276	74.5	1.14
MN4Y-63	4.5	0.15	0.2612	0.0063	0.1277	0.0037	1730	29	1496	32	2064	51	152.6	81	71	1.91
MN4Y-64	2.4	0.19	0.1241	0.0088	0.1395	0.0032	1235	57	753	50	2219	39	32	42	11.4	0.688
MN4Y-65	2.279	0.083	0.1269	0.0068	0.1368	0.0037	1215	25	769	39	2178	46	315	440	103	0.634
MN4Y-66	4.06	0.14	0.2584	0.0094	0.11644	0.00047	1643	28	1480	48	1902.1	7.2	242	221	91	2.48
MN4Y-67	3.565	0.089	0.2364	0.0053	0.11269	0.00068	1547	20	1367	27	1843	11	275.2	198.1	123.2	1.412
MN4Y-68	3.33	0.088	0.1984	0.005	0.12599	0.00057	1495	21	1166	27	2042.5	8	351	293	124.2	1.233
MN4Y-69	1.239	0.021	0.0752	0.0011	0.1207	0.0013	818.2	9.6	467.5	6.8	1967	20	871	669	226	1.357

Table 6.12: U-Pb geochronology of the Nagthat Fm. of outer Lesser Himalaya (Ghat-Gurna, Kumaun section)

Analysis	Isotopic ratio						Apparent age (Ma)						Content (ppm)			
	$^{207}Pb/^{235}U$	2σ	$^{206}Pb/^{238}U$	2σ	$^{207}Pb/^{206}Pb$	2σ	$^{207}Pb/^{235}U$	2σ	$^{206}Pb/^{238}U$	2σ	$^{207}Pb/^{206}Pb$	2σ	U	Th	Pb	U/Th
MN4Z-1	4.701	0.053	0.2448	0.0038	0.142	0.0016	1766.8	9.5	1411	19	2251	19	128.7	226	83	0.585
MN4Z-2	4.437	0.082	0.2421	0.0038	0.13575	0.00065	1720	16	1401	20	2174.5	8.2	253	213.4	119.2	1.192
MN4Z-3	5.63	0.32	0.2771	0.0051	0.151	0.0071	1913	49	1576	26	2329	83	203.7	170	148	1.272
MN4Z-4	3.832	0.042	0.2324	0.0028	0.1224	0.00032	1599.4	8.7	1347	15	1992.8	4	223.5	210.3	105.9	1.063
MN4Z-5	10.33	0.16	0.4526	0.0076	0.1701	0.0011	2466	15	2406	34	2558	10	126.6	114	115	1.125
MN4Z-6	7.81	0.13	0.3413	0.0061	0.16979	0.00081	2210	15	1893	29	2555.5	7.9	152.7	164.7	113	0.936
MN4Z-7	2.857	0.064	0.1543	0.0031	0.1376	0.001	1369	17	925	17	2199	13	332	460	153.9	0.745
MN4Z-8	0.111	0.0028	0.01687	0.00049	0.04882	0.00059	106.9	2.6	107.9	3.1	138	29	441	325	16.8	1.33
MN4Z-9	5.745	0.04	0.3253	0.0027	0.13094	0.00045	1937.9	6.1	1816	13	2110.4	6	166.9	50	36.62	3.33
MN4Z-10	3.513	0.024	0.2183	0.0011	0.11879	0.00045	1529.9	5.4	1273	5.7	1937.9	6.7	302.5	200	109.4	1.551
MN4Z-11	6.07	0.13	0.2997	0.007	0.1502	0.0003	1984	19	1689	35	2348.2	3.4	288	23.4	17.3	13.09
MN4Z-12	10.22	0.16	0.439	0.0075	0.17304	0.00031	2454	15	2345	34	2587.3	3	124.7	49.4	53.8	2.579
MN4Z-13	4.241	0.085	0.2583	0.0045	0.12139	0.00046	1680	17	1481	23	1977.9	7.1	332	33.91	27.59	10.01
MN4Z-14	4.452	0.034	0.2933	0.0019	0.11263	0.00052	1722.7	6.5	1658.1	9.5	1842	8.4	129.3	77.3	65	1.65
MN4Z-15	7.407	0.087	0.3134	0.0041	0.1751	0.00049	2161	11	1757	20	2607.8	4.9	239	216.6	152.8	1.105
MN4Z-16	8.55	0.23	0.359	0.011	0.17734	0.00088	2288	26	1976	53	2627.9	8.2	187	143	95.6	1.295
MN4Z-17	3.556	0.03	0.2649	0.0021	0.0997	0.00055	1540.7	7	1515	11	1618	10	93	61.2	54.4	1.595
MN4Z-18	3.351	0.056	0.2014	0.0027	0.1228	0.00068	1493	13	1183	14	1997.2	9.7	606	41.5	17.5	15.8
MN4Z-19	4.169	0.051	0.2494	0.0029	0.12437	0.00031	1668	10	1435	15	2019.8	4.3	280	55.1	23.4	5.57
MN4Z-20	5.393	0.084	0.2757	0.0045	0.14502	0.00061	1884	13	1569	23	2288	7.3	183.3	118.2	92	1.613
MN4Z-21	3.99	0.056	0.2239	0.0022	0.13281	0.00098	1632	11	1302	12	2135	13	272.1	266.3	122	1.038
MN4Z-22	3.067	0.03	0.2173	0.0017	0.10435	0.00063	1424.2	7.3	1267.6	9.1	1703	11	186.6	145.6	94.9	1.278
MN4Z-23	3.631	0.055	0.2201	0.0038	0.1216	0.0013	1556	12	1282	20	1981	19	146.9	135.3	63.6	1.05
MN4Z-24	3.127	0.04	0.2039	0.0032	0.11402	0.00037	1439	9.9	1196	17	1864.3	5.8	274.9	227	85.8	1.269
MN4Z-25	3.073	0.039	0.1976	0.0024	0.1138	0.00033	1425.3	9.7	1163	13	1860.9	5.3	488	12.13	7.29	41.8
MN4Z-26	6.47	0.17	0.3558	0.0094	0.13336	0.00029	2043	23	1960	45	2142.6	3.9	144.2	100	81.6	1.52
MN4Z-27	5.421	0.06	0.3297	0.0058	0.1192	0.00096	1887.9	9.5	1837	28	1944	14	142.5	43.5	32.1	3.49
MN4Z-28	4.457	0.092	0.2734	0.0064	0.11958	0.00048	1722	17	1558	32	1949.9	7.2	182	67.7	22.2	2.93
MN4Z-29	5.219	0.078	0.315	0.0045	0.12065	0.0007	1855	13	1765	22	1966	10	145.8	43.1	34.8	3.47
MN4Z-30	5.01	0.12	0.2846	0.007	0.12788	0.00066	1819	20	1620	33	2068.7	9.1	180.1	118.9	58.1	1.536

Continued-

Analysis	Isotopic ratio						Apparent age (Ma)						Content (ppm)			
	$^{207}Pb/^{235}U$	2σ	$^{206}Pb/^{238}U$	2σ	$^{207}Pb/^{206}Pb$	2σ	$^{207}Pb/^{235}U$	2σ	$^{206}Pb/^{238}U$	2σ	$^{207}Pb/^{206}Pb$	2σ	U	Th	Pb	U/Th
MN4Z-31	3.07	0.14	0.1718	0.0083	0.1291	0.0012	1424	35	1020	45	2085	17	319	192	78.9	1.701
MN4Z-32	4.55	0.2	0.2918	0.0089	0.1144	0.0018	1738	35	1649	45	1873	29	194.2	109.1	69.3	1.777
MN4Z-33	4.146	0.044	0.2542	0.003	0.1197	0.0003	1662.9	8.8	1460	16	1951.7	4.6	202.2	131.7	42.9	1.54
MN4Z-34	4.558	0.086	0.2797	0.0043	0.1193	0.0019	1743	16	1590	22	1943	27	177	81.9	55.4	2.164
MN4Z-35	4.56	0.11	0.2714	0.0064	0.12356	0.00035	1740	21	1547	32	2008.1	5.1	211	94.6	66.3	2.098
MN4Z-36	4.986	0.078	0.3335	0.0066	0.10976	0.00061	1816	13	1855	32	1795	10	126.5	58.2	52.3	2.212
MN4Z-37	3.657	0.079	0.2084	0.0051	0.12909	0.00055	1560	17	1220	27	2085.3	7.5	220.9	79.3	29.5	2.93
MN4Z-38	4.239	0.052	0.2791	0.0035	0.11202	0.0008	1681	10	1586	18	1834	13	157.7	73.4	55.1	2.181
MN4Z-39	12.17	0.41	0.509	0.014	0.1757	0.0017	2612	30	2649	57	2611	15	81.8	44	64.5	1.841
MN4Z-40	5.263	0.057	0.3255	0.0055	0.11799	0.00078	1862.3	9.2	1816	27	1925	12	143.2	65.4	51.2	2.226
MN4Z-41	7.37	0.15	0.3353	0.0057	0.16118	0.00091	2156	18	1863	28	2467.8	9.5	214.1	105.3	84.5	2.05
MN4Z-42	5.51	0.11	0.2603	0.0069	0.1566	0.0017	1901	18	1491	35	2419	19	176	74	57	2.47
MN4Z-43	5.26	0.1	0.2195	0.0042	0.1758	0.0011	1860	17	1279	22	2613	10	364	235.9	142.5	1.494
MN4Z-44	10.61	0.048	0.4596	0.0022	0.17069	0.00027	2489.5	4.2	2437.7	9.8	2564.4	2.7	70.4	28.85	35.8	2.505
MN4Z-45	5.02	0.12	0.289	0.0081	0.12711	0.00039	1820	21	1635	40	2058.3	5.4	175.8	43.2	31.6	4.24
MN4Z-46	5.136	0.044	0.3255	0.0027	0.1166	0.00071	1841.8	7.4	1817	13	1904	11	100.4	50	46.1	2.015
MN4Z-47	2.46	0.1	0.1422	0.0044	0.1272	0.0017	1255	30	857	25	2057	24	591	458	128.3	1.309
MN4Z-48	3.168	0.051	0.1991	0.0046	0.1183	0.0013	1449	12	1170	25	1933	19	194.7	268	79.8	0.744
MN4Z-49	4.518	0.04	0.2807	0.0029	0.11907	0.00025	1733.9	7.4	1595	14	1942.2	3.8	198.4	125.5	53.7	1.618
MN4Z-50	5.568	0.051	0.3248	0.0028	0.12679	0.0003	1912	7.7	1813	13	2053.9	4.1	159.6	55.2	25.4	2.84
MN4Z-51	4.561	0.041	0.2966	0.0022	0.11309	0.00036	1741.8	7.5	1674	11	1849.6	5.8	135.6	81.8	64.5	1.76
MN4Z-52	11.21	0.15	0.4784	0.0094	0.1738	0.0013	2541	13	2520	41	2594	12	84.8	28.9	44.6	3.01
MN4Z-53	8.47	0.21	0.3519	0.0083	0.1782	0.0013	2281	22	1943	40	2636	12	61	51.3	39.8	1.202
MN4Z-54	7.719	0.093	0.3401	0.0027	0.1678	0.0012	2198	11	1887	13	2535	11	196.9	86.9	74.3	2.33
MN4Z-55	4.32	0.046	0.2675	0.003	0.11922	0.00024	1697	8.7	1528	15	1944.5	3.6	247.7	64	23.5	4.82
MN4Z-56	3.309	0.066	0.2024	0.0038	0.12101	0.00058	1483	16	1188	20	1971.2	8.6	265.4	138.7	31.99	1.957
MN4Z-57	6.43	0.25	0.2247	0.0058	0.2106	0.0021	2033	34	1306	30	2910	16	399	188	107	2.28
MN4Z-58	11.6	0.26	0.3814	0.0086	0.22544	0.00049	2571	21	2082	40	3019.9	3.5	179.1	59.2	45.6	3.16
MN4Z-59	8.64	0.14	0.3519	0.0053	0.18168	0.00045	2299	15	1943	25	2668.2	4.1	197.8	194	153.4	1.027
MN4Z-60	2.49	0.042	0.1656	0.0024	0.11156	0.00033	1269	12	988	13	1824.9	5.3	386	155.7	51.5	2.537

Continued-

Analysis	Isotopic ratio						Apparent age (Ma)						Content (ppm)			
	$^{207}Pb/^{235}U$	2σ	$^{206}Pb/^{238}U$	2σ	$^{207}Pb/^{206}Pb$	2σ	$^{207}Pb/^{235}U$	2σ	$^{206}Pb/^{238}U$	2σ	$^{207}Pb/^{206}Pb$	2σ	U	Th	Pb	U/Th
MN4Z-61	5.225	0.081	0.3394	0.006	0.11468	0.0004	1860	14	1883	29	1874.7	6.3	109	54.6	45.3	2.025
MN4Z-62	4.047	0.085	0.2554	0.0055	0.11729	0.00076	1643	17	1466	28	1915	12	181.3	59.2	29.64	3.08
MN4Z-63	3.202	0.05	0.2004	0.0036	0.11801	0.00057	1457	12	1177	19	1926.1	8.6	229.6	82.7	36.2	2.79
MN4Z-64	4.743	0.059	0.2923	0.0034	0.12024	0.00072	1775	10	1653	17	1960	11	148	97.9	69.1	1.533
MN4Z-65	4.224	0.06	0.2436	0.0048	0.1285	0.0033	1678	12	1405	25	2074	46	201.9	150.4	77.1	1.371
MN4Z-66	9.909	0.074	0.4376	0.0045	0.16729	0.00082	2426.1	6.9	2340	20	2531.7	8	103.4	59.9	64.7	1.699
MN4Z-67	12.18	0.16	0.5062	0.0075	0.17849	0.00062	2620	13	2639	32	2638.7	5.7	86.4	55.1	76.9	1.59
MN4Z-68	9.34	0.14	0.3958	0.0056	0.17507	0.00048	2371	14	2149	26	2606.7	4.5	105.1	86.1	74.5	1.225
MN4Z-69	2.79	0.12	0.1616	0.0081	0.1277	0.0013	1364	35	964	44	2065	19	346	207	95.7	1.674
MN4Z-70	8.005	0.059	0.3459	0.003	0.17124	0.00048	2231.3	6.6	1917	14	2569.7	4.7	197.1	209.5	149.8	0.929
MN4Z-71	3.951	0.053	0.2295	0.0032	0.12821	0.00033	1624	11	1332	17	2073.5	4.5	243.2	92.6	45.1	2.54
MN4Z-72	2.705	0.096	0.1948	0.0065	0.10263	0.00067	1326	26	1146	35	1672	12	201.2	221	104.7	0.884
MN4Z-73	2.822	0.033	0.183	0.0024	0.11405	0.00017	1362.6	8.5	1086	12	1864.9	2.7	429	229.2	111.9	1.834
MN4Z-74	1.539	0.045	0.1023	0.0028	0.111	0.00023	944	18	628	17	1815.8	3.8	886	84.8	28.3	10.92
MN4Z-75	3.95	0.19	0.2305	0.004	0.125	0.0048	1616	36	1337	21	2013	63	188.2	233	87.4	0.822
MN4Z-76	9.516	0.072	0.4035	0.0032	0.17462	0.00025	2389	7	2185	15	2602.4	2.4	109	96	69	1.144
MN4Z-77	6.123	0.066	0.37	0.005	0.12228	0.00038	1995	10	2029	24	1989.6	5.5	87.7	29.7	25.3	3.062
MN4Z-78	3.947	0.08	0.2386	0.0045	0.12276	0.00026	1626	15	1379	23	1996.7	3.8	266	193	95.9	1.428
MN4Z-79	2.898	0.089	0.1838	0.0044	0.11599	0.00092	1380	22	1088	24	1895	14	503	121	44.7	4.43
MN4Z-80	3.163	0.049	0.1989	0.0022	0.1174	0.0012	1448	12	1170	12	1917	18	344	109.4	37.46	3.22
MN4Z-81	3.157	0.053	0.1861	0.0024	0.12509	0.00056	1446	13	1100	13	2029.9	8	274.1	244.1	91.3	1.153
MN4Z-82	4.983	0.076	0.2958	0.0034	0.1262	0.0027	1816	13	1670	17	2041	36	159.9	81.7	60.3	1.98
MN4Z-83	2.048	0.04	0.1302	0.003	0.1156	0.001	1131	13	789	17	1891	15	388	631	168	0.6
MN4Z-84	4.259	0.044	0.2707	0.0026	0.1153	0.00085	1685.1	8.5	1544	13	1887	14	170.8	84.4	60	2.01
MN4Z-85	2.38	0.18	0.148	0.011	0.11864	0.00046	1234	53	891	64	1935.9	6.9	374	236	95	1.574

CURRICULUM VITAE

Manju Negi

E-mail: manjunegi34@gmail.com

Contact No: 8755636931

Educational Qualifications:-

1. M.Sc. (Geology) from H.N.B. Garhwal University (2010-2012) with **71.3%**.
2. B.Sc. (Physics, Mathematics and Geology) from H.N.B. Garhwal University (2007-
   2010.) with **72.6%**.

Achievements:-

1. Awarded by **Rajendra Kulshreshtra Award** in 2011 for getting 2nd rank in
   B.Sc.
2. 2nd Prize for participating in the poster presentation in the "Industry-Academia
   Programme" under the aegis of GEO India (conference sponsored by ONGC)
   2011.

National & International Conferences:

Manju Negi, S. K. Rai and S. K. Ghosh. Petrographic and Sr-Nd isotopic
geochemistry of the lesser Himalayan clastic sediments constrains on
their provenance and model age. Himalaya-Karakoram-Tibet 2015
held at WIHG, Dehradun from October 6-8, 2015.

Manju Negi, Santosh K Rai, S.K. Ghosh, Uday Bhan and Saurabh Singhal.
Characterization of zircons in the Garhwal Lesser Himalayan clastic
sediments: a Morphological approach. "Earth system science with

special reference to Himalaya advancement and challenges" during May 16-18, 2018 held at WIHG, Dehradun.

Publications:

Ghosh, S.K., **Negi, M.**, Jalal, P. and Sinha, S., 2016. Proterozoic sedimentary successions in the Himalayan Orogen: stratigraphy, sedimentology and palaeobasinal conditions. *Himalayan Geology 37*(2), pp.121-140.

Tiwari, S.K., Rai, S.K., Bartarya, S.K., Gupta, A.K. and **Negi, M**., 2016. Stable isotopes (δ13C DIC, δD, δ18O) and geochemical characteristics of geothermal springs of Ladakh and Himachal (India): Evidence for CO_2 discharge in northwest Himalaya. *Geothermics*, *64*, pp.314-330.

Rai, S.K., Tiwari, S.K., Kharya, A., **Negi, M**. and Gupta, A.K., 2015. A Laser Based Fluorination (BrF_5) System for the Extraction of Oxygen (O_2) from Silicate Rocks of Himalaya and δ18O Measurements: Method Establishment and Implications. *Mapan*, *30*(3), pp.221-230.

Submitted:

Manju Negi, Santosh K. Rai, Sumit K. Ghosh, Uday Bhan, and Saurabh Singhal. Characterization of zircons from the Lesser Himalayan clastics: Implication for provenance appraisal. Himalayan Geology (commu.).

Workshop and Lecture series:

1. Participated in the "WIHG WINTER SCHOOL IN GEOMATHEMATICS" sponsored by Science and Engineering Research Board SERB, DST, GOVT of India to be organized at Wadia Institute of Himalayan Geology, Dehradun during 16-30 Dec 2013.
2. Participated in the Industry-Academia Workshop Recent Trends in Petroleum Exploration Technology Sponsored by ONGC in 2012.
3. Participated in the Geo-Gen Next Programme in 2011 Sponsored by ONGC.

4. Participated in the "Field Expedition and workshop in Himachal Pradesh (Nahan-Kangra Area)" organized by the Association of Petroleum Geologist in 2009.

5. Participated in the National Seminar "Science Communication through Creative Generes" in 2008.

CrossMark

SHORT COMMUNICATION

A Laser Based Fluorination (BrF$_5$) System for the Extraction of Oxygen (O$_2$) from Silicate Rocks of Himalaya and δ^{18}O Measurements: Method Establishment and Implications

S. K. Rai[1]* , S. K. Tiwari[1], A. Kharya[1], M. Negi[1] and A. K. Gupta[1,2]

[1]Wadia Institute of Himalayan Geology, 33 GMS Road, Dehra Dun 248001, India

[2]Department of Geology and Geophysics, Indian Institute of Technology, Kharagpur 721302, India

Abstract: Oxygen forms the majority of minerals constituting the terrestrial and planetary objects. Its chemical and isotopic compositions often bear signatures of the processes occurring within these objects on different time scales. Silicates are the common rocks in the Himalaya, the major feature on the Earth, which has witnessed different stages of metamorphism and got reworked during its evolution. Therefore, oxygen isotopes in silicate rocks can be used to reveal the processes pertaining to the Himalayan orogeny. These processes include petrogenesis, metamorphism, subduction and associated magmatic events, etc. Oxygen isotopic composition (δ^{18}O) is needed to be measured in silicate rocks which require special arrangements. Towards this, a vacuum line of stainless steel coupled with a computer controlled CO$_2$ laser system was fabricated, for the first time in India, to extract oxygen (O$_2$) from rock forming mineral in the BrF$_5$ environment. The line is equipped with suitable valves and traps for the efficient recovery of oxygen from the silicate minerals and reliable handling of hazardous oxidants (i.e., BrF$_5$, etc.) that are used as fluorination agents to break Si=O bonds. This extraction system is interfaced with a continuous flow stable isotope ratio mass spectrometer and is being used successfully for the oxygen isotopic (δ^{18}O) measurements in silicate and oxide minerals. Here we report the δ^{18}O results on a set of silicate rocks and standard reference materials including Norway olivine, Gee Whiz Garnet standard from University of New Mexico, olivine from Norway Fan (Lab Standard), silicate rocks from North West Himalaya (India) and NBS-28 quartz a standard reference material from International Atomic Energy Agency, Vienna. The average δ^{18}O values (relative to Vienna standard mean ocean water) and 2SD are 6.4 ± 0.3 ‰ ($N = 17$) for Norway olivine, 12.7 ± 0.2 ‰ ($N = 10$) for Gee Whiz Garnet and 9.5 ± 0.3 ‰ ($N = 12$) for NBS-28 quartz. In addition, some of the quartz vein and quartzites from the Garhwal Himalaya were also measured to establish the measurement protocols and procedures. Silicate rocks from the Himalaya near the main central thrust zone were tried to fix the end-member composition for oxygen isotopes (δ^{18}O). Such information is helpful to infer about the origin of quartzite and their relationship with possible protoliths in the region. Further, this technique finds applications in the analysis of biogenic silica (diatoms and phytoliths, etc.) for paleoclimatic reconstruction.

Keywords: Oxygen isotopes; BrF$_5$; Laser-fluorination; Silicates; Oxides

1. Introduction

Oxygen being one of the most abundant elements contributes to the formation of major common minerals in the solar system and terrestrial objects. Therefore, its chemical and isotopic composition contains valuable information on the processes operating on different time scales in the Earth and planetary system [1, 2]. This element has three stable isotopes ^{16}O, ^{17}O and ^{18}O with their terrestrial abundances of 99.76, 0.04 and 0.20 %, respectively. The analysis of oxygen isotopes in rock forming minerals are of vital importance in the field of geochemistry and cosmochemistry dealing with the origin and evolution of rocks. Oxygen isotope compositions of different reservoirs of the solar system vary as a result of initial heterogeneities, mixing of two or more distinct components processes leaving their imprints in form of isotopic fractionation. Hence isotopic

*Corresponding author, E-mail: rksant@wihg.res.in

Springer

Proterozoic Sedimentary Successions in the Himalayan Orogen: Stratigraphy, Sedimentology and Palaeobasinal conditions

SUMIT K. GHOSH[1]*, MANJU NEGI[1], POONAM JALAL[1,2], SUBHAJIT SINHA[3]

[1]*Wadia Institute of Himalayan Geology, Dehradun 248001, India*
[2]*Deparment of Geology, Kumaun University, Nainital 263001, India*
[3]*Department of Geology, Ballygunje Science College, Kolkata 700019, India*
*Email (Corresponding author) skgwihg@gmail.com

Abstract: The Himalayan orogen forms a 2500 km long and ~ 250 km wide arc along the leading margin of the Indian plate. The Higher, Lesser, and Sub-Himalaya are thus slices of the old Indian shield that have stacked over one another by transfer along a series of southward verging thrusts. Four prominent lithoevents are recorded in the Late Palaeoproterozoic to Early Palaeozoic sedimentary succession of the Lesser and Tethys Himalayan part: i) Palaeoproterozoic Argillite= Siliciclastic, ii) Mesoproterozoic Calcareous (limestone) > Argillite, iii) Neoproterozic Argillite=Siliciclastic, and iv) Late Neoproterozic- Early Palaeozoic Mixed Siliciclastic-Argillite-Calcareous (limestone). Based on geologic, sedimentologic and petrographic attributes, the central Lesser Himalayan (Garhwal and Kumaun) Proterozoic successions have been segregated into outer (southern) and inner (northern) domains. Of these the pre-Blaini sedimentary succession of the Outer Lesser Himalaya (OLH) is younger (Neoproterozoic) than Inner Lesser Himalaya (ILH) (Palaeoproterozoic-Meso-proterozoic). The gradual coarsening up succession, sub-aerially erupted volcanics, and occurrence of several gravelly beds suggest an unstable shallowing basin. A consistent northwest-southeast trending palaeo-shoreline from Neo- and Palaeoproterozoic successions of OLH and ILH has been visualized. The compositional consistency of OLH and ILH siliciclastics hints towards similar source area lithology (the Aravalli-Delhi Supergroup and less commonly the Banded Gneissic Complex and Bundelkhand Granite-gneiss). The presence of alluvial fan facies along the Tons thrust possibly hint towards the existence of a palaeo-high (horst) region of the rifted basin between OLH and ILH. The thinning and sagging of the basin floor of the basement and development of shallow marine set up is also consistent as some of the mafic bodies present within the studied sediments bear a "within plate basaltic" signature.It is also consistent with the palaeogeographic settings during the Proterozoic time, when no deep oceans existed around the Indian subcontinent. Precambrian stratigraphy of Himalaya has close proximity and resemblance with the Vindhyan basin which rests unconformably on the Bundelkhand and Aravalli cratons.Though the Vindhyan basin is traditionally considered intracratonic but it is in fact, an epicratonic basin located along the hinges of the Archean nuclei of the Indian shield and has a lots of similarities in sedimentation pattern with the Lesser Himalayan basin. Therefore, it will be appropriate to consider the Precambrian succession of Himalaya as a part in the Aravalli- Bundelkhand craton.

Keywords: Proterozoic, Himalaya, Stratigraphy, Sedimentology, Basin tectonics.

हिमालयी पर्वतजन में प्रोटेरोजोइक अवसादी अनुक्रमण: स्तरित शैलविज्ञान, अवसादिकी और पुराद्रोणीय स्थितियां

सुमित के. घोष[1], मंजू नेगी[1], पूनम जलाल[1,2], शुभजीत सिन्हा[3]

[1]*वाडिया हिमालय भूविज्ञान संस्थान, देहरादून 248001, भारत*
[2]*भूविज्ञान विभाग, कुमाऊं विश्वविद्यालय, नैनीताल 263001, भारत*
[3]*भूविज्ञान विभाग, बैलीगंज साइंस कॉलेज, कोलकाता 700019, भारत*

सारांशः हिमालयी पर्वतजन भारतीय प्लेट के अग्रणी किनारे की लम्बाई में 2500 कि. मी. लम्बी व 250 कि.मी. (औसत) चौड़ी एक चाप बनाता है। उच्चतर (हायर), कमतर (लेसर), व उप–हिमालय, पुरानी भारतीय शील्ड के कतले (स्लाइसेस) हैं जो दक्षिण की ओर झुकी हुई क्षेपों की एक श्रृंखला की लम्बाई में स्थानांतरण के कारण एक–दूसरे पर चढ़े हुए हैं। कमतर और टेथिस हिमालयी भाग में उत्तर पैलिओप्रोटेरोजोइक से पूर्व पैलिओजोइक तक के अनुक्रमणों में चार प्रमुख अश्म–घटनाएं (लिथोइवेंट्स) दर्ज हैं: i) पुराप्रोटेरोजोइक अर्जिलाइट=सिलिसिक्लास्टिक, ii) मीजोप्रोटेरोजोइक चूनेदार (चूनापत्थर) > अर्जिलाइट, iii) निओप्रोटेरोजोइक अर्जिलाइट=सिलिसिक्लास्टिक, और iv) उत्तर निओप्रोटेरोजोइक–पूर्व पैलिओजोइक मिश्रित सिलिसिक्लास्टिक–अर्जिलाइट–चूनेदार (चूना पत्थर)। केंद्रीय (सेंट्रल) कमतर हिमालयी (गढ़वाल व कुमाऊं) अनुक्रमणों को भूगर्भिक, अवसादिक और शैलवर्णनिक विशेषताओं के आधार पर बाहरी (दक्षिणी) व भीतरी (उत्तरी) प्रांतों (डोमेन्स) में पृथक किया गया है। इनमें से बाहरी कमतर हिमालय (ओ.एल.एच.) के ब्लेनी–पूर्व अवसादी अनुक्रमण की भूवैज्ञानिक आयु (निओप्रोटेरोजोइक) भीतरी कमतर हिमालय (आई.एल.एच.) के अवसादी अनुक्रमण की आयु (पुराप्रोटेरोजोइक–मीजोप्रोटेरोजोइक) से कम है। ऊपर की ओर उत्तरोत्तर बढ़ती हुई मोटाई वाले कणों वाला अनुक्रमण, भूपृष्ठिय (सब–एरियल) विस्फोट से बनी ज्वालामुखी शैल, तथा कई बजरी वाले संस्तरों का पाया जाना एक अस्थिर उथली होती द्रोणी की ओर इंगित करते हैं। ओ.एल.एच. और आई.एल.एच. के निओप्रोटेरोजोइक व पुराप्रोटेरोजोइक अनुक्रमणों के लिए एक अविरोधी उत्तरपश्चिम–दक्षिणपूर्व प्रवृत्ति

CHARACTERIZATION OF ZIRCONS FROM THE LESSER HIMALAYAN CLASTICS: IMPLICATION FOR PROVENANCE APPRAISAL

MANJU NEGI[1*], SANTOSH K. RAI[1], SUMIT K. GHOSH[1], UDAY BHAN[2], AND SAURABH SINGHAL[1]

*[manjunegi34@gmail.com]

[1]Wadia Institute of Himalayan Geology, 33 GMS Road, Dehradun-248001

[2]University of Petroleum and Energy Studies, Dehradun

ABSTRACT

Zircons are common, but a key resistant mineral found in the clastic rocks. These are useful to trace the provenance of sediments and their depositional regimes in varying basinal set ups. Due to its ability to survive magmatic, metamorphic and erosional processes, zircon is used as an important tool to infer detail information regarding the geological history and genesis of magmatic, metamorphic and sedimentary rocks.

The Proterozoic Lesser Himalayan basin largely consists of thick sequences of siliciclastic, argillite, and Limestone deposited under shallow marine shelf set up .The southern and northern parts of the Lesser Himalaya are divided on the basis of lithology, stratigraphy and tectonic settings and they are called as the Outer Lesser Himalaya (OLH) and Inner Lesser Himalaya (ILH).The clastic sediments have retained the accessory minerals such as, zircon, monazite and apatite, sourced from the Aravalli and Bundelkhand cratons of the peninsular India.Zircons from Proterozoic Lesser Himalayan clastic sediments differ in their response to magmatic and metamorphic processes with respect to their crystal morphology and internal structures.The present study attempts to categorizes the physical features perceived in the zircons of the two prominent lithounits –Neoproterozoic Jaunsar Group (Nagthat and Chandpur formations) and Paleoproterozoic Damtha (Rautgara Formation of ILH) of the Lesser Himalaya, in accordance to the processes responsible for their genesis. They are widely varied in terms of external morphology and internal textures. Zircon grains show zoning pattern of magmatic as well as metamorphic characteristics. Differences in morphological characteristics of different zircons suggest that each formation (Nagthat, Chandpur and Rautgara) of the Lesser Himalaya are sourced from a protoliths, which underwent different processes of zircon formation as well as different degree of transportation.